DEXTRAN IN SUGAR MANUFACTURE - PROBLEM EVALUATION AND ENZYME-BASED MITIGATION

vorgelegt von

M. Sc.

Karin Abraham

von der Fakultät III – Prozesswissenschaften,

der Technischen Universität Berlin

zur Erlangung des akademischen Grades

Doktor der Ingenieurwissenschaften

- Dr.-Ing. -

genehmigte Dissertation

Promotionsausschuss:

Vorsitzende:	**Prof. Dr.-Ing. habil. Cornelia Rauh**
Gutachter:	**Dr. Jan Maarten de Bruijn**
Gutachter:	**Prof. Dr.-Ing. Eckhard Flöter**
Gutachter:	**Dr. Lutz Popper**

Tag der wissenschaftlichen Aussprache: 20. Juni 2019

Berlin 2019

ABSTRACT

It is well-known that the presence of the microbial polysaccharide dextran in sugar beet and cane juices can affect sugar manufacture in many ways. However, a controlled mitigation of dextran-induced effects during sugar processing by enzymatic decomposition is still not established practice, which is what this work is aiming at.

The first step towards this is the detailed understanding of the effects of dextran as well as of enzymatically decomposed dextran during sugar manufacture. Therefore, laboratory juice purification and crystallisation experiments with synthetic thin and thick juices containing various dextran contents of different molecular masses were performed. This also includes enzymatic decompositions of dextran using various enzyme levels. Thereby, the most harmless reaction products with regard to these two process steps were identified.

For the purification process by means of lime and carbonation gas, it was shown that dextran is involved in size and shape modifications of calcium carbonate particles precipitated during carbonation. This could affect both, the filtration as well as the purification performance. The data indicate that the presence of dextran with molecular masses above 10 kDa promotes calcium carbonate agglomeration. This was most pronounced for broadly distributed intermediate but rather low molecular mass dextran. Thus, a mixture of high and low molecular mass dextran fractions as well as mildly, insufficiently decomposed high molecular mass dextran caused the most dramatic increase in the size of calcium carbonate particles. A size-related evaluation of particle shape parameters has additionally revealed that particularly the shape of large-sized agglomerates was modified. The shape data indicate that the calcium carbonate agglomeration in dextran-free samples as well as in samples loaded with low molecular mass dextran is oriented. Once dextran of higher molecular mass was present (>85 kDa), the shape data suggest that the agglomeration was non-oriented. Viscosity measurements have additionally shown that the effect of the dextran contents relevant for raw juices in the beginning of sugar manufacture on the flow behaviour is minor. Thus, the major cause for impeded filtration performances as a part of beet raw juice purification can be attributed to the just mentioned particle size and shape modifications. Thereby, it is assumed that the filter cake porosity is modified due to the presence of more round agglomerates with smoother surfaces, resulting from non-oriented agglomeration.

Similarly, the effects of different dextran fractions and enzymatically decomposed dextran on the size and shape distribution of sucrose crystals were investigated. The data from evaporative crystallisation experiments using synthetic thick juices indicate that three different crystal-shapes can be related to the presence of dextran, namely, cube-like, elongated as well as agglomerated crystals. The occurrence of these shapes seems to depend on the content of high molecular mass dextran, while low molecular mass dextran did not show a concentration dependency. For high contents of high molecular mass dextran and all contents of low molecular mass dextran, mainly an

increase in agglomerated crystals was found, accompanied by a rather low amount of elongated crystals. Here, again, it was found that mildly, insufficiently decomposed high molecular mass dextran still affects the sucrose crystal size and shape distribution, again negative effects were most pronounced for these broadly distributed intermediate but rather low molecular mass dextran fragments.

Consequently, it has been shown that high as well as low molecular mass dextran affect the characteristics of calcium carbonate particles as well as of sucrose crystal in an undesirable way. Depending on the progress in enzymatic decomposition and thus the molecular mass of the reaction products, these dextran-induced effects could be mitigated. When decomposing dextran to reaction products with molecular masses of less than 10 kDa, no effects on the size and shape of calcium carbonate particles were found anymore. Besides, no dextran-related effects on the sucrose crystal characteristics were found once dextran was decomposed to reaction products with molecular masses below 5 kDa.

A comprehensive study on the enzyme reaction on various dextran contents and initial molecular mass distributions was additionally done using size-exclusion and affinity chromatography. In doing so, it was found that, for all molecular mass distributions investigated, the molecular mass of dextran was gradually reduced with the increase in enzyme level and incubation time. However, the data also indicate that not only the total dextran content, but also the initial molecular mass distribution is decisive for the progress in enzymatic decomposition.

Thus, for targeted dextranase dosage, the dextran content as well as its molecular mass distribution need to be known. To pay attention to this aspect as well, a practical tool for dextran analysis in sugar industrial practice was developed and benchmarked against the commonly used but rather inaccurate Haze Method. The method proposed is based on determining differences in optical rotation caused by the mechanical separation of dextran as a macromolecule from the juices by membrane filtration. Thereby, it was found that the presence of sucrose advantageously improved the separation of dextran via ultrafiltration. Separation efficiencies as well as specific cut-off values (10 kDa and 50 kDa) for the separation of dextran from aqueous sucrose solutions for two polyethersulfone membranes were determined. The data indicate that the basic membrane setting (specific cut-off of 10 kDa) enables the complete separation and therefore the analytical quantification of the whole molecular mass spectrum relevant for dextran-related effects. For higher dextran contents, a combination of both membranes additionally enables the differentiation between a high and a low molecular mass dextran fraction. Thus, the results indicate that the complete and also a fractionated dextran analysis in sugar cane and beet juices is possible with this new principle. For the first time, comprehensive basic scientific findings on the whole dextran issue have been combined to a basic framework for dextranase application in sugar industrial practice.

ZUSAMMENFASSUNG

Die Anwesenheit von mikrobiellen Polysacchariden in Zuckerrüben- sowie Zuckerrohrsäften kann zu diversen Beeinträchtigungen bei der Zuckergewinnung führen. Für gewöhnlich werden diese Dextran-induzierten Effekte über den Einsatz von Enzymen reduziert. Trotz jahrelangem Bestehen dieser Problematik, gibt es immer noch keinen kontrollierten Einsatz von Dextranasen in der Zuckerindustrie, dessen Ermöglichung sich diese Arbeit zum Ziel gesetzt hat.

Dies setzt zunächst einmal das Verständnis der Prozesseffekte, die mit der Anwesenheit von Dextran und auch enzymatisch abgebautem Dextran einhergehen, voraus. Dafür wurden im Rahmen dieser Arbeit Saftreingungs- sowie Kristallisationsversuche im Labormaßstab mit synthetischen Dünn- und Dicksäften durchgeführt. Dabei wurden die Effekte von Dextran in Abhängigkeit der vorliegenden Konzentration und des Molekulargewichtes untersucht. Letzteres beinhaltet auch den enzymatischen Abbau von Dextran unter Verwendung verschiedener Enzymkonzentrationen. Als Resultat sollen für diese beiden bedeutenden Prozessschritte harmlose enzymatische Abbauprodukte und damit das Ziel des enzymatischen Abbaus identifiziert werden.

Die Durchführung von Saftreinigungsversuchen nach dem Kalk-Kohlendioxid-Prinzip hat gezeigt, dass Dextran die Größe und die Gestalt der bei der Karbonatation ausgefällten Kalziumkarbonatpartikel modifiziert. Eine veränderte Partikelgröße und -gestalt kann die Filtration, aber auch den eigentlichen Reinigungseffekt beeinträchtigen. Die Daten haben gezeigt, dass die Anwesenheit von Dextran mit Molekulargewichten über 10 kDa die Kalziumkarbonat-Agglomeration fördert. Dies war insbesondere der Fall, wenn breit verteiltes, intermediäres niedermolekulares Dextran anwesend war. Schließlich war die Zunahme der Partikelfläche am stärksten ausgeprägt für eine Mischung aus der nieder- und hochmolekularen Fraktion aber auch für geringfügig und damit unzureichend enzymatisch abgebautes hochmolekulares Dextran. Eine größenabhängige Auswertung von Gestaltsparametern hat außerdem gezeigt, dass insbesondere die Gestalt von großen Agglomeraten durch Dextran verändert wird. Dabei deuten die Daten daraufhin, dass die Agglomeration von Kalziumkarbonat in Abwesenheit und in Anwesenheit von niedermolekularem Dextran orientiert erfolgt. Sobald Dextran mit höherem Molekulargewicht (>85 kDa) anwesend war, deuten die Daten auf eine nicht-orientierte Agglomeration hin. Es konnte außerdem gezeigt werden, dass der Effekt der für Rohsäfte relevanten Dextrankonzentrationen am Anfang der Zuckergewinnung auf die Viskosität eher gering ist. So kann der Hauptgrund für eine verschlechterte Filtration als Teil der Reinigung von Zuckerrübenrohsäften auf veränderte Partikeleigenschaften zurückgeführt werden. Dabei wird angenommen, dass die Filterkuchenporösität durch die Anwesenheit von runderen Agglomeraten mit einer glatteren Oberfläche, resultierend aus der nicht-orientierten Agglomeration, reduziert wird.

Ebenso wurden die Effekte von verschiedenen Dextranfraktionen sowie von enzymatisch abgebautem Dextran auf die Größe und Gestalt von Zuckerkristallen untersucht. Die Resultate der

Verdampfungskristallisationsexperimente mit synthetischen Dicksäften deuten darauf hin, dass drei verschieden Kristallgestalten mit Dextran in Verbindung gesetzt werden können. Dabei handelt es sich um würfelförmige, deutlich verlängerte und agglomerierte Kristalle. Das Auftreten dieser Kristalle scheint von der vorhandenen Konzentration an hochmolekularem Dextran abhängig zu sein. Im Gegensatz dazu scheint es keine Konzentrationsabhängigkeit mit niedermolekularen Dextran zu geben. Für hohe Konzentrationen an hochmolekularem Dextran und für alle Konzentrationen an niedermolekularem Dextran konnte hauptsächlich ein höherer Anteil an Agglomeraten sowie ein vergleichsweise geringer Anteil an deutlich verlängerten Kristallen detektiert werden. Auch in diesem Fall hat sich gezeigt, dass ein unzureichender Abbau zu polydispersen, intermediären Dextranfragmenten die Eigenschaften der Saccharosekristalle deutlich verändert.

Schließlich konnte gezeigt werden, dass hoch- und auch niedermolekulares Dextran die Eigenschaften der Kalziumkarbonatpartikel sowie auch der Zuckerkristalle auf unerwünschte Weise modifiziert. In Abhängigkeit des enzymatischen Abbaugrades und damit des Molekulargewichtes der Abbauprodukte konnten die soeben erläuterten Dextran-induzierten Effekte reduziert werden.

Sobald Dextran zu Abbauprodukten mit einem Molekulargewicht, das kleiner als 10 kDa ist, abgebaut wurde, konnten keinerlei Effekte auf die Größe und Gestalt von Kalziumkarbonatpartikeln detektiert werden. Diese Grenze zu harmlosen Abbauprodukten konnte im Hinblick auf die Eigenschaften der Zuckerkristalle bei 5 kDa ermittelt werden.

Um die Enzymreaktion im Detail zu verstehen und die resultierenden Abbauprodukte zu identifizieren, wurde zusätzlich eine umfassende Studie zum enzymatischen Abbau von Dextran in Abhängigkeit der Konzentration und des Molekulargewichtes durchgeführt. Dafür wurde Größenausschluss- sowie Affinitätschromatographie verwendet. Es hat sich gezeigt, dass ausgehend von den verschiedenen Ausgangsmolmassenverteilungen das Molekulargewicht von Dextran bzw. deren Abbauprodukte mit der Erhöhung der Enzymkonzentration und der Inkubationszeit graduell reduziert wurde. Dabei zeigte sich, dass nicht nur die Dextrankonzentration, sondern auch die anfängliche Molmassenverteilung entscheidend ist für den Fortschritt im enzymatischen Abbau. Das macht die Kenntnis über die Konzentration sowie der Molmassenverteilung zu einer notwendigen Voraussetzung für einen gezielten Einsatz von Dextranasen.

Um auch diese Notwendigkeit zu berücksichtigen, wurde eine praktische Methode für die Bestimmung von Dextran in der Zuckerindustrie entwickelt und mit der bisher gängigen, aber ungenauen, Haze Methode verglichen. Das Prinzip der vorgeschlagenen Methode basiert auf der Messung von Differenzen in der optischen Rotation, verursacht durch die mechanische Abtrennung von Dextran aus den Zuckersäften mittels Membranfiltration. Es zeigte sich, dass die Anwesenheit von Saccharose die Abtrennung von Dextran mit Ultrafiltration deutlich verbessert.

Trenneffizienzen sowie spezifische Cut-off Werte (10 kDa und 50 kDa) für die Abtrennung von Dextran aus wässrigen Saccharoselösungen wurden für zwei Polyethersulfon-Membrane bestimmt. Die Daten zeigen ganz deutlich, dass eine vollständige Abtrennung und damit die Quantifizierung der gesamten Molekulargewichtsbreite, die für Dextran-induzierte Effekte relevant ist, möglich ist. Weiterhin konnte gezeigt werden, dass die Kombination der zwei Membranen zusätzlich die Differenzierung einer hohen und einer niedrigen Molekulargewichtsfraktion ermöglicht, wenn höhere Dextrankonzentrationen vorliegen. Schließlich deuten die gesammelten Erkenntnisse daraufhin, dass eine vollständige sowie auch fraktionierte Bestimmung von Dextran in Zuckerrüben- sowie Zuckerrohrsäften mit diesem neuen Prinzip möglich ist.

Abschließend lässt sich sagen, dass diese Arbeit erstmalig umfassende, wissenschaftliche Erkenntnisse zu der gesamten Dextranproblematik kombiniert und so ein grundlegendes Rahmenwerk für die Anwendung von Dextranasen in der Zuckerindustrie geschaffen hat.

ACKNOWLEDGEMENTS

This thesis was written with the department of Food Process Engineering of the Technische Universität Berlin. The work was based on a cooperative project with the company SternEnzym and financially supported by the WT.SH - Wirtschaftsförderung & Technologietransfer Schleswig-Holstein GmbH.

First of all, I would like to thank my supervisor Prof. Dr. Eckhard Flöter for his continuous support as well as his trust and belief he has always placed in me. His door was always open for scientific discussions and questions. The pleasant work atmosphere he provides gives proper space for personal growth and individual thinking.

Similarly, I would like to thank Dr. Susanne Rudolph-Flöter for being like a second supervisor. I have enjoyed every discussion with her and appreciated her engagement, pushing me to further improve my research and writings. I have learned a lot from her.

Besides, I would like to give many thanks to Dr. Lutz Popper and Dr. Jan Maarten de Bruijn for reading and assessing my thesis.

During my time at the department, I was honoured to supervise a couple of students in doing their thesis who helped me to generate data for my work. Of course, I would like to give many thanks to them as well.

Finally, I would like to thank all colleagues who surrounded me during the wonderful time of three years with the department of Food Process Engineering. I definitely enjoyed the work, which has always been accompanied by a lot of fun, but also by mutual respect. I would like to thank particularly those, who made me enjoy my daily life and also supported me in finishing my thesis in a variety of ways. It was not always about work, but also about meeting friends.

LIST OF PUBLICATIONS

Parts of the study presented were published as follows:

Publications in Journals

- Abraham, K.; Splett, L.; Köster, E.; Flöter, E. (2019). Effect of Dextran and Enzymatically Decomposed Dextran on Calcium Carbonate Precipitation. Journal of Food Process Engineering. https://doi.org/10.1111/jfpe.13072.
- Abraham, K.; Splett, L.; Flöter, E. (2019). Dextran-Induced Modifications of Particles Precipitated during Carbonation. submitted to the Sugar Industry in 2019.
- Abraham, K.; Rudolph-Flöter, E.S.J.; Schlumbach, K.; Schäfer, A.; Flöter, E. (2019). Comparative Analysis of Dextran-Induced Sucrose Crystal Modifications. submitted to the Journal of Crystal Growth in 2019.
- Abraham, K.; Brykczynski, H.; Rudolph-Flöter, E.S.J; Schlumbach, K.; Schäfer, A.; Flöter, E. (2019). Effect of Dextran and Enzymatically Decomposed Dextran on the Sucrose Crystal Shape Modifications. submitted to the Sugar Industry in 2019.
- Abraham, K.; Weigelt, J.; Rudolph, S.; Flöter E. (2019). Systematic Study on the Enzymatic Decomposition of Various Dextran Fractions. Journal of Process Biochemistry. https://doi.org/10.1016/j.procbio.2019.01.024.
- Abraham, K.; Flöter E. (2018). New approaches for the determination of dextran in the sugar production process. Sugar Industry, 143 (68), 138-146.
- Abraham, K.; Kunst, S.; Flöter E. (2019). Membrane Characterisation for Fractionated Dextran Analysis in Sugar Industry. Journal of Food Analytical Methods. https://doi.org/10.1007/s12161-019-01441-7.

Presentations and Posters

- Abraham, K.; Schlumbach K.; Thiesing D.; Flöter E. (16.08.2017): Insights into dextran analysis and dextran affected processing problems. 90th annual congress of the South African Sugar Technologists' Association (SASTA) – Durban, South Africa.
- Abraham, K.; Flöter, E. (22.05.2017): New Approaches for the Determination of Dextran in the Sugar Production Process. 5th biennial congress of European Society for Sugar Technology (ESST) – Dresden, Germany.
- Abraham, K.; Hußmann, J.; Flöter, E. (06.04.2017): Improving sugar manufacturing quality by efficient use of dextranase. 7th annual congress of Africa Sugar – Nairobi, Kenya.
- Abraham, K.; Flöter, E. (14.02.2017): New Approaches for the Determination of Dextran (Poster). ProcessNet - Jahrestreffen der Fachgruppe Lebensmittelverfahrenstechnik mit Lebensmittelbiotechnologie – Bruchsal, Germany.
- Abraham, K.; Hagen, S.; Schlumbach, K.; Flöter, E. (15.04.2016): Enzymeinsatz zur Optimierung des Zuckerproduktionsprozesses. Innovationsforum der Stern-Wywiol-Gruppe – Ahrensburg, Germany.
- Abraham, K.; Hagen, S.; Schlumbach, K.; Flöter, E. (18.03.2016): Enzymatischer Abbauprozess des Dextrans und Effekte auf die Kristallisation. Hauptversammlung Verein Deutscher Zuckertechniker (Zweigverein Nord) – Wernigerode, Germany.

TABLE OF CONTENTS

LIST OF SYMBOLS, INDICES AND ABBREVIATIONS

Symbol	Description	Unit
A	Area	m^2
a	Activity	-
c	Concentration	mol l^{-1}, kg m^{-3}
c_F	Concentration in the feed	g/100g
c_P	Concentration in the permeate	g/100g
d	Diameter	m
d_{50}	Mean aperture	m
D	Diffusion coefficient	m^2 s^{-1}
G	Gibbs free Energy	kg m^2 s^{-2}
g	Gravitational acceleration	m s^{-2}
H	Enthalpy	kg m^2 s^{-2}
h	Height	m
J	Mass transfer	m s^{-1}
k	Permeability	m^2
k_D	Constant for diffusion reaction	m s^{-1}
k_R	Coefficient for surface reaction	m s^{-1}
k_G	Overall crystal growth coefficient	m s^{-1}
k_B	Boltzmann constant	J K^{-1}
K_M	Michaelis-Menten constant	-
l	Length	m
m	Mass	kg
N	Number	-
p	Pressure	Pa
R	Gas constant	kg m^2 s^{-2} mol^{-1} K^{-1}
R	Rejection coefficient for membrane separation	%
r	Radius	m
r_m	Radius of a molecule	m
r_{crit}	Critical radius of crystals	m
R_g	Radius of gyration of a macromolecule	m
S	Supersaturation (ratio of concentrations c/c)	-
T	Time	s
T	Temperature	K
W	Velocity	m s^{-1}

V	Volume	m^3
w	Mass content	% (m/m)
$X^{\ddagger}$	Transition state	-
y_{sat}	Saturation coefficient	-
y_{SS}	Supersaturation	-
γ	Activity coefficient	-
γ	Surface energy	J m^{-2}
γ	Degree of polymerisation	-
γ_{CL}	Interfacial tension between crystalline solid and liquid	J m^{-2}
γ_{SC}	Interfacial tension between foreign and crystalline solid	J m^{-2}
γ_{SL}	Interfacial tension between foreign solid and liquid	J m^{-2}
$\dot{\gamma}$	Shear rate	s^{-1}
Γ	Thermodynamic factor	-
δ	Layer thickness	m
ε	Porosity	-
η	Dynamic viscosity	Pas
ν	Kinematic viscosity	m^2 s^{-1}
θ	Contact angle	°
μ	Chemical potential	J mol^{-1}
τ	Tortuosity	-
ρ	Density	kg m^{-3}
σ	Specific surface tension	kg s^{-2}
σ	Shear stress	Pa
ϕ	Factor for free energy of heterogeneous nucleation	-

Abbreviations	Description
BCF	Burton-Cabrera-Frank
Circ.	Circularity
E	Enzyme
ELSD	Evaporative Light Scattering Detector
ICUMSA	International Commission for Uniform Methods of Sugar Analysis
j.	Juice
MW	Molecular weight
MWCO	Molecular weight cut-off
P	Product
RDNS	Roundness
S	Substrate
SAXS	Small-angle X-ray scattering
SEC	Size exclusion chromatography
sat	Saturated state
sol	Solute
suc.	Sucrose
TU	Technische Universität
TS	Total Solids
T2000	Dextran with average molecular mass of 2000 kDa
T500	Dextran with average molecular mass of 500 kDa
T40	Dextran with average molecular mass of 40 kDa
T2000+T40	Equal-mass mixture of T2000 and T40
Vs	Versus
W/L	Width-to-length ratio
W	Water

1 INTRODUCTION

Sugar is still unique in its functionality (sweetness, bulking property, texture) among all sweeteners and still represents an important energy source in the world's nutrition. Furthermore, sugar production, trade and research employ a large number of people and is thus of great economic importance in sugar-producing countries. In the last century, the world sugar production increased from roughly 10 million metric tons, raw value (in 1900) to about 150 million metric tons, raw value (in 2005). Depending on the climatic conditions, the sugar producing countries either cultivate beet (moderately cold) or cane (in tropical and subtropical areas). The case that the climatic conditions allow to cultivate both crops is rather seldom but still possible (e.g. Egypt, Iran, United States) (Asadi, 2007). All in all, more than 130 countries currently produce sugar from sugar cane and/or beet (International Sugar Organization, 2018).

More recently, the data collected by the United States Department of Agriculture (USDA) illustrate that the world sugar production has still slightly increased in the last years, reported to be 185 million metric tons in 2018. The sugar production has generally been driven by its increasing demand. Thus, sugar consumption has similarly increased like the production, as illustrated in Figure 1-1 (United States Department of Agriculture (USDA), 2018).

Thereby, the main proportion of high market-quality white and crystalline sugar is used as an ingredient in food products (e.g. soft drinks). The quality of white sugar, meaning purified and crystallised sucrose, is determined by various criteria, such as purity, ash content, colour as well as the crystal size and shape distribution. White sugar, in comparison with other substances, is extremely high in purity with sucrose contents rarely lower than 99.7 %.

From the crystallisation of sucrose, a large mixture of crystals with different sizes are generally obtained. However, it should as far as possible be uniformly distributed with narrow size distributions and a small proportion of fine crystals. This is due to the fact that the size distribution affects the appearance of sugar and also its behaviour during industrial processing as well as in its final application in food products.

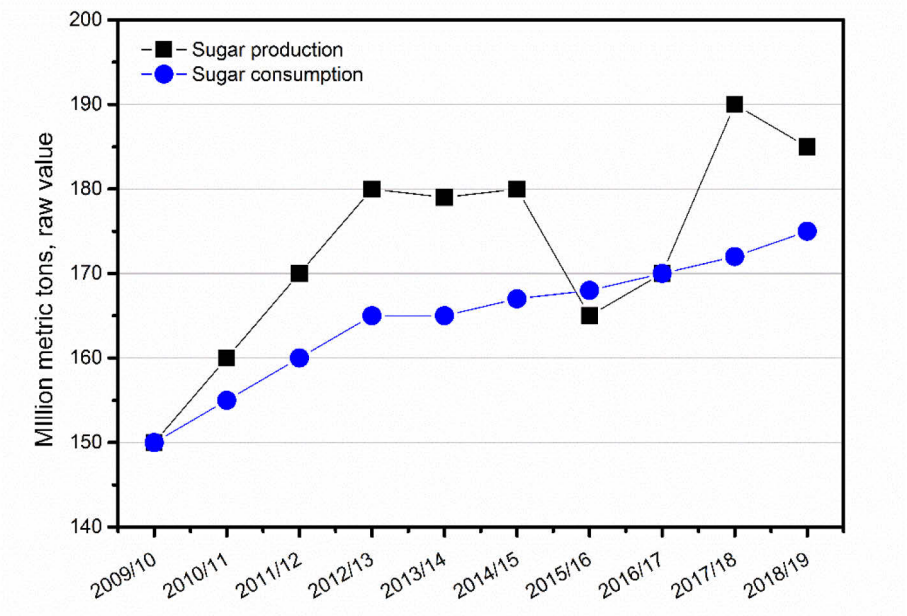

Figure 1-1 Global sugar production and consumption according to data collected from the USDA (reprinted from United States Department of Agriculture (USDA), 2018).

It is a well-known fact that the presence of impurities in cane and beet juices can impede sugar processing and can also detrimentally affect the above-mentioned quality criteria of final sucrose crystals. Thereby, the presence of polysaccharides plays an important role. One of the most important representatives is the microbial polysaccharide dextran, which is still a major problem during sugar manufacture from both, cane and beet (van der Poel et al., 1998).

Dextran is especially relevant for the cane sugar industry mainly due to the abundant occurrence of mesophilic bacteria in the area, where sugarcane is cultivated. Nevertheless, the presence of dextran in sugar beet juices is not negligible either, which is in this case mainly initiated by freeze-thaw-cycles (Abdel-Rahman, 2007). The latter is currently particularly gaining in importance due to prospective prolongations of sugar beet campaigns as a result of changes of the European legislation in 2017 (Adjari Rad et al., 2014).

Thus, for instance, an increase in viscosity, a reduction in purity as well as abnormal crystal size and shape distributions can result from the presence of dextran of various molecular masses (Promraksa, 2008). For both, cane and beet, it is well-known that dextran affects the sub-process steps of sugar manufacture, whereas purification processes as well as the sucrose crystallisation seem to be most relevant. Impeded juice purification performances not only disturb processing, but also leads to a lower purity of the final sucrose crystals (colour and other impurities) (Asadi, 2007). Besides, a decrease in sugar quality due to modified sucrose crystal size and shape distributions is one of the most well-known results of the presence of dextran of varying molecular masses (Abdel-Rahman, 2007). In case microbial contamination has already taken place, the decomposition of

dextran by enzyme application is the method of choice for mitigating the dextran-related process effects (Khalikova et al., 2005).

Even though dextran has been an issue in sugar manufacture for years, a targeted mitigation of dextran contamination by enzymes is still not established practice, which is what this work aims at. Thereby, the following three main issues have been dealt with in this thesis.

1. Analysis of dextran-induced process effects with regard to juice purification and sucrose crystallisation
2. Investigations on the enzyme reaction and identification of corresponding reaction products
3. Analysis of dextran in sugar raw juices as a substrate for the enzyme reaction

To be able to follow the respective sub-topics in detail, the necessary fundamentals are firstly given in the following chapter 2 of this thesis. The results obtained from laboratory juice purification and crystallisation experiments with synthetic thin and thick juices containing various contents of different molecular mass dextran fractions are discussed in chapter 3 to 6. Thereby, implementation of suitable analytical tools to adequately analyse the characteristics of calcium carbonate particles and sucrose crystals (image analysis) was also key to this study.

The characterisation of the enzyme reaction pattern as well as the identification of the resulting reaction products were done by means of highly accurate size exclusion and affinity chromatography (see chapter 7). By combining the results from the investigations on dextran-induced process effects and on the enzyme reaction most harmless reaction products resulting from the decomposition of dextran with regard to juice purification and sucrose crystallisation could be identified. This means the actual target for controlled dextranase application in sugar industry has been identified. To obtain these targeted reaction products by adequately dosing dextranase, the initial total dextran content and at best also its molecular mass distribution need to be analysed. Thus, also a part of the work presented, a new method for complete and fractionated dextran analysis suitable for sugar industrial practice has been developed, see detailed explanation and results in chapter 8 and 9.

This way, for the first time, combined scientific knowledge on the entire dextran topic has been created. Finally, an overall conclusion gives a survey on all findings of this work and combines them to a fundamental framework for dextranase application in sugar industrial practice.

References

Abdel-Rahman, E.-S. (2007). Investigations on the influence of dextran during beet sugar production with special focus on crystal growth and morphology (PhD). Technische Universität Berlin, Berlin.

Adjari Rad, M., Adjari Rad, A., & Schrevel, G. (2014). Evaluation of juice purification in sugar factories. *Sugar Industry*, *139*(12), 734–744.

Asadi, M. (Ed.). (2007). *Beet-Sugar Handbook*. New Jersey: John Wiley & Sons.

International Sugar Organization. (2018). The Sugar Market. Retrieved from https://www.isosugar.org/sugarsector/sugar, accessed on 12th of march 2019.

Khalikova, E., Susi, P., & Korpela, T. (2005). Microbial dextran-hydrolyzing enzymes: fundamentals and applications. *Microbiology and Molecular Biology Reviews*, *69*(2), 306–325. https://doi.org/10.1128/MMBR.69.2.306-325.2005

Promraksa, A. (2008). Reduction of Dextran Contamination in Raw Sugar Production (PhD). Suranaree University of Technology, Nakhon Ratchasima.

United States Department of Agriculture (USDA). (2018). Sugar: World Markets and Trade. Retrieved from https://usdasearch.usda.gov, accessed on 12th of march 2019.

Van der Poel, P. W., Schiweck, H., & Schwartz, T. (1998). *Sugar Technology: Beet and Cane Sugar Manufacture*. Berlin: Dr. Albert Bartens KG.

2 FUNDAMENTALS

2.1 Industrial Sugar Production

2.1.1 Sugar Beet and Cane - Plant and Composition

The two main sources for sugar manufacture, sugar cane and beet, cover roughly 40 % and 60 % of the world's sugar production, respectively.

Sugar beets are conical plant organs of the biennial plant *Beta vulgaris saccharifera*, which mainly grows in moderate climate zones in the northern hemisphere. During the first year of vegetation, the roots and leaves grow. During the second year of vegetation, flowering and seed production takes place. The manufacturing target, the disaccharide sucrose, is mainly stored in the roots, which hence represent the starting material for sugar manufacture from beets. Thus, beet harvesting is done in the first year of vegetation (Asadi, 2007).

In contrast to beet, sugar cane (*Saccharum officinarum*) cultivation requires warm temperatures (293 to 303 K) and adequate moisture. It is hence mainly grown in tropical and subtropical regions. The tropical grass of the family *Gramineae* accumulates sugar in its stems as the main result of photosynthesis, providing the energy for the plant to grow (Chen & Chou, 1993).

In the main, both starting materials for sugar manufacture are composed of three main parts: water, soluble and insoluble dry substance. For both, beet and cane, water is the major component, ranging between 70-77 % (m/m). The insoluble matter generally originates from the cell wall and the semipermeable cell membrane. The material remaining after the aqueous extraction of water soluble components is known as beet marc (5 % (m/m)) and cane bagasse (10 % (m/m/)), respectively (van der Poel et al., 1998). The composition of these two residual fibrous materials are generally relatively similar. Both, beet marc and cane bagasse, are mainly composed of cellulose, hemicellulose, lignin and proteins. Beet cells additionally contain pectin as a cell wall component, while cane cells have a considerably higher amount of lignin. The main component of the soluble dry substance contained in beet and cane juices is, of course, sucrose, ranging from 14 to 20 % (m/m) and 10 to 18 % (m/m) in beet and cane raw juices, respectively. Apart from sucrose, several other soluble non-sucrose components (referred to as non-sugars) are co-extracted along

with the sucrose and can subsequently act as impurities during sugar manufacture. These are only partially removed during processing. Nitrogenous non-sugars can barely be removed during processing and mainly end up in the molasses, particularly concerning glutamine, asparagine and for beet also betaine. The nitrogen-free components include several saccharides, colourings, minerals as well as organic acids. The most important small-sized saccharides in beet and cane juices are glucose and fructose, which occur in reasonably higher amounts in cane juices. Besides, in beets, varying amounts of raffinose can additionally occur (van der Poel et al., 1998). Especially important for processing is the amount and kind of soluble polysaccharides, either originating from cell plant material (e.g. pectin, starch, soluble hemicelullose) or from microbial contamination (e.g. dextran and levan) (Cuddihy et al., 2001). In view of microbial polysaccharides, the glucose polymer dextran in particular plays an increasingly important role for both, sugar cane and beet processing, thus, being key to this study,

The general outline of sugar manufacture from beet and cane is relatively similar. However, some parts considerably differ due to the different structure and also due to varying compositions of beet and cane. Thus, the amount and kind of non-sugars vary from beet to cane and can also vary depending on several climatic and environmental conditions. Therefore, the following chapter provides a basic overview of sugar manufacture from cane and beet, schematically illustrated in Figure 2-1 and 2-2.

2.1.2 General Outline of Sugar Manufacture from Cane and Beet

2.1.2.1 Harvest and Preparation

Sugar beets are harvested once the temperature drops below 288 K and has to be completed before the first frost. The latter is especially relevant for avoiding cell damage, which initiates beet quality loss due to microbial contamination, inter alia leading to dextran formation. The beets are generally mechanically harvested (tractor-drawn and self-propelled). After that, the top and the crown of the beets are removed. Trash (e.g. soil, stones) and tare attached to the beet surface decisively lowers the beet quality and need hence also to be removed (Asadi, 2007). Similarly, sugar cane harvest aims at delivering high quality cane stalks to the factory, which is also measured by sucrose and trash (tops, leaves, root, soil) contents. Dry (vibration) as well as wet (wash water) cleaning methods are used to remove impurities from the surface of beet and cane (Chen & Chou, 1993).

In general, cane is much more prone to deterioration, which is mainly attributable to the climatic conditions but also to the cane plant properties. Even before harvesting, deterioration can occur more often, caused by diseases, pest or weather damage. After cutting, chemical (acids), microbial (lactic acid bacteria) and enzymatic (invertase) processes can cause rapid deterioration and thus quality loss. Consequently, different from beets, cane stalks cannot be stored for a long time due to rapid deterioration, necessitating that harvest and processing are simultaneously done. Thus, cane

quality distinctly decreases due to cane damage and particularly due to a delay in cane delivery. In order to reduce deterioration as far as possible, cane harvest is usually done during the cooler, drier months of the year. Here again, the cane tops need to be removed because of low sucrose contents and high contents of starch and reducing sugars. The best harvesting method with regard to cane quality is still cutting by hand. However, due to the general endeavour of increasing efficiency, mechanical harvesting has increasingly been used in the last decades. This way, burning of cane prior to harvest has gained in popularity to reduce the higher trash content coming with mechanical harvesting. However, it also removes protective waxes on the cane surface and causes cooking of the peripheral storage tissue of the stalk. The more intense the burning procedure, the greater the damage and thus the higher the risk of microbial contamination. The latter also means that dextran contamination is distinctly increased due to burning (Chen & Chou, 1993).

The sugar beet roots and cane stalks are then transported to the factory (Asadi, 2007). After unloading the beet roots and cane stalks, sampling and laboratory analysis are done. Mostly, the growers' payment is not only based on weights, but also on the sucrose content, which is usually determined by polarimetric analysis (van der Poel et al., 1998).

2.1.2.2 Beet Slicing and Cane Preparation

The cleaned beets are then transferred to the beet hoppers, which deliver the beets into the slicer. The slicer cuts the beets into the so-called cossettes, generating a higher contact area between the surrounding water and the beet, increasing the diffusion of sucrose. In doing so, the desired V-shape with uniform width (3 to 6 mm) and length (30 to 60 mm) is pursued. Slicing is done by several knives held in blocks in the drum of the slicer. The cossettes are then transferred to the diffuser via a belt conveyer (Asadi, 2007).

Cane stalks have to get prepared for extraction as well, aiming at breaking the hard structure and rupturing cells. Therefore, revolving knives (cut stalks into chips, no juice extraction), hammer-mill shredders (separation of cane chips into shreds, no juice extraction) and grooved crusher rolls (break cane and additionally cause juice extraction) are used, either separately or in combination (Chen & Chou, 1993).

2.1.2.3 Extraction

The targeted component sucrose is dissolved in the aqueous solution of the cellular structure of sugar beet and cane. For beet raw juice extraction, the diffusion-based solid-liquid extraction is used to initiate the movement of sucrose to the surrounding solvent, the diffusion water. Similarly, extraction by diffusion is also partly used for cane raw juice extraction. Most deviating here is the mechanical preparation of cane prior to diffusion, which is mainly due to the diverging characteristics of the two starting materials.

Anyhow, thermal denaturation is necessary to overcome the semi-permeability of the protoplasm (cell membrane). Thereby, the heat induces the coagulation of proteins, representing the protoplasm's main component, to enable the diffusion of sucrose to the diffusion water. The diffusion process can generally be described by Fick's law. In general, the driving force of the diffusion process is attributable to a gradient in chemical potential of sucrose. This is often simplified by a difference in sucrose concentration between the inside and the outside of the beet cells, which is used in Fick's law. Apart from the gradient in chemical potential, the temperature, the surface area of the cossettes/shreds as well as the retention time affect the extraction. Beyond control at this point, the inherent properties of the beet material, affected by the storage conditions (e.g. potential diseases and frost damage), can affect the diffusion success as well.

Juice diffusion from beet cossettes and cane shreds is usually done in counter-current manner. This means, cossettes and hot water are guided in opposite direction. The optimum temperature of the hot diffusion water is 343 to 346 K balancing the positive (e.g. improved diffusion and denaturation, lower bacterial activity) and negative (release of cell wall components such as pectin, pulp pressability) aspects of high temperatures (van der Poel et al., 1998).

Even though diffusion is also applied for cane raw juice extraction, milling is still the predominant process for the extraction of raw juice from cane. The mills for cane manufacture usually consist of multiple units, each consisting of a three-roller combination through which the crushed cane passes. Thereby, three rolls are combined to a triangular form, whereby the two bottom rolls are fixed in position. The prepared cane is fed via the opening between the adjustable top roll and the two fixed bottom rolls. To additionally increase the sucrose yield, water or thin juice is sprayed on the crushed cane, known as imbibition. This way, about 95 % of the sugar passes into the raw juice. The remaining cane and beet material is mainly composed of woody fiber, water and also the residual unextracted sugar (Chen & Chou, 1993).

The raw juice resulting from the extraction is of dark-grey colour and contains suspended solids as well as colloidal substances, which are supposed to be removed as far as possible during the following purification step (van der Poel et al., 1998).

2.1.2.4 Juice Purification

The raw juice resulting from extraction is still acidic and contains several co-extracted non-sugars, which are heterogeneous in composition. The aim of juice purification is to increase the purity as well as the processibility of the raw juices.

The sugar beet raw juice purification is usually done by means of lime and carbonation gas. In doing so, the raw juice is progressively limed in order to stepwise precipitate certain non-sugars. This first step of lime addition is known as pre-liming. During subsequent main-liming, a dramatic increase of the pH and alkalinity in the main liming step take place, which aims at decomposing invert sugar

and partly amides. The subsequent addition of carbonation gas initiates calcium carbonate crystallisation. Hence, the simultaneous dissolution of $Ca(OH)_2$ and CO_2 leads to the formation of $CaCO_3$ while H^+ and OH^- form water molecules. The calcium carbonate particles subsequently grow, agglomerate and additionally serve as adsorption points for non-sugars. The calcium carbonate crystals and their agglomerates with adhering non-sugars are then separated by settling and filtration. The result is known as thin juice, in which all insoluble and partially soluble substances are removed. As a result, about 20-30 % (m/m) of the non-sugars in beet raw juices are removed by purification using lime and carbonation gas. This way, beet thin juices are generally thermostable juices of low colour and high purity. It is further free of insoluble substances and should have minimal solution hardness (Asadi, 2007).

The purification process of cane raw juice differs from that. This is mainly due to a distinctly higher amount of invert sugar. For cane raw juice purification, lime and heat are mainly used as clarifying agents. Thereby, the juice is only moderately limed to neutralise the acidity of the juice while forming insoluble lime salts (mostly calcium phosphate). The limed juice is subsequently heated to boiling in order to coagulate albumins and some fats, waxes and partly gums. The drastic increase of pH is in this case avoided because the amount of acid and colour resulting from the decomposition of invert sugar would be too high. The precipitate is known as mud, which is separated from the thin juice by sedimentation. The mud is then filtered in order to maximise juice and thus sugar yield. The corresponding filter cake is mainly used as fertiliser. The clarified thin juices from beet and cane are then further processed in the evaporation station (Chen & Chou, 1993).

2.1.2.5 Evaporation

Multiple-stage evaporation is likewise used for the evaporation of water from beet and cane thin juices. In doing so, the thin juice, containing roughly 15 % (m/m) dry substance, is concentrated to the so-called thick juice, containing about 65 % (m/m) dry substance. From now on, further processing of beet and cane thin juices to solid sucrose crystals is relatively similar. Flash evaporation is commonly used, meaning the conversion of liquid to vapour by the simultaneous application of heat and vacuum. The latter reduces the boiling point of water and consequently reduces the heat supply required for evaporation. The steam for the first evaporator is generated in a steam boiler by burning of fuel. Subsequently, the steam coming from an evaporator is used to heat the respective following evaporator. Due to heat losses and boiling point elevation from evaporator to evaporator, the temperature successively decreases and hence also the pressure is stepwise reduced from one evaporator to the next one (Asadi, 2007).

Sugar beet thin juices have a pH of about 8.5 to 9.0, representing the most suitable pH to prevent sucrose loss, thus representing a thermostable juice. Due to the higher stability, higher temperatures

can be applied. Thus, boiling temperatures range from 398 to 408 K in the first evaporator down to 353 to 368 K in the last evaporator during sugar beet thin juice evaporation. Since cane thin juices are thermolabile, generally lower temperatures are applied. Thus, the highest temperatures are set to 383 to 388 K in the first evaporator and to about 346 to 361 K in the last evaporator. This way, excessive colour formation and sucrose loss is supposed to be reduced (van der Poel et al., 1998).

2.1.2.6 Crystallisation and Centrifugation

A detailed view on the basic theory of crystallisation, including the effects of impurities, is given in chapter 2.2.3.3. This chapter gives a general survey of industrial sucrose crystallisation. During crystallisation, the sucrose molecules dissolved in aqueous beet and cane thick juices are transferred from the liquid to the solid state.

Thereby, sucrose crystals of high quality are aimed at, meaning high purity, including an appearance which is as close to white as possible, as well as uniform crystal size and shape distributions. The driving force for crystallisation is the supersaturation. In sugar industry, this is either achieved by the evaporation of water or by cooling resulting in a decrease in solubility. The former refers to the most commonly used flash evaporation, again meaning the simultaneous application of heat and vacuum. The latter has the advantage of reducing the boiling point of the syrup, preventing colour formation and sucrose inversion. Evaporative crystallisation of cane and beet thick juices is usually performed at 333 to 363 K.

The supersaturation is carefully managed in a way that the metastable zone is reached, exclusively allowing existing crystals to grow while avoiding nucleation. This is a necessary prerequisite to ensure narrow crystal size and shape distributions. To establish this, once the desired supersaturation is reached, seed crystals are added (seeding point), which subsequently further grow due to the attachment of dissolved sucrose molecules on the solid crystal surface rather than forming further nuclei. Therefore, a sugar-isopropanol suspension or seed magma crystals (slurry from B- or C-sugars) can be used. The supersaturation diminishes as a consequence of the crystallisation processes, which necessitates to continuously pursue evaporation to maintain the desired supersaturation. Besides, syrup is continuously added until the entire volume of the crystalliser is filled, which also compensates water evaporation. Crystallisation runs until about 50-55 % (m/m) of crystalline material is generated. This point is identified by either analysing the dry substance or by indirect measurements of the viscosity (van der Poel et al., 1998).

To exploit the maximum amount of sucrose contained in the thick juices, a three-stage crystallisation is most commonly used. The most high-grade sucrose coming from the first crystallisation (A-crystallisation) is known as the so-called white sugar. The remaining molasses from the first crystallisation are successively processed during B- and C-crystallisation, leading to ‘raw sugar’ and ‘after product’, respectively (Asadi, 2007).

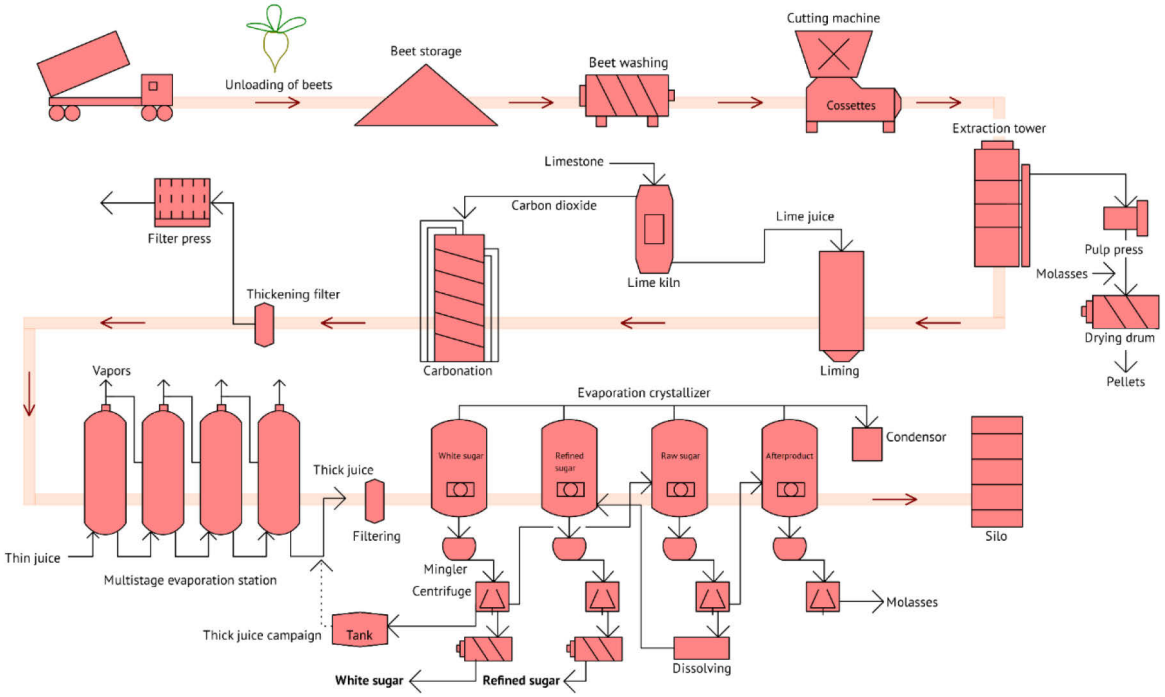

Figure 2-1 Process scheme of sugar manufacture from beet.

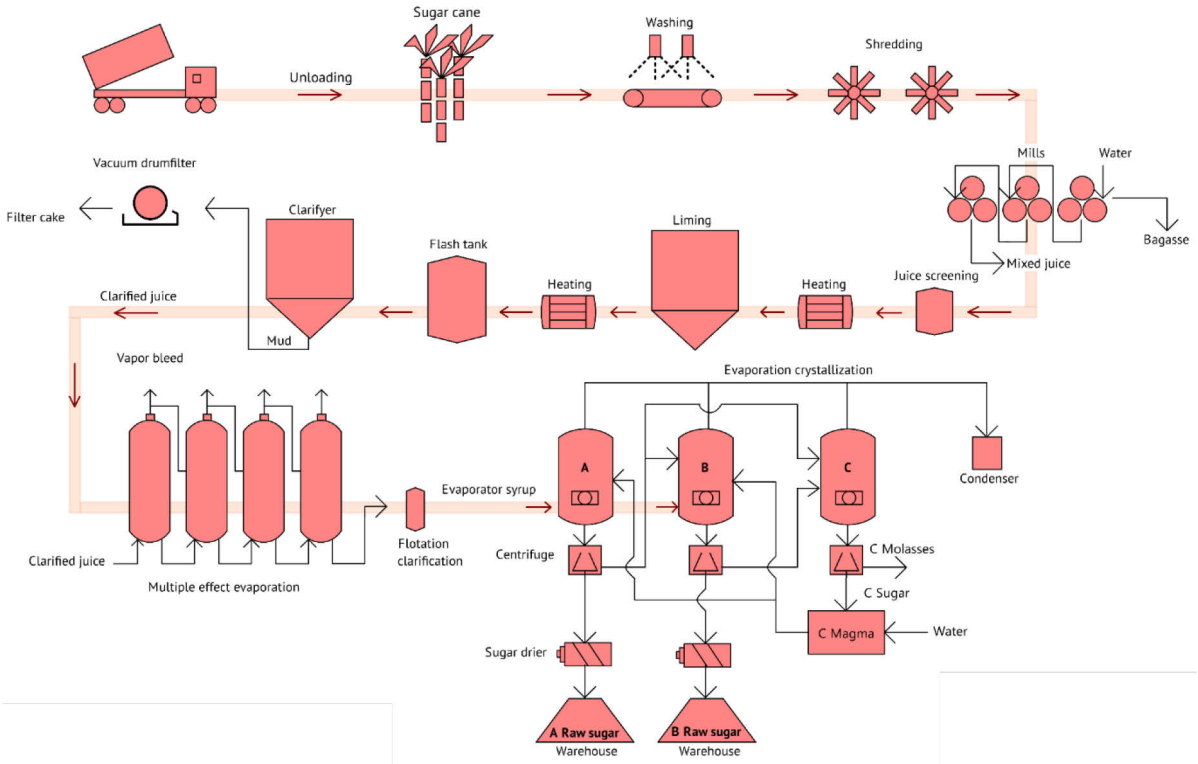

Figure 2-2 Process scheme of raw sugar manufacture from cane.

In contrast, cooling crystallisation uses a temperature decrease to reduce the solubility of sucrose creating the supersaturation necessary for crystallisation. In this case, the dry substance is not changed for creating the supersaturation, but decreases as a consequence of the crystallisation process. Seeding takes place once the desired supersaturation is reached, which is maintained due to further cooling until the desired crystal content is reached. Cooling crystallisation is rather important for C-crystallisation and for seed magma production (van der Poel et al., 1998).

The suspension of sucrose crystals in the aqueous liquid phase, the mother liquor, is called massequite. Centrifugal forces are used to separate the mother liquor from the crystals. Thereby, the liquid passes through a screen of the cylindrical basket, while the sucrose crystals are retained on the screen (Chen & Chou, 1993).

2.2 Dextran in Sugar Production

2.2.1 General Introduction to Carbohydrates in Sugar Manufacture

Carbohydrates, or rather saccharides, are carbon-based molecules with several hydroxyl groups attached. The smallest units of carbohydrates are known as monosaccharides, in which, apart from one, every C-atom is connected to a hydroxyl group. The remaining one has a carbonyl group attached instead, which either has its position at the end or inside of the chain, referring to the term aldose or ketose, respectively (Blumenthal et al., 2006). Monosaccharides can further be distinguished based on the number of C-atoms within their chain. Monosaccharides with 3, 4, 5 and 6 C-atoms forming their chain are referred to as triose, tetrose, pentose and hexose, respectively. Saccharides are generally known to be optically active, which means they are able to rotate the direction of an incident beam of polarised light according to specific angles. As mentioned, this is particularly useful to determine the concentration of an optically active solute when dissolved in an optically inactive solvent (Bannwarth et al., 2007). According to the ICUMSA (International Commission for Uniform Methods of Sugar Analysis), the optical activity of sugar beet and cane juices is commonly used to determine the sucrose concentration in sugar industry practice (van der Poel et al., 1998).

As above-mentioned, the most common monosaccharides in sugar beet and cane raw juices are the aldose glucose and the ketose fructose, both possessing the same formula ($C_6H_{12}O_6$) (van der Poel et al., 1998). In aqueous solutions, monosaccharides exist almost exclusively in ring forms. The so-called Harworth projection for glucose and fructose is shown in Figure 2-3. In case of glucose, the aldehyde group connected to the carbon atom C1 of the glucose monomer reacts with the hydroxyl group of the carbon atom C5, resulting in an intramolecular hemiacetal. Such a six-unit ring is known as pyranose. Similarly, the ketone group connected to the carbon atom C2 of the fructose combines either with the hydroxyl group connected to the carbon atom C5 or C6, forming a five-unit or six-unit ring, furanose or pyranose, respectively (Berg et al., 2018).

The fact that the two monosaccharides form a hemiacetal/hemicetal ring indicates reducing characteristics, easily enabling unwanted colour formation via Maillard reaction during sugar manufacture. In ring form, the previously free carbonyl group subsequently forms an additional asymmetric C-atom. An axial or equatorial position of the corresponding hydroxyl group is possible, known as α- and β-configuration, respectively. The different anomers resulting from the different configurations show distinctly different characteristics, such as melting point, water solubility as well as specific optical activity. The associated change in optical rotation until chemical equilibrium is reached, is known as mutarotation. In chemical equilibrium, roughly one third consists of α- D-glucopyranose and two thirds of β-D-glucopyranose (ratio of 36:64). This

composition results in a specific dextrorotatory optical rotation of +52.5° (at 293 K) (Belitz et al., 2008).

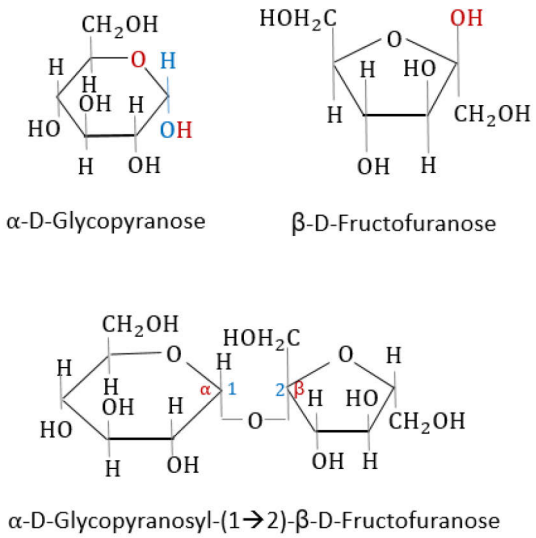

Figure 2-3 Harworth projection of the two monosaccharides glucose and fructose and their combination to the disaccharide sucrose (Berg et al., 2018).

In case of fructose, mutarotation becomes more complex due to the possible occurrence of furanose and pyranose configurations in aqueous solutions, which both occur in α- and β-configuration (Berg et al., 2018). The exact distribution of these configurations in chemical equilibrium has not been precisely determined yet. However, Cockman et al. identified β -fructopyranose, β -fructofuranose and α-fructofuranose as the major components (Cockman et al., 1987). However, it is known that in chemical equilibrium fructose is characterised by a specific laevorotatory optical rotation of -92° (at 293 K) (Belitz et al., 2008). Monosaccharides can be linked via glycosidic bonds between the anomeric C-atom and the oxygen atom of an hydroxyl group under the release of water (Bannwarth et al., 2007). Thereby, the two monomers, fructose and glucose, combine to the disaccharide sucrose ($C_{12}H_{22}O_{11}$), constituting the main and targeted component in sugar beet and cane juices. In this specific case, a fullacetal is formed giving sucrose its non-reducing characteristics. Thus, advantageously, it is not participating in Maillard reactions. The functional groups of the two monosaccharides, namely the aldehyde and ketone group, are the connection points for the glycosidic linkage. Hence, α-D-glycopyranose and β-D-fructofuranose are connected via the carbon atom C1 of the glucose ring and the carbon atom C2 of the fructose ring, forming α-D-(+)-glycopyranosyl-(1,2)-β-D-(-)-fructofuranose, see Figure 2-3 (Berg et al., 2018). Sucrose possesses a positive specific optical rotation of +66.5° (at 293 K), while the unwanted hydrolysis of this dimer to equal amounts of glucose and fructose, known as invert sugar, is in total laevorotatory (van der Poel et al., 1998).

The molecules originating from the linkage of more than two monomers are referred to as oligo- and polysaccharides. The number of ten monomers linked in one molecule gives the upper limit to allow the use of the term oligosaccharide. The most important oligosaccharide in sugar industry, mainly for the sugar beet industry, is the trisaccharide raffinose. It is composed of an α-D-galactopyranose unit attached to a sucrose molecule, possessing a specific optical rotation of +123.2° (at 293 K). Besides, it also shows reducing characteristics and is highly soluble in water (van der Poel et al., 1998).

The characteristics of polysaccharides in aqueous solutions, such as solubility and viscosity, clearly differ from the ones of the small-sized saccharides discussed above (e.g. solubility, viscosity). In general, homogenous and heterogeneous polysaccharides can be distinguished depending on the linkage of either a single kind or different kinds of monomers, respectively. Apart from the chemical composition, the characteristics of a polysaccharide are furthermore determined by its configuration, meaning the type of glycosidic linkages connecting the monomers. Both, monomer and glycosidic linkages affect the molecular conformation, which is of great relevance for several aspects discussed in this work (flow behaviour, separation via membrane filtration and enzymatic decomposition). In view of this, macromolecules can generally adopt a rod or rather ribbon-, a compact sphere- or a loosely jointed random coil-type conformation (Belitz et al., 2008).

The presence of polysaccharides in sugar cane and beet juices can diversely affect sugar manufacture, depending on the characteristics (e.g. molecular conformation) in aqueous solution. These polysaccharides can either originate from cell plant material or from microbial activity (Cuddihy et al., 2001).

In both, sugar cane and beet plants, cellulose and hemicellulose belong to the major polysaccharides originating from the plant. Cellulose is composed of glucose monomers linked via β-(1→4) glyosidic linkages resulting in a ribbon-type conformation (Belitz et al., 2008). Due to its insolubility in water, it does not pass into the raw juice and is therefore of marginal relevance for sugar manufacture. In contrast, it is known that little amounts of soluble hemicelluloses can pass into sugar beet and cane raw juices. Process effects related to hemicellulose are rarely mentioned in literature, though (van der Poel et al., 1998).

In contrast, starch accounts for a large proportion of sugar cane plant polysaccharides, which is known to detrimentally affect sugar cane processing. This comprises two fractions, amylose and amylopectin, which are both composed of glucose units mainly linked via α-(1→4) glycosidic linkages (Cuddihy et al., 2001). Amylose is again a linear molecule, but has additionally helical arrangements. Amylopectin has additionally branching points at α-(1→6) linkages (Belitz et al., 2008).

In sugar beets, starch is not known to play a decisive role. In this case, pectin is one of the main plant polysaccharides, of which about 4-6 % (m/m) of the pectic substances pass into the raw

juice (van der Poel et al., 1998). Similar to the conformation of cellulose, but distinctly stronger folded, sugar beet pectin possesses a ribbon-type conformation. The main chain of these rather complex polysaccharides are composed of α-(1→4) linked galacturonic acids (Belitz et al., 2008). The linear conformation of pectin with comparatively low molecular mass was confirmed by other authors as well (Morris & Ralet, 2012). The diffusion conditions decisively contribute to the co-extraction of pectin. Anyhow, pectin is mostly removed during sugar beet raw juice purification (Asadi, 2007). The total amount of soluble polysaccharides significantly increases due to microbial contamination. Polysaccharides formed by microorganisms mainly concern levan and dextran for both, sugar cane and beet juices. Levan consists of fructose monomers, which are linked via β-(2→6) glycosidic bonds. It is highly soluble in water and has, as expected, a negative optical rotation of -39° to -41° (293 K). Although it was determined that the effect of levan on the viscosity is comparatively low, there is generally little knowledge about the related process effects during sugar manufacture (van der Poel et al., 1998). Momentarily, it has not even been clarified whether levan occurs in considerable amounts in cane or beet juices.

Thus, for both, sugar cane and beet industry, dextran seems to be the most relevant microbial polysaccharide, known to detrimentally affect sugar processing (Cuddihy et al., 2001). Dextran is composed of glucose units, which are mainly linked via α-(1→6) glycosidic bonds. These particularly flexible bonds give dextran, among the polysaccharides relevant for sugar industry, a conspicuous random coil conformation in aqueous solution (Hirata et al., 2003). In contrast to levan, many reports on the presence of dextran and related process effects are given in literature. However, a targeted mitigation of negative dextran-induced effects is still not established practice, which is what this work is aiming at. Thus, the following chapters are specifically concerned with more detailed information on dextran contamination in sugar industry.

2.2.2 Formation and Characteristics of Dextran

The α-(1→6) glycosidic linkages in dextran's main chain are generally known to account for 50 % to 97 %. The remaining bonds can be attributed to branching points via α-(1→2), α-(1→3) and α-(1→4) glycosidic linkages. The kind and amount of branching points in dextran's main chain depends on the microbial origin (Klemm, 2006). It is a well-known fact that lactic acid bacteria, more specifically *Leuconostoc Mesenteroides* species, are responsible for dextran formation in sugar cane and beet juices (Promraksa, 2008). Structural analysis by nuclear magnetic resonance spectroscopy (NMR) revealed that dextran originating from these species contains 95 % α-(1→6) linkages and 5 % linkages, mainly via α-(1→3), with randomly distributed branching points (Klemm, 2006). Besides, Cheetham et al. found that these latter linkages have relatively short side chains. Only 15 % of these side chains starting from α-(1→3) branching points were found to be

longer than two glucose units. The remaining side chains due to branching are equally composed of one or two glucose unit length (Cheetham et al., 1985).

The biosynthesis of dextran is catalysed by enzymes produced by the respective bacterial strain. The participating enzymes are summarised by the name dextransucrase, which is generally used for the family of enzymes which synthesises dextran from sucrose (Robyt et al., 2008). To do so, the dimer sucrose is hydrolysed due to the attack of nucleophiles at the active site of the enzyme, yielding β-glycosyl intermediates. Glycosyltransferase activity is furthermore necessary for the formation of glycosidic bonds with the sugar nucleotide as a substrate. Thus, the primary hydroxyl group of one glycosyl intermediate attacks the carbon atom C1 of another glycosyl intermediate forming the above-mentioned α -(1→6) glycosidic linkage, while releasing a free enzyme nucleophile. The unoccupied nucleophile attacks another sucrose molecule, again releasing a glycosyl intermediate. The primary hydroxyl group of the latter again attacks the carbon atom C1 of the previously formed isomaltose unit. Thus, the dextran chain grows due to the alternate transfer of glycosyl and dextranosyl groups between the nucleophils. The dextran polymerisation of the glucose monomers proceeds and finally results in high molecular mass dextran chains (Klemm, 2006). A simplified scheme of the dextran formation is shown in Figure 2-4 below.

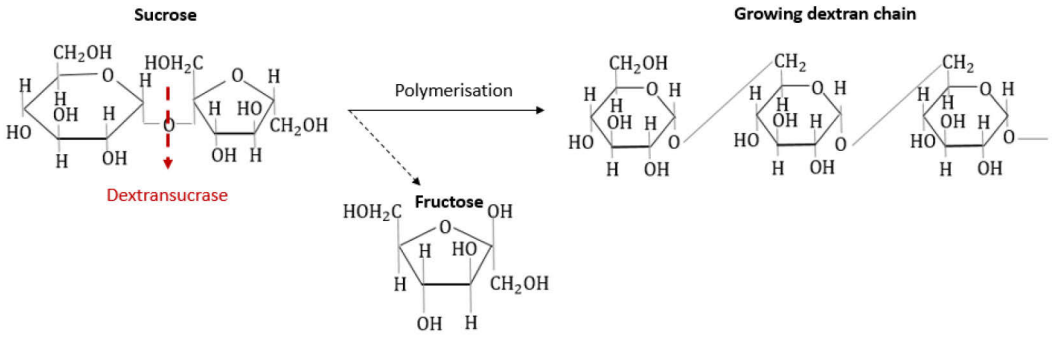

Figure 2-4 Dextran formation catalysed by dextransucrase enzymes produced by *Leuconostoc Mesenteroides* (inspired by Chen & Chou, 1993).

Naturally produced dextran is generally of relatively high average molecular mass and high polydispersity. Thus, it was found that dextran with molecular masses in the range of 15 kDa to 2,000 kDa potentially occur in sugar raw juices (Chen & Chou, 1993).

The total amount as well as the structure and especially the molecular mass distribution of dextran is affected by several parameters during synthesis, including the sucrose content, the dextransucrase content as well as the presence of acceptor molecules. Acceptor molecules, such as maltose and isomaltose, can interfere during the dextran chain growth due to displacing dextran from the active site (Tsuchiya et al., 1955). In such a case, branching can occur due to the attack of the hydroxyl group of the carbon atom C3 of an acceptor molecule on the glycosyl or dextranosyl groups (Klemm, 2006).

Besides, Falconer et al. have found that the final average molecular mass of dextran increases with higher sucrose contents as well as with higher temperatures. Also according to that study, the average molecular mass of dextran is inversely proportional to the dextransucrase content, directly correlating with the microbial contamination (Falconer et al., 2011). This clearly indicates that the total content as well as the average molecular mass distribution of dextran is not uniform in sugar cane and beet juices. Instead, it varies depending on the climatic and harvesting conditions. As already mentioned, the α-(1→6) glycosidic linkages in dextran's main chain gives the molecule conspicuous characteristics. The kind of monosaccharides and the type of glycosidic linkage decisively affect the molecular conformation of a macromolecule in solution. Polysaccharides containing glycosidic linkages at the primary hydroxyl group have an additional rotation angle. Two glucose units linked via an α-(1→6) bond can hence occur in various conformations depending on the three rotation angles, illustrated in Figure 2-5.

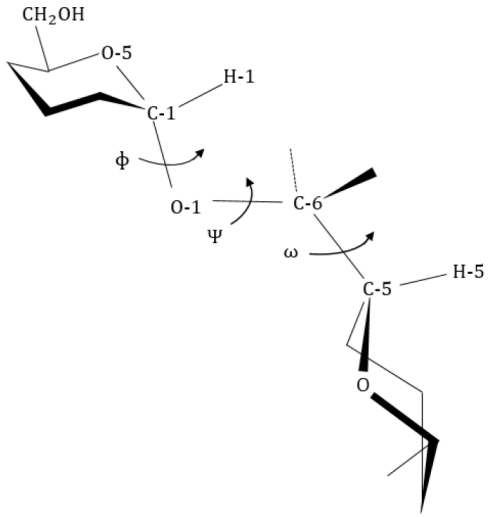

Figure 2-5 Schematic illustration of two α-1,6-linked glucose units with three different rotation angles (Tvaroska et al., 1978).

This unusual flexible back bone of dextran allows a large number of conformations, which can easily be transformed into each other (Lee et al., 2004). It is assumed and confirmed by several authors that high molecular mass dextran exhibits characteristics of an expandable random coil (Hirata et al., 2003). Besides, Gasciolli et al. also identified from viscosity measurements a random coil conformation of high molecular mass dextran, but also found an elongated rod-like conformation of low molecular mass dextran molecules, less than an average-number molecular mass of 2000 Da (Gasciolli et al., 1991).

Thus, the predominant presence of α-(1→6) glycosidic linkages leads to a higher chain mobility and is also responsible for dextran's good solubility in various solvents (e.g. water, formamide, DMSO). Consequently, the solubility of dextran not only correlates with the solvent properties but

also with the molecular mass distribution as well as the degree and kind of branching (Klemm, 2006).

2.2.3 Results of Dextran Formation

2.2.3.1 Effects on the Sucrose Content

Due to the consumption of sucrose during dextran biosynthesis, sucrose loss is an unavoidable and irreversible result once microbial infestation has been initiated. Besides, it was found that the amount of sucrose in the final molasses is higher when dextran was present, additionally leading to an increased sucrose loss during sugar processing (Abdel-Rahman, 2007). According to the official ICUMSA method, the determination of sucrose contents in sugar industry is based on polarisation measurements (ICUMSA, 2011). As already mentioned, dextran is optically active itself. The specific optical rotation of dextran (ranging from +195 to +205 °) is about three times higher in comparison with the specific optical rotation of sucrose (+66.5°). Thus, the dextrorotatory optical activity of dextran contributes to the overall polarisation of juices, leading to a falsification of the measurement of the sucrose content in beet and cane, affecting payment and quality assessment (Chen & Chou, 1993).

2.2.3.2 Viscosity

The viscosity is a fundamental characteristic of a liquid decisively affecting practically every chemical and physical reaction. It is defined as the internal resistance of a liquid to flow and is therefore a measure of frictional properties. In general, two terms can be distinguished, dynamic and kinematic viscosity. The dynamic viscosity refers to the tangential force required to slide one layer (A) against another fixed one (B), while the two layers are maintained at a unit distance *y*, see Figure 2-6 below.

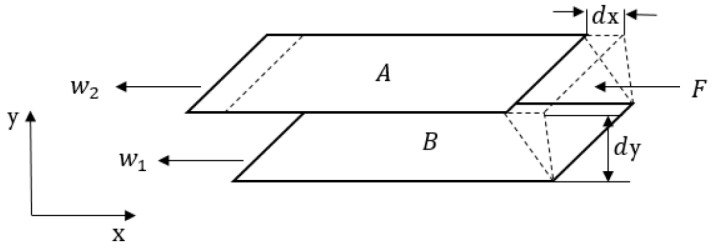

Figure 2-6 Shear between two adjacent layer (Viswanath et al., 2007).

The shear stress σ refers to the force per area. The shear rate $\dot{\gamma}$ can be described as the ratio of the velocity $w = \frac{dx}{dt}$ to the distance between the two layers *y*, see equation (2-1).

$$\dot{\gamma} = \frac{dw}{dy} \tag{2-1}$$

The dynamic viscosity η describes the dependence of the shear stress σ on the shear rate $\dot{\gamma}$, see equation (2-2).

$$\eta = \frac{\sigma}{\dot{\gamma}} = \sigma \frac{dy}{dw} \tag{2-2}$$

The kinematic viscosity ν is related to the dynamic viscosity η via the density ρ (Viswanath et al., 2007).

$$\nu = \frac{\eta}{\rho} \tag{2-3}$$

The viscosity of a liquid is affected by the presence of polymers. Polymer segments represent an additional resistance, which need to be circumvented by the solute molecules and induces, for instance, an increase in the dynamic viscosity and the density. The change of the flow characteristics relates to the sum of the disturbances of all polymer segments (Lechner et al., 2010). Polysaccharides, such as dextran, can hence detrimentally affect the viscosity of sugar beet and cane juices (van der Poel et al., 1998). As is well-known, the kind of the solvent as well as the environmental conditions, such as temperature, contribute to the viscosity of a solution. Apart from that, a polymer-related viscosity increase correlates with the concentration, the molecular mass distribution as well as the molecular conformation of the polysaccharide in solution (Norton et al., 2011). The latter is due to the fact that the viscosity correlates with the effective volume occupied by the molecule, which is described by a sphere, whose diameter depends on to the longest linear expansion of the molecule (Figure 2-7).

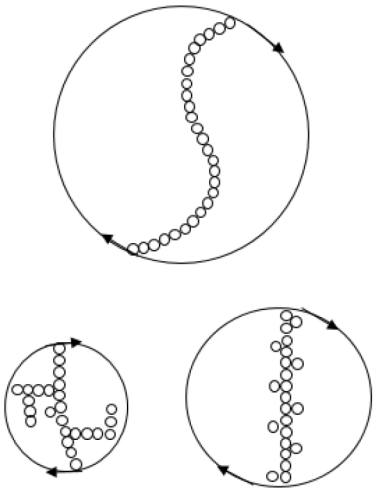

Figure 2-7 Schematic illustration of the effective volume of polysaccharides of different molecular conformations (Belitz et al., 2008).

Apart from the effects due to varying molecular masses, this volume is higher for more expanded molecules in comparison with branched and coil structured polysaccharides (Belitz et al., 2008).

As a result, ribbon-type macromolecules, to which starch and pectin belong, affect the solution's viscosity distinctly stronger in comparison with the coil-shaped dextran molecule, provided that similar molecular masses are considered.

Nevertheless, it is well-known that dextran depending on its concentration and its molecular mass causes an increase of the viscosity in aqueous solutions. Thus, there is general agreement that the viscosity of beet and cane juices is mainly affected by high molecular mass dextran. The increase of the viscosity with higher concentration and molecular mass is hence attributable to an increase of the effective volume occupied. The correlation of viscosity with concentration and molecular mass was found by several authors (Figure 2-8).

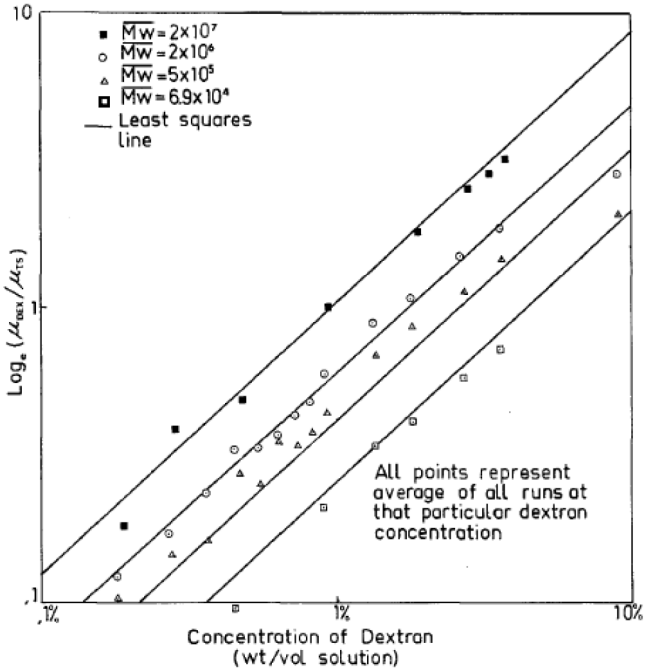

Figure 2-8 Effect of the concentration and molecular mass of dextran on the viscosity (Geronimos & Greenfield, 1978).

Based on this data set, the authors postulated the following exponential mathematical correlation, in which the effect of the concentration as well of the molecular mass clearly become apparent.

$$\eta_{Dext} = \eta_{TS}\left[exp(k_1'\gamma^{k_2'}c^{k_3'})\right] \tag{2-4}$$

Here, η_{Dex} represents the viscosity of the dextran-loaded solution and η_{TS} is the viscosity of a solution containing the same total solids but no dextran. k_1', k_2' and k_3' are parameters fitted by least square regression. The effect of the weight average degree of polymerisation γ and the dextran concentration c also becomes apparent in this equation (Geronimos & Greenfield, 1978).

2.2.3.3 Crystallisation

The crystalline state is an ordered and rigid arrangement of molecules, atoms or ions, which can generally be obtained from melts, vapour phases or solutions. Therefrom, the crystallisation from

aqueous solutions is key to crystallisation processes during sugar manufacture (van der Poel et al., 1998). In general, a solution is a homogenous mixture of two or more substances, whereby the solvent as well as the solute are the two main constituents (Mullin, 2001). In order to induce the transfer from the liquid to the solid state, supersaturation needs to be established and kept as the driving force for crystallisation. A supersaturated solution can generally be obtained by reducing the temperature, removing the solvent or by adding certain reactants (Mersmann, 2001). The former two, referring to cooling and especially evaporative crystallisation, are commonly used for sucrose crystallisation in sugar industrial practice. Besides, crystallisation by precipitation (adding a reactant) is used to obtain calcium carbonate crystals from aqueous solutions during sugar beet raw juice purification (van der Poel et al., 1998). Since the crystallisation of sucrose is key to this study, the following chapter firstly focuses on the fundamental theory of crystallisation with regard to sucrose. Subsequently, further specific details on crystallisation by precipitation of calcium carbonate is given in 2.2.3.3.6.

2.2.3.3.1 Driving Force for Crystallisation

The driving force for crystallisation is the difference in chemical potential of the component to be crystallised in the liquid and the solid phase. This is commonly approximated by the supersaturation (Letcher et al., 2004). In a saturated solution, the solid and the liquid phase are in equilibrium at given temperature and pressure and thus the chemical potential of the dissolved component and therefore also of the solid phase is equal. The chemical potential μ_i^α of component *i* in the respective phase α is generally defined as follows:

$$\mu_i^\alpha = \mu_i^{0,\alpha}(T,p) + RTln(a_i^\alpha) \tag{2-5}$$

Here, *R* and *T* refers to the gas constant and the temperature, respectively. a_i^α is the activity of component *i* in the respective phase α. Using the Lewis-Randall state for the standard chemical potential, the standard state chemical potential is solely a function of pressure and temperature. The solid-liquid phase equilibrium describes the state which a system assumes by itself without changes from outside. Thus, the equilibrium state gives the conditions to which a system strives if a driving force exists (Schaber & Mayinger, 2010).

In case of the crystallisation process, a difference in the chemical potential of component *i* in the liquid phase and in the solid phase is a necessary prerequisite to initiate and keep the mass transfer of component *i* from the dissolved to the solid state, see equation (2-6).

$$\Delta\mu_i^L = \mu_i^L - \mu_i^{L,sat} \tag{2-6}$$

In this case, the system endeavours to establish equilibrium, which is achieved by nucleation and crystal growth (Mullin, 2001). The fundamental driving force for a real system can hence be expressed with the equation (2-7).

$$\Delta\mu = RTlna_i^L - RTlna_i^{L,sat} \tag{2-7}$$

Additionally using the definition of the activity reveals equation (2-9), in which γ_i^L and x_i^L refer to the activity coefficient and the mole fraction of component *i* in the liquid phase, respectively. p_i^{sat} is the vapour pressure of component *i* at given temperature and pressure.

$$a_i^L = \frac{x_i^L \cdot \gamma_i^L}{p_i^{sat}} \tag{2-8}$$

$$\frac{\Delta\mu}{RT} = \frac{lna_i^L}{lna_i^{L,sat}} = \frac{ln\left(\frac{x_i^L \cdot \gamma_i^L}{p_i^{sat}}\right)}{ln\left(\frac{x_i^{L,sat} \cdot \gamma_i^{L,sat}}{p_i^{sat}}\right)} = \frac{ln\left(x_i^L \cdot \gamma_i^L\right)}{ln\left(x_i^{L,sat} \cdot \gamma_i^{L,sat}\right)} \tag{2-9}$$

Assuming an ideal solution, meaning equal interactions between all molecules in solutions, the activity coefficient of the actual solution ($\gamma_i^L = 1$) and of the saturated solution ($\gamma_i^{L,sat} = 1$) approaches one. This way, the equation is further simplified, see equation (2-10).

$$\frac{\Delta\mu}{RT} = ln\left(\frac{x_i^L}{x_i^{L,sat}}\right) \tag{2-10}$$

In general, the mole fraction and concentration are defined as follows:

$$x_i^L = \frac{n_i^L}{n^L} \; and \; x_i^{L,sat} = \frac{n_i^{L,sat}}{n^L} \tag{2-11}$$

$$c_i^L = \frac{n_i^L}{V_{sol}^L} \; and \; c_i^{L,sat} = \frac{n_i^{L,sat}}{V_{sol}^L} \tag{2-12}$$

Assuming a constant solution volume, the mole fractions of component *i* can be replaced by the concentration of component *i* in the liquid phase at its actual state and at saturation (equilibrium), in which the ratio of the activity values of the actual solution and of the saturated solution is replaced by the ratio of the respective concentrations (Schaber & Mayinger, 2010). The latter is referred to as the supersaturation *S*.

$$\frac{\Delta\mu}{RT} = ln\left(\frac{x_i^L}{x_i^{L,sat}}\right) = ln\left(\frac{c_i^L}{c_i^{L,sat}}\right) = lnS \tag{2-13}$$

In case of low degrees of supersaturation (*S* approaching 0), *ln(S)* can be approximated by *S-1* (Taylor series expansion) and equation (2-13) can further be simplified. By additionally replacing the term *S-1* by the so-called relative supersaturation σ, another common simplified expression of the driving force is obtained (Letcher et al., 2004).

$$\sigma = \frac{\Delta\mu}{RT} = \left(\frac{c_i^L}{c_i^{L,sat}} - 1\right) = \frac{c_i^L - c_i^{L,sat}}{c_i^{L,sat}} \tag{2-14}$$

In sugar industry, crystallisation concerns the mass transfer of sucrose molecules dissolved in an aqueous solution (thick juice) from the liquid to the solid state. Thereby, a uniform crystal size and shape distribution and a high purity are targeted (Asadi, 2007).

The sucrose molecule possesses eight hydroxyl groups, as shown in Figure 2-9. Three of these hydroxyl groups form intramolecular hydrogen bonds. The remaining five can participate in intermolecular bond formation and are responsible for the dissolution of sucrose molecules in aqueous solutions and, hence, also for sucrose crystallisation. In case that sucrose is completely dissolved, all intermolecular hydroxyl groups are solvated by water molecules. The fact that these five hydroxyl group can form hydrogen bonds with water molecules is the main reason for the high solubility of sucrose in water. If the sucrose concentration increases, the number of water molecules is insufficient to form hydrogen bonds with all hydroxyl groups. In such a case, sucrose molecules start to aggregate and form nuclei, which, if the critical radius is exceeded, can further grow. Crystallisation is hence based on the fact that the amount of dissolved solute molecules in a specific solvent is limited (van der Poel et al., 1998).

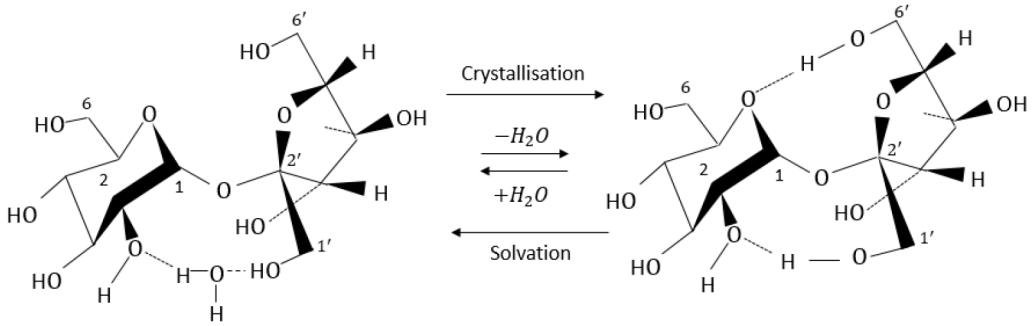

Figure 2-9 Schematic illustration of a solvated and crystallised sucrose molecule (Wittenberg, 2000).

In sugar industry practice, the following terms are usually used to describe the state of a sucrose solution. The solubility coefficient $q_{S/W,sat,binary}$ is the ratio of the mass fraction of sucrose w_S and water w_w in a binary saturated aqueous sucrose solution at a certain temperature. More precisely, it describes the amount of dissolved sucrose per gram of water (van der Poel et al., 1998).

$$q_{S/W,sat,binary} = \left(\frac{w_S}{w_w}\right)_{sat,binary} \tag{2-15}$$

In this case, the solubility of sucrose exclusively depends on the temperature (and to a lesser extent on the pressure) (Asadi, 2007). However, in multi-component aqueous sucrose solutions, the solubility of sucrose is known to be additionally affected by the amount and kind of impurities in solution. In case of technical sucrose solutions, the so-called saturation coefficient γ_{sat} is better suitable to describe the solubility of succrose. It refers to the ratio of the mass fraction ratios of sucrose to water in the multi-component and in the binary aqueous sucrose solution, respectively.

$$\gamma_{sat} = \frac{\left(\frac{w_S}{w_w}\right)_{sat,multi-comp}}{\left(\frac{w_S}{w_w}\right)_{sat,binary}} = \frac{q_{S/W,sat,multi-comp}}{q_{S/W,sat,binary}} \tag{2-16}$$

To describe the saturation state of a sucrose solution, the supersaturation coefficient γ_{SS} is commonly used in industrial practice. It is obtained by dividing the ratios of the mass fractions of sucrose and water in a given solution and in the saturated solution at the same temperature.

$$\gamma_{SS} = \frac{w_S/w_w}{\left(w_S/w_w\right)_{sat}} \tag{2-17}$$

The solubility curve for a number of solute-solvent systems are given in literature and can be used to determine the actual degree of supersaturation (Vedantam & Ranade, 2013). The plot of the solubility $q_{S/W}$ and saturation coefficient γ_{SS} as a function of the temperature reveals the well-known solubility curve for sucrose (Figure 2-10). It represents a solubility curve for solutes with a positive temperature coefficient of solubility, e.g. one with increasing solubility with increasing temperature.

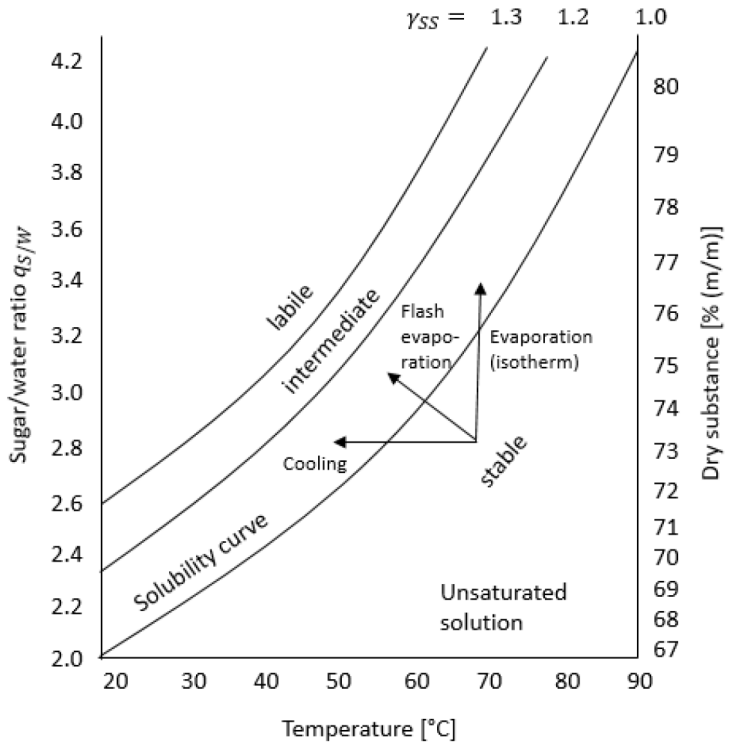

Figure 2-10 Solubility curve of sucrose (van der Poel et al., 1998).

Therefrom, different supersaturation zones can be distinguished. Their knowledge enables to define the conditions for a controlled crystallisation, accounting for nucleation as well as crystal growth. The area below the solubility curve refers to the unsaturated state ($\gamma_{SS} < 1$) implying that the solute is still properly dissolved in the solvent and that even more solute could be dissolved in the solvent.

As already mentioned, leaving this unsaturated state, and hence initiating supersaturation ($\gamma_{SS} > 1$), can either or both be done by an increase of the solute's concentration (removal of solvent→evaporation) or by changes in solubility (temperature change→cooling). The probability of nucleation in the labile zone ($\gamma_{SS} > 1.2$) is very high, which is undesirable for controlled industrial crystallisation as the crystal size cannot be controlled. It is hence the target to set the supersaturation within the metastabile zone ($1.0 < \gamma_{SS} < 1.2$) in order to allow a controlled crystallisation. In this region, nucleation can be supressed by adding seed crystals such that exclusively growth occurs (van der Poel et al., 1998).

2.2.3.3.2 Nucleation

The crystallisation process can be divided into two main steps: nucleation and crystal growth. As already mentioned, at a sufficient degree of supersaturation, solute molecules start to form an ordered and stable unit acting as crystallisation centres. These aggregates can further grow once stable three-dimensional nuclei of a certain critical size are formed, necessitating to overcome a certain energy barrier. In general, primary and secondary nucleation can be distinguished. The latter originates from existing crystals of the solute to be crystallised, e.g. caused by mechanical stress such as agitation. Primary nucleation can further be caused homogenously or heterogeneously, referring to the spontaneous collision of the constituent molecules to be crystallised and the presence of foreign particles serving as crystalline sites, respectively.

Homogenous nucleation can be described by the classical theory of nucleation, which describes the total change in free energy ΔG between the solid crystalline solute and the dissolved solute (Mullin, 2001). Crystallisation in general is an exothermic process implying that energy is being released (Mersmann, 2001). The free energy is composed of the positive surface energy ΔG_S and the negative volume energy ΔG_V. The former is necessary to create crystal nucleus surface and is proportional to the square of the radius of the molecule r^2. The latter is caused by the transition from the dissolved to the solid state (decrease of molecular motion) and is proportional to r^3 (Mullin, 2001). A system always strives to its energetically most favourable state which, when comparing the Gibbs energy of the various states, is characterised by the lowest Gibbs energy. Thus, characterising the driving force of a process by the change of the Gibbs energy from the initial to the final state, the process occurs spontaneously when the change of the Gibbs energy becomes negative (Schaber & Mayinger, 2010).

Ideally assuming spherical nuclei, the total change of Gibbs energy from the liquid to the solid state can be described by the following equation (2-18), in which V_M refers to the volume of the molecule, r to the radius of the crystallising sphere, γ to the specific surface energy and $\Delta\mu$ to the difference in chemical potential between dissolved and crystalline state.

$$\Delta G = -\Delta G_V + \Delta G_S = -\frac{4\pi}{3V_M} \cdot r^3 \Delta\mu + 4\pi \cdot r^2 \cdot \gamma \quad (2\text{-}18)$$

Depending on the size of the nuclei, it can either dissolve or grow, generally aiming at the decrease in Gibbs energy change, as shown in Figure 2-11.

In case of small nuclei, the contribution of the surface energy predominates, which are therefore unstable and can easily be dissolved. The minimum size of a nucleus for which it is more favourable to grow is referred to as the critical radius. On attainment of the critical radius r_{crit} indicated by the maximum change of Gibbs energy, it is energetically more favourable to grow and thus the change of Gibbs energy decreases (van der Poel et al., 1998).

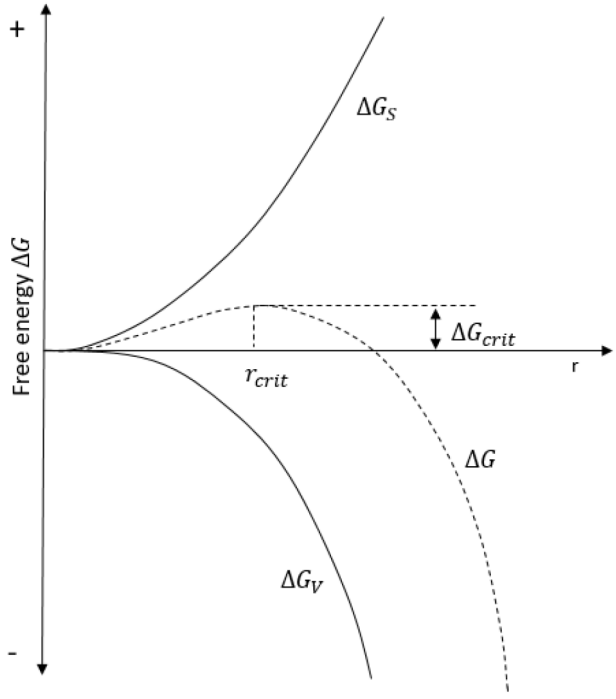

Figure 2-11 Free energy for homogenous three-dimensional nucleation (Mullin, 2001).

The critical radius corresponds to the maximum of the change of the Gibbs energy, which refers to $\frac{d\Delta G}{dr} = 0$. This way, equation (2-18) becomes:

$$\frac{d\Delta G}{dr} = \frac{4\pi}{V_M} \cdot r^2 \Delta\mu + 8\pi \cdot r \cdot \gamma = 0 \quad (2\text{-}19)$$

Thus, the minimum size of a stable nucleus of radius r_{crit} can be expressed as follows:

$$r_{crit} = \frac{2\gamma V_M}{\Delta\mu} \quad (2\text{-}20)$$

Insertion of equation (2-20) into equation (2-18) reveals the critical change of Gibbs energy ΔG_{crit}.

$$\Delta G_{crit} = \frac{16}{3}\pi V_M^2 \cdot \frac{\gamma^3}{(\Delta\mu)^2} \tag{2-21}$$

Additionally using equation (2-5) for the chemical potential, the following expression for the change of the critical Gibbs energy is obtained.

$$\Delta G_{crit} = \frac{16}{3}\pi V_M^2 \cdot \frac{\gamma^3}{(RT)^2(lnS)^2} \tag{2-22}$$

Obviously, the energy barrier decreases with the increase of temperature *T* and supersaturation *S* (as *S* is greater than 1) (van der Poel et al., 1998).

The number of stable nuclei created per unit volume and unit time is known as the nucleation rate *J*, which can be expressed by the Arrhenius equation.

$$J = A \cdot exp\left(\frac{-\Delta G_{crit}}{k_B T}\right) = A \cdot exp\left(\frac{16\pi V_M^2 \gamma^3}{k^3 T^3 (lnS)^2}\right) \tag{2-23}$$

Here, A and k_B are the Arrhenius and Boltzmann constant, respectively. According to the Arrhenius-type of equation, the nucleation rate follows an exponential curve. Theoretically, this implies that the nucleation rate is low before a critical supersaturation is reached and then dramatically increases. However, due to a viscosity increase induced by the increase in supersaturation, the nucleation rate has a maximum value before it decreases, as shown in Figure 2-12 (Mullin, 2001).

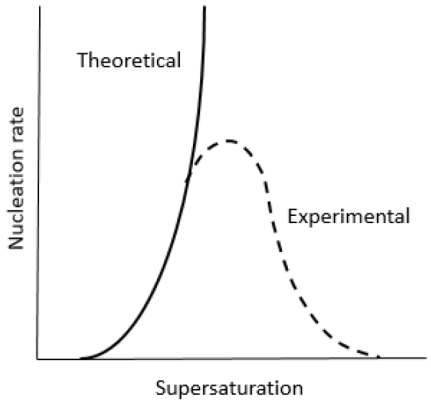

Figure 2-12 Nucleation rate as a function of supersaturation (Mullin, 2001).

Equation (2-23) illustrates that the nucleation rate is determined by three main factors: the temperature *T*, the supersaturation *S* and the surface energy γ. With the increase of the temperature and the supersaturation, the activation energy and therefore the critical radius decreases. Different from homogenous nucleation, the surface energy can be affected due to the presence of foreign particles, referring to the above-mentioned heterogeneous nucleation. The presence of foreign particles or crystal fragments reduces the surface energy and therefore also contributes to a reduced activation energy. The critical change of Gibbs energy for heterogeneous nucleation ($\Delta G'_{crit}$) is

hence lower in comparison with the one for homogeneous nucleation (ΔG_{crit}), which can be described by equation(2-24), including a geometric correction factor ϕ which is smaller than 1.

$$\Delta G'_{crit} = \phi \Delta G_{crit} \tag{2-24}$$

In case of heterogeneous nucleation, the surface energy is the main impact factor. In general, the surface Gibbs energy describes the energy required to form a new surface, e.g. interfacial area. For the description the interfacial tension γ is used. As shown in Figure 2-13, it is composed of three parts: the interfacial tension between the solid crystallite and the liquid γ_{CL}, between the solid and the liquid γ_{SL} and between the solid phase and the solid crystallite γ_{SC}.

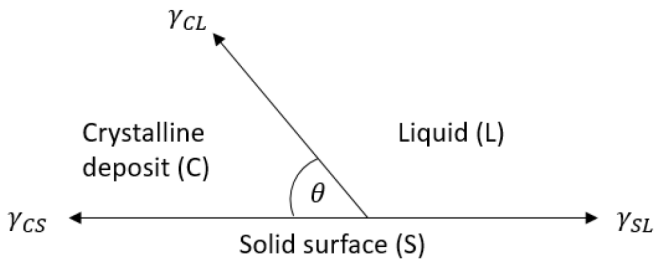

Figure 2-13 Interfacial tension of heterogeneous nucleation between the foreign solid, the crystalline solid and the liquid phase (Mullin, 2001).

In horizontal direction, assuming force equilibrium, the following equation can be stated.

$$\gamma_{SL} = \gamma_{CS} - \gamma_{CL} cos\theta \tag{2-25}$$

Therein, θ describes the contact angle between the crystalline material (*C*) and the solid surface of foreign particles (*S*).

$$cos\theta = \frac{\gamma_{CS} - \gamma_{SL}}{\gamma_{CL}} \tag{2-26}$$

The geometric factor (derived from the volume of a nucleus related to that of a sphere) differentiating the free energy of heterogeneous and homogenous nucleation is defined as follows:

$$\phi = \frac{(2 + cos\theta)(1 - cos\theta)^2}{4} \tag{2-27}$$

In case of a contact angle θ of 180°, the factor ϕ is 1, implying that the change of the Gibbs energy of heterogeneous nucleation is equal to the one of homogeneous nucleation. This implies that there is no affinity between the foreign material and the crystallising component so that the component does not preferably crystallises on the foreign material. The factor ϕ varies for contact angles between 0 and 180°. Generally, the factor is lower than 1, thus, the change of the Gibbs energy of heterogeneous nucleation is lower than the one of homogenous nucleation and is, therefore, easier to achieve. This is commonly referred to as partial affinity.

For complete affinity, the contact angle θ is 0°, resulting in $\Delta G'_{crit} = 0$. The latter applies to the situation of seeding in a supersaturated solution where no nucleation occurs but growth on the

surface of the seed crystals. This is the case for industrial sucrose crystallisation and thus also for the sucrose crystallisation experiments performed in this study (Mullin, 2001).

2.2.3.3.3 Crystal Growth

Once stable crystal nuclei are formed, crystal growth takes place, which is mainly described by two theories: the diffusion and the adsorption layer theory. The former describes the transport of sucrose molecules from a supersaturated solution to the crystal surface. The latter deals with the incorporation phenomena of these molecules, also called growth units, into the crystal lattice (van der Poel et al., 1998). As shown in Figure 2-14, the growth unit diffuses to the crystal surface (1), loosely adsorbs (2) and diffuses along the surface (3) until it gets incorporated at energetically favoured positions (kinks) (4).

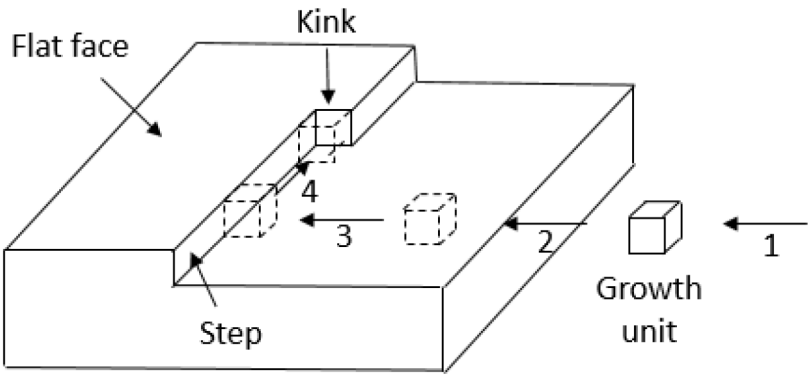

Figure 2-14 Steps during crystal growth. 1) Transport of the growth unit to the crystal surface. 2) Loose adsorption on the crystal surface. 3) Diffusion to energetically favoured kinks. 4) Incorporation into crystal lattice (Mersmann, 2001).

Thus, the diffusion theory applies to two steps: the transport of molecules from the liquid phase to the surface of the solid phase and the diffusion of these molecules within a stagnant film in order to arrange themselves into the crystal lattice (Mullin, 2001).

In general, Fick's law is most commonly used to describe diffusion processes. Assuming a time-independent constant flux and thus a steady-state diffusion, Fick's first law can generally be expressed by equation (2-28), in which D is the diffusion coefficient and $\frac{dc}{dx}$ is the difference in concentration related to the spatial coordinate x.

$$\mathrm{J} = -\mathrm{D}\frac{\mathrm{dc}}{\mathrm{dx}} \tag{2-28}$$

Additionally considering the time dependence of diffusion, Fick's second law is obtained, which is the most well-known model to describe the unsteady state diffusion (Kärger et al., 2012).

$$\frac{dc}{dt} = -D\frac{d^2c}{d^2x} \tag{2-29}$$

Commonly, Fick's law is used to describe the diffusion of sucrose from the bulk liquid phase to the crystal surface (see equation (2-30)). The diffusion of sucrose through the adsorption layer is usually described by a quasi-chemical approach, meaning the change of the mass of sucrose with time is described by a chemical reaction, the so-called surface reaction, of order *z* (see equation (2-31))).

$$\frac{dm}{dt} = k_D \cdot A \cdot (c - c_i) \tag{2-30}$$

$$\frac{dm}{dt} = k_R \cdot A \cdot (c_i - c_*)^z \tag{2-31}$$

Here, *A* refers to the crystal surface area. k_D is the coefficient of mass transfer by diffusion and k_R represents the rate constant for the surface reaction, which are determined by the crystallisation conditions (e.g. temperature, agitation and impurities). Besides, *c* refers to the sucrose concentration of the bulk solution, c_i to the sucrose concentration of the boundary layer crystal/solution and c_* to the sucrose concentration of the solid-liquid equilibrium and *z* gives the reaction rate of the assumed surface reaction. Assuming that the surface reaction is of first order ($z = 1$), solving the equations for the concentration differences and subsequently adding these two equations, one obtains the generally postulated equation for sucrose crystallisation (2-33), in which k_G is the overall crystal growth coefficient (van der Poel et al., 1998).

$$k_G = \frac{(k_D \cdot k_R)}{(k_D + k_R)} \tag{2-32}$$

$$\frac{dm}{dt} = k_G \cdot A \cdot (c - c_*) \tag{2-33}$$

Despite this usual approach, it should be kept in mind that the fundamental driving force for diffusion is still the difference in chemical potential rather than just the difference in concentration (Mersmann, 2001).

$$J = -D \frac{d\mu_i}{dx} \tag{2-34}$$

Using the equation (2-5) for the chemical potential μ_i of component *i*, the gradient in chemical potential can be expressed by equation (2-35) (Schaber & Mayinger, 2010).

$$\frac{d\mu_i}{dx} = \frac{d\mu_i^0}{dx} + RT \frac{dlna_i}{dx} \tag{2-35}$$

The change in standard chemical potential μ_i^0 with the coordinate *x* is zero. Using the diffusion coefficient $D^* = RTD$ and the definition of the activity a_i according to equation (2-8), in which γ_i and x_i refer to the activity coefficient and the mole fractions of component *i*, equation (2-34) becomes:

$$J = -D^* \frac{dlna_i}{dx} = -D^* \frac{dln(x_i.\gamma_i)}{dx} \tag{2-36}$$

As elucidated in chapter 2.2.3.3.1, assuming a constant solution volume, the mole fraction x_i can be replaced by the concentration c_i of component *i*.

$$J = -D^* \left(\frac{dlnc_i}{dx} + \frac{dln\gamma_i}{dx} \right) \tag{2-37}$$

Using $lnc_i = c_i - 1$ (Taylor series expansion) reveals equation (2-38).

$$J = -D^* \left(\frac{dc_i}{dx} + \frac{dln\gamma_i}{dx} \right) \tag{2-38}$$

Comparing it with the usually mentioned Maxwell-Stefan equation (2-39)

$$J = -D^* \Gamma \frac{dc_i}{dx} \tag{2-39}$$

$$\Gamma \frac{dc_i}{dx} = \frac{dc_i}{dx} + \frac{dln\gamma_i}{dx} \tag{2-40}$$

reveals the equation for the thermodynamic factor Γ (Demirel, 2014).

$$\Gamma = 1 + \frac{dln\gamma_i}{dc_i} = 1 + \frac{dln\gamma_i}{dlnc_i} \tag{2-41}$$

The activity coefficient γ_i describes the interactions between the molecules in solution. If it takes a value of 1, then an ideal solution with uniform interactions between the molecules is described. For all other values, the deviation from ideal behaviour is accounted for (Schaber & Mayinger, 2010). The thermodynamic factor hence describes deviations from an ideal behaviour. Thus, in case of ideal conditions in a binary dilute solution, the thermodynamic factor is 1 and the equation of Fick and Maxwell-Stefan would be equal (Rehfeldt, 2009).

In view of the above-described, the widespread profile of the driving force for sucrose crystallisation should be modified in a way that the chemical potential as a driving force for crystallisation is used instead of the concentration, illustrated in Figure 2-15.

The arriving crystal growth unit is not immediately incorporated into the crystal lattice, but is firstly loosely adsorbed, forming the just mentioned adsorption layer. If equilibrium between the solid and the liquid phase is established, the chemical potentials of solute *i* in the solid phase (crystal) and in the liquid phase (bulk) are the same. Before equilibrium is reached, the growth units, which have reached the adsorption layer, first need to diffuse along the flat surface until it gets incorporated, preferentially at energetically favoured places. Figure 2-16 schematically illustrates the different growth positions on the surface of a crystal. The crystal surface is composed of flat and stepped regions. The stepped regions can also be interrupted forming so-called kinks. The probability of incorporation relates to the number of possible binding sites between the growth unit and the different positions on the crystal surface.

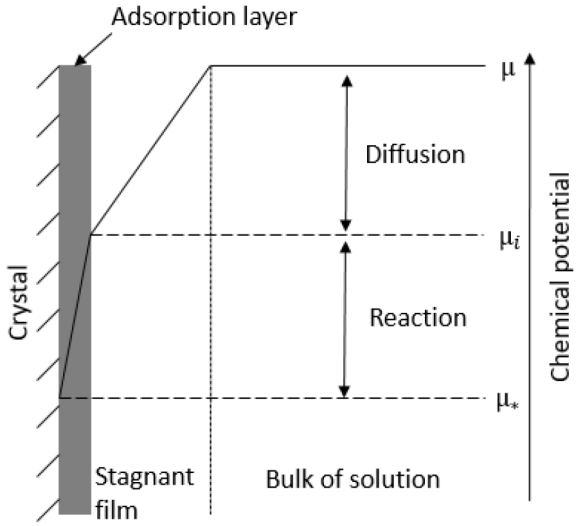

Figure 2-15 Profile of the chemical potential as the fundamental diving force for crystallisation (inspired by Mullin, 2001).

Kinks are hence favoured for incorporation due to highest number of possible binding sites and hence attractive forces. As a result, kinks grow the fastest, followed by stepped and then flat regions. Ideally, the build-up takes place stepwise until a flat face is completed, see Figure 2-16 (B). In this case, further growth necessitates the formation of new steps or kinks on the surface. In case of ideally completed flat faces, this is caused by two-dimensional nucleation on the surface, see Figure 2-16 (C). Similar to three-dimensional homogenous nucleation described in 2.2.3.3.2 above, a certain barrier of energy must be overcome. Then, small islands are formed on the flat surface leading to new steps and kinks enabling further crystal growth.

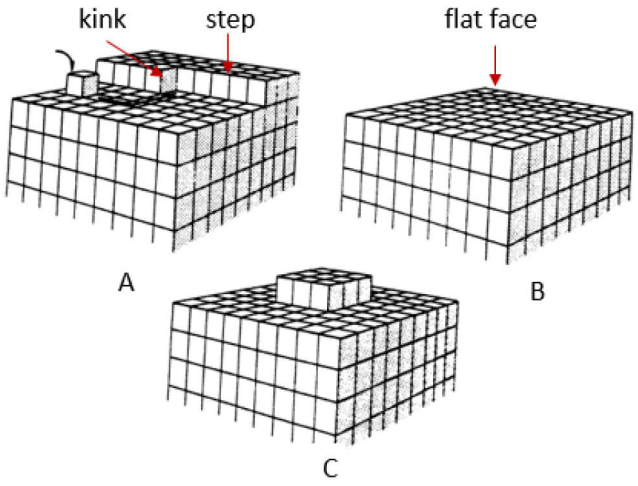

Figure 2-16 Model of crystal growth. A) migration of growth unit to the crystal surface and incorporation in a kink. B) completed flat layer. C) island formation on a flat surface due to two-dimensional surface nucleation (Mullin, 2001).

Even though the critical Gibbs energy of two-dimensional nucleation is lower than that of a homogenous three-dimensional nucleation, relatively high local supersaturations would be necessary to initiate it. However, realistic crystals mostly contain dislocations implying that the faces are basically never completely flat. In case of realistic crystals, dislocations (rough surfaces) are present forming new steps and kinks, which continuously promote growth. In particular, so-called screw dislocations are important, enabling persistent growth following a spiral pattern, as shown in Figure 2-17. Once a screw dislocation has been formed, a complete flat face does not occur anymore, so that crystal growth continuous. This is described by the BCF-theory (Burton, Cabrera, Frank) in detail, which assumes ongoing adsorption of growth units also at lower supersaturations (Mullin, 2001).

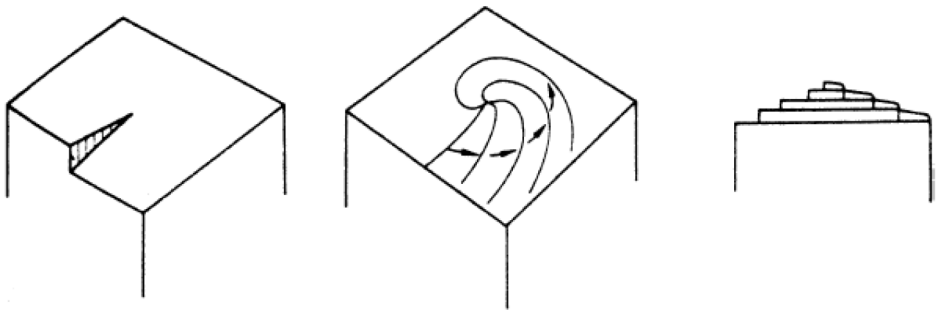

Figure 2-17 Theoretic demonstration of the spiral growth initiated by a screw location. A) initial kink (screw location). B) indication of growth direction. C) illustration of crystal from the side (Mullin, 2001).

Summarising, it can be stated that the overall crystallisation rate is hence controlled by both, the diffusive transport of molecules from the liquid to the crystal surface and their incorporation into the crystal lattice. In general, the slower process controls the overall growth rate. In view of the above-mentioned, two main factors act against each other, the supersaturation, which promotes growth, and the viscosity, which slows down growth. Both are in turn affected by the temperature, dry substance concentration and the presence of impurities (Asadi, 2007). For sucrose crystallisation, it is generally assumed that at lower temperatures, the surface reaction dominates the overall growth rate (< 313 K), while at higher temperatures diffusion dominates (> 323 K) (van der Poel et al., 1998).

2.2.3.3.4 Sucrose Crystal Morphology

As already mentioned, a crystal is a spatial lattice obtained from the repeating arrangement of its unit cell. Its polyhedral shape is framed by specific crystallographic faces, which are regularly repeated. These faces can be related to a common system of coordinates. Based on the lengths and angles of the respective axes, seven different crystal systems can be distinguished. Within each crystal system, several symmetry-related crystal classes can further be differentiated. A theoretical

three-dimensional sucrose crystal shape is shown in Figure 2-18, in which the three main crystallographic axes are depicted (A, B, C).

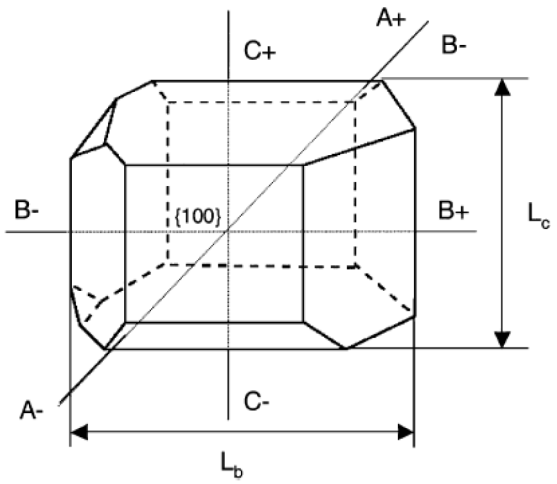

Figure 2-18 Three-dimensional theoretical sucrose crystal shape (Bubnik & Kadlec, 1992).

The sucrose crystal belongs to the monoclinic crystal system, implying that the length of the three axes differ from one another. It can further be assigned to the sphenoidic crystal class, characterised by a twofold axis of symmetry, which in this case coincides with the B-axis of the sucrose crystal. The sucrose crystal is polar along the B-axis. At different positions along the B-axis, different polarities are observed. As a consequence of this asymmetry, the negative left and the positive right pol along the B-axis are crystallographically different and thus have different chemical and physical properties (e.g. growth rate, quantity and quality of faces). Thus, in binary aqueous sucrose solutions, the positive right pol (+) grows faster than the negative left pole (-). The overall crystal habit is determined by the growth kinetics of the different crystallographic faces, which in turn mainly depend on the temperature, the supersaturation as well as the presence of impurities, such as dextran of varying molecular mass (Vavrinecz, 1965). The specific effects of impurities during sucrose crystallisation, particularly focusing on crystal habit modifications, is given in chapter 2.2.3.3.5.

2.2.3.3.5 Effects of Impurities during Crystallisation

The presence of impurities in sugar cane and beet juices decisively complicates the understanding of crystallisation. As already mentioned, for crystallisation, the crystal growth unit firstly diffuses to the crystal surface, it loosely adsorbs and diffuses along the flat surface until it gets incorporated at energetically favoured kinks (see Figure 2-14). Impurities can either or both modify the solution characteristics or interact with the growing crystal faces. This way, the overall growth rate and/or the crystal habit can be affected. As pointed out in detail above, the driving force for crystallisation is the supersaturation, which is a function of the solubility of the solute in the liquid solution (mother

liquor). It is a well-known fact that organic and inorganic non-sugars present in the liquid phase, depending on their type and concentration, can either increase or decrease the solubility of the crystallising solute. For instance, most inorganic salts tend to decrease, while invert sugar tend to increase the solubility of sucrose in aqueous beet and cane juices. It is also assumed that polysaccharides, such as dextran, can affect the solubility of sucrose, even though consistent and detailed knowledge still lacks.

Some authors assume that the presence of dextran causes an unfolding of two intramolecular hydrogen bonds of the sucrose molecule, which then enables intermolecular bond formation between dextran and water molecules, thus decreasing the solubility of sucrose. An easier approach was made by the general assumption that low non-sugar to water ratios reduces the solubility of sucrose, while higher non-sugar to water ratios are known to increase the solubility. An increase in solubility leads to a decrease in supersaturation and thus to reduced growth rates (van der Poel et al., 1998).

When the necessary driving force exists, the next step during crystallisation is the diffusive mass transfer of sucrose molecules to the crystal surface. As pointed out in chapter 2.2.3.2, the flow behaviour might be affected by the presence of impurities, in particular those of higher molecular mass. On the one hand, this leads to an increased thickness of the boundary layers. On the other hand, the diffusion coefficient D decreases with increasing the viscosity, as illustrated by the Stones-Einstein-relation (2-42). In this equation, k_B, T and r represent the Boltzmann constant, the temperature as well as the radius of an ideal spherical molecule, respectively (Mullin, 2001).

$$D = \frac{k_B T}{6\pi r \eta} \tag{2-42}$$

Obviously, an increase in viscosity η slows down diffusion and thus leads to reduced growth rates. Apart from diffusion-related effects, an increase in viscosity is generally known to impede other process steps of sugar manufacture as well (e.g. centrifugation). Thus, the overall processability of sugar cane and beet juices is hampered by higher viscosities (Asadi, 2007).

Furthermore, impurities can interact with the crystal surface affecting the overall crystal growth and, therefore, the habit. As mentioned in the previous chapter, the crystal habit is determined by the growth rate of the different crystallographic faces. The growth of the respective faces is related to the crystallisation conditions and to the crystal surface structure. The adsorption of impurities on growing crystal faces can either impede or promote the deposit of solute molecules. In general, it is assumed that the adsorption of impurities impedes the crystal growth (Mullin, 2001).

In case that there is a structural affinity between the impurity and the crystallising component, the foreign molecules remain on the surface, forming a localised impurity layer and thus hindering further attachment of solute molecules. This would cause a reduction of the growth rate of this specific face. If the interaction between the impurity and the crystal surface is weak, the adsorbed

impurity competes with sucrose and thus might be removed by crystallising sucrose molecules (Mathlouthi & Reiser, 1995).

During sucrose crystallisation starting from beet and cane thick juices, impurities can be allocated to three different places. Firstly, mother liquor, containing several impurities, might adsorb on the crystal surface, which is mostly removed by affination. Secondly, impurities might be incorporated into the crystal lattice, which in this case cannot be removed by affination. Thirdly, non-sugars can be located at the crystal surface captured by adsorption forces. A detailed understanding of the effects of the different impurities is especially difficult since various non-sugars are simultaneously dissolved in the mother liquor. Their amount and kind detrimentally vary, e.g. depending on the plant origin and microbial contamination. In addition, several parameters such as the temperature during crystallisation, pH as well as synergistic effects even complicate the phenomena (van der Poel et al., 1998).

Generally speaking, it seems likely that non-sucrose carbohydrates, such as dextran, interact with the growing sucrose crystal surface since they are composed of the same structural units. There are several studies about dextran-related sucrose crystal modifications, however, revealing discrepant statements. These potentially result from different experimental conditions (crystallisation conditions and analytical procedures), potential synergistic effects and also from the use of dextran with different characteristics, in particular concerning different molecular mass distribution. However, it was mostly reported that dextran causes a specific elongation along the initially shorter C-axis of the sucrose crystal. So far, it was assumed that this relates to a reduction of the growth of the initially longer B-axis rather than an increase of the growth of the initially shorter C-axis. The formation of such elongated needle-shaped crystals results in detrimental technological problems, e.g. danger of crystal fragmentation (Mathlouthi & Reiser, 1995).

2.2.3.3.6 Specifics of Calcium Carbonate Crystallisation by Precipitation

As elucidated in chapter 2.1.2, sugar beet raw juice purification is usually done by means of lime and carbonation gas. In doing so, lime is added to precipitate certain non-sugars. After that, carbonation gas is added to initiate calcium carbonate crystallisation according to the following chemical reaction.

$$Ca(OH)_2 + CO_2 \rightarrow CaCO_3 \downarrow + H_2O \tag{2-43}$$

The calcium carbonate crystals subsequently grow, agglomerate and serve as adsorption points for other non-sugar components. These calcium carbonate particles are then removed by settling and filtration (Asadi, 2007).

In general, the crystallisation by precipitation is initiated by a chemical reaction of two soluble components forming a less soluble product, which then crystallises (Mersmann, 2001). Thereby, the basic theory of crystallisation, which is explained in detail in the previous chapter, also applies

to the precipitation of calcium carbonate during beet raw juice purification. Different from conventional crystallisation, crystallisation by precipitation is comparatively fast and often reveals insoluble precipitates, such as for calcium carbonate in aqueous solutions. Due to a comparatively high supersaturation, nucleation with a comparatively large number of nuclei and subsequent growth occur very fast. Here, primary nucleation continues to occur during crystal growth until a sufficient large crystal surface area has been formed, which causes a rapid decrease in supersaturation. In contrast, secondary nucleation is general known to play a minor role during precipitation (Mullin, 2001). In contrast to sucrose, calcium carbonate is known to be polymorph and can thus occur in different crystalline phases. Polymorphs differ in their type of lattice and thus have different microscopic crystalline habits. However, the macroscopic crystal habit is not necessarily changed for the different polymorphs. The respective polymorphs have different physical properties, such as density and solubility. In general, the most stable one has the lowest Gibbs energy and thus the lowest solubility (Kaempfe, 2011). Depending on the operational conditions, calcium carbonate can nucleate in three different anhydrous polymorphic forms, namely calcite (trigonal), aragonite (orthorombic) and vaterite (hexagonal), listed in ascending order of increasing solubility and thus of decreasing thermodynamic stability. Consequently, the former two are most commonly found (Butler et al., 2006). Besides, amorphous calcium carbonate is known to additionally occur, which is obviously the least stable one. During crystallisation, according to Ostwald's phase rule, the most stable polymorph is not immediately formed because this would cause the highest decrease in Gibbs enthalpy compared to the initial situation. Instead, the polymorph with the lowest difference in Gibbs enthalpy in comparison with the educts is firstly formed. Thus, the least stable one crystallises first, which is step by step transformed to the most stable form according to the Ostwald's rule, shown in Figure 2-19.

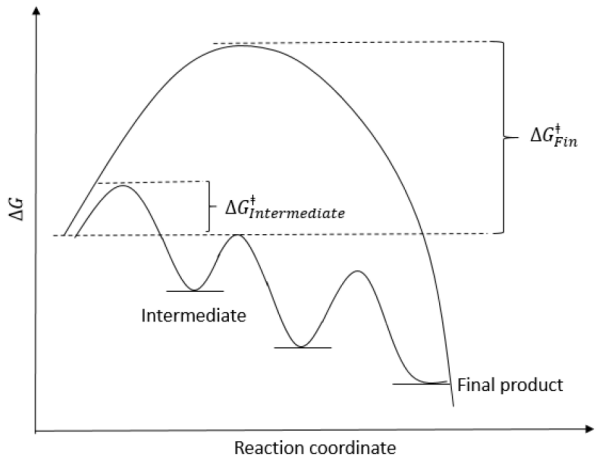

Figure 2-19 Energy profile of the gradual transformation of polymorphs according to Ostwald's rule (Kaempfe, 2011).

This means amorphous calcium carbonate is firstly formed as a precursor phase, which is then gradually transformed to vaterite and then to aragonite and calcite. The occurrence of the different

calcium carbonate polymorphs can be controlled by temperature, supersaturation as well as the presence of several additives.

The temperature dependency is illustrated in Figure 2-20. At a low temperature (< 30°C), calcite is predominantly formed. An increase in temperature causes a decrease of the calcite abundance and vaterite dominates. Above 40°C, which is the case for carbonation during sugar beet raw juice purification, aragonite is formed accompanied, to a much lower degree, by calcite (Sawada, 1997).

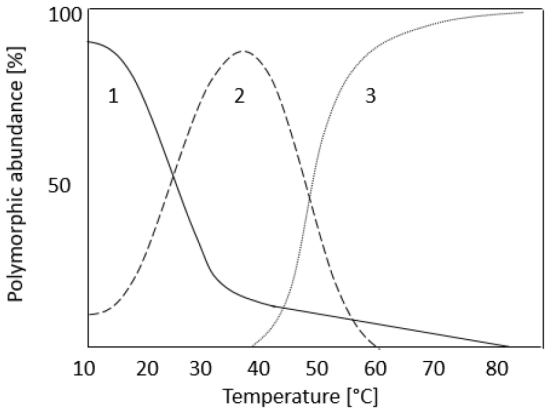

Figure 2-20 Polymorphic abundance as a function of temperature. Curve 1) calcite. Curve 2) vaterite. Curve 3) aragonite (Sawada, 1997).

Apart from the basic steps of crystallisation (nucleation, growth), two additional secondary steps usually profoundly affect the final crystalline precipitate, namely agglomeration and aging. Due to inter-particle collisions, small enough particles can be permanently attached to each other due to stronger Van der Waals forces than gravitational forces. Perikinetic and orthokinetic agglomeration can generally be distinguished, referring to the situation of a static fluid and an agitated dispersion, respectively. The latter one predominantly occurs during stirred precipitation of calcium carbonate during industrial beet raw juice purification. For orthokinetic agglomeration, the agglomerate size d can be related to the time t via the following equation, in which A and B are particle-fluid system constants. It is important to mention here that this equation exclusively applies to early stages of agglomeration since the agglomerate size is generally limited to a maximum value (Mullin, 2001).

$$ln\, d(t) = A + Bt \tag{2-44}$$

When solid particles are dispersed in their own saturated solution, smaller particles tend to dissolve and the solute to be deposited attaches to larger particles. Particle coarsening is the result, known as Ostwald ripening, which is driven by a difference in solubility of small and large particles, illustrated by the Gibbs-Thomson equation. The Gibbs-Thomson equation is derived from the equation by Thomson which gives the change of the vapour pressure as function of the radius of a bubble. Accordingly, the solubility of small particles of size r, assuming a spherical shape, can be expressed as:

$$c(r) = c^* \cdot exp\left(\frac{2\sigma v}{\vartheta RTr}\right) \quad (2\text{-}45)$$

Here, c^* represents the equilibrium saturation concentration for large particles of infinite size. σ is the interfacial tension of the particle (solid) with respect to the liquid phase and v is the molar volume of the solution. Besides, ϑ refers to the number of ions, which is for non-electrolytes equal to one. All the parameters in the exponential function take positive values, so that it is clear that *c(r)* is larger than $c(r \rightarrow \infty)$ (Mullin, 2001). The difference between $c(r)$ and c^* causes the transfer of atoms from small to large particles. Thus, the average size increases and the total number of particles as well as the Gibbs surface energy of the system decrease with time (Baldan, 2002). The final size and shape distribution of calcium carbonate precipitates hence relates to a complex combination of various processes, including nucleation, chemical equilibrium (or reaction rate), growth, phase transformation, agglomeration as well as ripening (Mullin, 2001).

As mentioned above, the calcium carbonate crystals and their agglomerates act as adsorbents during raw juice purification (Asadi, 2007). Thus, non-sugar components dissolved in the raw juice, such as colorants, accumulate at the calcium carbonate surface. The adsorbent, here calcium carbonate, provides the surface for the substances to be adsorbed, here non-sugar components (adsorbate). Depending on the forces of attraction, physical (physiosorption) and chemical (chemisorption) adsorption can be distinguished. The former one mainly refers to weak Van der Waals forces characterised by a low enthalpy of adsorption. As the physiosorption works without sharing or transferring electrons, it is reversible. On the other hand, chemisorption is due chemical bonds characterised by a comparatively high enthalpy of adsorption and is mostly irreversible (Mukherjee, 2011).

The size and shape of calcium carbonate crystals and their agglomerates are hence decisive for the purification performance since they provide the adsorption surface for non-sugar components. Besides, for the filtration process which completes the juice purification, the porous filter cake structure directly correlates with the filtration performance and is determined by the characteristics of the calcium carbonate precipitate.

2.2.3.4 Filtration

Filtration is a mechanical process to separate solid particles from liquid suspensions with the help of a semipermeable filter medium (Bohnet, 2004). The driving force for filtration is a pressure gradient, either caused by vacuum or by an applied pressure. The solid particles can either or both be retained on the surface or within the pores of the filter medium, distinguishing surface and depth filtration, respectively (Figure 2-21). The separation mechanism of surface filtration is based on geometric conditions, implying that the particle diameter is larger than the filter pore diameter. In case of depth filtration, concerning particles with diameters smaller than the pore size diameter,

adhesive forces cause the retention within the porous channels leading to modified filter and/or filter cake pore structures. Due to the fact that both, the size distribution of the filter pores and the particles to be separated cover mostly a broad range, usually both separation mechanisms simultaneously occur (Tien, 2012).

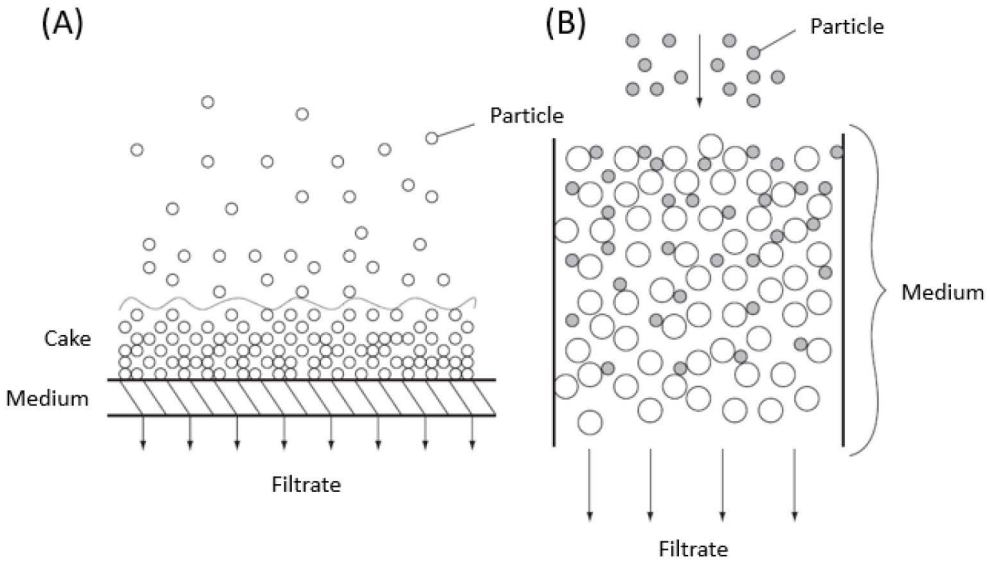

Figure 2-21 Schematic illustration of surface (A) and depth filtration (B) (Tien, 2012).

Surface filtration can be performed in static and dynamic manner. In dynamic filtration, also known as cross flow filtration, the solution to be filtered is perpendicular to the permeate flow. This way, a deposit on the surface of the filter medium is continuously removed avoiding filter cake formation. This method is particularly used for solutions with high solid contents. However, most relevant for the work presented is the static mode, considering both, the currently discussed conventional filtration and the prospectively discussed membrane filtration (see chapter 2.3). In static filtration, also known as dead-end filtration, the flow of the solution to be filtered flows perpendicular to the alignment of the filter medium. As a result, particles are retained on the surface of the filter medium forming a filter cake (Cardew & le, 1998). The height of the filter cake increases with filtration time. The filter cake itself forms a porous structure through which the liquid needs to pass, which hence additionally contributes to the filtering functionality. This way, especially the retention of fine particles is improved. Filter cake formation leads to increased drag coefficients, which reduces the flow rate of the liquid (Schubert, 2012).

In general, a porous medium (filter medium and cake) can be characterised by the porosity ε, which is defined as the relation of pore volume V_{pore} to the total volume V_{total}, see equation (2-46) below.

$$\varepsilon = \frac{V_{pore}}{V_{total}} \tag{2-46}$$

Besides, the tortuosity τ is known as the ratio of pore length *l* to the thickness *h* of the porous media.

$$\tau = \frac{l}{h} \tag{2-47}$$

For perfectly shaped cylindrical pores, the tortuosity is 1. However, realistic filter and membrane pores are not regularly shaped and mostly follow a more worming pass in a way that the tortuosity is higher than 1. Thus, the pore shape and also the pore size distributions of porous media are generally heterogeneous. These rather irregular pore features generally complicate a detailed understanding of the separation process (Baker, 2004). The permeability k is an experimentally determined parameter and describes the ability of a porous medium to allow a fluid to flow through it (Bear, 1972). The laminar flow Q through porous media is most commonly described by Darcy's law, see equation (2-48).

$$Q = -\frac{A \cdot \Delta p \cdot k}{\eta h} \tag{2-48}$$

Where A is the cross-sectional area of the porous medium through which the medium flows, η is its dynamic viscosity and Δp the pressure gradient over the length of the porous medium h. The filtration velocity v can then be expressed by equation (2-49).

$$v = \frac{Q}{A\varepsilon} = -\frac{\Delta p k}{\eta h \varepsilon} = -\frac{\Delta p}{\eta h r} \tag{2-49}$$

The ratio of the porosity and the permeability is referred to as the specific resistance r. Obviously, the velocity is directly proportional to the pressure difference Δp as the driving force for filtration. Besides, according to Darcy's law, the filtration velocity is inversely proportional to the dynamic viscosity η, the height of the porous layer h and to the specific resistance r (the ratio of the porosity ε and the permeability k of the medium) (Gasper, 2005).

Thus, here, too, a viscosity increase due to the presence of high molecular mass dextran can be a relevant factor contributing to impeded filtration processes, meaning reduced velocity, during sugar manufacture. In addition, the size and shape distribution of particles participating in filter cake formation need to be considered to fully understand the effects on the filtration performance. The resistance of the filter cake is a function of the inner surface and the diameter of the pores, affecting the porosity and permeability, which are in turn influenced by the size and shape of the particles deposited on the filter medium (Schubert, 2012).

Several authors have found that dextran is not only involved in viscosity effects, but also causes modifications of the characteristics of the particles precipitated during purification processes prior to filtration (Wojtczak et al., 2015). Conclusively, the two aspects, viscosity increase as well as particle modifications, need to be considered to holistically elucidate the dextran-related effects during purifications processes, including filtration, as a part of sugar manufacture.

2.3 Membrane Filtration as a Preparatory Step for Dextran Analysis

The previous chapters have illustrated that the presence of dextran can diversely affect sugar manufacture. To assess as well as to mitigate these dextran-related effects, the quantitative and qualitative determination of dextran in sugar cane and beet raw juices is necessary. However, dextran analysis in sugar industrial practice is still a great challenge, particularly hampered by the low contents and broad molecular mass distributions. The issue of dextran analysis as well as a survey of existing methods including their limitations are given as an introduction to the proposal of a new method in chapter 8 and 9. The new membrane method proposed is based on differences in polarisation caused by the mechanical removal of dextran by ultrafiltration. Therefore, the following chapter provides more detailed knowledge about the separation of dextran as a macromolecule via membrane filtration.

2.3.1 General Introduction to Membrane Technology

The main principle of membrane filtration is similar to the one of conventional filtration discussed in the previous chapter 2.2.3.4, whereby the main difference is the average pore size. Membranes are selective barriers having one input stream and at least two output streams, of which one contains the targeted component (see Figure 2-22). The penetrating output stream is known as the permeate, whereas the rejected output refers to the term retentate (Cardew & Le, 1998).

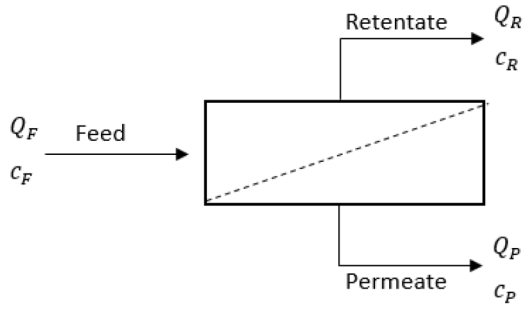

Figure 2-22 General scheme of a membrane separation process (Cardew & Le, 1998).

In membrane technology, four different procedures can be distinguished in order to selectively separate certain components: microfiltration, ultrafiltration, reverse osmosis and electrodialysis, shown Figure 2-23. These methods not only differ in their pore sizes, but also in their separation mechanisms. Here, too, static and dynamic filtration can be distinguished. For the membrane separation of dextran from raw juices as a preparatory step for dextran analysis, static dead-end filtration was used since solid content and permeate volume needed are comparatively low (Baker, 2004).

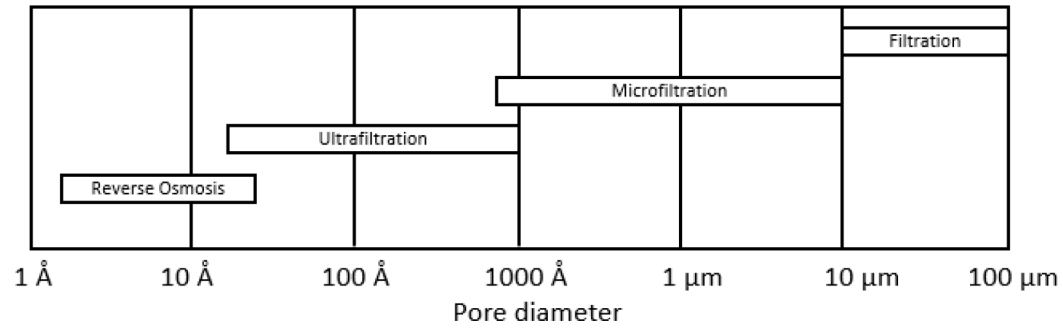

Figure 2-23 Membrane filtration procedures differing in their average pore size diameter (Baker, 2004).

2.3.2 Membrane Transport Models

Two transport models can be distinguished: the solution-diffusion model and the pore flow model. For the solution-diffusion model, permeants (components passing the membrane) dissolve in the membrane material and diffuse through it driven by a gradient in chemical potential, which is often approximated by the concentration gradient (dense membrane). Separation in this case is caused by differences in solubility and mobility of solutes in the membrane. This model e.g. applies to reverse osmosis but is not relevant for the separation of macromolecules via ultrafiltration being key to this study.

To describe separation via ultrafiltration, the pore-flow model applies, basically referring to molecular sieving. In this case, permeants are transported through tiny pores driven by a pressure difference, while components of certain sizes are retained (Baker, 2004).

In the main, the flow behaviour and separation phenomena of conventional filtration and membrane filtration are similar. Thus, the liquid flow through membrane pores can also ideally be described by Darcy's law (see equation (2-48) in chapter 2.2.3.4). According to the corresponding equation, the flow rate is again proportional to the pressure difference representing the driving force for membrane filtration (Ohlrogge & Ebert, 2006).

Here, too, apart from the flow rate, particles can be retained in two ways, screen and depth filtration. In case of screen filtration, the pore size diameter is smaller than the particles to be retained. Depth filtration concerns the retention of particles in the interior of the membrane. Thus, solutes are small enough to pass into the membrane pores but are held back by constrictions or adsorption. In case of the separation of macromolecules via membrane filtration, both mechanisms can occur, but screen filtration is generally the dominating and targeted one (Baker, 2004).

During screen filtration, the steric hindrance hampers the solute molecule to pass through the membrane pores. The heterogeneous pore structure of membranes generally impedes the formulation of specific equations for the pore flow model. This is due to the fact that the above-mentioned heterogeneous pore size and shape distributions deviate from uniform geometries (mind

the tortuosity above). Nevertheless, Ferry firstly established a model, in which an ideal assumption of equal circular pore shapes with the radius *r* is used (see Figure 2-24).

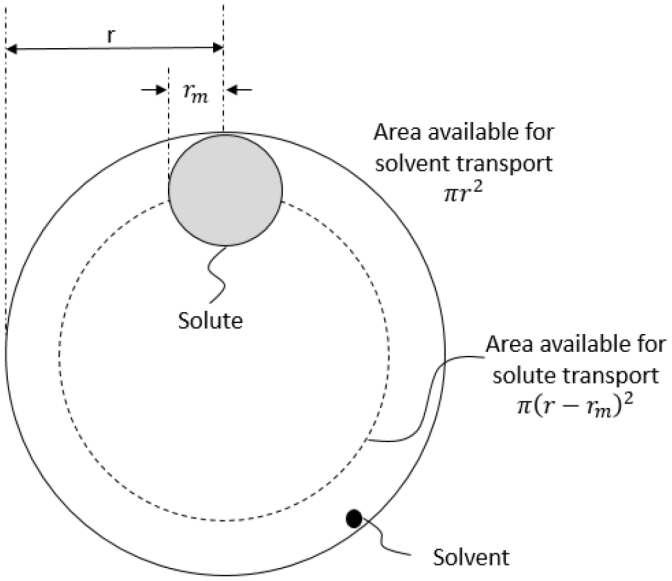

Figure 2-24 Ferry model for mechanical retention of solute molecules in membrane pores (Baker, 2004).

A circular molecule with radius r_m can only pass through a membrane pore within the area of a circle with the radius $(r - r_m)$ in a way that the virtual area for solute transport is $A = \pi(r - r_m)^2$. In relation to the area of the opening available for solvent transport $A_0 = \pi r^2$, the fractional area for solute transport is given by equation (2-50) (Baker, 2004).

$$\frac{A}{A_0} = \frac{(r - r_m)^2}{r^2} \tag{2-50}$$

Renkin modified this model and took also the parabolic velocity profile of the fluid while passing through the membrane into account, caused by frictional resistance (empirically determined) (Renkin, 1955). The fractional area available for solutes can then be described as stated below. It is equal to the ratio of the solute concentration, which should be retained by the membrane, in the feed c_F and in the permeate c_P.

$$\left(\frac{A}{A_0}\right)' = 2\left(1 - \frac{r_m}{r}\right)^2 - \left(1 - \frac{r_m}{r}\right)^4 = \frac{c_P}{c_F} \tag{2-51}$$

Using the general equation for the rejection coefficient *R*,

$$R = \left[1 - \frac{c_P}{c_F}\right] \cdot 100\% \tag{2-52}$$

the Ferry-Renkin equation (2-53) describing the membrane rejection is obtained. The latter can be used to estimate the pore size of an ultrafiltration membrane when using a solute of known radius.

$$R = \left[1 - 2\left(1 - \frac{r_m}{r}\right)^2 - \left(1 - \frac{r_m}{r}\right)^4\right] \cdot 100\% \tag{2-53}$$

Obviously, higher solute diameters r_m reduce the area available for penetration, thus retention is increased (Baker, 2004). To estimate the diameter of a macromolecule, the radius of gyration is often used, which is defined as the root mean square distance of the building blocks from their centre of mass (Lechner et al., 2010). Thus, an increase in molecular mass results in an increase of the radius of gyration and therefore in higher membrane separation efficiencies. For instance, poor solvents generally cause a molecular compaction and thus a decrease of the radius of gyration (Klemm, 2006). Retention caused by depth filtration is more complex in comparison with screen filtration. Thereby, four mechanisms can contribute to the capture of particles in the depth of the membrane porous structure (see Figure 2-25). This includes, on the one hand, the geometric mechanisms of molecular sieving and, on the other hand, the inertial impaction of molecules in the tortuous pores in the interior of the membrane. These mechanisms are rather applicable to larger particles. For smaller particles, Brownian motion is also of relevance, which brings them randomly into contact with the pore walls, where they get captured by surface adsorption. In addition, electrostatic adsorption can cause a capture of molecules within the membrane pore structure due to different charges of membrane and colloidal material (Baker, 2004).

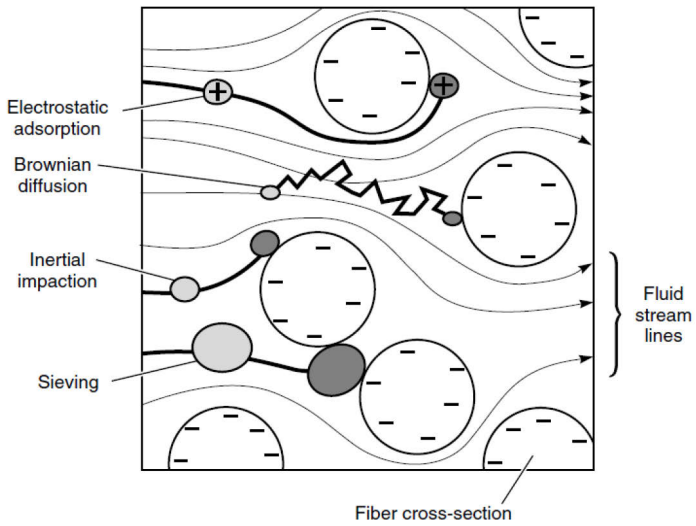

Figure 2-25 Mechanism for particle capture during depth filtration (Baker, 2004).

2.3.3 Separation of Macromolecules by Ultrafiltration

To separate the macromolecule dextran from aqueous sugar beet and cane raw juices, ultrafiltration membranes are suitable. Ultrafiltration commonly uses asymmetric membranes with pores sizes of about 10 Å to 1000 Å (see Figure 2-23 above). As shown in Figure 2-26, a surface skin layer with

such fine pores, the actual separation layer, is deposited on a microporous support layer. The latter gives the membrane mechanical stability. The surface layer enables a selective size-related retention of macromolecules.

In case of ultrafiltration, the separation limit is usually characterised by the so-called molecular weight cut-off (MWCO). This term refers to the molecular mass of a globular marker protein that is rejected by 90 % (m/m). It is important to mention here that a congruent definition of this parameter is still missing. The previous chapter 2.3.2 illustrates that the ratio of the solute radius to the pore size radius is decisive for the separation. However, not only the pore and solute size distribution, but also the shape of macromolecules in solution differ from ideal geometries. Linear molecules are hence rather able to pass through the membrane pores than globular coil shaped molecules, as illustrated in Figure 2-26 below (Baker, 2004).

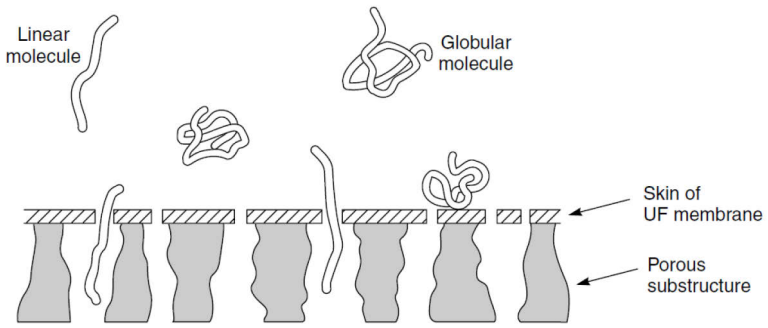

Figure 2-26 Effect of molecule shape on membrane separation (Baker, 2004).

Proteins are stable wound coils held together by hydrogen bonds making it resistant against deformation and, therefore, are usually used for the determination of the just mentioned MWCO. For non-rigid molecules, as is the case for dextran, Brownian motion additionally causes random rotations and a continuous change in molecular conformation. Thus, internal Brownian motion can continuously induce changes of the molecular conformation enabling to “snake through” pores with a radius smaller than the “effective” radius of the molecule (Cardew & Le, 1998). Apart from such spontaneous molecular fluctuations, modifications due to the application of pressure, the driving force for membrane filtration, is assumed to contribute to this. This is especially relevant when α-1,6 linkages dominate in the polymer structure, which is, as explained in 2.2.2 above, the case for dextran molecules (Lee et al., 2004).

2.3.4 Adsorption – Concentration Polarisation

Similar to the formation of a filter cake during conventional filtration, solute molecules retained by membranes can form an additional layer on the membrane’s surface, additionally contributing to the overall functionality. In membrane technology, this refers to the term “fouling”, caused by concentration polarisation. It results from the interaction between membrane and solute molecules,

either on the membrane surface or in the porous structure. The deposit of colloidal and macromolecular matter results in a filter cake composed of multiple molecular layers, which can distinctly affect the filtration performance, concerning flow rate and separation characteristics (Ohlrogge & Ebert, 2006).

The accumulation of solute molecules on the surface of the membrane is caused by the forced convective flux towards the membrane surface $J_v c_i$, as the liquid is 'pressed' through the membrane. As a result, an exponential concentration profile was found, see Figure 2-27. However, due to the difference in concentration, there is a diffusive transport back to the bulk $D_i \frac{dc_i}{dx}$, which is, however, comparatively low.

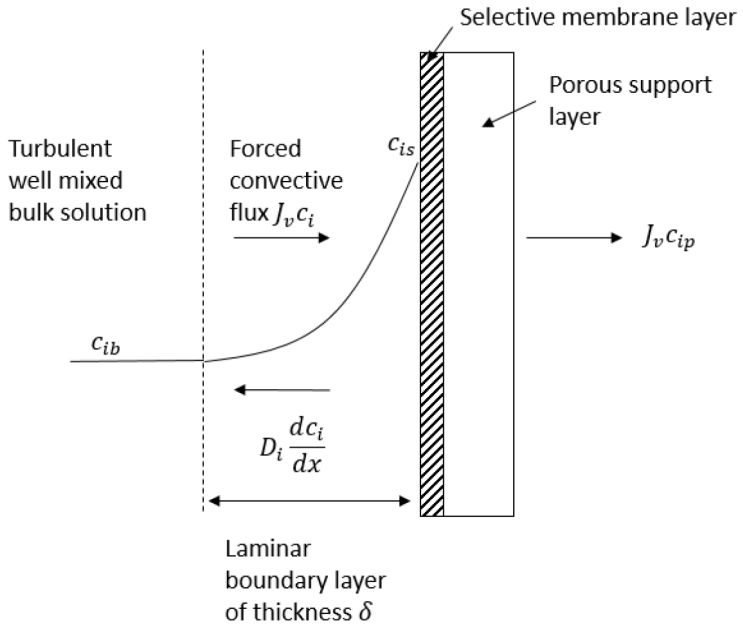

Figure 2-27 Schematic illustration of concentration polarisation at the membrane surface (Baker, 2004).

In steady state, the balance of the convective flux $J_v c_i$ towards the membrane surface and the diffusive flux $D_i \frac{dc_i}{dx}$ backwards to the bulk can be expressed by the following equation, in which c_i and D_i are the concentration of solute and the diffusion coefficient of component *i* in the boundary layer, respectively. J_v refers to the volume flux.

$$J_v c_i = D_i \frac{dc_i}{dx} \tag{2-54}$$

Integration over the boundary layer thickness δ results in the so-called polarisation *P*.

$$P = \frac{c_{is}}{c_{ib}} = exp\left(\frac{J_v \delta}{D_i}\right) \tag{2-55}$$

Here, c_{is} and c_{ib} refer to the concentration of component *i* in the bulk and on the membrane surface. According to this, polarisation increases with the increase in flux rate and the decrease in diffusivity (Cardew & Le, 1998).

Consequently, the filtration velocity is generally assumed to be lower for high molecular mass dextran in comparison with low molecular mass dextran due to higher viscosities and thus decreased molecular mobilities. In addition, concentration polarisation is also affected by the diffusivity and is therefore also supposed to be higher for high molecular mass dextran. Thus, the filtration time necessary to obtain a certain permeate volume is supposed to increase with dextran's molecular mass, affecting the overall experimental time for the analytical method proposed. However, the actual separation of dextran is, if any, slightly improved with increasing time due to this phenomenon.

2.4 Mitigation of Dextran-Induced Process Effects by Enzymatic Decomposition

2.4.1 Basics of an Enzyme Reaction

Enzymes are globular proteins with a complex structure. The building blocks of proteins are amino acids, which are covalently linked via peptide bonds. The amino acid sequence is characteristic of a protein and is known as its primary structure. The secondary structure refers to the spatial arrangement of a peptide chain due to interaction of amino acids, which are situated close to each other, resulting in periodic folding of polypeptide chains. Interaction between amino acids located far from one another determines the tertiary structure (non-periodic folding of secondary structures). A functional protein composed of several polypeptide chains can be described by the quaternary structure (Berg et al., 2018).

An enzyme is composed of at least one folded polypeptide chain. The three-dimensional structure of proteins arises from physicochemical interactions between side chains, amide groups and solvent molecules. The folded globular protein has an inward-looking hydrophobic core and a hydrophilic exterior. The folding of the enzyme is a sign of complete functionality, which can easily be destroyed by energy changes (e.g. temperature) (Illanes, 2008).

An enzyme reaction is generally composed of three main steps: the formation of an enzyme-substrate complex, the catalytic reaction and finally the product dissociation. The specific region of an enzyme involved in the catalysis of chemical reactions is known as the active centre. It is made of functional groups coming from the amino acid sequence and resembles a cavity or gap form, actually representing just a small part of the protein. However, the overall mobility of the protein contributes to the binding of the substrate at the active site. The latter is caused by weak non-covalent interactions (electrostatic interaction, Van-der-Waals forces and hydrogen bonds) with specific amino acid residues. The catalytic reaction is caused by other amino acid residues present in the non-polar active centre. The interaction between specific functional groups of enzyme and substrate is responsible for the high specificity of an enzyme. Due to the short local range of these forces, a complementary unique geometric shape of the substrate and the active site of the enzyme was initially assumed, referring to the lock and key principle. However, more recently, it has been suggested that the active site of an enzyme sterically adapts in order to bind the substrate, while orienting the participating catalytic groups accordingly. The latter is known as the so-called induced-fit model. Anyhow, after the formation of an enzyme-substrate-complex, the catalytic conversion takes place and the product is finally dissociated. Thereby, the enzyme is released unchanged and enzymatic catalysis continues (Berg et al., 2018).

2.4.2 Classification of Enzymes and Origin of Dextranases

The catalytic reaction of an enzyme is specific with regard to either or both, the substrate and the type of catalysed reaction (Christen et al., 2016). In view of this, six enzyme classes can be distinguished, which are summarised in Table 2-1.

Table 2-1 Enzyme classification (Storhas, 2013).

Enzyme class	**Catalytic functionality**
Oxidoreductase	Redox reactions, electron transfer
Transferase	Group transfer reactions
Hydrolase	Hydrolytic reaction
Lyase	Reaction at double-bonds
Isomerase	Isomerisation
Ligase	Reaction of two molecules while consuming energy-rich compounds (e.g. ATP)

Enzymes specifically hydrolysing α-(1→6) glycosidic bonds in dextran molecules are known as dextranases, which hence belong to the group of hydrolases. The globular protein structure of a dextranase originating from a *Penicillium minioluteum* is exemplary illustrated in Figure 2-28. Dextranase can bind to varying substrate molecules, such as dextran with different molecular masses, isomalto-oligosaccharides and iso-maltose. In general, dextranases have varying microbial origins (fungi, yeast, bacteria), whereby fungi represent the most important sources for commercial applications. Depending on the origin, an exo- (acting from the end of the chain) and an endo-mode (acting from the middle of the chain) of action can be distinguished (Khalikova et al., 2005). Among the industrial applications of dextranase, whereby a major part constitutes the sugar industry, endo-dextranases are commonly used, decomposing dextran in a gradual manner (Eggleston & Monge, 2005).

Based on the amino acid sequence, which in turn determines the secondary and tertiary structure of a protein, the carbohydrate-active enzymes database was established (CAZy). Thereby, structural and mechanical similarities rather than substrate specificity are considered to assign enzymes to the same family. According to this, endo-dextranase can be assigned to the glycoside hydrolase family 49 and 66 (Khalikova et al., 2005). The dextranase used in this study originates from a *Chaetomium gracile* strain and therefore belongs to the glycoside hydrolase family 49.

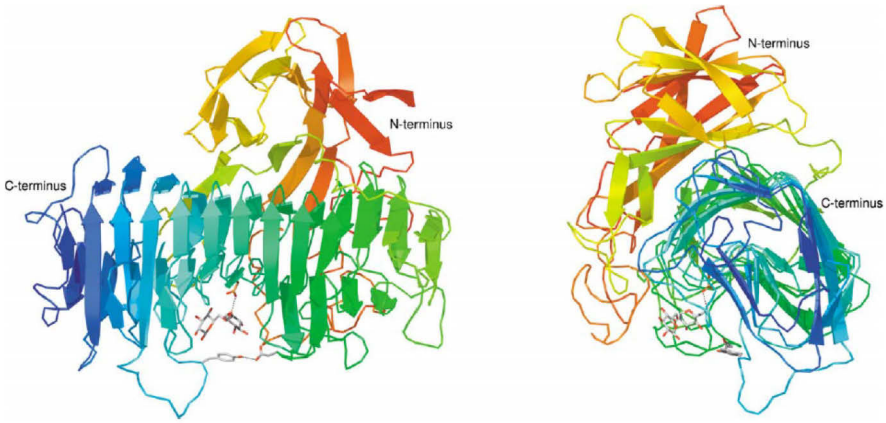

Figure 2-28 Exemplary illustration of a dextranase originating from a *Penicillium minioluteum* strain (Larsson et al., 2003).

2.4.3 Thermodynamics of an Enzyme Reaction

In the main, a chemical reaction is characterised by two thermodynamic features. First, the difference in Gibbs energy ΔG between the initial substrate and the final product. If its value is negative, the reaction occurs spontaneously into the direction of the products. The second one refers to the energy necessary to introduce the conversion of the substrate to the product via a transition state. Enzymes are catalysts, which are able to affect the latter, thus lowering the Gibbs energy of the transition state so that less energy is required for the reaction to occur spontaneously. An enzyme is hence not able to affect the overall thermodynamic equilibrium, which exclusively depends on the difference in energy between the initial substrate and the final product (Figure 2-29).

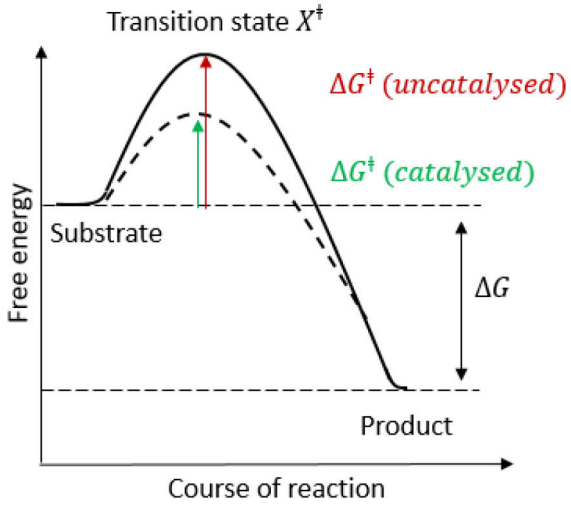

Figure 2-29 Energy profile of an enzyme reaction (Berg et al., 2018).

Thus, the chemical reaction from a substrate S to a product P passes through a transition state $X^{\ddagger}$, see schematic chemical reaction equation (2-56). This transitional state possesses a higher Gibbs energy in comparison with both, the initial substrates and the final products and is therefore highly

unstable. The difference in Gibbs energy between the transition state $\Delta G_X^{\ddagger}$, maximum in Figure 2-29, and the substrate ΔG_S is known as the activation energy $\Delta G^{\ddagger}$, see equation (2-57).

$$S \rightarrow X^{\ddagger} \rightarrow P \tag{2-56}$$

$$\Delta G^{\ddagger} = \Delta G_X^{\ddagger} - \Delta G_S \tag{2-57}$$

Enzymes reduce this activation energy and thus facilitate to achieve the transition state without changing the net Gibbs energy ΔG for the conversion of substrate to product. This is due to the fact that the formation of an enzyme-substrate-complex provides a new reaction path way, providing a lower Gibbs energy in comparison with the usual transition state. An energy release coming from the interaction between enzyme and substrate is related to this (exergonic reaction). This energy contribution due to enzyme action is responsible for the decrease in activation energy (Berg et al., 2018).

2.4.4 Enzyme Kinetics

The enzyme activity represents the catalytic potential of an enzyme and is hence a matter of reaction velocity. The reaction velocity can either be described by the substrate consumption or by the product generation with time *t* (Illanes et al., 2014).

$$activity = v_{t=0} = -\frac{dS}{dt}_{t=0} = \frac{dP}{dt}_{t=0} \tag{2-58}$$

Ideally, it is assumed that the enzyme activity correlates linearly with the enzyme concentration. Nevertheless, the substrate concentration is also known to be a key variable in enzyme kinetics (Illanes, 2008).

Based on work initially suggested by Henri, Michaelis and Menten formulate the fundamental and well-known model to describe the enzyme kinetic, relating the enzyme activity to the enzyme and substrate concentration. Here, again, the three main steps of an enzyme reaction are given in the chemical reaction equation (2-59).

$$E + S \underset{k_{-1}}{\overset{k_1}{\rightleftharpoons}} ES \underset{k_{-2}}{\overset{k_2}{\rightleftharpoons}} E + P \tag{2-59}$$

Further simplification is made when focusing on the beginning of the reaction, where the product concentration is still low. In this case, the backwards reaction from product to enzyme-substrate-complex can be neglected.

$$E + S \underset{k_{-1}}{\overset{k_1}{\rightleftharpoons}} ES \overset{k_2}{\rightarrow} E + P \tag{2-60}$$

The first step of substrate binding is much faster than the second step of producing *P*. The latter is hence reaction rate-determining and used to describe the reaction velocity, which can be described by the following equation (Illanes et al., 2014).

$$\frac{dP}{dt} = v = k_2[ES] \tag{2-61}$$

Obviously, the rate is directly proportional to the concentration of the enzyme-substrate-complex, which is in turn proportional to the concentration of the two participating reactants, enzyme and substrate.

$$\frac{d[ES]}{dt} = k_1 \cdot [E] \cdot [S] \tag{2-62}$$

$$\frac{d[ES]}{dt} = (k_2 + k_{-1}) \cdot [ES] \tag{2-63}$$

Additionally, considering the steady-state theory proposed by Briggs and Haldane, in which it is assumed that the formation as well as the disintegration rate of the enzyme-substrate-complex is balanced, the two equations above can be equalised.

$$k_1[E] \cdot [S] = (k_2 + k_{-1})[ES] \tag{2-64}$$

$$[E] \cdot [S] = \frac{k_2 + k_{-1}}{k_1}[ES] \tag{2-65}$$

The rate constants are then combined to the well-known Michaelis-Menten constant K_M and the enzyme concentration is expressed as $[E] = [E_{total}] - [ES]$.

$$K_M = \frac{k_2 + k_{-1}}{k_1} \tag{2-66}$$

Then, equation (2-65) becomes

$$[ES] = \frac{[E_{total}] \cdot [S]}{K_M + [S]} \tag{2-67}$$

Thus, the rate-determining step can be expressed by the equation (2-68).

$$v = k_2[ES] = \frac{k_2 \cdot [E_{total}] \cdot [S]}{K_M + [S]} \tag{2-68}$$

In case that all catalytic binding sites of the enzymes are occupied by substrate, the concentration of $[ES]$ is equal to $[E_{total}]$. Thus, the maximum velocity v_{max} is obtained, which refers to the reaction velocity at substrate surplus.

$$v_{max} = k_2 \cdot [E_{total}] \tag{2-69}$$

This way, the well-known Michaelis-Menten equation is obtained, in which v_0 refers to the initial reaction velocity at a substrate level *S*.

$$v_0 = k_2[ES] = \frac{v_{max} \cdot [S]}{K_M + [S]} \tag{2-70}$$

The Michaelis-Menten constant K_M is determined by the substrate content $[S]$ at half of the maximal velocity. It is a measure of substrate affinity, whereby low values indicate high affinity. The maximum velocity, and therefore also the Michaelis-Menten constant, is characteristic of an enzyme. By plotting the reaction rate as a function of the substrate content, a hyperbolic curve is obtained, see Figure 2-30 (Berg et al., 2018).

At low substrate contents when $K_M < S$, the reaction velocity linearly correlates with the substrate concentration, according to a reaction of first order. At higher substrate contents when $K_M > S$, the curve asymptotically approaches the maximum velocity. In this case, the reaction rate is hence independent of the substrate concentration reducing the reaction order to zero (Mikkelsen & Cortón, 2004).

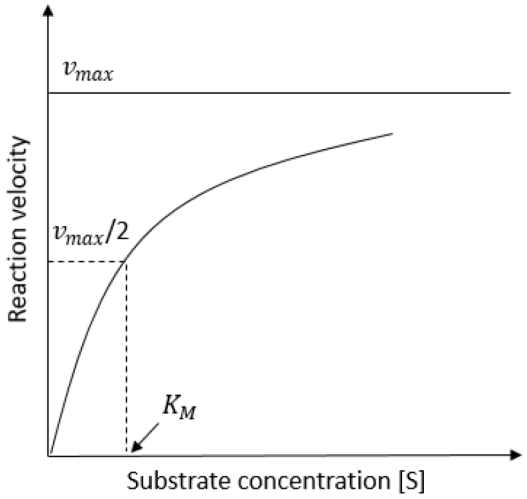

Figure 2-30 Enzyme reaction velocity as a function of the substrate concentration according to the Michaelis-Menten theory (Berg et al., 2018).

2.4.5 Factors Affecting an Enzyme Reaction

The previous chapter has illustrated the effect of the two key parameters of an enzyme reaction, substrate and enzyme concentration. Thereby, it is generally acknowledged that an increase of the enzyme concentration is directly proportional to the enzyme activity, whereas deviations potentially occur. By means of the Michaelis-Menten theory, it was illustrated that an increase in substrate concentration leads to an increase in reaction rate until approaching a maximum value, provided that the enzyme concentration is kept constant. At low substrate contents, the active centres of enzymes are not completely occupied and thus the enzyme is not saturated with substrate. An increase in substrate concentration hence leads to a higher number of occupied active centres, implying that the enzyme action is increasingly exploited. In case that all active centres are bound to a substrate, an increase in substrate concentration does not affect the reaction rate anymore (Berg et al., 2018).

Apart from the effects due to varying enzyme and substrate concentrations, the activity as well as the stability of an enzyme can be affected by several environmental parameters. The most important ones are the temperature as well as the pH, which are known to affect both, activity and stability (Illanes et al., 2014).

The amino acids of polyionic enzymes partly contain charged functional groups, which can participate in the catalytic reaction or in the formation of the tertiary structure (Chmiel, 2011). A change in pH results in a change of concentrations of hydrogen (H^+) and hydroxyl ions (OH^-). Therefore, the ionisation state of the active centre and the charge distribution of the enzymes surface can hence easily be changed by pH variation (Illanes et al., 2014). Here, it is assumed that small deviations from the optimum cause reversible pH-induced changes. In contrast, irreversible changes are usually caused when the pH dramatically deviates from the optimum, leading to protein denaturation (Chmiel, 2011).

In general, a higher temperature leads to increased rates of chemical reactions. As a result, the enzyme activity is increased. Since enzymes are labile proteins prone to configurational changes, higher temperatures reduce the stability of an enzyme due to an increase in enzyme inactivation. The compromise between activity and stability refers to the optimum temperature for the use of an enzyme in a certain reaction (Illanes et al., 2014).

The activity of an enzyme can furthermore be affected by the presence of inhibitors. As elucidated in chapter 2.1.1, sugar beet and cane raw juices contain various non-sugar components, which potentially play a role as inhibitors during enzymatic decomposition of dextran in industrial practice. In this case small molecule or ions can interact with the globular enzyme at different positions, distinguishing competitive and non-competitive inhibition. Competitive inhibitors are in most cases similar to the substrate enabling to bind at the active centre of the enzyme as well. Thus, inhibitor and substrate compete for binding at the catalytic centre of the enzyme. An increase in substrate concentration can hence reduce this kind of inhibition, while making the substrate superior to the inhibitor. In case of non-competitive inhibition, inhibitor and substrate simultaneously bind to the enzyme, but at different sites. Thus, the complementary shape of the active centre is modified, which reduces the efficiency of functional enzyme (Berg et al., 2018). It is widely assumed that sucrose contained in sugar beet and can juices affects the enzymatic decomposition of dextran (Eggleston & Monge, 2005). On the one hand, this could be related to a higher viscosity, but on the other hand, non-competitive inhibition could also play a role.

2.4.6 Diffusional Restrictions of an Enzyme Reaction

As mentioned above, an enzyme reaction is composed of three main steps: substrate binding, catalytic reaction and dissociation of enzyme and product. For the first step, the encounter of the two participating reactants, enzyme and substrate, is the prerequisite. This is followed by a loose

adhesion until the active site of the enzyme is reached. These steps are diffusion-controlled processes, whereas the subsequent catalytic step is reaction controlled (Bisswanger, 2000). Thus, the reaction rate is not only a function of the above-described catalytic potential of enzymes, but is also affected by the mass transfer of substrate molecules to the binding sites of the enzymes. As a result, concentration differences in the vicinity of the enzyme surface occur (Illanes et al., 2014).

Fick's first law can be used to ideally describe the diffusion-controlled reaction. Assuming that at the beginning of the enzyme reaction, enzyme and substrate are equally distributed. With ongoing enzyme action, substrate is consumed and thus becomes depleted in the vicinity of the enzyme surface, leading to local lower substrate concentrations. The net flow ∅ of substrate can hence be described by equation (2-71).

$$\emptyset = \frac{dn}{dt} = DA\frac{dc}{dr} \tag{2-71}$$

Where n is the net surplus of substrate molecules passing through an area A in time t. c represents the concentration of substrate located at distance r from the enzyme molecule.

The diffusional part is distinctly determined by the diffusion coefficient D, which relates to the type of the medium and its temperature as well as to the concentration and the size of the molecules. As already explained above, the diffusion coefficient in liquids is most commonly expressed by the Stokes-Einstein relation (equation (2-72), in which k_B is the Boltzmann's constant and T is the temperature. Besides, η and r represent the viscosity and the solute radius, respectively.

$$D = \frac{k_B \cdot T}{6\pi\eta r} \tag{2-72}$$

Here again, the Stokes-Einstein relation clearly illustrates that the diffusion coefficient is inversely proportional to the viscosity. As elucidated in chapter 2.2.3.2, the viscosity η is a function of the concentration as well as of the molecular mass of dextran. Thus, apart from the substrate content, the flow behaviour, and thus the diffusion-controlled processes, can obviously be affected by the molecular mass distribution of the substrate (Bisswanger, 2000).

The Stokes-Einstein relation ideally assumes the diffusion of rigid solute spheres in a liquid solvent. However, the molecular shape of polymers usually deviates from this ideal assumption. For random coil shapes, which applies to dextran in aqueous solutions, the radius of the sphere in equation (2-72) can be replaced by the equivalent radius of the polymer R_e (Cussler, 2009).

$$D = \frac{k_B \cdot T}{6\pi\eta R_e} \tag{2-73}$$

$$R_e = 0.676\,\langle R^2\rangle^{1/2} \tag{2-74}$$

In this approach, $\langle R^2\rangle^{1/2} = R_g$ represents the above-mentioned root mean square radius of gyration, representing a common measure of a polymer in solution (Cussler, 2009).

The molecular shape of a polymer affects the radius of gyration as well as the viscosity of its solvent, which are both inversely proportional to the diffusion coefficient. The molecular shape in turn depends on the molecular mobility, determined by the type of linkages connecting the monomers and the type of solvent. Thus, more rigid molecules have a lower mobility and thus lower diffusion coefficients.

As elucidated in chapter 2.2.2, glucose monomers in dextran's main chain are connected via highly flexible α-(1→6) glycosidic linkages. In case of such a non-rigid molecule, Brownian motion additionally causes random rotations and thus a continuous change in molecular conformation. Permanent molecular movement is the result, which distinctly increases the enzyme-substrate collision (Cardew & Le, 1998).

Consequently, the molecular mass as well as the conformational structure of a polysaccharide functioning as a substrate for enzyme reactions is decisive for the reaction rate as well as the final decomposition products. Due to the broad molecular mass distribution of dextran in sugar cane and beet juices mentioned in chapter 2.2.2, this is of great relevance for targeted mitigation of dextran contamination in sugar industrial practice, necessitating complete and fractional dextran analysis.

References

Abdel-Rahman, E.-S. (2007). Investigations on the influence of dextran during beet sugar production with special focus on crystal growth and morphology (PhD). Technische Universität Berlin, Berlin.

Asadi, M. (Ed.). (2007). *Beet-Sugar Handbook*. New Jersey: John Wiley & Sons.

Baker, R. W. (2004). *Membrane technology and applications* (2nd ed.). Chichester, New York: J. Wiley.

Baldan, A. (2002). Progress in Ostwald ripening theories and their applications to nickel-base superalloys: Part I: Ostwald ripening theories. *Journal of Material Science*, *37*(11), 2171–2202. https://doi.org/10.1023/A:1015388912729

Bannwarth, H., Kremer, B. P., & Schulz, A. (2007). *Basiswissen Physik, Chemie und Biochemie*. Heidelberg: Springer-Verlag.

Bear, J. (1972). *Dynamics of Fluids in Porous Media*. New York: American Elsevier.

Belitz, H.-D., Grosch, W., & Schiberle, P. (2008). *Lehrbuch der Lebensmittelchemie* (6. Auflage). Berlin Heidelberg: Springer Berlin Heidelberg.

Berg, J. M., Tymoczko, J. L., Gatto, G. J. jr., & Stryer, L. (2018). *Stryer Biochemie* (8. Auflage). Heidelberg: Springer Spektrum.

Bisswanger, H. (2000). *Enzymkinetik: Theorie und Methoden* (3. Auflage). Weinheim: Wiley-VCH.

Blumenthal, G., Linke, D., & Vieth, S. (Eds.). (2006). *Chemie - Grundwissen für Ingenieure*. Wiesbaden: Teubner.

Bohnet, M. (2004). *Mechanische Verfahrenstechnik*. Weinheim: Wiley-VCH Verlag GmbH & Co. KGaA.

Bubnik, Z., & Kadlec, P. (1992). Sucrose crystal shape factors. *Sugar Industry*, *117*(5), 345–350.

Butler, M. F., Glaser, N., Weaver, A. C., Kirkland, M., & Heppenstall-Butler, M. (2006). Calcium Carbonate Crystallization in the Presence of Biopolymers. *Crystal Growth & Design*, *6*(3), 781–794. https://doi.org/10.1021/cg050436w

Cardew, P. T., & le, M. S. (1998). *Membrane Processes: A Technology Guide*. Cambridge: The Royal Society of Chemistry.

Cheetham, N. W., Taylor, C., & Walker, G. J. (1985). Application of High-Performance Liquid Chromatography to a Study of Branching in Dextrans. *Carbohydrate research*, *137*, 1–12. https://doi.org/10.1016/0008-6215(85)85144-2

Chen, J. C., & Chou, C. C. (1993). Cane Sugar Handbook: A Manual for Cane Sugar Manufacturers and Their Chemists (12th ed.). New York: John Wiley & Sons.

Chmiel, H. (2011). *Bioprozesstechnik* (3. Auflage). Heidelberg: Springer Spektrum.

Christen, P., Jaussi, R., & Benoit, R. (2016). *Biochemie und Molekularbiologie*. Berlin Heidelberg: Springer Spektrum.

Cockman, M., Kubler, D. G., Oswald, A. S., & Wilson, L. (1987). The Mutarotation of Fructose and the Invertase Hydrolysis of Sucrose. *Journal of Carbohydrate Chemistry*, *6*(2), 181–201. https://doi.org/10.1080/07328308708058870

Cuddihy, J. A., Porro, M. E., & Raiih, J. S. (2001). The Presence of Total Polysaccharides in Sugar Production and Methods for Reducing their Negative Effects. *Journal American Society of Sugarcane Technologists*, *21*, 73–91.

Cussler, E. L. (2009). *Diffusion: Mass transfer in Fluid Systems* (3rd ed.). Cambridge: Cambridge University Press.

Demirel, Y. (2014). Nonequilibrium Thermodynamics: Transport and Rate Processes in Physical, Chemical and Biological Systems (3rd ed.). Amsterdam: Elsevier.

Eggleston, G., & Monge, A. (2005). Optimization of sugarcane factory application of commercial dextranases. *Process Biochemistry*, *40*(5), 1881–1894. https://doi.org/10.1016/j.procbio.2004.06.025

Falconer, D. J., Mukerjea, R., & Robyt, J. F. (2011). Biosynthesis of dextrans with different molecular weights by selecting the concentration of Leuconostoc mesenteroides B-512FMC dextransucrase, the sucrose concentration, and the temperature. *Carbohydrate Research*, *346*(2), 280–284. https://doi.org/10.1016/j.carres.2010.10.024

Gasciolli, V., Choplin, L., Paul, F., & Monsan, P. (1991). Viscous properties and molecular characterization of enzymatically size-controlled oligodextrans in aqueous solutions. *Journal of biotechnology*, *19*, 192–202. https://doi.org/10.1016/0168-1656(91)90058-4

Gasper, H. (Ed.). (2005). *Handbuch der industriellen Fest/Flüssig-Filtration* (2. Auflage). Weinheim: Wiley-VCH.

Geronimos, G. L., & Greenfield, P. F. (1978). Viscosity Increase in Concentrated Sugar Solutions and Molasses due to Dextrans. *Proc. 45th Conf. Queensland*, 119–126.

Hirata, Y., Sano, Y., Aoki, M., Shohji, H., Katoh, S., Abe, J., Yamamoto, H. (2003). Small-angle X-ray scattering studies of moderately concentrated dextran solution. *Carbohydrate polymers*, *53*(3), 331–335. https://doi.org/10.1016/S0144-8617(03)00107-3

ICUMSA (Ed.). (2011). *ICUMSA Method Book*. Berlin: Dr. Albert Bartens KG.

Illanes, A. (2008). *Enzyme Biocatalysis: Principles and Applications* (1st ed.). New York: Springer.

Illanes, A., Wilson, L., & Vera, C. (2014). *Problem Solving in Enzyme Biocatalysis* (1st ed.). West Sussex: John Wiley & Sons.

Kaempfe, P. D. (2011). Kristallisation, Modifikation und Adsorptionseigenschaften von Calciumcarbonat sowie Untersuchungen eines oszillierenden Kristallisationssystems (PhD). Universität Duisburg-Essen, Kiel.

Kärger, J., Ruthven, D. M., & Theodorou, D. N. (2012). *Diffusion in Nanoporous Materials* (1st ed.). Weinheim: Wiley-VCH.

Khalikova, E., Susi, P., & Korpela, T. (2005). Microbial dextran-hydrolyzing enzymes: fundamentals and applications. *Microbiology and Molecular Biology Reviews*, *69*(2), 306–325. https://doi.org/10.1128/MMBR.69.2.306-325.2005

Klemm, D. (2006). *Polysaccharides II* (1st ed.). Berlin Heidelberg: Springer-Verlag.

Larsson, A. M., Andersson, R., Ståhlberg, J., Kenne, L., & Jones, T. (2003). Dextranase from Penicillium minioluteum: Reaction Course, Crystal Structure, and Product Complex. *Structure*, *11*(9), 1111–1121. https://doi.org/10.1016/S0969-2126(03)00147-3

Lechner, M. D., Gehrke, K., & Nordmeier, E. H. (2010). Makromolekulare Chemie: Ein Lehrbuch für Chemiker, Physiker, Materialwissenschaftler und Verfahrenstechniker (4. Auflage). Basel: Birkhäuser Basel.

Lee, G., Nowak, W., Jaroniec, J., Zhang, Q., & Marszalek, P. E. (2004). Molecular dynamics simulations of forced conformational transitions in 1,6-linked polysaccharides. *Biophysical Journal*, *87*(3), 1456–1465. https://doi.org/10.1529/biophysj.104.042879

Letcher, T., Teja, A. S., & Rousseau, R. W. (Eds.). (2004). *Chemical thermodynamics for industry*. Cambridge: RSC.

Mathlouthi, M., & Reiser, P. (1995). *Sucrose Properties and Application: Properties and Application* (1st ed.). Frimley: Blackie Academic & Professional.

Mersmann, A. (2001). *Crystallization technology handbook* (2nd ed.). New York: Marcel Dekker.

Mikkelsen, S. R., & Cortón, E. (2004). *Bioanalytical chemistry*. Hoboken N.J.: John Wiley & Sons.

Morris, G. A., & Ralet, M.-C. (2012). The effect of neutral sugar distribution on the dilute solution conformation of sugar beet pectin. *Carbohydrate polymers*, *88*(4), 1488–1491. https://doi.org/10.1016/j.carbpol.2012.02.020

Mukherjee, S. (2011). Applied Mineralogy: Applications in Industry and Environment. New Dehli: Springer Netherlands.

Mullin, J. W. (2001). *Crystallization* (4th ed.). Oxford: Butterworth-Heinemann.

Norton, I. T., Spyropoulos, F., & Cox, P. (2011). *Practical food rheology: An interpretive approach*. West Sussex: Wiley-Blackwell.

Ohlrogge, K., & Ebert, K. (Eds.). (2006). *Membranen: Grundlagen, Verfahren und industrielle Anwendungen*. Weinheim: Wiley-VCH Verlag GmbH & Co. KGaA.

Promraksa, A. (2008). *Reduction of Dextran Contamination in Raw Sugar Production* (PhD). Suranaree University of Technology, Nakhon Ratchasima.

Rehfeldt, S. (2009). *Mehrkomponentendiffusion in Flüssigkeiten* (PhD). Technische Universität München, München.

Renkin, E. M. (1955). Filtration, Diffusion and Molecular Sieving Through Porous Cellulose Membranes. *J. Gen. Physiol.*, *38*, 224-242.

Robyt, J. F., Yoon, S.-H., & Mukerjea, R. (2008). Dextransucrase and the mechanism for dextran biosynthesis. *Carbohydrate Research*, *343*(18), 3039–3048. https://doi.org/10.1016/j.carres.2008.09.012

Sawada, K. (1997). The mechanisms of crystallization and transformation of calcium carbonates. *Pure and Applied Chemistry*, *69*(5), 921–928. https://doi.org/10.1351/pac199769050921

Schaber, S., & Mayinger, S. (2010). *Thermodynamik: Band 2: Mehrstoffsysteme und chemische Reaktionen* (15. Auflage). Heidelberg: Springer.

Schubert, H. (2012). *Handbuch der Mechanischen Verfahrenstechnik*. Hoboken: John Wiley & Sons.

Storhas, W. (2013). *Bioverfahrensentwicklung* (2. Auflage). Weinheim: Wiley-VCH Verlag GmbH & Co. KGaA.

Tien, C. (2012). *Principles of Filtration* (1st ed.). Oxford: Elsevier.

Tsuchiya, H. M., Hellman, N. N., Koepsel, H. J., Corman, J., Stringer, C. S., Rogovin, S. P., Jackson, R. W. (1955). Factors Affecting Molecular Weight of Enzymatically Synthesized Dextran. *Journal of the American Chemical Society*, *77*(9), 2412–2419. https://doi.org/10.1021/ja01614a016

Tvaroska, I., Pérez, S., & Marchessault, R. (1978). Conformational Analysis of (1->6)-alpha-D-Glucan. *Carbohydrate research*, *61*, 97–106. https://doi.org/10.1016/S0008-6215(00)84470-5

Van der Poel, P. W., Schiweck, H., & Schwartz, T. (1998). *Sugar Technology: Beet and Cane Sugar Manufacture*. Berlin: Dr. Albert Bartens KG.

Vavrinecz, G. (1965). *Atlas der Zuckerkristalle*. Berlin: Verlag Dr. Albert Bartens.

Vedantam, S., & Ranade, V. (2013). Crystallization: Key thermodynamic, kinetic and hydrodynamic aspects. *Sadhana*, *38*(6), 1287–1337. https://doi.org/10.1007/s12046-013-0195-4

Viswanath, D. S., Ghosh, T. K., Prasad, D. H. L., Dutt, N. V. K., & Rani, K. Y. (2007). *Viscosity of Liquids: Theory, Estimation, Experiment, and Data*. Dordrecht: Springer.

Wittenberg, A. (2000). *Beitrag zur Optimierung der teschnischen Saccharosekristallisation* (PhD). Technische Universität Berlin, Berlin.

Wojtczak, M., Gruska, R., MIkos, P., Antczak-Chrobot, & Aneta (2015). Dextran molecular mass effect on particle size distribution of CaCO3 for 1st and 2nd carbonatation. *Sugar Industry*, *140*(11), 703–706.

3 Effect of Dextran and Enzymatically Decomposed Dextran on Calcium Carbonate Precipitation

Abraham, K. [a b], Splett, L. [a], Köster, E. [a], Flöter, E. [a]

[a] TU Berlin, Department of Food Process Engineering, Seestraße 13, 13353 Berlin, Germany

[b] SternEnzym, Kurt-Fischer-Str. 55, 22926 Ahrensburg, Germany

Originally published in the Journal of Food Process Engineering (2019).

https://doi.org/10.1111/jfpe.13072

Abstract

The effect of dextran's molecular mass distribution (T40, T500, T2000 and enzymatically decomposed T2000) on the size and shape of calcium carbonate particles precipitated during carbonation, a step in the sugar manufacturing process, was investigated. Image analysis combined with size exclusion chromatography (SEC) were used to distinguish harmful and harmless dextran sizes aiming at targeted mitigation of dextran-related effects by dextranase. The data indicate that dextran with molecular masses above 10 kDa promotes agglomeration, indicated by an increase in particle projection area. This effect was especially found for broadly distributed intermediate but rather low molecular mass dextran (10 kDa to 85 kDa). Based on particle shape data, the agglomeration of calcium carbonate crystals in the absence and in the presence of low molecular mass dextran (< 85 kDa) appears to be oriented and similar to each other. In contrast, the data suggest that high molecular mass dextran (>85 kDa) promotes non-oriented agglomeration and an increase in surface roughness. Once dextran was significantly decomposed by enzyme action (10 or 50 mg/kg juice) to smaller molecules in the size range below 10 kDa, no dextran-related effects on particle size and shape were found anymore.

3.1 Introduction

The presence of polysaccharides in sugar cane and beet juices can diversely affect sugar manufacture. In beet juices, the disadvantageous presence of polysaccharides is mainly initiated by exposure of beets to freeze-thaw cycles. The associated beet cell wall destruction leads, on the one hand, to a more pronounced solubilisation of cell wall components (mainly pectin) and, on the other hand, gives microorganisms access to infestation. Microbial contamination of beet cells or juices inter alia results in the formation of dextran with broad molecular mass distributions. Lactic acid bacteria, mainly *Leuconostoc mesenteroides* species, produce the enzyme dextransucrase, which catalyses dextran formation due to sucrose hydrolysis and glucose polymerisation. Thus, dextran molecules are homogenously composed of glucose monomers, which are mainly linked via α-(1→6) glycosidic linkages (van der Poel et al., 1998). Besides, sugar industry relevant species are known to produce dextran with up to 5 % branching points via α-(1→2), α-(1→3) and α-(1→4) glycosidic linkages (Khalikova et al., 2005). The presence of dextran in sugar beet juices is currently gaining in importance due to prospective prolongations of sugar beet campaigns as a result of changes of the European legislation in 2017 (Adjari Rad et al., 2014).

Dextran produced in cane and beet juices is generally of relatively high average molecular mass and high polydispersity. Thus, it is known that dextran with molecular masses ranging between 15 kDa to 2,000 kDa can occur in cane and beet juices (Chen & Chou, 1993). Besides, two major groups could be identified, consisting of a lower and a higher dextran fraction of molecular masses in the 10^1 kDa- and 10^3 kDa-range, respectively. A rather low occurrence rate of intermediate dextran fractions in the 10^2 kDa-range was additionally found (Aquino & Franco, 2009). The latter is particularly gaining in importance when gradually decomposing high molecular mass dextran by dextranase (Eggleston et al., 2009).

Apart from the dextran concentration as a key parameter, the dextran-related process problems also depend on the molecular mass distribution present. The latter has especially gained interest in previous work, in which interactions between dextran fractions with high and low molecular masses were assumed (Abraham et al., 2019).

Up to now, there has been general agreement that high molecular mass dextran is mainly responsible for a viscosity increase adversely affecting the filtration, evaporation as well as the crystallisation rate during sugar manufacture (Chen & Chou, 1993). Besides, high as well as low molecular mass dextran fractions have been found to modify the size and shape of sucrose crystals during crystallisation (Abdel-Rahman, 2007). Furthermore, particle formation during juice purification by means of lime and carbon dioxide appears to be influenced by dextran (Wojtczak et al., 2015).

However, there is still insufficient understanding of the specific role of high and low molecular mass dextran fractions and especially of the polydispersity of dextran during the purification

process. It is, however, necessary to design specific mitigation actions on dextran contamination by enzymatic decomposition.

In this procedure, the raw juice is progressively limed in order to stepwise precipitate certain non-sugars. This is followed by a dramatic increase of the pH value and alkalinity in the main liming step, which aims at the decomposition of invert sugar and amides. The subsequent addition of carbonation gas (CO_2) leads to the conversion of calcium hydroxide and carbon dioxide to calcium carbonate and water. Once calcium carbonate crystals have formed, they also serve as adsorbents for non-sugars (Asadi, 2007). This results in a polydisperse system containing calcium carbonate crystals, their aggregates as well as adsorbed non-sugars (Sarka, E. Bubnik, Z. Hinkova, A., 2006). The calcium carbonate crystals with adhering non-sugars are subsequently separated from the juice by settling and filtration. The filtrate is known as the thin juice, which is preferably of a high purity, low colour and good thermostability (Asadi, 2007).

During this procedure, the flow behaviour as well as the particle characteristics are decisive for the process execution and purification performance. A modified flow behaviour of the continuous phase of the carbonation slurry can influence reaction rates during purification as well as the flow through filter and cake pores during subsequent filtration. Changes in particle size and shape can obviously affect the adsorption surface for non-sugars and thus the actual purification effect (Sarka, E. Bubnik, Z. Hinkova, A., 2006). Besides, subsequent filtration can also be impaired by modified particle sizes leading to modified filter cake pore structures (Schubert, 2012).

On the one hand, Hein et al. stated that the above-mentioned viscosity increase can contribute to particle size modifications (Hein et al., 2012). On the other hand, Kontrec et al. observed dextran adsorption on the mineral surface of calcium carbonate, which has been assumed to be related to hydrogen-bonds between the oxygen ion of the hydroxyl groups of dextran molecules and the calcium ions (Kontrec et al., 2011). Both aspects, a viscosity increase as well as interactions with the surface of growing calcium carbonate crystals, could hence be instrumental in dextran-induced modifications of calcium carbonate crystals and their agglomerates.

Dextranase from various microbial origins can be used to depolymerise high molecular mass dextran to smaller, preferentially harmless low molecular mass dextran fragments. However, a controlled and targeted enzyme application is still not established practice. Harmless molecule sizes, and therefore the target of dextranase applications, need still to be identified. Assuming that the decomposition follows a gradual decrease of the molecular mass, as Eggleston et al. stated, decomposition products with intermediate molecular masses need to be considered as well (Eggleston & Monge, 2005). An insufficient decomposition could only transform the processing problems during sugar manufacture, instead of solving them. Thus, for targeted mitigation of dextran contaminations by enzymatic decomposition, the specific role of different molecular mass

fractions as well as the polydispersity of the molecular mass distribution need to be understood. Only then, enzyme application can be accomplished in a targeted manner.

While there is broad consensus about dextran-related viscosity effects, the mechanisms of dextran-induced particle modifications depending on its level and molecular mass distribution have not been investigated in detail yet. This endeavour is burdened with the challenge of accurately analysing the particle characteristics, either single crystals or agglomerates. In the past, laser diffraction was often used to analyse dextran-induced modifications of the size distribution of calcium carbonate particles (Wojtczak et al., 2015). This method is, however, afflicted with some disadvantages when analysing irregular particle shapes. Laser diffraction algorithms generally assume spherical shapes making it prone to misinterpretations. When analysing non-spherical particles, the evaluation is also affected by the orientation of the particles to be analysed, which is reported to be affected by the flow of the dispersion medium. Besides, the usage of dispersing units entails the danger of modifying the particle characteristics during sample preparation (Gabas et al., 1994). This widely used method is hence a good tool to analyse the size distribution of rather regularly sphere-shaped particles, but it is of limited value to analyse the size and especially the shape of rather irregular particle shapes. Interdisciplinary, image analysis is a widely used tool for particle size and in particular for particle shape analysis. Depending on the scale considered, the particle shape is determined by the form (large scale) as well as the surface roughness (small scale), for which several parameters can be used as indicators (Liu et al., 2015).

The work presented aims at specifically analysing dextran-induced modifications of particles precipitated during carbonation as a part of the sugar beet raw juice purification. This study mainly focuses on effects due to dextran fractions with varying molecular mass distributions. This also includes molecular mass variations due to enzymatic decompositions using different enzyme levels. On the one hand, this approach necessitates chromatographic analysis to characterise the different dextran fractions as well as enzymatically decomposed dextran. On the other hand, two-dimensional static image analysis based on light microscopy was key to this study to determine size and shape distributions of the precipitated particles contained in the carbonation slurries. For the more challenging shape analysis, parameters relating to the particle form as well as the surface texture were considered (circularity, roundness, solidity). In doing so, this study aims at unravelling the relation between the molecular mass distribution of dextran and the crystallisation and/or agglomeration of calcium carbonate crystals.

3.2 Material and Methods

3.2.1 Materials

The specific effects of dextran fractions with varying molecular mass distributions on the size and shape of calcium carbonate particles were investigated using laboratory carbonation tests. A

synthetic thin juice of 15 % (m/m) refined sucrose (Nordzucker, extra-white sugar) was used. Dextran fractions with mass-average molecular masses of 2,000 kDa (T2000: Sigma-Aldrich, dextran with a molecular mass distribution ranging from 1,500 to 2,800 kDa), 500 kDa (T500: Carl Roth, dextran 500) and 40 kDa (T40: Carl Roth, dextran 40) were used. All dextran fractions originate from the lactic acid bacteria *Leuconostoc Mesenteroides* strain B512. Milk of lime (Grüssings, milk of lime 120 g CaO/L) and carbonation gas (Linde, carbon dioxide) with a purity > 99.5 % were used.

For the enzymatic decomposition of the T2000 dextran fraction, a non-genetically modified dextranase originating from a *Chaetomium gracile* strain (Sugazym DX L, SternEnzym) was used. Its temperature and pH optimum range from 328 K to 338 K and from 4 to 7, respectively. The enzyme is known to specifically and randomly hydrolyse α-(1→6) glycosidic linkages in dextran molecules (Khalikova et al., 2005). According to the manufacturer, the activity of this dextranase is 7000 U/g. Here, one dextranase unit refers to the activity of the amount of enzyme which liberates one micromole isomaltose per minute under specific conditions (pH 6.0, 310 K, reaction time of 30 min, 2 % (m/m) dextran 500).

3.2.2 Enzyme Reaction

Aqueous sucrose solutions containing T2000 dextran were incubated using varying enzyme levels. Incubation of these samples took place in a shaking water bath in order to ensure good mixing. Temperature was monitored and the respective enzyme level was dosed once the desired temperature of 328 ± 1 K was reached. This is defined as the starting point of the enzymatic decomposition process. The enzymatic reaction was terminated after 10 minutes by thermal inactivation, for which the samples were kept at a temperature of 353 K ± 1 K using a second water bath for 20 min. Prior to chromatographic analysis, the samples were cooled to room temperature. Previous experiments verified that dextran remains well-dissolved during this procedure. In general, every enzyme reaction was performed in duplicate.

3.2.3 Chromatographic Analysis

Chromatographic analysis in aqueous solutions was performed using high pressure liquid chromatography (Chromaster system, Hitachi) equipped with an evaporative light scattering detector (ELSD 90 LT-Low Temperature, VWR). Two polymeric size exclusion columns with a separation range of 0.1 kDa to 70 kDa (ABOA SuperOH-P-250, AppliChrom) and 2.5 kDa to 1,000 kDa (ABOA SuperOH-P-350, AppliChrom) were applied in series to enhance separation based on size exclusion. The mobile phase was distilled water and kept constant according to an isocratic application. The flow rate was set to 1 ml/min and the injection volume was 20 µl. The temperature of the oven and the detector were set to 293 K and 323 K, respectively. Calibration for molecular

mass analysis was performed using pullulan standards of low polydispersity (Pulkit 08, Polymer Standard Service), see Figure 3-1.

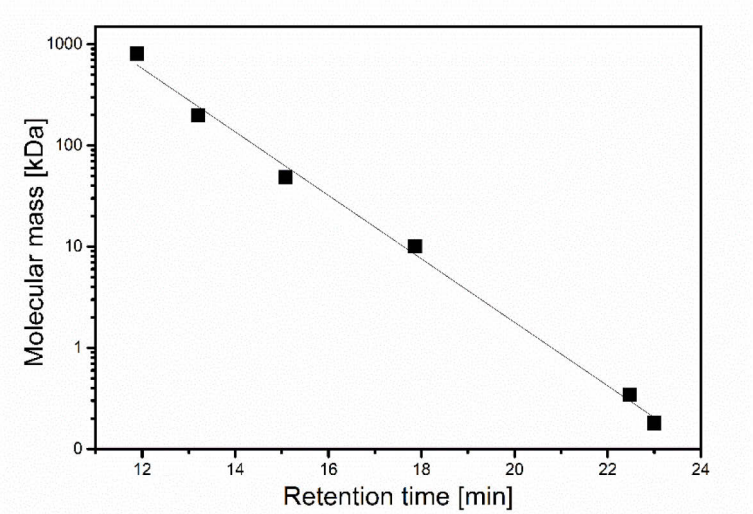

Figure 3-1 SEC-calibration data. Molecular mass as a function of the retention time deduced from calibration using two polymeric size exclusion columns (ABOA SuperOH-P-250 and ABOA SuperOH-P-350, AppliChrom).

The chromatograms of each duplicate determination were subsequently analysed using the Peakfit software 4.12. In doing so, broad and multiple peaks could be separated by using a manually modified deconvolution method. The peaks were described by Gaussian peaks at their local maxima. If necessary, when two peaks were not completely separated, two different Gaussian peaks were separated at the so-called valley in between these two peaks. The peak width of the single peaks was adapted in a way that the total area under the chromatogram was completely covered. To exclude noise of the baseline in the data processing, a fixed minimum amplitude was set.
The area A_i and molecular masses M_i of the individual peaks were determined. Subsequently, these were used to calculate the average molecular masses of the sample according to equation (3-1). M_i was obtained from relating the maximum respective peak retention time to the pullulan calibration curves (see Figure 3-1).

$$Average\ molecular\ mass = \Sigma \frac{A_i}{A_{total}} * M_i \tag{3-1}$$

3.2.4 Juice Purification on Laboratory Scale

3.2.4.1 Juice Purification Plant

The juice purification experiments were performed in a 1 liter lab-scale, double-walled glass cylindrical vessel. The temperature was controlled by a hot water flow through the double wall jacket of the vessel. A thermostat (Julabo, F12-ED) was used to keep the heating medium at the desired temperature. To allow a rapid temperature change from pre-liming to main-liming a second thermostat (Julabo, F32-ME) was connected via a three-way valve. A blade stirrer with holes

connected to an agitator (RZR 2102 control, Heidolph Instruments GmbH & Co. KG) ensured appropriate mixing inside the vessel. Process control was maintained by a Pt100 thermo-element and a pH electrode (Mettler Toledo, InLab Expert Pro) immersed in the juice. A second glass pH electrode was used to determine the pH value at 393 K after rapid cooling of the sample in an ice bath. Milk of lime was added volumetrically into the opening of the vessel using a plastic syringe meeting the targeted pH values. A pressure reducing valve and a flow meter were used to set and control the carbon dioxide flow passing through the gas piping ending in a perforated ring on the bottom of the vessel. Sampling and discharge of the slurry were done via the outlet valve at the vessel's bottom. Separations of particles precipitated were performed using vacuum filtration with filter papers of defined pore sizes (Schleicher & Schnell, filter paper circles 589 black ribbon, particle retention of 12-25 µm).

3.2.4.2 Process Execution

The juice purification process includes liming and carbonation, further sub-divided into pre- and main-liming as well as first and second carbonation. During the first step of pre-liming, the temperature was set to 328 K and milk of lime was gradually added according to a specific pattern necessary for progressive precipitation of certain non-sugars. The temperature as well as the pH value were continuously monitored during the process. For verification purposes, pH-determination at 293 K was performed after sampling and rapid cooling in an ice bath. The final pH value of the pre-limed juice was set between 11.0 and 11.4 (293 K). To initiate the main-liming step, an even higher alkalinity and pH value as well as a higher temperature are required. By adding the required amount of lime all at once, an alkalinity of 0.8 to 1.0 g CaO/100 ml and pH values of 12 to 12.5 were achieved. After the addition of milk of lime, the temperature was increased to 358 K. A holding phase of 20 min completed the main liming step. The first carbonation was initiated by the introduction of carbon dioxide. Continuous gassing for 10 min reduced the pH to the targeted value of 11.0 to 11.4 (293 K). And again, pH values were determined at 293 K via sampling and rapid cooling in an ice bath. The particles precipitated during carbonation were separated by vacuum filtration. Prior to the filtration, samples for particle analysis were taken from the slurry. The filtrate obtained is usually subjected to a second carbonation and filtration to produce actual industrial thin juice. This, however, was not investigated in the current study. Multiple determination was selectively performed. Therefore, the juice purification of the dextran-free reference was performed eightfold. Additionally, the T2000 dextran loaded sample was performed fourfold. The process for all other samples was performed in duplicate.

3.2.5 Static Image Analysis

Light microscopic images of the particles precipitated during first carbonation were recorded by Zeiss-Axio Scope A1 microscope and subsequently analysed by ImageJ. The samples for image

analysis were taken directly from the slurry and subsequently diluted 1 to 4 with distilled water to separate single calcium carbonate particles and agglomerates in order to avoid artefacts. Prior to the actual particle size and shape analysis, image editing and calibration are necessary prerequisites, illustrated in Figure 3-2. Thereby, a threshold was set and the function 'fill holes' were used to fill the background of the particles. Besides, particles were smoothed and isolated pixels were removed by the function 'open' and 'close'. This way, the original microscopic images (Figure 3-2 (A)) were transferred to black and white images with two-dimensional particles, as shown in Figure 3-2 (B). To exclude unrealistically perfectly round particles, the circularity was furthermore limited to a maximum value of 0.95.

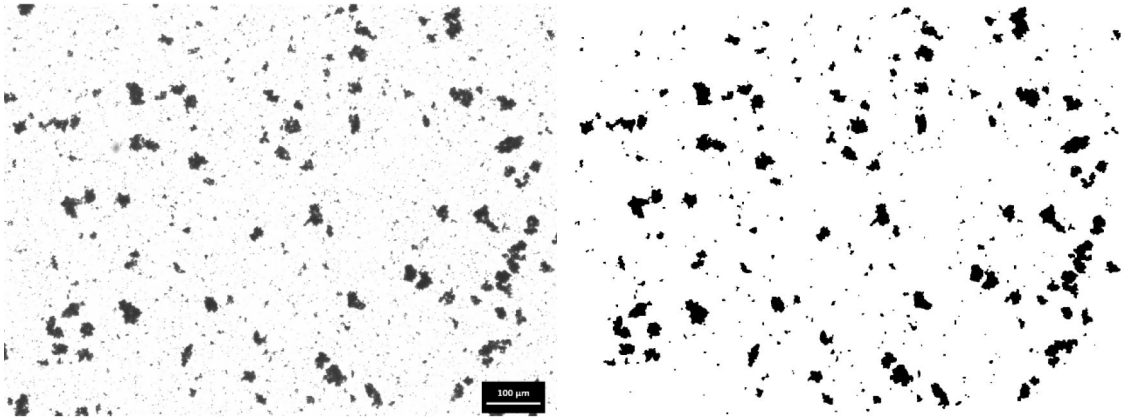

Figure 3-2 Image editing as a part of the static image analysis for the analysis of calcium carbonate particles contained in the carbonation slurry. A) Original light microscopic image. B) Light microscopic image after image editing.

To analyse the particle size distribution, the particle projection area, expressed as average values and relative frequencies according to four categories (<50 µm^2, 50 to 100 µm^2, 100 to 500 µm^2 and >500 µm^2), was evaluated.

The particle shape is affected by two major factors, the particle form and the surface roughness. Thus, parameters indicating changes in either or both form and roughness were taken into account. In this study, the circularity was primarily used to detect changes of the particle shape, which is affected by both particle form and roughness, see equation (3-2). A perfect circle has a circularity of 1.

$$Circularity = 4\pi \frac{Area}{Perimeter^2} \tag{3-2}$$

According to Liu et al., the roundness as well as the solidity are useful indicators for changes in particle form and roughness, respectively (see equation (3-3) and (3-4)) (Liu et al., 2015).

$$Roundness = 4 \times \frac{Area}{\pi \times [Major\ axis]^2} \tag{3-3}$$

$$Solidity = \frac{Area}{Convex\ Area} \tag{3-4}$$

The data corresponding to the shape parameters are depicted as total and area-related averaged values.

3.3 Results and Discussion

3.3.1 Chromatographic Analysis

3.3.1.1 Characterisation of the Different Dextran Fractions

Figure 3-3 (A) shows the chromatograms of the different non-decomposed molecular mass dextran fractions. For all dextran fractions, a constant dextran level of 5000 mg/kg sucrose was added, which represents relatively high but still realistic dextran contents in contaminated sugar raw juices. A secondary x-axis relates the molecular masses to the respective retention times as deduced from the calibration using pullulan standards and size-exclusion columns with defined separation ranges (see Figure 3-1). As usual, the retention time increases with decreasing molecular mass. Thus, large molecules, such as T2000 dextran, elute first (continuous line). The broad and overlapping peaks of the T2000 chromatogram suggest a relatively high polydispersity, covering a molecular mass range from 60 kDa to 3000 kDa, according to the calibration system used. The analysis of T40 dextran indicates a monomodal, but still relatively broad main peak (dashed line), covering a range from 3 kDa to 100 kDa. Even though T2000 and T40 dextran fractions are obviously composed of molecules with different molecular masses, the proximity of the peaks indicates that T40 and T2000 dextran fractions partially comprise dextran molecules of similar molecular masses. Surprisingly, the dextran fraction with an intermediate average molecular mass of 500 kDa (T500) shows an even higher polydispersity (dashed-dotted line), spanning over the molecular mass range of both, T2000 and T40 (3 kDa to 3000 kDa). The equal-mass mixture of the T2000 and T40 dextran fraction consistently also covers both individual fractions (dotted line), but with a higher load of intermediate but rather low molecular mass dextran fragments (in the range of 85 kDa to 3 kDa) in comparison with T500 dextran.

3.3.1.2 Characterisation of Enzyme Reaction Products

Figure 3-3 (B) shows the chromatograms of the reaction products resulting from the enzymatic decomposition of T2000 dextran at 328 K and pH 6 for 10 min. Under these conditions - optimal for the dextranase activity according to the supplier – the effect due to varying enzyme levels was investigated. Obviously, the increase of the enzyme level leads to a gradual decrease of the molecular mass indicated by a successive shift of the peaks towards higher retention times. Thus, high molecular mass dextran molecules were gradually converted into smaller molecules. The application of a comparatively low dextranase level of 4 mg/kg juice on a rather high T2000 content of 5000 mg/kg sucrose resulted in broadly distributed low molecular mass dextran fragments (dashed line in Figure 3-3 (B)). According to the secondary x-axis deduced from the calibration

system described above, these reaction products covered a molecular mass range of 2 kDa to 300 kDa. From the chromatogram in Figure 3-3 (B), two main peaks can be identified. The maximum of the first and second peak can be assigned to a molecular mass of approximately 85 kDa and 10 kDa, respectively. Interestingly, apart from the relatively high molecular masses above 300 kDa, the chromatogram of these reaction products is quite similar to that of the non-decomposed equal-mass mixture of the T40 and the T2000 dextran fraction.

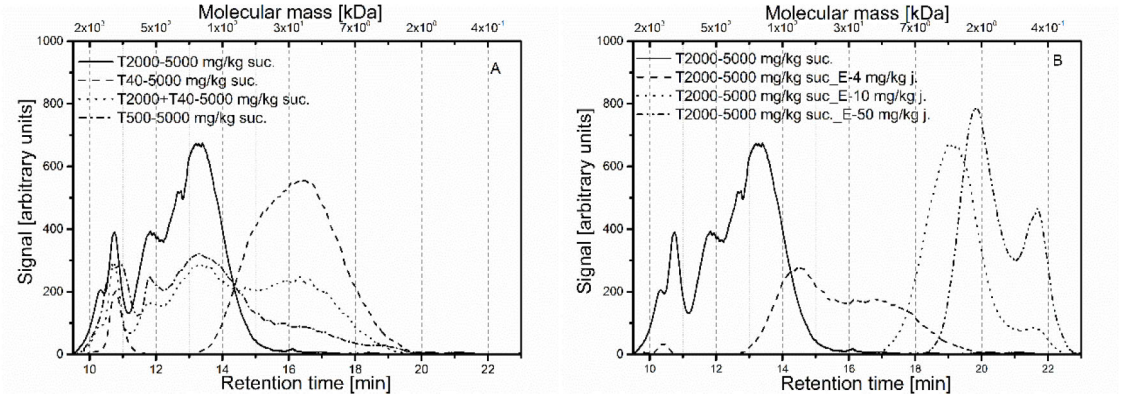

Figure 3-3 SEC-Chromatograms of dextran fractions with varying molecular mass distributions. A) Non-decomposed dextran fractions (continuous line-T2000, dashed line-T40, dash-dot line-T500, dotted line-equal-mass mixture of T2000 and T40). B) Enzymatically decomposed T2000 dextran (continuous line-initial T2000 substrate, dashed line-enzyme level of 4 mg/kg j., dotted line-enzyme level of 10 mg/kg j., dash-dot-dot line-enzyme level of 50 mg/kg j.).

The application of higher enzyme levels of 10 mg/kg juice resulted in a distinctly progressed decomposition. The data suggest more clearly a bimodal distribution, whereby the maximum of the main peak relates to a molecular mass of about 3 kDa. The smaller side peak indicates the additional presence of molecules possessing a molecular mass of about 0.6 kDa. Overall, the curve deviates from the base line at retention times belonging to molecular masses ranging from 0.4 kDa to 10 kDa. Similarly, the application of a higher enzyme level of 50 mg/kg juice leads to an even further shift of the main peak towards higher retention times corresponding to a molecular mass of 2.3 kDa (peak maximum). Besides, the side peak indicating a molecular mass of 0.6 kDa is distinctly increased. In this case, signals were obtained at retention times corresponding to molecular masses of 0.4 kDa to 5 kDa. Thus, the increase of the enzyme level leads to a gradual reduction of the average molecular mass, resulting in reaction products of low molecular mass and reduced polydispersity.

3.3.2 Particle Analysis

3.3.2.1 Particle Size Analysis

3.3.2.1.1 Average Particle Projection Area

The dextran fractions with varying molecular mass distributions described above were used to study the effect of dextran's molecular mass distribution on the size and shape of calcium carbonate particles precipitated during carbonation. A constant dextran level of 5000 mg/kg sucrose was considered. Figure 3-4 (A) shows the average values of the projection area of calcium carbonate particles precipitated in the presence of the different dextran fractions. It illustrates an increase in the average area for either dextran addition in comparison with the dextran-free reference. However, the extent of this increase in area appears to correlate with the molecular mass distributions present. At this certain dextran level of 5000 mg/kg sucrose, the effect of T40 and T2000 dextran on the average area seems to be quite similar, both fractions caused roughly a doubling compared to the reference (increase from 125 μm^2 to about 230 μm^2). Interestingly, the presence of T500 dextran caused an even stronger increase in the average area, to 325 μm^2. As mentioned above, this fraction is characterised by a distinctly higher polydispersity in comparison with the individual T2000 and the T40 dextran fraction, as deduced from the chromatograms in Figure 3-3 (A). The presence of the equal-mass mixture of T2000 and T40 dextran leads to an even higher average area, tripled in comparison with the reference (375 μm^2). As elucidated above, this equal-mass mixture is characterised by a molecular mass distribution similar to the T500 dextran fraction, but contains a distinctly higher amount of low molecular mass dextran fractions in the range of 85 kDa to 3 kDa. Thus, the dextran-related increase in the average area appears to correlate with the molecular mass distribution present. For one thing, the data suggest that an increase in the polydispersity resulted in a systematic increase in the average particle projection area. Besides, the presence of intermediate but rather low molecular mass dextran fractions (85 kDa to 3 kDa) seems to additionally promote the increase in the average area and thus the agglomeration of calcium carbonate crystals.

Figure 3-4 (A) additionally shows the average area of the particles precipitated during carbonation in the presence of enzymatically decomposed T2000 dextran using the above-discussed enzyme levels (4, 10 and 50 mg/kg juice). The presence of the reaction products, obtained from the application of the low dextranase level of 4 mg/kg juice to T2000 dextran contaminated juice, resulted in an even further increase in the average area of the calcium carbonate particles. The average area determined is, however, relatively similar to that obtained in the presence of the equal-mass mixture of T2000 and T40.

As already pointed out, apart from really high molecular masses above 300 kDa, the chromatograms of these two samples (see Figure 3-3 above), non-decomposed equal-mass mixture (3 kDa to 3000 kDa) and enzymatically decomposed T2000 by 4 mg/kg juice (2 kDa to 300 kDa), are quite

similar. This indicates again that the above-mentioned intermediate but rather low molecular mass dextran fragments additionally exacerbated the dextran-promoted agglomeration. During carbonation of the juices that have been treated with the two higher enzyme levels of 10 and 50 mg/kg juice - reduced dextran molecular masses ranging from 0.4 kDa to 10 kDa and 0.4 kDa to 5 kDa, respectively - the average areas of the resulting calcium carbonate particles approached the reference value (Figure 3-4 (A)).

Conclusively, the increase in the average projection area of the calcium carbonate particles appears to depend on the polydispersity of the dextran present. It was most pronounced for broadly distributed dextran molecules of intermediate but rather low molecular masses roughly ranging from 10 kDa to 10^2 kDa.

3.3.2.1.2 Relative Frequency Calculation of the Particle Projection Area

For a better understanding of the data previously cumulated in average values, relative frequencies relating to four different area categories (<50 μm^2, 50 to 100 μm^2, 100 to 500 μm^2 and >500 μm^2) were calculated. The relative frequencies for particles precipitated in the presence of the different non-decomposed dextran fractions are shown in Figure 3-4 (B). The presence of T40 dextran resulted in a shift to larger particles. The occurrence of particles with areas between 100 and 500 μm^2 and particles with areas of more than 500 μm^2 were both increased, each by 5 to 7 %. For the particle sizes of more than 500 μm^2, this equals a twofold increase. Obviously, this increase in large-area particles was at the expenses of particles with smaller areas, both categories were reduced by 5 to 7 %, respectively.

Similar effects were observed for particles contained in T2000 dextran loaded carbonation slurries, whereby the changes for the respective categories marginally moved further to larger particle sizes. The presence of the equal-mass mixture of T2000 and T40 dextran caused reductions of the particles belonging to the two small-area-categories similar to those caused by the individual T2000 and T40 dextran fractions (<50 μm^2 and 50 to 100 μm^2). Interestingly, the amount of particles with areas between 100 and 500 μm^2 is not apparently affected. Instead, the equal-mass mixture caused a dramatic increase of the amount of large particles with areas of more than 500 μm^2, by 15 %. The same trend could be observed for the polydisperse T500 dextran fraction, also resulting in a significant increase of large particles (13 %). Thus, in case of broad distributions, a distinctly higher amount of particles with really high areas (> 500 μm^2) could be observed, which is in good agreement with the increase in the average area discussed above.

Figure 3-4 (C) shows the relative frequency calculation of particles precipitated in the presence of the enzymatically decomposed T2000 dextran. In this case both, the non-contaminated juice and the non-treated T2000 contaminated juice serve as reference.

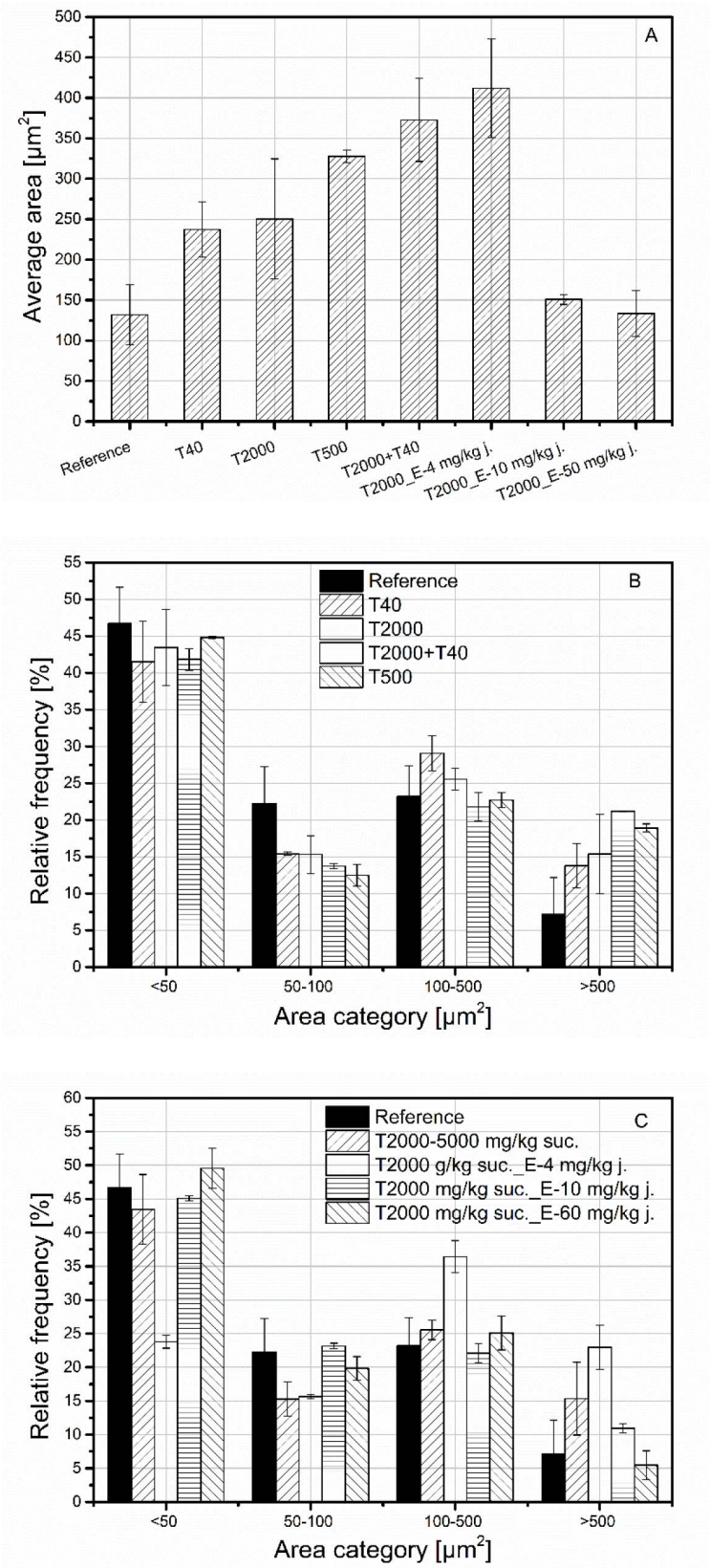

Figure 3-4 Projection area of calcium carbonate particles. A) Total average values. B) Relative frequencies according to four area-categories for the different dextran fractions. C) Relative frequencies according to four area-categories for enzymatically decomposed T2000 dextran.

In line with Figure 3-4 (A), most dramatic effects were found for juices treated with 4 mg enzyme per kg juice. The occurrence of small particles (areas lower than or equal to 50 μm^2) was halved compared to both references. For the sample containing mildly decomposed dextran, the highest proportion is in the size range between 100 μm^2 and 500 μm^2 (36 %). The percentage increase is, however, most prominent, for particles with areas above 500 μm^2 , plus 18 %. In contrast to Figure 3-4 (A), the relative frequency calculation indicates a clear distinction between the effects of the equal-mass mixture of T2000 and T40 contamination and the mildly decomposed T2000.

With increased progression of the decomposition reaction (enzyme level of 10 and 50 mg/kg juice), it was observed that the profile of the calcium carbonate particle sizes approached that of the dextran-free reference. Thus, the presence of broadly distributed molecular masses comprising intermediate but rather low dextran fractions again caused most pronounced effects on the relative frequency distribution of the particle projection area. Consequently, the average value as well as the relative frequency calculation illustrate that too low dextranase-to-dextran ratios, or for that matter reaction times, could result in an insufficient decomposition of dextran. Reaction products of molecular masses in the range of 10 to 85 kDa actually seem to exacerbate the dextran-related size increase of calcium carbonate particles.

Conclusively, all dextran fractions lead to higher amounts of large-sized particles at the expense of small-sized particles, indicating pronounced agglomeration. However, significant differences arose due to increasingly broad molecular mass distributions and in particular due to the presence of intermediate but rather low molecular mass dextran fractions. Due to the number-based evaluation, this effect is probably even underrepresented. Pronounced agglomeration of calcium carbonate crystals during the industrial sugar beet raw juice purification can obviously affect the adsorption surface for other non-sugars and thus the actual purification performance. The actual consequences for industrial practice need, however, to be elucidated in more detail, which is beyond the scope of the study presented. Nevertheless, in line with the findings of this study, Kontrec et al. also found irregular aggregation of calcium carbonate crystals with high specific surface areas and broad size distributions due to the presence of dextran (Kontrec et al., 2011). Thus, the data obtained confirm the general effect of agglomeration, but additionally reveal a specific dependency on the molecular mass distribution of dextran.

3.3.2.2 Particle Shape Analysis

3.3.2.2.1 Average Circularity

The circularity, defined by equation (3-1) above, is affected by changes of both, the particle form and surface roughness (Liu et al., 2015). Figure 3-5 shows the total average circularity of particles contained in the dextran-free and dextran-loaded samples discussed above. It illustrates that the average circularity generally slightly decreased due to either dextran addition, mind the scale of the

y-axis. However, the extent of this decrease in average circularity is again subject to dextran's molecular mass distribution present. Among the non-decomposed dextran-loaded samples, the biggest drop can be seen for T40 dextran loaded samples and for the equal-mass mixture of T2000 and T40 dextran (from 0.69 to 0.64). The average value of the circularities of calcium carbonate particles precipitated in the presence of enzymatically decomposed T2000 dextran are also shown in Figure 3-5.

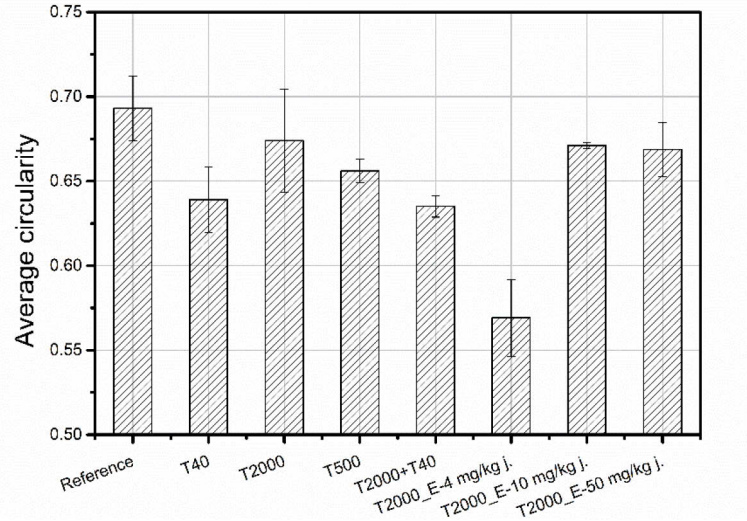

Figure 3-5 Average values of the circularity of particles precipitated in the presence of dextran fractions with different molecular mass distributions.

Surprisingly, the reaction products resulting from the application of the low enzyme level of 4 mg/kg juice of broadly distributed intermediate molecular masses caused the overall lowest total average circularity, 0.57. This is distinctively different from both the dextran-free and the T2000 contaminated references. For the slurries treated with higher enzyme levels of 10 and 50 mg/kg juice, the average circularity approached the reference value.

3.3.2.2.2 Area-Related Average Shape Parameters

The changes in average circularity discussed above give reason to assume that the presence of dextran additionally affects the particle shape during agglomeration. To understand this in more detail, a size-related evaluation of the circularity and two further shape parameters, roundness and solidity, were considered. For a basic understanding of the calcium carbonate particle formation in the dextran-free reference sample, the average values of these shape parameters corresponding to the above-discussed four area-categories (<50 μm^2, 50 to 100 μm^2, 100 to 500 μm^2 and >500 μm^2) are shown in Figure 3-6. Therefrom, it is obvious that the average circularity systematically decreases from the small-area-category (0.8) to the large-area-category (0.35), see squares in Figure 3-6. From the circularity, it cannot be concluded whether this relates to changes of either or both

the actual particle form or the surface roughness. Therefore, the roundness as well as the solidity were additionally evaluated, affected by the particle form and surface roughness, respectively.

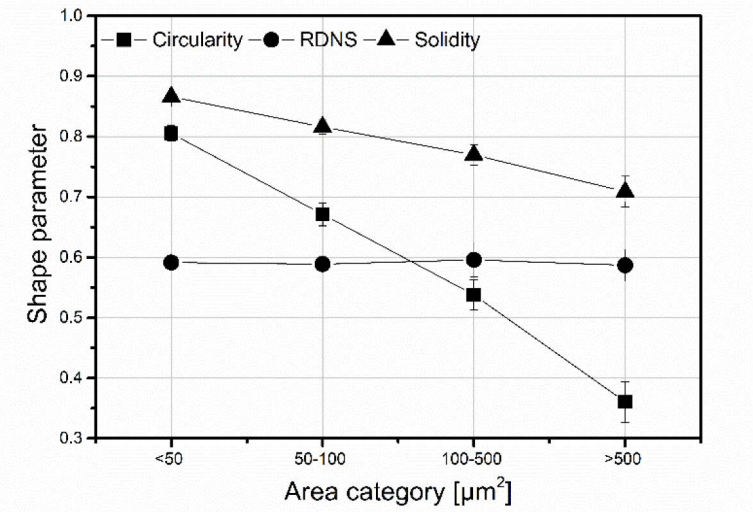

Figure 3-6 Particle shape parameters per area-category of the reference particles. Squares: circularity (affected by the particle form and roughness). Dots: Roundness (affected by the particle form). Triangles: Solidity (affected by the particle roughness).

The average solidity also decreases from the small-area-category (0.86) to the large-area-category (0.71), suggesting that particularly the particle roughness decreases with the increase of the particle size. Interestingly, the roundness appears to be constant all over the four area-categories, which suggests that the actual particle form is independent of the particle size. Thus, the changes in circularity as a function of the particle size for the dextran-free reference appears to be driven by changes in the surface roughness during the agglomeration of calcium carbonate crystals. Increasingly irregular perimeters hence caused the decrease in circularity with the increase in area. Thus, it is a general fact that a higher number of agglomerates with large areas, as found for the dextran-loaded samples, is accompanied by an overall decrease of the circularity. The data have hence to be interpreted in combination with Figure 3-4 (B). The average values of the three shape parameters corresponding to the four area-categories were also calculated for the dextran-loaded samples. The data indicate that the average circularities within the two small-area-categories (<50 µm^2 and 50 to 100 µm^2) are not greatly affected due to either dextran addition in comparison with the dextran-free reference. In general, the average circularity of agglomerates corresponding to the two large-area-categories (100 to 500 µm^2 and >500 µm^2) respectively increased due to either dextran addition. Since the presence of dextran caused most prominently an increase of large particles, the average values of the three shape parameters are exclusively shown for the large-area-category (>500 µm^2), see Figure 3-7.

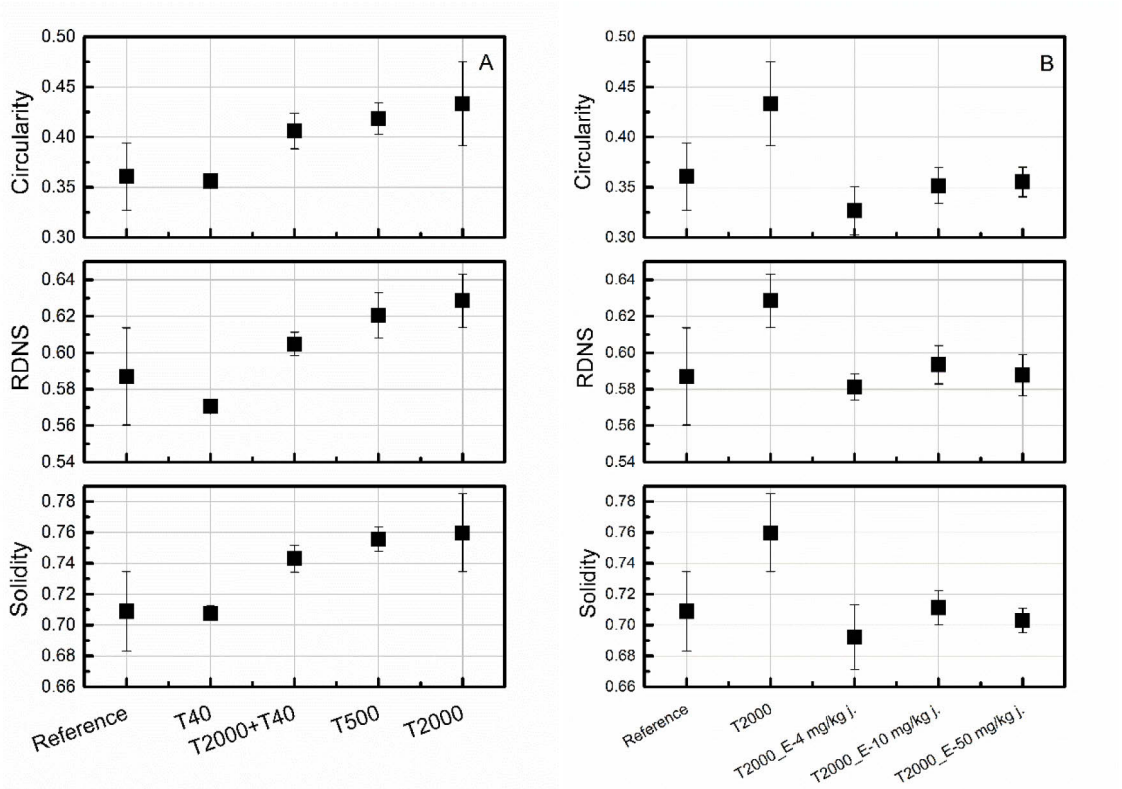

Figure 3-7 Average values of the particle shape parameters for large area agglomerates (>500 μm^2). A) Particles affected by non-decomposed dextran fractions of different molecular mass. B) Particles affected by enzymatically decomposed T2000 dextran.

Interestingly, the sample containing T40 showed a similarly low circularity for the large-area agglomerates as the reference (approximately 0.35), see squares in Figure 3-7 (A). Besides, the average values of the roundness (dots) as well as the solidity (triangles) appear to be unaffected by T40 dextran.

In contrast, throughout the data set, it appeared that the presence of T2000 and T500 caused an increase in the average circularity of large particles, 0.42 and 0.44 for the large area category, respectively (squares in Figure 3-7 (A)). The equal-mass mixture of T2000 and T40 has an intermediate position. Similar molecular mass dependent changes were found for the roundness and the solidity.

Even though the differences found were most pronounced for the large particles, the overall trend indicates that agglomeration might be oriented in the absence of dextran and in the presence of T40 and non-oriented when T2000 or T500 were present. In addition to the change of the form due to non-oriented agglomeration, the increase in the average solidity additionally indicates that the surface roughness is also increased when T500 and T2000 dextran were present.

Thus, the consideration of the different shape parameters suggests that the dextran-induced increase in circularity of large area agglomerates is caused by changes in both surface roughness and particle form.

Figure 3-7 (B) illustrates in how far the enzymatic decomposition products influence the shape parameters for the large-area category (>500 μm^2). Again, two references are shown, non-contaminated juice and T2000 contaminated juice. Here, too, the data on the enzyme treated juices confirm the general trend that larger agglomerates reveal a lower circularity.

Focussing on the large agglomerates, the sample treated with 4 mg/kg juice shows a slightly lower but quite similar circularity than the non-treated reference. Again, very similar data trends were found for the roundness as well as the solidity, see Figure 3-7 (B). Compared to the sample containing T2000, the difference is distinctly bigger. In this context, it should be noted again that for the sample treated with the low enzyme level, large agglomerates are most prominently present, see Figure 3-4 (C). The data indicate again that the differences in circularity found are most likely not only due to agglomerate size but also subject to the orientation of the agglomerate growth and the surface roughness.

Here, again, the application of higher enzyme levels of 10 and 50 mg/kg juice shows unaffected shape parameters for the large agglomerates close to the reference values, just as the T40 loaded samples. Thus, for these two higher enzyme levels, all data evaluated indicate that the particle size and shape characteristics approached those of the dextran-free reference suggesting a sufficient enzymatic decomposition to harmless reaction products.

In summary, for the reference, it was found that the circularity and the solidity decrease with increasing agglomerate size, whereas the roundness appears to be size-independent. In contrast to T40, which practically does not change these three shape parameters within a size category, T2000 increased the three shape parameters of large agglomerates the most. With respect to the circularity of the large agglomerates, T500 and the mixture of T2000 and T40 were found to cause similar effects as T2000. Strikingly, the juice which was treated with 4 mg/kg juice resulted in the presence of many large agglomerates with particularly low circularities. This indicates that the two samples with high polydispersity in the intermediate size range (equal-mass mixture of T2000 and T40 and mildly decomposed T2000) promotes agglomeration, while the shape of agglomerates is not affected by dextran of intermediate but rather low molecular mass (10 kDa to 85 kDa). The data gathered do not allow to formulate a mechanistic hypothesis concerning the shape of the calcium carbonate agglomerates, but indicate that more detailed work is necessary to unravel the specific influence of dextran on the form and roughness of calcium carbonate agglomerates in more detail.

3.4 Conclusion

The specific effects of dextran with varying molecular mass distributions on the size and shape of calcium carbonate particles precipitated during carbonation were key to this study. Therefore, the effects on the particle characteristics due to the presence of high, middle and low molecular mass dextran fractions (T2000, T500 and T40, respectively) and an equal-mass mixture of T2000 and T40 dextran in synthetic thin juices were investigated. Furthermore, effects due to dextranase

applications on T2000 dextran using varying enzyme levels were investigated, aiming at implementing targeted mitigation of dextran-related effects.

Particle analysis combined with size exclusion chromatography (SEC) enabled to detect harmful and harmless dextran fragments with regard to particle modifications during carbonation. SEC analysis of the non-decomposed dextran fractions (T40, T2000 and T500) generally indicated a relatively high polydispersity, listed in ascending order. Consequently, the equal-mass mixture of T2000 and T40 dextran comprised an even broader molecular mass distribution (totally covering molecular masses from 3 kDa to 3000 kDa). SEC analyses of enzymatically decomposed T2000 dextran indicate a successive decrease in the average molecular mass of the reaction products with the increase of the enzyme level. The application of the low enzyme level of 4 mg/kg solution leads to broadly distributed low molecular mass dextran fragments (covering a range from 2 kDa to 300 kDa), which is, apart from the high molecular mass end, similar to the equal-mass mixture of T2000 and T40. The application of higher enzyme levels of 10 and 50 mg/kg solution resulted in a further decrease in the molecular mass of the reaction products (covering 0.4 kDa to 10 kDa and 0.3 kDa to 5 kDa, respectively).

Particle analysis revealed that the average area of the calcium carbonate particles increased due to every dextran addition, pointing towards pronounced agglomeration. This effect appears to systematically correlate with the polydispersity of dextran. Besides, the presence of intermediate but rather low molecular mass dextran fractions (3 kDa to 85 kDa) have additionally promoted the agglomeration of calcium carbonate crystals. Thus, the biggest effect on the average area was found for the equal mass mixture of T2000 and T40 and the samples treated with the low enzyme level of 4 mg/kg juice.

The data gathered on the shape of the calcium carbonate particles (circularity, roundness, solidity) indicate that every dextran addition lead to higher amounts of particles with lower circularities (indicator for form and roughness). The additional area-related evaluation revealed that the circularity generally decreased with the increase in particle area. The same applies to the solidity (indicator for roughness), while the roundness (indicator for form) appears to be size-independent for the dextran-free reference particles. This suggests that the increased presence of larger agglomerates drives the changes in circularity, which is mainly caused by an increase in surface roughness. Once the dextran was significantly decomposed by enzyme action (10 or 50 mg/kg juice) to smaller molecules, in the size range of 10 kDa and below, no dextran-related effects on particle size and shape were found anymore.

A closer look at the data reveals that the polydispersity of dextran and the spread of the molecular mass are key parameters for agglomerate characteristics. The comparison of the effects of mildly decomposed T2000 (4 mg/kg juice) and the equal-mass mixture of T2000 and T40 indicates that both induced the highest number of large agglomerates (> 20%). This mainly relates to the abundant

presence of dextran in the intermediate range of molecular masses from 10 kDa to 85 kDa. Strikingly, the circularity of calcium carbonate agglomerates differs between these two samples. It seems that the particles affected by mildly decomposed dextran possess rather low circularities similar to the reference. Even though the data do not allow to formulate any specific hypothesis for a mechanism of the agglomeration, this suggests that the agglomeration is possibly oriented in the presence of exclusively small dextran fragments while dextran of higher molecular masses promote non-oriented agglomerate growth and the increase in surface roughness.

The findings reported here certainly need further confirmation. In order to connect them to industrial practices, it is necessary to study realistic sugar beet raw juices, taking synergistic effects with other impurities and interactions within compacted filter cakes into account.

Nevertheless, this work clearly illustrates that successful dextranase application to mitigate dextran contamination necessitates a detailed understanding of micro-processes to ensure a sufficiently small molecular mass of the reaction products.

References

Abdel-Rahman, E.-S. (2007). Investigations on the influence of dextran during beet sugar production with special focus on crystal growth and morphology (PhD). Technische Universität Berlin, Berlin.

Abraham, K., Kunst, S., & Flöter, E. (2019). Membrane Characterisation for Fractionated Dextran Analysis in Sugar Industry. *Food Analytical Methods*. Advance online publication. https://doi.org/10.1007/s12161-019-01441-7

Adjari rad, M., Adjari Rad, A., & Schrevel, G. (2014). Evaluation of juice purification in sugar factories. *Sugar Industry*, *139*(12), 734–744.

Aquino, F. W., & Franco, D. W. (2009). Molecular mass distribution of dextran in Brazilian sugar and insoluble deposits of cachaça. *Food Chemistry*, *114*, 1391–1395. https://doi.org/10.1016/j.foodchem.2008.11.019

Asadi, M. (Ed.). (2007). *Beet-Sugar Handbook*. New Jersey: John Wiley & Sons.

Chen, J. C., & Chou, C. C. (1993). Cane Sugar Handbook: A Manual for Cane Sugar Manufacturers and Their Chemists (12th ed.). New York: John Wiley & Sons.

Eggleston, G., & Monge, A. (2005). Optimization of sugarcane factory application of commercial dextranases. *Process Biochemistry*, *40*(5), 1881–1894. https://doi.org/10.1016/j.procbio.2004.06.025

Eggleston, G., Monge, A., Montes, B., & Stewart, D. (2009). Application of dextranases in sugar cane factory: Overcoming practical problems. *Sugar Tech*, *11*(2), 135–141. https://doi.org/10.1111/j.1468-0254.2009.00285.x

Gabas, N., Hiquily, N., & Laguérie, C. (1994). Response of Laser Diffraction Particle Sizer to Anisometric Particles. *Particle & Particle Systems Characterization*, *11*(2), 121–126. https://doi.org/10.1002/ppsc.19940110203

Hein, W., Bauer, H., & Emertorfer, F. (2012). Processing of long-stored sugar beet. *Sugar Industry*, *137*(1), 25–32.

Khalikova, E., Susi, P., & Korpela, T. (2005). Microbial dextran-hydrolyzing enzymes: fundamentals and applications. *Microbiology and Molecular Biology Reviews*, *69*(2), 306–325. https://doi.org/10.1128/MMBR.69.2.306-325.2005

Kontrec, J., Ukrainczyk, M., Babić-Ivančić, V., & Kralj, D. (2011). Synthesis of Calcium Carbonate by Semicontinuous Carbonation Method in the Presence of Dextrans. *Croatica Chemica Acta*, *84*(1), 25–32. https://doi.org/10.5562/cca1746

Liu, E. J., Cashman, K. V., & Rust, A. C. (2015). Optimising shape analysis to quantify volcanic ash morphology. *GeoResJ*, *8*, 14–30. https://doi.org/10.1016/j.grj.2015.09.001

Sarka, E. Bubnik, Z. Hinkova, A. (2006). Changes in particle size of carbonation slurry. *Sugar Industry*, *131*(8), 551–557.

Schubert, H. (2012). *Handbuch der Mechanischen Verfahrenstechnik*. Hoboken: John Wiley & Sons.

Van der Poel, P. W., Schiweck, H., & Schwartz, T. (1998). *Sugar Technology: Beet and Cane Sugar Manufacture*. Berlin: Dr. Albert Bartens KG.

Wojtczak, M., Gruska, R., MIkos, P., Antczak-Chrobot, & Aneta. (2015). Dextran molecular mass effect on particle size distribution of CaCO3 for 1st and 2nd carbonatation. *Sugar Industry*, *140*(11), 703–706.

4 Dextran-Induced Modifications of Particles Precipitated During Carbonation

Abraham, K. [a b], Splett, L. [a], Flöter, E. [a]

[a] TU Berlin, Department of Food Process Engineering, Seestraße 13, 13353 Berlin, Germany

[b] SternEnzym, Kurt-Fischer-Str. 55, 22926 Ahrensburg, Germany

Submitted to the Sugar Industry (2019).

Abstract

The effects of high and low molecular mass dextran (T2000 and T40) on the size and shape of particles precipitated during carbonation and their correlation with filtration performances were key to this study. Varying contents of T2000 and T40 dextran in synthetic thin juices were investigated. For particle size and shape analysis, static image analysis and laser particle size analysis were used. Both methods, static image analysis and laser diffraction, revealed that the presence of T2000 and T40 dextran leads to a higher amount of large-sized particles at the expense of small-sized particles, indicating pronounced agglomeration. The additional evaluation of shape parameters (circularity, roundness, solidity) obtained from static image analysis indicates that the agglomeration is oriented in the absence and in the presence of lower T40 dextran contents. Besides, non-oriented agglomeration, resulting in more round agglomerates with smoother surfaces, was found for samples loaded with T2000 dextran and high T40 dextran levels. Only the latter samples have shown to negatively affect the filtration performance. Thus, in the presence of T2000 dextran and high T40 dextran contents, the filtration was hampered. This appears to be mainly caused by a tighter packing of more round calcium carbonate agglomerates in the porous structure of the filter cake.

4.1 Introduction

The presence of deterioration products originating from microbial contamination in sugar cane and beet juices are widely known to affect sugar manufacture. Lactic acid bacteria, mainly *Leuconostoc mesenteroides* species, inter alia produce dextran with broad molecular mass distributions. Dextran is a prevailing topic in the sugar cane industry due to higher microbial activity in the areas, where sugar cane is cultivated. Nevertheless, dextran formation is of interest for the sugar beet industry as well, mainly initiated by exposure of sugar beets to freeze-thaw cycles. The latter is of increasing relevance due to prospective elongations of sugar beet campaigns as a result of changes of the European legislation in 2017 (Adjari Rad et al., 2014).

Dextran is composed of glucose units, which are mainly linked via α-(1→6) glyosidic linkages (van der Poel et al., 1998). Besides, it is known that sugar industry-relevant species produce dextran containing up to 5 % branching points, mainly via α-(1→3) glycosidic linkages, which cause deviations from a strictly uniform structure (Khalikova et al., 2005). Dextran produced in cane and beet juices is generally of relatively high average molecular mass and high polydispersity. This refers to the potential occurrence of molecular masses ranging between 15 kDa and 2,000 kDa (Chen & Chou, 1993). Aquino et al. further identified two major groups, a lower and a higher fraction possessing molecular masses in the 10 kDa- and 10^3 kDa-range, respectively (Aquino & Franco, 2009).

Dextran is co-extracted along with sucrose and is hence present in dissolved form. The presence of these water-soluble, homogenous polysaccharides can subsequently affect various stages of sugar processing. It is widely accepted that dextran-induced process effects relate to specific molecular mass fractions. So far, there is general agreement that high molecular mass dextran is mainly responsible for a viscosity increase negatively affecting the filtration, evaporation as well as the crystallisation rate (Chen & Chou, 1993). Besides, high as well as low molecular mass dextran are known to modify the size and shape of sucrose crystals during crystallisation (Abdel-Rahman, 2007). Furthermore, the calcium carbonate precipitation during juice purification appears to be influenced by dextran (Wojtczak et al., 2015). For the latter, there is still uncertainty about the specific role of high and low molecular mass dextran fractions.

The sugar beet raw juice purification is usually achieved by means of lime and carbonation gas. In doing so, the raw juice is progressively limed in order to stepwise precipitate certain non-sugars. This is followed by a dramatic increase of the pH value and alkalinity in the main liming step, which aims at the decomposition of invert sugar and amides. The subsequent addition of carbonation gas leads to the formation of calcium carbonate crystals. This relates to the conversion of $Ca(OH)_2$ and CO_2 to $CaCO_3$ and water. Once calcium carbonate crystals have formed, they also function as adsorption surfaces for non-sugars. The calcium carbonate crystals and their agglomerates with

adhering non-sugars are subsequently separated from the juice by settling and filtration (Asadi, 2007).

It is generally acknowledged that dextran, depending on the molecular mass distribution, impairs the juice purification process (van der Poel et al., 1998). On the one hand, this relates to an increase of the viscosity of the continuous phase. According to Darcy's law, the viscosity inversely correlates with the flow rate through porous media, e.g. filter media and cakes. An increase of the solution viscosity hence results in modified flow characteristics, mainly caused by high molecular mass dextran (Stieß, 2009). The pore structure of the filter cake is, however, not considered in this interpretation. Apart from the effects due to increased viscosities, dextran-induced particle modifications also play a crucial role in hampering filtration processes. The size and shape of particles precipitated during carbonation determine the filter cake pore structure. Different cake structures can lead to increased drag coefficients or even blocked filters and filter cake pores (Schubert, 2012). Besides, the adsorption surface for non-sugars that is generated is relevant for the purification performance. Thus, changes in the particle characteristics also directly affect the purification process (Asadi, 2007).

On an interdisciplinary level, it is known that the operation conditions as well as the presence of additives, also including dextran, can affect the size and shape of precipitated calcium carbonate crystals, potentially concerning nucleation, growth and agglomeration of crystallites (Kontrec et al., 2011).

In sugar industry, a detailed understanding of such particle modification effects specifically caused by dextran fractions with different molecular masses have received scant attention up to now. While there is broad consensus about dextran-related viscosity effects, the mechanisms of dextran-induced particle modifications have not been investigated in detail yet.

This endeavour is burdened with the challenge of accurately analysing the particle characteristics, either single crystals or agglomerates. In the past, laser diffraction was often used to analyse dextran-induced modifications of calcium carbonate particles (Wojtczak et al., 2015). This method is, however, afflicted with some disadvantages when analysing irregular particle shapes. Laser diffraction algorithms generally assume spherical shapes making it prone to misinterpretations. When analysing irregular non-spherical particles, the evaluation is also affected by the orientation of the particles to be analysed, which is reported to be affected by the flow of the dispersion medium. Irregular particle shapes can hence cause "ghost" particles leading to artefacts. Besides, the usage of dispersing units entails the danger of modifying the particle characteristics during sample preparation (Gabas et al., 1994).

This widely used method is hence a good tool to analyse rather regularly sphere-shaped particles, but is probably of limited value to generate a reliable characterisation of rather irregular particle shapes. When considering irregularly modified particles and their agglomerates, this appears

especially relevant. The presence of dextran in particular is suspected to stimulate these phenomena. A detailed study on dextran-induced changes of particles hence necessitates to apply an additional analytical tool.

Similar to Kontrec et al., previous work using image analysis has indicated that dextran promotes agglomeration, varying with the dextran molecular mass distribution (Abraham et al., submitted for publication in 2019). Specifically, the data have indicated differences in orientation of agglomeration for the different dextran fractions. Thereby, calcium carbonate agglomeration appeared to be non-oriented in the absence as well as in the presence of low molecular mass dextran. In contrast, high molecular mass dextran caused oriented agglomeration of calcium carbonate. In this study, however, variation of concentration was not considered.

The current study is supposed to complement this previous work and particularly aims at unravelling concentration-dependencies of these particle modifications for the two main dextran fractions, T2000 and T40. Thus, the work presented aims at adequately detecting dextran-induced modifications of particles precipitated during carbonation as a part of the sugar beet raw juice purification. Effects of varying contents of either high or low molecular mass dextran fractions were investigated using two different analytical methods. Static image analysis based on light microscopy was used to characterise the particle size and shape distribution. The widely used laser particle size analysis was additionally used for reasons of comparison. In addition, correlations of particle changes with the filtration performance were made by additionally consulting the filtration test according to Brieghel-Müller.

4.2 Material and Methods

4.2.1 Materials

The effects of high and low molecular mass dextran fractions (T2000 and T40) on particles precipitated during carbonation were analysed. Experiments were performed in synthetic thin juices, meaning 15 % (m/m) aqueous sucrose solutions. For this purpose, refined sucrose (Nordzucker, extra-white sugar) was used. The effects of varying dextran concentrations as well as molecular masses were investigated. Dextran fractions with mass-average molecular masses of 2,000 kDa (T2000: Sigma-Aldrich, dextran with a molecular mass distribution ranging from 1,500 kDa to 2,800 kDa) and 40 kDa (T40: Carl Roth, dextran with a molecular mass distribution ranging from 35 kDa to 45 kDa) were systematically added. All dextran fractions originate from the lactic acid bacteria *Leuconostoc Mesenteroides* strain B512. Besides, milk of lime (Grüssings, milk of lime 120 g CaO/L) and carbonation gas (Linde, carbon dioxide) with a purity > 99.5 % were used.

4.2.2 Juice Purification at Laboratory Scale

4.2.2.1 Juice Purification Plant

The juice purification experiments were performed at 1 liter labscale in a double-walled glass cylindrical vessel. The temperature was controlled by a hot water flow through the double-wall jacket of the vessel. A thermostat (Julabo, F12-ED) was used to keep the heating medium at the desired temperature. To allow a rapid temperature change from pre-liming to main-liming, a second thermostat (Julabo, F32-ME) was connected via a three-way valve. A blade stirrer with holes connected to an agitator (RZR 2102 control, Heidolph Instruments GmbH & Co. KG) ensured appropriate mixing inside the vessel. Process control was maintained by a Pt100 thermo-element and a pH electrode (Mettler Toledo, InLab Expert Pro) immersed in the juice. A second glass pH electrode was used to measure the pH of the sample at 293 K after rapid cooling in an ice bath. Milk of lime was added volumetrically into the opening of the vessel using a plastic syringe meeting the targeted pH values.

A pressure reducing valve and a flow meter were used to set and control the carbon dioxide flow passing through the gas piping ending in a perforated ring on the bottom of the vessel. Sampling and discharge of the slurry was done via the outlet valve at the vessel's bottom. The separation of the particles precipitated was performed using vacuum filtration with filter papers of defined pore sizes (Schleicher & Schnell, filter paper circles 589 black ribbon, particle retention of 12-25 μm).

4.2.2.2 Process Execution

The juice purification process includes liming and carbonation, further sub-divided into pre-liming and main-liming as well as first and second carbonation. This study focuses on the calcium carbonate crystals and their agglomerates formed during the first carbonation using synthetic thin juices.

During the first step of pre-liming, the temperature was set to 328 K and milk of lime was gradually added according to a specific pattern necessary for progressive precipitation of certain non-sugars. The temperature as well as the pH were continuously monitored during the process. For verification, sampling followed by rapid cooling in an ice bath allowed pH-measurements at 293 K. The final pH of the pre-limed juice was set between 11.0 and 11.4 (293 K).

Even higher alkalinities and pH values are required to decompose invert sugar and amides during main-liming. By adding the required amount of lime all at once, an alkalinity of 0.8 to 1.0 g CaO/100 ml and pH values of 12 to 12.5 were achieved, respectively. After the addition of milk of lime, the temperature was increased to 358 K. A holding phase of 20 min completed the main liming step.

The first carbonation was initiated by introduction of carbon dioxide. Continuous gassing for 10 min reduced the pH to the targeted value of 11.0 to 11.4 (293 K). And again, pH values were measured at 293 K via sampling and rapid cooling in an ice bath. The particles precipitated during carbonation were separated by vacuum filtration. Prior to the filtration, samples for particle analysis were taken from the slurry. The filtrate obtained is usually subjected to the second carbonation and subsequent filtration to produce actual thin juice. However, this is not subject of the current study.

4.2.3 Laser Particle Size Analysis

The particles contained in the first carbonation slurry were analysed using laser particle size analysis (Fritsch, Analysette 22). Distilled water was used as the suspension medium. Samples were added via wet dispersion using a stirring unit. The data obtained are depicted as relative distribution curves, referring to a volume-based evaluation.

4.2.4 Static Image Analysis

Light microscopic images of the particles precipitated during first carbonation were recorded by Zeiss-Axio Scope A1 microscope and subsequently analysed by ImageJ. The samples for image analysis were taken directly from the slurry. Prior to the actual particle size and shape analysis, image editing and calibration are necessary prerequisites. Particle size parameters include the area as well as the maximum feret diameter. The size data are depicted as total average values and relative frequencies respectively according to four categories.

The shape of calcium carbonate particles is mainly affected by their form and their surface roughness. Thus, parameters indicating changes in either or both, form and roughness, were taken into account. In this study, the circularity was primarily used to detect changes of the particle shape, which is affected by both, particle form and roughness, see equation (4-1). A perfect circle has a circularity of 1. To further make an approach to distinguish form and surface roughness, the roundness as well as the solidity were additionally considered (see equation (4-2) and (4-3)) (Liu et al., 2015). The data corresponding to the shape parameters are depicted as average values according to the above mentioned area-categories.

$$Circularity = 4\pi \frac{Area}{Perimeter^2} \tag{4-1}$$

$$Roundness = 4 \times \frac{Area}{\pi \times [Major\ axis]^2} \tag{4-2}$$

$$Solidity = \frac{Area}{Convex\ Area} \tag{4-3}$$

4.2.5 Filtration Test

The filtration test according to Brieghel-Müller was performed using the filtration-coefficient measuring instrument provided by Putsch GmbH & Co. KG. A 10 ml measuring burette was used

to record the filtration time per filtrate volume unit, which is connected to a vacuum pump via a connecting hose. The vacuum pump is used to build up a constant pressure difference of 533 mbar as a driving force for filtration. The filter head of the burette, equipped with a filter paper, was immersed into the carbonation slurry to be filtered. The latter is continuously stirred. The filtration test was performed at 338 K. The filtration coefficient was calculated using the time difference of the fifth (t_2) and the first volume (t_1) unit multiplied with the conversion factor q = 0.25, see equation (4-4) below.

$$FK = q \cdot (t_2 - t_1) \tag{4-4}$$

4.3 Results and Discussion

4.3.1 Static Image Analysis

4.3.1.1 Particle Size

To elucidate the specific effects of T2000 and T40 dextran on the shape and size of the particles precipitated during carbonation, experiments in synthetic thin juices were performed. Sucrose solutions (15 % (m/m)) containing varying contents of either T2000 or T40 dextran were studied. The dextran contents are, as usual, given as mg per kg sucrose. The particles precipitated during carbonation were analysed using static image analysis. Here, particle size analysis includes well-known size parameters, the particle projection area as well as the maximum feret diameter.
Figure 4-1 (A) indicates that the average values for the particle projection area increase due to the presence of either dextran fraction in comparison with the reference.

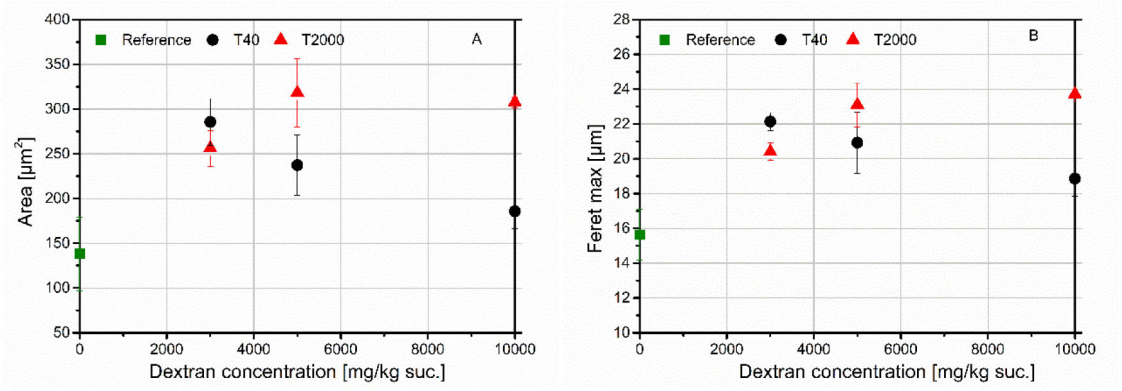

Figure 4-1 Average values of the particle size parameters obtained from static image analysis. A and B relate to the area and the maximum feret diameter, respectively.

Surprisingly, on studying the T40 dextran concentration from 3,000 to 5,000 and 10,000 mg/kg sucrose, the average values increased dramatically with the addition of dextran. However, the initial jump in the projection area is followed by a systematic decrease on further T40 dextran addition. Anyhow, final values are still higher than the reference (black dots in Figure 4-1 (A)). In contrast, on T2000 dextran addition, the initial increase in the projection area is maintained and appeared

constant at twice the value of the reference sample (red triangles in Figure 4-1 (A)). Similar trends were found for the average values of the maximum feret diameter (Figure 4-1 (B)). The data appear quite consistent because the relative difference between the diameter and the area scale is quadratic, which is in line with assuming regular shapes.

Looking at the statistical distribution behind these average values, the relative frequencies corresponding to four different categories show clear dose-dependent changes for both dextran fractions and size parameters, projection area (Figure 4-2 (A) and (B)) and maximum feret diameter (Figure 4-2 (C) and (D)).

The most conspicuous change found is a significant reduction in the occurrence of small-sized particles with an area of less than or equal to 50 μm^2. Independent of the T40 dextran dosage, this value was reduced by approximately 15 % (Figure 4-2 (A)). This decrease was accompanied by a systematic increase in prevalence of particles with intermediate areas (100 to 500 μm^2). In this case, the addition of T40 dextran revealed a systematic dose-response change as well (nearly 15 % increase for the highest dextran content). The amount of particles with large areas of more than 500 μm^2 is also increased, roughly doubled in comparison with the reference.

In essence, the same effect was found for T2000 dextran-loaded samples. Here, an almost linear dose response was found with a reduction of the small-sized particles up to 20 % for the highest dextran dosage of 10,000 mg/kg sucrose (Figure 4-2 (B)). However, since the prevalence of the small-sized particles was reduced more dramatically, the relative occurrence of the particles with larger areas is also increased more clearly. Similar to T40 dextran, the amount of particles with areas between 100 and 500 μm^2 also increased systematically with dextran dosage. Besides, the amount of even larger particles with areas above 500 μm^2 is much higher in comparison with T40 dextran-loaded samples. Thus, the data clearly indicate that large-sized particles occurred more often when dextran was present, which applies in particular to T2000 dextran. Consistently, a very similar pattern was found for the relative frequencies corresponding to the maximum feret diameter. For both dextran fractions, an increase of particles with a maximum diameter in the intermediate range at the expense of particles with small maximum feret diameters is obvious (Figure 4-2 (C) and (D)). Again, the reduced occurrence rate of small-sized particles is more sensitive to T2000 dextran compared to T40 dextran. For T40 dextran-loaded samples, this reduction again appeared to be dose independent in the range studied. Not surprisingly, the reduction in the relative occurrence of small diameters, less than or equal to 20 µm, was accompanied by a systematic increase in larger diameters, here mainly between 20 and 40 µm. Both dextran fractions hence showed the same trend, but the presence of T2000 dextran, provoke stronger and more systematic effects on the area as well as on the maximum feret diameter.

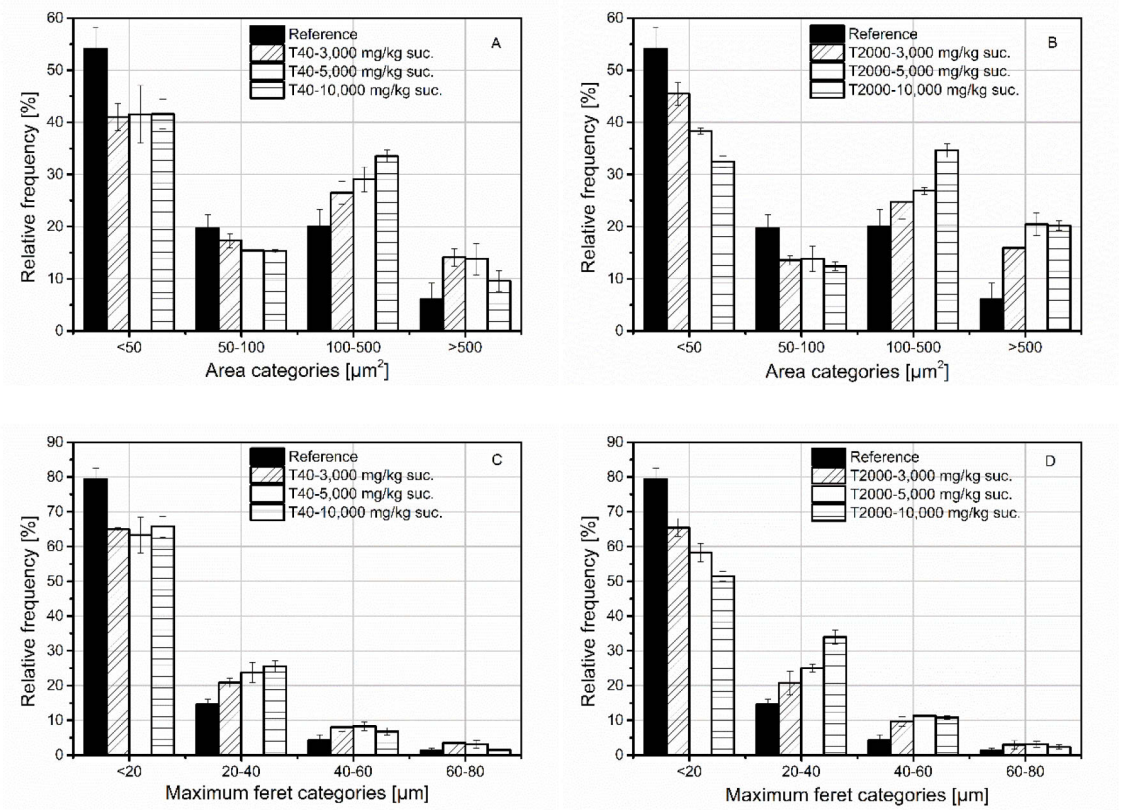

Figure 4-2 Relative frequency distribution [%] of particle size parameters obtained from static image analysis (number-based evaluation). A and B relate to the area for T40 and T2000, respectively. C and D relate to the maximum feret diameter for T40 and T2000, respectively.

Conclusively, both size parameters indicate that T2000 as well as T40 dextran cause a change of the particle size distribution indicated by a shift of the distribution towards larger particle sizes. This is clearly indicated by both, an increase of the projection area as well as the maximum feret diameter. This effect is more pronounced for T2000 dextran. It is important to mention that the applied number-based evaluation even tends to underestimate this effect. The occurrence of increased amounts of the large-sized matter suggests a more pronounced calcium carbonate crystal agglomeration due to dextran addition.

4.3.1.2 Particle Shape

For the respective shape parameters, the average values in relation to the above-discussed area categories were calculated. For a basic understanding of the calcium carbonate particle formation in the dextran-free reference sample, the average values of these shape parameters corresponding to the above-discussed four area-categories (<50 µm², 50 to 100 µm², 100 to 500 µm² and >500 µm²) are firstly depicted, see Figure 4-3. The average circularity obviously systematically decreases from the small-area-category (0.8) to the large-area-category (0.35), see squares in Figure 4-3. The circularity is affected by both, particle form and surface roughness. To further distinguish these two aspects, the roundness as well as the solidity were additionally evaluated. Similar to the

changes in circularity, the average solidity also decreases from the small-area-category (0.86) to the large-area-category (0.71), suggesting that particularly the particle roughness increases with the increase of the particle size. Interestingly, the roundness seems to be constant over the four area-categories, which suggests that the actual particle form is independent of the particle size. Thus, the changes in circularity as a function of the particle size for the dextran-free reference appear to be driven by changes in the surface roughness (increased perimeter) during the agglomeration of calcium carbonate crystals.

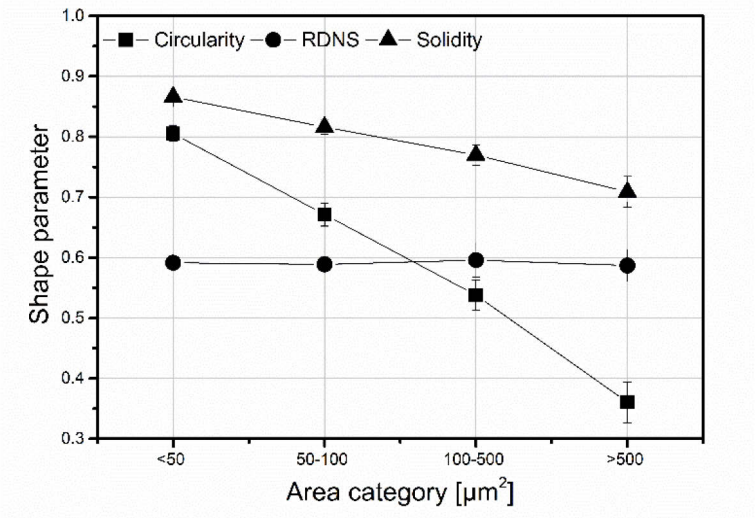

Figure 4-3 Particle shape parameters per area-category of the reference particles. Squares: circularity (affected by the particle form and roughness). Dots: Roundness (affected by the particle form). Triangles: Solidity (affected by the particle roughness).

Figure 4-4 (A), (B) and (C) show the area-related average circularity, roundness and solidity for the samples loaded with the different T40 dextran contents, respectively. The shape parameters corresponding to the calcium carbonate agglomerates formed in the presence of the two lower T40 contents appear unaffected, as found in previous work. In this case, T40 dextran only causes changes in the size rather than the shape of calcium carbonate agglomerates. However, the highest T40 dextran content caused a minute increase in circularity mainly for the two intermediate agglomerates.

In addition, the roundness and the solidity are also increased for the two intermediate area categories, indicating more round agglomerates with a lower surface roughness. The consideration of the different shape parameters hence suggests that the dextran-induced increase in circularity of these agglomerates is caused by changes in both, surface roughness and particle form. The area-related average circularity corresponding to T2000 dextran-loaded samples systematically increases with dextran dosage, which, in this case, mainly concerns the two large area categories. Thus, for the agglomerates with the largest area (>500 μm^2), the average circularity increased from roughly 0.35 to 0.45.

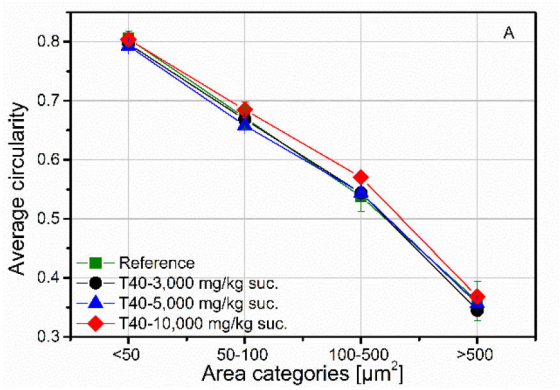

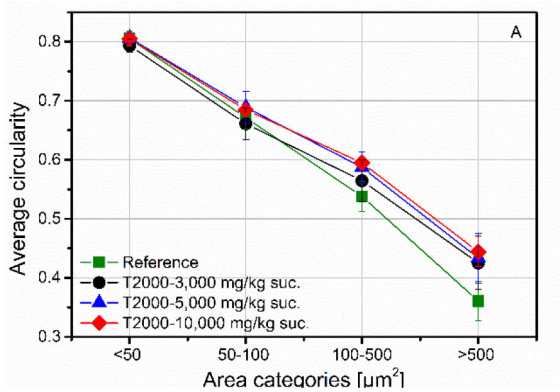

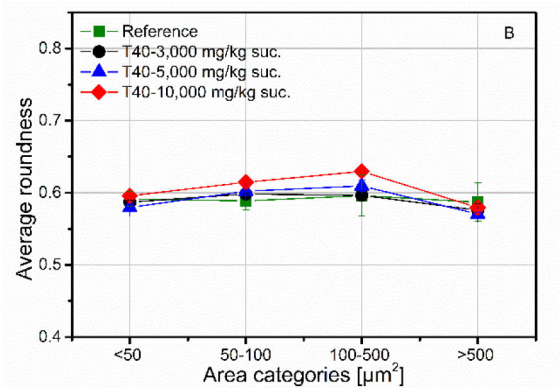

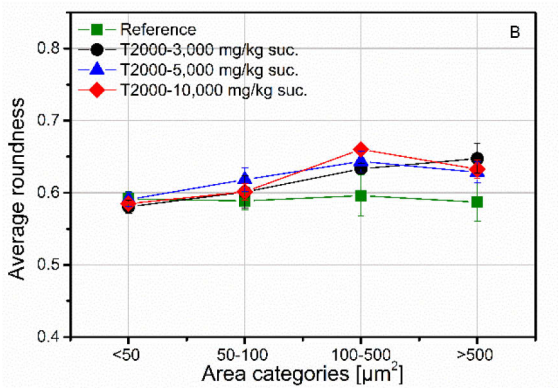

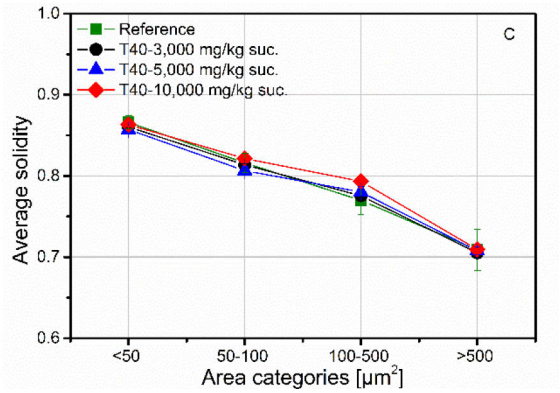

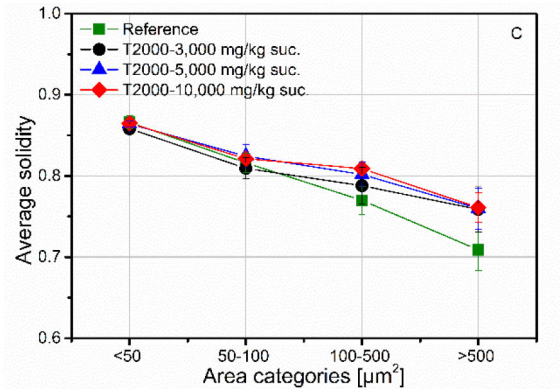

Figure 4-4 Area-related particle shape data for samples containing varying T40 dextran contents. A) Average circularity. B) Average roundness. C) Average solidity.

Figure 4-5 Area-related particle shape data for samples containing varying T2000 dextran contents. A) Average circularity. B) Average roundness. C) Average solidity.

The average roundness (Figure 4-5 (A)) as well as the solidity (Figure 4-5 (B)) also increased particularly for these large-area agglomerates. Thus, the previously assumed non-oriented agglomeration in the presence of T2000 dextran could also be confirmed in this study. Additionally, a systematic correlation with the T2000 dextran dosage was found. Besides, oriented agglomeration in the absence of dextran and in the presence of lower T40 dextran contents could be confirmed as well. However, it was found that the high T40 dextran content also causes shape modifications of calcium carbonate agglomerates as T2000 dextran.

Thus, the combined findings of the shape parameters suggest that T2000 dextran as well as the high T40 dextran contents induce the formation of more round calcium carbonate agglomerates with a smoother surface. In view of filtration performances, it seems reasonable that these agglomerates with a higher roundness (non-oriented agglomeration) can rather cause a reduction in filter cake porosity than more elongated particles (oriented agglomeration), which is discussed further down.

4.3.2 Laser Particle Analyser

The particles formed during carbonation were additionally analysed using laser light diffraction. The corresponding relative distribution curves are shown in Figure 4-6. The data of the reference material indicate a bimodal distribution with a main peak at diameters of about 30 µm and a smaller side peak at diameters of about 10 µm (cube-shaped data points). The particle sizes determined per definition slightly deviate from the particle sizes determined by static image analysis because of different order parameters. The fact that calcium carbonate crystal agglomerates differ from a perfect spherical shape further emphasises the differences between these two analytical methods.
Nevertheless, the laser data indicate that the presence of T2000 and T40 dextran generally leads to a broader size distribution. The peak representing particles of about 10 µm, found in the reference sample, diminishes due to the presence of T2000 and T40 dextran. The most common size of particles was consistently found to be approximately 32 µm.
Instead, the presence of T40 dextran leads to higher amounts of particles with diameters of 10 to 30 µm. This shift of the smaller fraction of agglomerates appears to be systematic with the increase of the T40 dextran dosage (Figure 4-6 (A)). Laser diffraction data of the T2000 dextran-loaded samples are increasingly difficult to interpret. Analogous to the T40 addition, instead of the small particles (below 10 µm) present in the reference samples, particles with diameters of 20 to 25 µm appeared massively. Their occurrence increases with higher dosages of dextran. Different from T40, T2000 additionally affected the peak maxima. A T2000 dextran content of 3,000 mg/kg sucrose shifted the peak maximum towards higher particle sizes, 40 µm compared to the previous 32 µm.
Surprisingly, on higher dextran dosage the peak maximum approached the original peak maximum matching it for samples loaded with 10,000 mg T2000 per kg sucrose (Figure 4-6 (B)). Thus, the laser data also indicate that agglomeration increasingly occurred. However, the data gathered by the two methods of characterisation are difficult to combine to a consistent interpretation. One fundamental difference between the methods is the sample addition. While samples for static analysis were practically untreated, it was necessary for the laser particle analysis to apply wet dispersion equipped with a stirring unit. The latter possibly cause a destruction of agglomerates. Additionally, the laser based particle analysis is prone to errors when analysing non-spherical particles with irregular shape and size distributions.

For the reference samples, most stable particles have a dimension of approximately 10 µm. The size of these smallest aggregates appeared to shift to values around 20 µm in the presence of dextran. This could indicate that dextran stabilizes agglomerates, making them more stable against shear induced desagglomeration. However, the most prominent size fraction found in laser based size analysis remained constant in presence of T40 dextran and varied when T2000 was present. In conclusion the laser particle size data also indicate a shift towards larger agglomerate sizes, roughly confirming the findings obtained from static optical analysis.

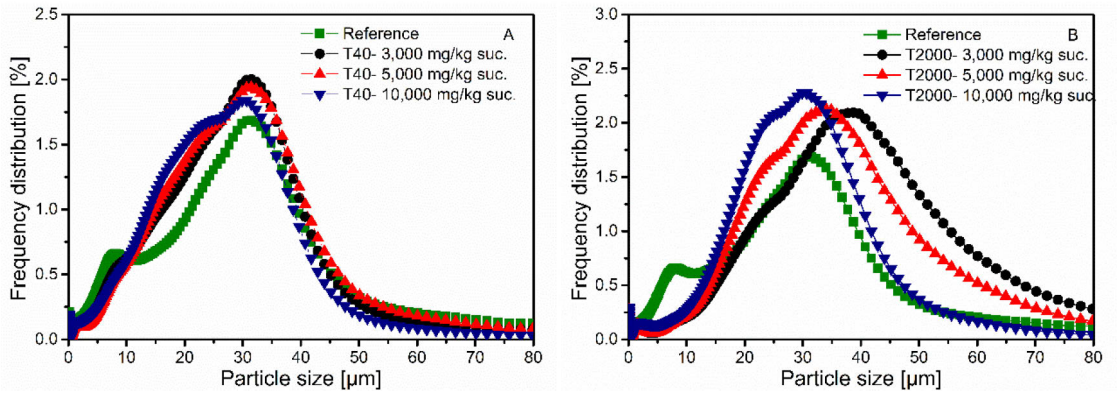

Figure 4-6 Laser particle size analysis. A and B relate to T40 and T2000 dextran-loaded samples, respectively.

4.3.3 Filtration Test

Figure 4-7 shows the data obtained from the filtration test performed with the respective carbonation slurries at 338 K. Thereby, the filtration time per filtrate volume as well as the filtration coefficient were considered (Figure 4-7 (A) and (B), respectively).

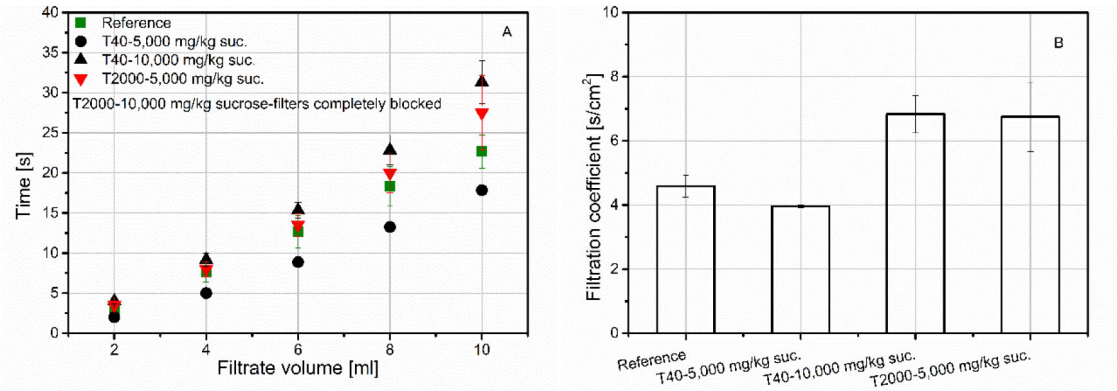

Figure 4-7 Data from the filtration test according to Brieghel-Müller performed with the carbonation slurries loaded with T2000 and T40 dextran.

In comparison with the reference, the filtration seems to be slightly accelerated for the lower T40 dextran content of 5000 mg/kg sucrose (black dots Figure 4-7 (A), respectively). The filtration coefficient for this sample is, however, not significantly affected, indicating that the pore structure is not dramatically affected, see Figure 4-7 (B). The increase of the T40 dextran dosage to 10,000

mg/kg sucrose increases the filtration time (black triangles) as well as the filtration coefficient (from roughly 4 to 6.5 s/cm^2).

The filtration behaviour of the slurry containing the lower T2000 dextran content of 5000 mg/kg sucrose is very similar to the one containing 10,000 mg T40 per kg sucrose. Affected most badly, the filtration test with the carbonation slurry loaded with 10,000 mg T2000 dextran per kg sucrose could not be executed due to non-filterability and complete filter blockage.

To fully consider the impact of dextran on filtration, the viscosities of 15 % (m/m) sucrose solution containing the different T40 and T2000 dextran contents were additionally determined, see Figure 4-8.

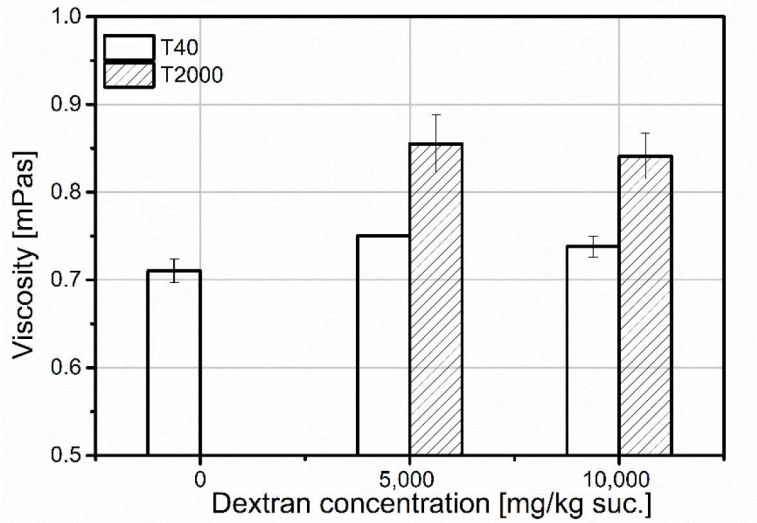

Figure 4-8 Viscosity of 15 % (m/m) sucrose solutions containing varying contents of T40 and T2000 dextran determined at 338 K (temperature for filtration test).

The viscosity appears to be relatively unaffected by the presence of T40 dextran. As expected, the presence of T2000 has a higher impact on the viscosity. Thus, the viscosity slightly increased from 0.7 mPas to 0.85 mPas due to the dextran content of 5000 mg/kg sucrose (corresponding to 0.075 g/100g). A further increase of the T2000 content to 10,000 mg/kg sucrose (corresponding to 0.15 g/100g solution) did not cause an additional increase of the viscosity. Thus, at these rather low dextran contents in the beginning of sugar manufacture, a modified filtration behaviour cannot exclusively be attributed to changes in viscosity, especially relevant for the samples loaded with the high T40 concentration. However, as discussed above, particle modifications are obvious and appear to decisively contribute to impeded filtration performances. For both T40 and T2000, the changes in size due to pronounced agglomeration correlates with the dextran content, which is, however, generally higher for T2000 dextran. Besides, shape modifications of calcium carbonate agglomerates appear with increasing T2000 concentrations and high T40 concentrations. The data hence suggest that lower contents of T40 dextran contamination are not critical for the filtration. The presence of higher amounts of agglomerates with unchanged shape parameters, probably leads

to a more porous filter cake. However, changes in filtration time were minutes, as the filtration coefficient remains unchanged.

T2000 dextran as well as the highest T40 dextran content obviously impeded the filtration process. The higher amount of agglomerates which are increasingly round and possess a smoother surface could be related to a tighter packing in the filter cake and thus reduced porosities. Thus, in synthetic juices, an impeded filtration performance can mainly be related to modified shapes of calcium carbonate agglomerates, whereas more round agglomerates with smoother surfaces (non-oriented agglomeration due to T2000 and high contents of T40) seem to affect the filter cake pore structure.

4.4 Conclusion

The analysis of specific dextran-induced effects on the size and shape of calcium carbonate particles precipitated during carbonation were key to this study. The effect due to the presence of varying contents of high and low molecular mass dextran fractions (T2000 and T40) in synthetic thin juices were investigated. To do so, static image analysis and laser particle size analysis were used. The additional consideration of a filtration test and viscosity measurements is supposed to identify correlations of the particle characteristics and flow behaviour with the filtration performance of the carbonation slurries.

The particle size data obtained from static image analysis clearly suggest that the exclusive presence of either T2000 or T40 dextran in synthetic thin juices lead to higher amounts of large-sized particles at the expense of small-sized particles, indicating more pronounced agglomeration. The dextran-related pronounced agglomeration was found to be caused by both dextran fractions, but to be more pronounced and systematic for T2000 dextran.

Laser data on dispersion seem generally less suitable for analysing the size of dextran-affected calcium carbonate agglomerates because of desagglomeration during sample addition. Nevertheless, the data also indicate an increased occurrence of agglomerates at the expense of small-sized particles. However, this resulted in higher amounts of agglomerates of intermediate size. It is assumed that desagglomeration during sample dosage via wet dispersion for laser measurement can occur. However, it seems that the presence of dextran stabilizes the agglomerates resulting in the shift observed.

The particle shape data obtained from static image analysis confirm the oriented agglomeration in the absence as well as in the presence of low T40 dextran contents. Besides, non-oriented agglomeration in the presence of T2000 dextran could be confirmed. In addition, it was found that the latter systematically correlates with the T2000 concentration. Interestingly, the shape modification induced by T2000 dextran was also found for the highest T40 dextran concentration.

An impairment of the filtration performance could be observed for high T40 and all T2000 dextran contents studied. This corresponds to effects on the shape of calcium carbonate agglomerates. Viscosity measurements have shown that the flow behaviour is not affected by T40 dextran and

only slightly changed due to T2000 dextran. Thus, the negative impact of higher dextran contents on the filtration performance is believed to be mainly caused by the particle modifications mentioned above. Thereby, it is assumed that a higher number of agglomerates with a higher roundness and a smoother surface, as found for samples loaded with T2000 dextran and high T40 dextran contents, reduce the porosity of the filter cake.

The fundamental findings reported here still need further confirmation. Investigations using realistic sugar beet raw juices taking synergistic effects with other impurities into account are much to be recommended. These are necessary prerequisites for establishing a connection to industrial applications. Nevertheless, this study delivers fundamental insights into the calcium carbonate precipitation in the presence of dextran. This way, it contributes to a more in-depth understanding of dextran induced problems encountered during the juice purification process.

References

Abdel-Rahman, E.-S. (2007). Investigations on the influence of dextran during beet sugar production with special focus on crystal growth and morphology (PhD). Technische Universität Berlin, Berlin.

Abraham K., Splett, L., Köster, E., & Flöter, E. Effect of Dextran and Enzymatically Decomposed Dextran on Calcium Carbonate Precipitation. *Submitted for Publication in 2019*.

Adjari Rad, M., Adjari Rad, A., & Schrevel, G. (2014). Evaluation of juice purification in sugar factories. *Sugar Industry*, *139*(12), 734–744.

Aquino, F. W., & Franco, D. W. (2009). Molecular mass distribution of dextran in Brazilian sugar and insoluble deposits of cachaça. *Food Chemistry*, *114*, 1391–1395. https://doi.org/10.1016/j.foodchem.2008.11.019

Asadi, M. (Ed.). (2007). *Beet-Sugar Handbook*. New Jersey: John Wiley & Sons.

Chen, J. C., & Chou, C. C. (1993). Cane Sugar Handbook: A Manual for Cane Sugar Manufacturers and Their Chemists (12th ed.). New York: John Wiley & Sons.

Gabas, N., Hiquily, N., & Laguérie, C. (1994). Response of Laser Diffraction Particle Sizer to Anisometric Particles. *Particle & Particle Systems Characterization*, *11*(2), 121–126. https://doi.org/10.1002/ppsc.19940110203

Khalikova, E., Susi, P., & Korpela, T. (2005). Microbial dextran-hydrolyzing enzymes: fundamentals and applications. *Microbiology and Molecular Biology Reviews*, *69*(2), 306–325. https://doi.org/10.1128/MMBR.69.2.306-325.2005

Kontrec, J., Ukrainczyk, M., Babić-Ivančić, V., & Kralj, D. (2011). Synthesis of Calcium Carbonate by Semicontinuous Carbonation Method in the Presence of Dextrans. *Croatica Chemica Acta*, *84*(1), 25–32. https://doi.org/10.5562/cca1746

Liu, E. J., Cashman, K. V., & Rust, A. C. (2015). Optimising shape analysis to quantify volcanic ash morphology. *GeoResJ*, *8*, 14–30. https://doi.org/10.1016/j.grj.2015.09.001

Schubert, H. (2012). *Handbuch der Mechanischen Verfahrenstechnik*. Hoboken: John Wiley & Sons.

Stieß, M. (Ed.). (2009). *Mechanische Verfahrenstechnik - Partikeltechnologie 1* (3. Auflage). Berlin Heidelberg: Springer.

Van der Poel, P. W., Schiweck, H., & Schwartz, T. (1998). *Sugar Technology: Beet and Cane Sugar Manufacture*. Berlin: Dr. Albert Bartens KG.

Wojtczak, M., Gruska, R., MIkos, P., Antczak-Chrobot, & Aneta. (2015). Dextran molecular mass effect on particle size distribution of CaCO3 for 1st and 2nd carbonatation. *Sugar Industry*, *140*(11), 703–706.

5 Comparative Analysis of Dextran-Induced Sucrose Crystal Modifications

Abraham, K. [a b], Rudolph-Flöter, E.S.J. [a], Schlumbach, K. [a], Schäfer, A. [a], Flöter, E. [a]

[a] TU Berlin, Department of Food Process Engineering, Seestraße 13, 13353 Berlin, Germany

[b] SternEnzym, Kurt-Fischer-Str. 55, 22926 Ahrensburg, Germany

Submitted to the Journal of Crystal Growth (2019).

Abstract

The analysis of sucrose crystal size and shape modifications induced by the presence of dextran was key to this study. Therefore, evaporative crystallisation experiments using synthetic thick sucrose juices containing various contents of high molecular mass dextran (T2000) were performed. HPLC analysis of the dissolved sucrose crystals revealed that T2000 dextran gets incorporated into the sucrose crystal, indicating that dextran-related crystal size and shape modifications occur. For analysing the sucrose crystal size and shape distribution, static image analysis was implemented and compared to common sieve analysis as well as dynamic image analysis (Camsizer). All methods consistently indicate an increase of crystals with lower minimum and especially lower maximum feret diameters due to the presence of T2000 dextran. For the sucrose crystal shape analysis, average values and relative frequency distributions were evaluated. For more detail, the shape data were further processed using a crystal size-dependent evaluation. Thereby, it was found that cube-shaped crystals, elongated needle-shaped crystals and agglomerates can be related to the presence of dextran. The data suggest that the occurrence of the three dextran-related shapes depend on the dextran content present and also relate to certain sucrose crystal sizes. This way, cube-shaped crystals could be related to small-sized crystals, predominantly occurring at lower dextran contents. Agglomeration and distinct elongation were found to be related to mid- and especially large-sized crystals. The latter two, especially distinct elongation, seem to increasingly occur when higher dextran contents were present.

5.1 Introduction

The presence of microbial polysaccharides in sugar beet and cane juices is widely known to affect the crystallisation process during sugar manufacture (Asadi, 2007). Infestation of sugar cane and beet cells with lactic acid bacteria, more specifically *Leuconostoc Mesenteroides* species, inter alia results in the production of dextran (Abdel-Rahman, 2007). Dextran is homogenously composed of glucose units, which are mainly linked via α-(1→6) glycosidic linkages. Besides, it was reported that sugar industry-relevant species produce dextran containing up to 5 % branching points via α-(1→2), α-(1→3) and α-(1→4) glycosidic bonds (Khalikova et al., 2005). The molecular mass distribution of dextran in sugar raw juices is known to cover a broad range from 15 to 2,000 kDa (Chen & Chou, 1993).

It is widely assumed that not only the total dextran content, but also the molecular mass distribution is relevant for the extent and kind of the dextran-induced effects during sucrose crystallisation. In general, the final sucrose crystal characteristics depend on various internal and external process conditions during nucleation and subsequent crystal growth. Hydrodynamic solution properties, the degree of supersaturation as well as the characteristics of the growing crystal surface are the main departure points for understanding the phenomena during crystallisation. Modified solution characteristics concerning the flow behaviour as well as the sucrose solubility are directly linked to crystallisation kinetics. It is further a well-known fact that impurities can interact with the growing crystal surfaces leading to modified crystal habits (van der Poel et al., 1998). Dextran is known to affect both, hydrodynamics as well as crystal characteristics, which is assumed to depend on the molecular mass distribution present (Abdel-Rahman et al., 2007). So far, there is general agreement that high molecular mass dextran is mainly responsible for a viscosity increase negatively affecting diffusion processes and thus the crystallisation rate (Kaur & Kaler, 2008). Besides, high as well as low molecular mass dextran are known to be involved in modifications of the final sucrose crystal characteristics with regard to size and shape distributions (Abdel-Rahman et al., 2007).

Reviewing the literature (see for instance (Abdel-Rahman, 2007)), the dextran-related effects on the viscosity appear reasonably well understood. There is also a substantial amount of studies about the effects of dextran on the sucrose crystal characteristics. However, reports on these dextran-related sucrose crystal modifications are divergent, implying that the specific mechanism is not fully understood yet. Even though the statements differ, it was consistently stated that dextran is responsible for modifications deviating from the desired sucrose crystal shape. A theoretical three-dimensional sucrose crystal shape is shown in Figure 5-1, illustrating the horizontal B- and vertical C-axis. The A-axis is perpendicular to the observation plot. Its allocation to the monoclinic crystal system inter alia implies that the length of the three axes (A, B, C) differ from one another.

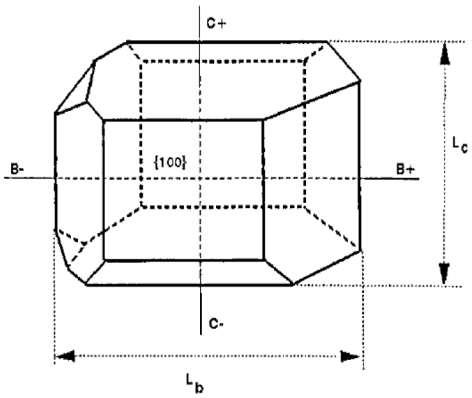

Figure 5-1 Theoretical sucrose crystal shape (Bubnik & Kadlec, 1992).

Several different faces are able to grow, whereby the most important eight faces are visible and identifiable on the final sucrose crystal shape. The initial faces for growth are of flat, stepped or kinked character. The most rapid growth occurs on the latter two. The crystal morphology directly correlates with the growth rate of the different crystallographic faces. Regarding the lengths of the crystal axes grown in pure sucrose solutions, the B-axis is generally known to be the elongated one. A ratio of the C- to the B-axis of 0.7 for a sucrose crystal grown in a pure aqueous sucrose solutions has been reported (van der Poel et al., 1998). Similarly, Faria et al. determined a ratio of the C-axis to the B-axis of 0.79 for sucrose crystals grown in a pure aqueous sucrose solution (Faria et al., 2002). However, the crystallisation conditions as well as the presence of impurities, such as dextran, are known to affect the growth along the respective crystal axes (Mathlouthi & Reiser, 1995). In general, impurities can get in contact with the growing crystal surface in different ways. First of all, impurities can be attached to the sucrose crystals in form of residual mother liquor, which can be removed by an additional affination step. Besides, impurities can be attached by adsorptive forces or can get incorporated into the crystal lattice (van der Poel et al., 1998).

It is mainly reported that the presence of dextran causes an elongation along the initially shorter C-axis of the sucrose crystal, which was for instance found by Mantovani et al. (Mantovani et al., 1960). In contrast, Faria et al. found that elongated crystals occur only occasionally. Instead, cube-shaped crystals and pronounced agglomeration was predominantly related to the presence of dextran (Faria et al., 2002). Similar to Faria et al., previous work of ours has shown that indeed the presence of dextran alters the crystal shape in different ways (cube-shaped, elongated and agglomerated crystals). However, no clear preference to one of the crystal shapes observed could be identified (Abraham et al., 2016).

Thus, the specific action of dextran appears to be more complex, which certainly also relates to the crystallisation conditions, e.g., concentration, temperature, and supersaturation (Abdel-Rahman et al., 2008). Anyhow, the simultaneous occurrence of different crystal shapes complicates a clear evaluation of crystal shape data. Therefore, consideration of averaged data obtained from the image

analysis of two-dimensional crystals can easily be misinterpreted and does not allow to distinguish between different shapes.

The study presented aims at adequately analysing sucrose crystal characteristics allowing to identify dextran-induced modifications using different methods by comparison. Therefore, sucrose crystals were produced by evaporative crystallisation experiments using synthetic thick juices with varying dextran contents. For the analysis of the crystal size and shape distribution, static image analysis was implemented and compared to two common particle analysis methods, especially sieve analysis as well as dynamic image analysis (Camsizer).

Average values as well as relative frequency distributions were calculated and used to identify the crystal size and shape distribution present. Different to previous investigations, the static image analysis was additionally used for a crystal size-dependent evaluation of particle shape parameters in order to distinguish different sucrose crystal shape modifications caused by dextran.

5.2 Material and Methods

5.2.1 Materials

Evaporative crystallisation experiments using synthetic thick juices (66 % (m/m) sucrose solutions) with varying amounts of high molecular mass dextran (T2000: Sigma-Aldrich, dextran 2000 with a molecular mass distribution of 1,500 to 2,800 kDa) were performed. Therefore, refined sucrose (Nordzucker, extra-white sugar) was used. The T2000 dextran originate from lactic acid bacteria, more specifically from the *Leuconostoc mesenteroides* strain B512.

5.2.2 Crystallisation Experiments

5.2.2.1 Crystallisation Pilot Plant

Evaporative crystallisation experiments were performed using a crystallisation pilot-plant with a volume of 5 litre followed by centrifugation and drying. The plant design as well as the experimental procedure is described in detail elsewhere (Schlumbach et al., 2017). Schlumbach et al. also verified the experimental set-up on reproducibility and suitability for the production of sugar possessing industry relevant quality. The crystallisation unit is composed of a double wall stainless-steel vessel with a cylindrical glass vessel mounted on top. Both vessels are individually temperature controlled via two thermostats (F32-HD and F12-MC, Julabo). A Pt-100 thermocouple as well as a process refractometer (iPR 2-3, Schmidt & Haensch GmbH & Co) are attached on top and on the bottom of the vessel, respectively. This allows continuous monitoring of temperature and dry substance content throughout the crystallisation run. The vacuum is built up and held constant using a vacuum pump (PC 3001, Vacuubrand GmbH & Co KG). An agitator (RZR 2102 control, Heidolph Instruments GmbH & Co. KG) is used to move a stirrer inside the vessel. A gastight permanent magnetic coupling on top of the vessel guarantees the vessel to be tightly sealed

in order to maintain the vacuum at which the crystallisation is done. The agitator is further applied to determine the torque serving as reliable indication for the end of the crystallisation run. The experimental set-up is computer-controlled and the data (temperature, pressure, dry substance) are recorded online using an in-house written code in Lab-VIEW. Furthermore, all input and output flows are manually recorded in order to allow mass balance calculations. An inlet and an outlet valve at the bottom of the vessel allow filling and sampling, respectively. The steam resulting from evaporation leaves the system on top of the vessel, where it enters a vent condenser connected to an Anschuetz-Thiele receiver, enabling the quantification of the condensate produced. After discharging the crystal slurry from the crystallisation equipment, the sucrose crystals are separated from the mother liquor in a temperature-controlled centrifuge, which is equipped with a washing unit with a flat-jet nozzle enabling the removal of residual syrup from the sucrose crystal surface. To finish, the sugar is dried in a fluidized bed dryer (Fluid bed dryer TG 1, Retsch).

5.2.2.2 Experimental Procedure

Different feedstocks were prepared as 66 % (m/m) aqueous sucrose solutions with varying additions of high molecular mass dextran (T2000: Sigma-Aldrich, dextran 2000 with a molecular mass distribution of 1,500 to 2,800 kDa). Filling of the crystallisation unit was done via the inlet valve supported by the pressure below atmospheric pressure within the vessel. With the help of the in-house code, the saturation of the solution is computed from the in-situ data of temperature, refractive index and density determined. Once a supersaturation of 1.05 was reached, seed crystals of defined sizes (180 – 250 µm) were added to initiate the crystal growth. In agreement with industrial practice, addition of seed crystals to the system being in the metastable zone of supersaturation is supposed to avoid nucleation. Consequently, the number of crystals is basically constant throughout the crystallisation run and only their size increases due to crystal growth.
The required amount of seed crystals of known diameter can accordingly be calculated using the equation based on the d^3-rule (Witte, 1987), in which $n_{Cr,i}$ and $m_{Cr,i}$ refer to the number and mass of crystals, respectively. The indices 0 and 1 are related to the starting and end point of a crystallisation strike. Thereby, not only the desired size of the produced crystals but also the number and mass of crystal at the end of the crystallisation need to be given.

$$m_{Cr,0} = m_{Cr,1} \times \left(\frac{d_{Cr,0}}{d_{Cr,1}}\right)^3 \times \frac{n_{Cr,0}}{n_{Cr,1}} \tag{5-1}$$

The process was subsequently controlled in a way that, at practically constant supersaturation of 1.05, approximately 50 % (m/m) crystalline material within the slurry was generated. This end point of the crystallisation run was indicated by the increase of the agitator's torque of 0.06 Nm compared to its initial value. The resulting crystals were then separated from the mother liquor via centrifugation, whereby the residual syrup attached to the crystal surface was removed by spraying

wash water on them. A fluidized bed dryer was further used to dry the sugar at 333 K for 5 minutes. The experimental procedure was proven reliable by repeating the crystallisation of the dextran-free reference system four times. The results have indicated good repeatability. Subsequent crystallisation experiments using the synthetic thick juices containing various contents of high molecular mass dextran were performed in duplicate.

5.2.3 Chromatographic Analysis

The dextran content included in or adsorbed onto the final sucrose crystals were chromatographically analysed prior to and following an additional affination step. Therefore, the sucrose crystals were dissolved in distilled water in a way that 10 % (m/m) aqueous sucrose solutions were obtained. The dextran content in these aqueous sucrose solutions was chromatographically determined. The chromatographic measurements in aqueous solutions were performed using high pressure liquid chromatography (Chromaster system, Hitachi) with an evaporative light scattering detector (ELSD 90 LT-Low Temperature, VWR). A single separation column was used to separate the saccharides based on affinity (ABOA SugarSep-Ca, AppliChrom). An isocratic method with distilled water as the mobile phase was applied. The flow rate was set to a constant value of 0.5 ml/min and a sample volume of 20 µl was injected. The temperature of the oven and the detector were set to 353 K and 323 K, respectively. The samples were pre-filtered using 0.45 µm syringe filters (Chromafil GF/PET-45/25, Macherey-Nagel) and were transferred into 1.5 ml vials. The chromatograms obtained were analysed using the Peakfit software 4.12. A calibration curve of the area as a function of the T2000 dextran content was created and used to determine the dextran content of the samples. The dextran concentration determined has then been related to the mass of sucrose in the samples, expressed as milligram per kg sucrose.

5.2.4 Analysis of Sucrose Crystals

5.2.4.1 Sieve Analysis

Classical sieve analysis was done according to the ICUMSA Method GS2/9-37 (ICUMSA, 2011). The mean aperture was calculated according to the Powers Method. Besides, the mass-based data were used to calculate percentage distributions retained on each sieve. Class of sieves with aperture sizes of 180, 315, 400, 560, 630, 710, 800 and 900 µm were used.

5.2.4.2 Static Image Analysis

Static image analysis combines light microscopy with the ImageJ software 1.51k (Ferreira & Rasband, 2012). Light microscopy images were recorded using a Zeiss-Axio Scope A1 microscope. Microscope slides were loaded with the dry sucrose crystals in a way that the whole slide is used. With the help of the tile function included in the Zeiss software, images of the microscopic slides

were completely recorded. The resulting images of three microscopic slides of each sample were subsequently analysed using ImageJ. This way, a minimum crystal number of about 400 for each sample composition was analysed.

In order to properly analyse the crystal size and shape, calibration as well as image editing are necessary. Thus, two-dimensional crystal shapes were analysed, while assuming that the crystals lay on the largest 100-surface. In order to reduce potential errors due to dust or foreign matter, only crystals with a circularity of at least 0.8 were considered. This limit value was chosen and proven to give reliable results based on preliminary experiments of sucrose crystals.

The size parameters, maximum and minimum feret diameter, are depicted as relative frequency distribution curves, corresponding to certain size ranges in steps of 200 µm.

According to the ImageJ user guide, the maximum and minimum feret diameter refer to the longest and shortest distance between any two points along the selection boundary, respectively. Thus, the minimum and the maximum distance between two parallel tangents on opposite sides of the projection area are respectively used to determine the maximum and minimum feret diameter (Fernlund, 1998). The ratio of the minimum and the maximum feret diameter refers in this study to the width-to-length ratio, see equation (5-2).

$$Width/Length = \frac{Minimum\ diameter}{Maximum\ diameter} \tag{5-2}$$

The circularity is defined by the following equation (5-3) (Ferreira & Rasband, 2012).

$$Circularity = 4\pi \times \frac{Area}{Perimeter^2} \tag{5-3}$$

The two shape parameters are depicted as average values and relative frequency distributions. Besides, a size-dependent shape analysis of the sucrose crystals according to the maximum feret diameter was established. Three categories were chosen in a way that each category is sufficiently represented by a similar crystal number. Therefore, three categories were used, sucrose crystals with a maximum diameter of less than 1000 µm, ranging between 1000 and 1250 µm and greater than 1250 µm, respectively.

5.2.4.3 Dynamic Image Analysis

Dynamic image analysis was done using the Camsizer P4 (at the department of geo-technical engineering at the Technical University of Berlin, Ernst-Reuter-Platz 1, 10587 Berlin, Germany). An amount of 500 g of each sample was analysed, no preparation necessary. The greatest advantages of this method are hence a minimum of preparation effort as well as the coverage of a comparatively high number of crystals. For reasons of comparison, size and shape parameters possessing the same definitions were applied to both, static and dynamic image analysis. These are the maximum and minimum feret diameter of the crystals as well as the circularity and the width-to-length ratio. The size parameters, maximum and minimum feret diameter, are depicted as relative

frequency distribution curves. The shape parameters, namely circularity and width-to-length ratio, are illustrated as average values.

5.3 Results and Discussion

5.3.1 Chromatographic Analysis of Sucrose Crystals

From literature, it is known that dextran influences the growth of sucrose crystals. From the physico-chemical view, the influence of non-sugar components on the sucrose crystallisation should be distinguished in components that are only loosely attached to the surface of the crystal and those which are incorporated into the crystal lattice. So far, there are only limited data available quantifying the amount of dextran attached to or incorporated into the sucrose crystal. To distinguish between loosely adsorbed non-sugar components and non-sugar components that are incorporated into the crystal, an additional affination step was done. During this step, the loosely adsorbed non-sugar components are removed. HPLC analysis before and after affination were performed in order to determine the amount of dextran incorporated into the crystal and the amount adsorbed to the crystal surface. Therefore, a defined amount of sucrose crystals before and after affination was dissolved in distilled water. Figure 5-2 (A) shows the chromatograms of 10 % (m/m) solutions containing sucrose crystals obtained from the crystallisation of the synthetic thick juices loaded with the highest dextran content of 15,000 mg/kg sucrose before and after the affination step (solid and dashed line, respectively). The similar course of these two chromatograms indicates practically unchanged dextran contents. For more detail, the chromatograms were evaluated using Peakfit 4.12, which reveals dextran contents of roughly 350 mg/kg sucrose for both, the non-affinated and the affinated samples (duplicate), see Figure 5-2 (B). The data reveal that the total dextran content in the crystals determined did not change significantly due to the additional affination step. This fact clearly indicates that dextran was incorporated into the crystal lattice. This suggests that crystal size and/or shape modifications are driven by an incorporation mechanism. Taking into account that the feed solution had a dextran content of 15,000 mg/kg sucrose, an incorporation factor of approximately 2 % was found. This approach reflects industrial practice. It has, however, to be considered that during the crystallisation process, the non-sugar components, and hence also dextran, were concentrated by a factor of approximately 2.5 in the mother liquor. Applying simple mass balances, a partition factor (growing crystal surface to mother liquor) of approximately 1.15 % emerges.

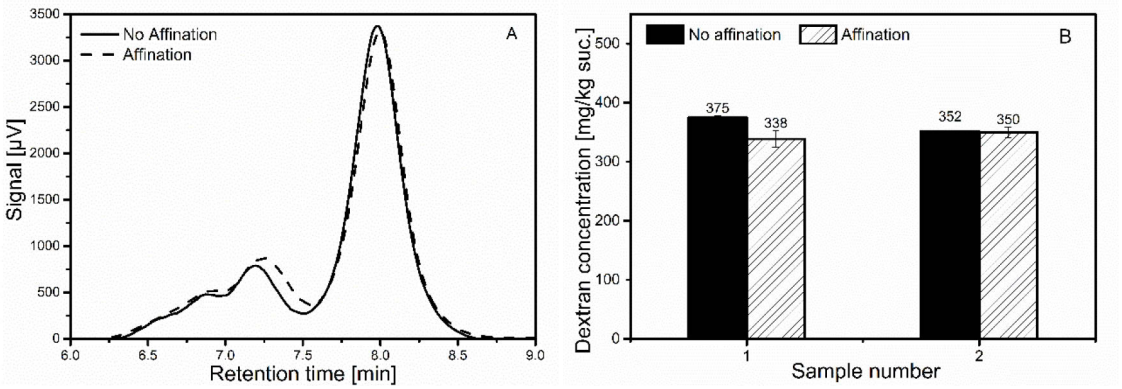

Figure 5-2 HPLC analysis of the sucrose crystals produced in the presence of 15,000 mg T2000 dextran/kg sucrose. A) HPLC-chromatograms before (solid line) and after (dashed line) affination. B) Dextran concentration determined before (filled bars) and after (hatched bars) affination [mg/kg sucrose].

5.3.2 Impact of Dextran on Sucrose Crystal Characteristics

5.3.2.1 Sucrose Crystal Size Distribution

The sucrose crystal size distribution was analysed using the three different particle analysis methods, sieve analysis and dynamic as well as static image analysis.

Classical sieve analysis uses the mass of the sucrose crystals retained on sieves with different aperture sizes. Thus, the minimum diameter of the sucrose crystals is decisive for the retention on the respective sieve apertures. Assuming a Gaussian distribution, the mean aperture can be calculated, shown in Figure 5-3 (A). Obviously, the mean aperture decreases from roughly 635 µm for the dextran-free reference to 615 µm for the sample loaded with 5000 mg dextran/kg sucrose. The mean aperture slightly further decreases with the increase of the T2000 dextran content, resulting in a reduction of up to 30 µm for the highest T2000 content of 15,000 mg/kg sucrose. In addition, the mass-based percentages retained on each sieve of a certain mean aperture size was calculated, see Figure 5-3 (B). The percentage distribution clearly shows that the decreasing mean aperture size is due to the fact that in particular more particles were retained by an aperture size of 560 µm and 630 µm when dextran was present. Thus, a maximum increase of 15 % at an aperture size of 560 µm for the highest dextran load of 15,000 mg/kg sucrose was found. Additionally, a slight increase of retained crystals was observed at a distinctly lower aperture size of 180 µm. Clearly fewer crystals were retained by sieves with an aperture size larger than 630 µm for the dextran-loaded samples. However, when dealing with modified crystal shapes, sieve analysis can be prone to misinterpretation. Furthermore, classical sieve analysis is not capable to deduce information about crystal shapes (e.g. needle-shaped crystal can still pass through apertures).

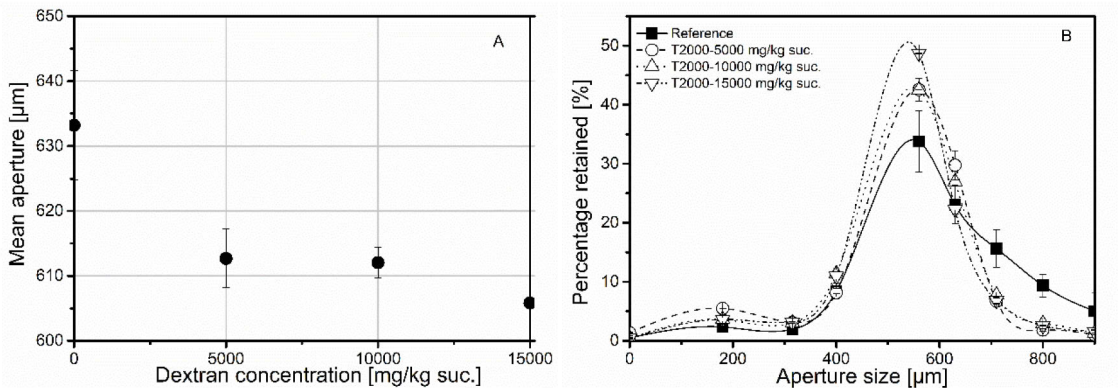

Figure 5-3 Sucrose crystal size analysis by sieve analysis. A) mean aperture and B) distribution curve with respect to aperture size.

To reveal more details on the crystals shape and size, dynamic as well as static image analysis were additionally used. For both methods, the minimum and maximum feret diameter of the sucrose crystals were determined and depicted as relative frequency distributions. Figure 5-4 (A) and (B) show the frequency distribution of the two diameters obtained from dynamic image analysis (Camsizer). For the dextran-free reference (solid line), it was found that the main proportion of the sucrose crystals possessed minimum diameters ranging from 600 µm to 1000 µm (Figure 5-4 A). Interestingly, in this case, the curves of the dextran-free and dextran-loaded samples deviate only slightly. For all samples, the maximum of the distribution curve of the minimum feret diameter was found at diameters of 800 µm. For the dextran-loaded samples, the number of particles with minimum feret diameters of more than 1000 µm is slightly lower, while the number of particles with smaller diameters below 800 µm is slightly higher in comparison with the dextran-free reference.

The distribution curves of the maximum feret diameter show more clearly the difference between the dextran-free reference and the dextran-loaded samples (Figure 5-4 (B)). The distribution curve of the reference material shows a maximum of the distribution curve at a diameter of 1250 µm. For this and larger diameters, there are more particles found in the reference sample than in the dextran-loaded samples. The maxima of the distribution curves of the dextran-loaded samples shifted to a diameter of 1000 µm. Basically, the samples of the crystals produced in the presence of the different dextran contents show similar distribution curves. Interestingly, the samples of the crystals produced in presence of the lowest dextran content show additionally a local maximum at diameters of 400 µm.

The samples loaded with higher dextran contents do not display a maximum at 400 µm, but slightly more crystals with maximum feret diameters of larger than 1200 µm were found, compared to the sample with the lowest dextran content. Combination of the distribution curves of the maximum and minimum feret diameter clearly shows that the mean diameter decreases with increasing dextran content, just as the sieve analysis revealed.

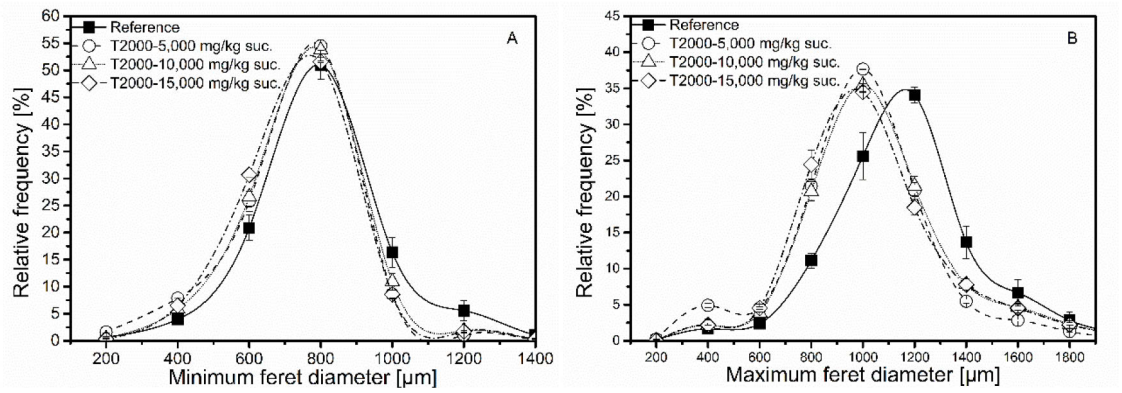

Figure 5-4 Sucrose crystal size analysis by dynamic image analysis (Camsizer). Relative frequency distribution curves with respect to A) the minimum and B) maximum feret diameter.

The static image analysis applied in this work is generally distinctive to the other two methods due to a number-based evaluation. Thus, effects due to the presence of more small-sized crystals are generally even more pronounced. The data obtained from static image analysis are shown in Figure 5-5. Here, again, the main proportion of the sucrose crystals contained in the dextran-free reference possesses minimum diameters of 600 to 1000 µm with a maximum at 800 µm, which is in good agreement with the data obtained from dynamic image analysis (peak maximum of the solid line in Figure 5-5 (A)).

Different to the dynamic image analysis, the data of the minimum and the maximum feret diameter of the dextran-loaded samples differ quite clearly from the data of the reference samples. In general, the maxima of the minimum feret diameter of the dextran-loaded samples were found at slightly higher diameters. At the low dextran content of 5,000 mg/kg sucrose, a higher amount of crystals with slightly higher minimum diameters of 800 to 1000 µm can be seen, more precisely it is increased by 15 %. However, this effect systematically decreases on further dextran addition and was not found for the highest dextran load of 15,000 mg/kg sucrose anymore. Instead, a higher number of crystals with lower minimum diameters of 400 to 600 µm was found. Besides, a considerable increase of crystals with even lower minimum diameters of about 200 to 400 µm was found for the samples containing higher dextran contents of 10,000 and 15,000 mg/kg sucrose, roughly tripled in comparison with the dextran-free reference.

Again, the relative frequency distribution according to the maximum diameter shows even more pronounced and systematic changes of the diameter distribution. The distribution curves corresponding to the dextran-loaded samples are either bimodal or spread out over a wider diameter range. The maxima of the maximum feret diameter were found at slightly lower values in comparison with the reference, except from the highest dextran load of 15,000 mg/kg sucrose.

Similar to the data obtained from dynamic image analysis, Figure 5-5 (B) reveals that the main proportion of the reference crystals possesses maximum diameters of 1000 to 1400 µm with a maximum at 1200 µm.

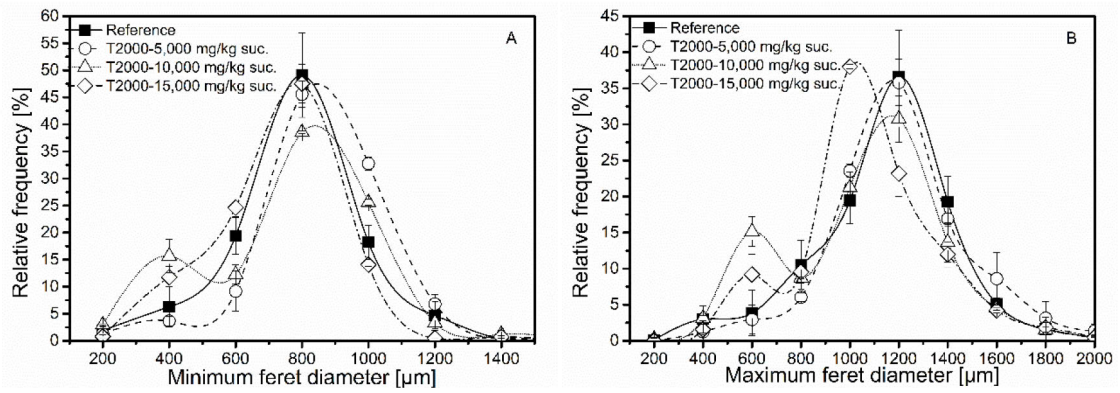

Figure 5-5 Sucrose crystal size analysis by static image analysis. Relative frequency distribution curves with respect to A) minimum and B) maximum feret diameter. A minimum crystal number of about 400 per sample was analysed.

In the range between 1200 and 1400 µm, the occurrence of particles systematically decreases on T2000 dextran dosage, ending in a maximum reduction of 12 %. Lower maximum feret diameters of 1000 µm increasingly occur with increasing dextran content. Especially the highest load of 15,000 mg/kg sucrose caused an increase by roughly 18 %. Besides, an additional local maximum was found at 600 µm for samples containing 10,000 and 15,000 mg/kg sucrose.

In general, all three methods applied consistently indicate that the presence of T2000 dextran caused an increased occurrence of sucrose crystals with a lower (mean) diameter size. Dynamic as well as static image analysis additionally indicate that this is mainly related to reduced maximum diameters. The sieve analysis as well as static image analysis further indicate a slight reduction of the minimum diameter.

In conclusion, the size data of the maximum to the minimum feret diameter, indicate increased amounts of smaller cube-shaped crystals due to the presence of dextran. To substantiate this initial assessment, additional data processing is necessary.

5.3.2.2 Crystal Shape Analysis

5.3.2.2.1 General Understanding of the Shape Parameters

Dynamic as well as static image analysis additionally reveal particle shape parameters, which can be used to detect modifications of the sucrose crystal morphology. Two crystal shape parameters have been chosen to detect dextran-induced sucrose crystal shape modifications, the circularity and the width-to-length-ratio (see equation (5-2) and (5-3) above). The advantage of using these parameters is that these are determined from the number of pixels of the projections of the various crystals.

To initially better understand the size and shape analysis, different theoretical geometrical forms were chosen and evaluated by the static method, see Figure 5-6. For two-dimensional sucrose crystal analysis, cubic (A) and rectangular shapes ((B) and (C)) are of relevance. Besides,

agglomerates, consisting of different single crystal forms, can occur during sucrose crystallisation. The latter is approximated by different artificial agglomerate shapes, see (D) to (F) in Figure 5-6.

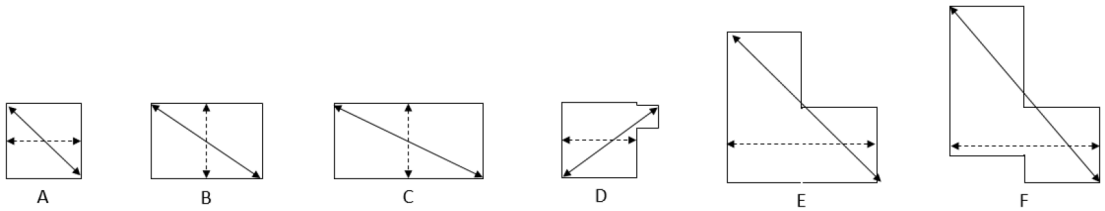

Figure 5-6 Determination of the maximum and minimum feret diameter for theoretical geometrical shapes by ImageJ. Perfect square (A); Rectangles with different maximum feret diameters (B) and (C); Artificial agglomerate shapes (D) to (F).

Table 5-1 Circularity and width-to-length ratio (=minimum feret/maximum feret) determined by Image J for the geometrical forms shown in Figure 5-6.

Shape parameter	Cube (A)	Rectangle (B)	Rectangle (C)	(D)	(E)	(F)
Circularity	0.8	0.77	0.7	0.71	0.6	0.5
Width/Length	0.7	0.55	0.44	0.65	0.71	0.65

As mentioned above, the maximum and minimum feret diameter refer to the longest and shortest distance between any two points along the selection boundary. In squares and rectangles ((A), (B) and (C)), this means that the maximum feret is represented by the maximum diagonal (see Figure 5-6). For irregular forms, such as the agglomerate shapes (D) to (F), the minimum and maximum feret length are determined based on the shortest and longest straight lines which fits into the contour of the particle/crystal.

To illustrate the two shape parameters, the circularity and the width-to-length ratio, were determined for the 2-D projections of these defined geometrical forms, see Table 5-1. The perfect cube has the highest values for both, the circularity and the width-to-length ratio, being the closest to a perfect circle, for which both values would theoretically be equal to 1. More precisely, a cube-shaped crystal is characterised by a circularity of 0.8 and a width-to-length ratio of 0.7. As expected, an elongation of the maximum diameter, as it is the case for the two rectangles, the width-to-length ratio as well as the circularity decrease. The more elongated a rectangular crystal is, the lower the width-to-length ratio and the lower the circularity.

Keeping the determination of the maximum and minimum feret diameter for irregular shapes in mind, the artificial agglomerate shapes show a similar width-to-length ratio as the cube-form due to the way the minimum and maximum feret length are determined. However, the circularity is most prominently decreased for the artificial agglomerate shapes (E) and (F), most deviating from a cube-shape.

To distinguish between the different degrees of elongation, the width-to-length ratio would be enough. However, the single crystal data have shown that the circularity in combination with the

width-to-length ratio need to be considered in order to distinguish between agglomerates and cube-shaped crystals. Thus, the combined evaluation of these two shape parameters is mandatory to detect sucrose crystal shape modifications.

More practically, single crystal analysis of realistic sucrose crystal shapes identified in the dextran-free and dextran-loaded samples were additionally considered and compared to the theoretical shapes discussed above, see Figure 5-7. Crystal type (A) is a representative shape of a reference crystal and (B) to (D) are crystal shapes found in the dextran-loaded samples. Here, too, the circularity and the width-to-length ratio are compared to the values of the reference crystal shape, see crystal (A) in Figure 5-7. The crystal shape-related changes of these shape parameters are shown and compared to the values of the reference crystal in Table 5-2. Four crystal types could be identified, which are quite similar to some of the theoretical geometrical forms suggested in Figure 5-6 and Table 5-1, namely the cube-, the rectangular and the agglomerate L-shape. The latter three crystal types illustrated in Figure 5-7 were previously individually found to be related to the presence of dextran by different authors (Faria et al., 2002). In view of this, the two-dimensional analysis of a reference crystal (type (A)) appears to be closest to a rectangular shape with a width-to-length ratio of 0.6 and a circularity of 0.75.

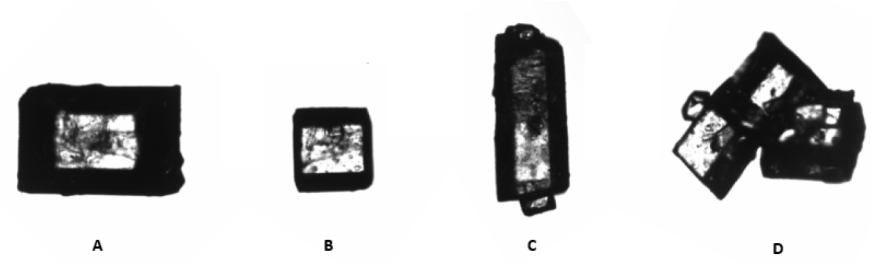

Figure 5-7 Sucrose crystal types identified from single crystal analysis by ImageJ, including a reference crystal (A), cube-shaped crystal (B); distinctly elongated crystal (C) and an agglomerated crystals (D).

Table 5-2 Circularity and width-to-length ratio (=minimum feret/maximum feret) determined by Image J for the sucrose crystals identified in dextran-free and dextran-loaded samples shown in Figure 5-7.

Shape parameter	Reference	Cube-shape	Elongated shape	Agglomerates
Circularity	0,75	0,78 ↑	0,58 ↓	0,51 ↓
Width/Length	0,6	0,75 ↑	0,39 ↓	0,83 ↑

Similar to the findings from the just discussed theoretical shapes, for an approach to a cube-shape (type (B)), both shape parameters increase in comparison with the reference crystal. Quite the opposite parameter change was found for distinctly elongated crystals (type (C)), for which the circularity as well as the width-to-length ratio distinctly decrease. As exemplary shown by the artificial crystal type (E) in Figure 5-6 above, in case of agglomerates, the width-to-length ratio might be about the same as the value of a cube-shaped crystal. However, the circularity value is

clearly smaller than the value of the cube-shaped crystal (see Table 5-1 and Table 5-2). Thus, in comparison with the reference, a significant decrease of the circularity combined with higher width-to-length-ratios can be attributed to agglomerates (type (D)). First and foremost, the single crystal analysis confirmed that the latter three shapes (type (B) to (D)) simultaneously occur when T2000 dextran was present during sucrose crystallisation.

5.3.2.2.2 Evaluation of Average Values of the Shape Parameters – Dynamic and Static Image Analysis

To compare dynamic and static image analysis, the two shape parameters are depicted as total average values including the data of all crystals analysed. Figure 5-8 (A) shows the average values of the circularity obtained from dynamic (open dots) and static (filled dots) image analysis. In general, the data points obtained from the two methods are slightly different but show a very similar pattern. The values obtained from the dynamic image analysis are generally larger than those from the static analysis. Considering the reference sample, the dynamic data give a slightly higher average circularity as the analysis of the single reference crystal, while the static method gives an average circularity just slightly below this value of the exemplary reference single crystal. Both deviations are within 1.3 %.

The fact that both methods give the same trend of behaviour is in particular interesting because of the fact that fewer particles were used for the static image analysis as for the dynamic image analysis. The data obtained from dynamic image analysis suggest an increase of the average circularity due to a T2000 dextran content of 5000 mg/kg sucrose (from 0.76 to 0.79). After this initial jump, the average values of the circularity slightly decrease when further increasing the T2000 dextran content but remain still slightly higher in comparison with the reference (at about 0.77). The data obtained from static image analysis generally revealed slightly lower values in comparison with dynamic image analysis, but similarly, a slight increase is observed when comparing the average circularity of the reference with the circularity of the crystals produced in presence 5000 mg/kg sucrose (from 0.74 to 0.75). Here, too, a subsequent decrease could be observed by increasing the dextran concentration, which in this case, debark just slightly below the reference value (0.735).

The average values of the width-to-length-ratio obtained from dynamic and static image analysis are shown in Figure 5-8 (B). Again, the same general dependence of the width-to-length ratio on the dextran content is found for both analytical methods.

Considering the definition of this parameter, the width-to-length ratio never exceeds a value of 1, not even for a perfect cube shape (0.7). In this case as well, the average values of the width-to-length-ratio show an increase due to the presence of the lower dextran content of 5000 mg/kg sucrose (from 0.62 to 0.66 and from 0.65 to 0.69 for dynamic and static image analysis,

respectively). Again, after an initial jump, the average values subsequently slightly decrease with the increase of the dextran content but remain slightly higher for both methods in comparison with the reference.

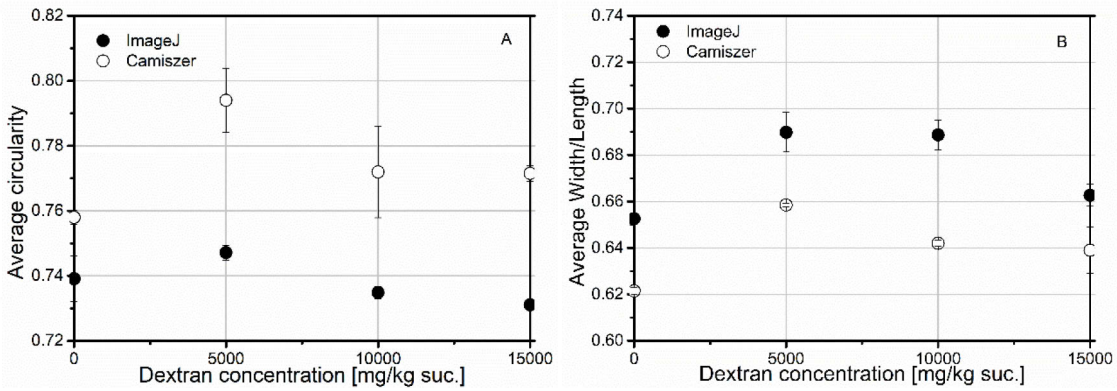

Figure 5-8 Average values of the circularity (A) and the width-to-length ratio (B) obtained from static (filled dots) and dynamic (open dots) image analysis including all sucrose crystals analysed.

According to Table 5-1 and Table 5-2, a simultaneous increase of the circularity and the width-to-length ratio points towards a higher amount of cube-shaped crystals, which was found for the analysis of the crystals produced in in the presence 5000 mg/kg sucrose. Analyses of the other dextran-loaded samples revealed that further addition of dextran results in a decrease of both, the circularity and the width-to-length ratio, in comparison with the sample containing the low dextran content. Nevertheless, a clear interpretation based on these average values appears rather difficult due to the varying and partly opposing contributions of the above-discussed crystal shapes (cube-shaped and elongated crystals as well as agglomerates, see Figure 5-7 above). Thus, a more detailed evaluation is necessary to clearly determine and potentially to distinguish different crystal shapes. Therefore, the relative frequencies of the circularity and width-to-length ratio were additionally determined.

5.3.2.2.3 Relative frequency Distributions – Static Image Analysis

The relative frequency distribution of the circularity and the width-to-length-ratio are shown in Figure 5-9 (A) and (B). In general, the distribution curves corresponding to the circularity are relatively similar for all samples, differences are minor. The distribution of the dextran-free reference has its maximum at relatively high circularities between 0.75 and 0.8, which can be represented by rectangular reference crystals or cube-shaped crystals (filled squares in Figure 5-9 (A)). The width-to-length ratio of the reference sample spreads from 0.55 to 0.8 with its maximum at 0.65, which is characteristic of rectangular reference crystal shapes.

In view of all crystals analysed, a dextran content of 5000 mg/kg sucrose results in a slight increase of crystals with higher circularities between 0.75 and 0.8 at the expense of intermediate circularities

of 0.7 and 0.75, which is in alignment with the slightly higher average value shown in Figure 5-8 (A) .

Taking into account the distribution curve corresponding to the width-to-length ratio (open circles, Figure 5-9 (B)), it was found that the maximum of the distribution curve is at values of about 0.75, which matches reasonably well to the cube-like crystal type (B) introduced in Figure 5-7. A width-to-length ratio of 0.7 represents a perfect cube, see Figure 5-6 above. Width-to-length ratios above this value imply non-rectangular crystal shapes, e.g. round shapes or agglomerates. For all dextran contents, the amount of crystals with high width-to-length ratios above 0.7 or rather 0.75 is increased at the expense of intermediate width-to-length ratios of 0.6 to 0.7. For the low dextran content of 5000 mg/kg sucrose, the simultaneous increase of the circularity (0.75 to 0.8) and the width-to-length ratio (0.75) again suggests a higher amount of cube-shaped crystals.

In contrast, the presence of 10,000 and 15,000 mg dextran/kg sucrose causes a slight increase of crystals with lower circularities ranging between 0.6 and 0.7 (open diamonds and triangles, Figure 5-9 (A)), which explains the slightly lower average values in comparison with the lower dextran content of 5,000 mg/kg suc. (see Figure 5-8 (A)).

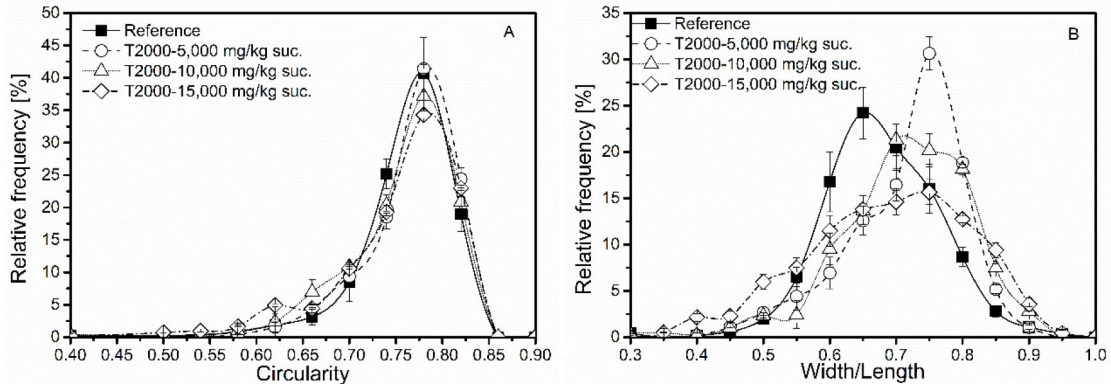

Figure 5-9 Sucrose crystal shape analysis by static image analysis. Relative frequency distribution curves of A) the circularity and B) the with-to-length ratio.

The distribution curves of the width-to-length ratio for the samples with high dextran contents are broader than for the dextran-free reference and the samples with the low dextran content. Thereby, about 45 % of the crystals produced in the presence of high dextran contents have a ratio bigger than 0.7. Again, this points towards more round crystal shapes or agglomerates. This effect systematically decreases with the increase of the dextran content.

For the highest dextran content of 15,000 mg/kg sucrose, a higher number of crystals with distinctly lower width-to-length ratios below 0.5 were additionally found. Thus, the highest dextran load of 15,000 mg/kg sucrose causes an increase of both extremes, crystals with low (<0.5) and high width-to-length-ratios (>0.7) in comparison with the dextran-free reference. The distribution curves at width-to-length ratios lower than 0.7 give the impression that by increasing the dextran content

more crystals are elongated than for the dextran-free reference sample. Thus, the highest dextran load of 15,000 mg/kg sucrose seems to cause higher amounts of both, agglomerates and elongated crystals.

From the relative frequency data, it can be concluded that the T2000 dextran-induced shape modifications seem to depend on the dextran content present. Thereby, cube-shaped crystals seem to be related to lower dextran contents, while elongated and agglomerated crystals increasingly occur for samples with higher dextran contents. In the further course, a size-related evaluation of these shape parameters according to the maximum feret diameter is supposed to additionally unravel to what extent these different dextran-related shapes occur.

5.3.2.2.4 Crystal Size Dependent Evaluation – Static Image Analysis

To further elucidate the dextran-related effects, the shape parameters were additionally evaluated according to three different crystal size categories. Static image analysis data were used for this purpose. Categorisation was done according to the maximum feret diameter of the sucrose crystals. The crystal size-dependent shape analysis refers to three categories, crystals with maximum diameters of less than 1000 µm, ranging from 1000 to 1250 µm and greater than 1250 µm, respectively.

First of all, the percentages of these categories with respect to the crystal number were calculated, see Figure 5-10. Thereby, it is important to mention that the number-based evaluation emphasises the contribution of small-sized crystals. Besides, it is important to keep in mind that if the particles are distributed into categories, the number of particles per category becomes smaller. It should be kept in mind when analysing the data that this renders the data potentially less reliable.

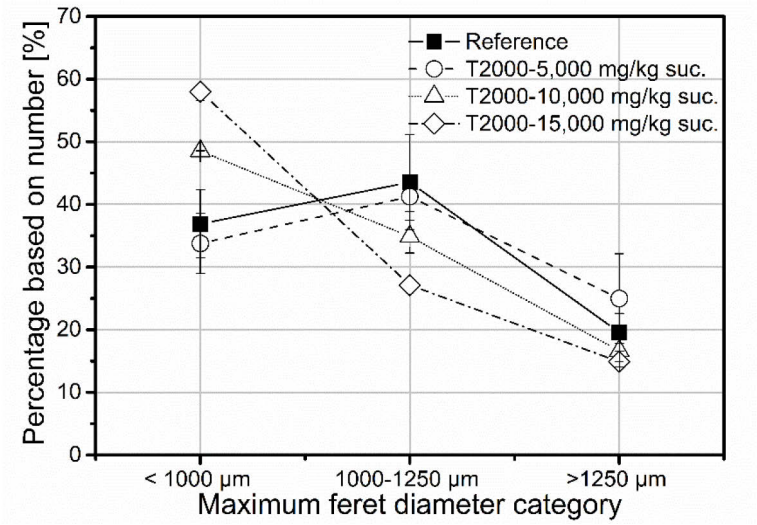

Figure 5-10 Percentages of the sucrose crystal categories based on the crystal number.

For the reference, the number of crystals within the small- and large-sized category constitutes about 40 % and 20 % of all crystals analysed, respectively. The percentage distribution over the

categories for the sample loaded with the low dextran content of 5000 mg/kg sucrose is quite similar to the one of the reference. For the higher dextran contents, the percentage distribution confirms a higher amount of crystals within the small-sized category in comparison with the reference, 50 % and nearly 60 % for 10,000 and 15,000 mg/kg sucrose, respectively.

Figure 5-11 (A) and (B) show the average values for the circularity according to these crystal size-categories. For the dextran-free reference, the average values of the circularity and the width-to-length ratio (0.65) for the respective size categories are relatively similar, implying that the two shape parameters are widely size-independent (filled squares). Besides, the average values for the circularity (roughly 0.74) and the width-to-length ratio (0.65) match reasonably well to the shape data of the reference crystal introduced in Figure 5-7.

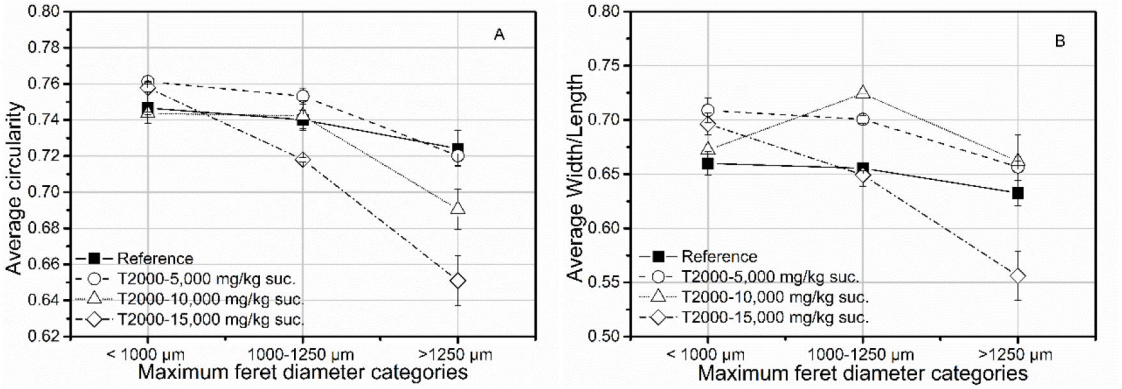

Figure 5-11 Average values of A) the circularity and B) the width-to-length-ratio of sucrose crystals according to the different maximum feret diameter-related categories.

In contrast, the average values of the circularity and the width-to-length ratio of the dextran-loaded samples decrease from the small-sized to the large-sized category, while the extent of this decrease correlates with the dextran content. For all dextran contents, the average values of the circularity of crystals with low maximum feret diameters of less than 1000 µm are either slightly increased or unchanged in comparison with the reference (Figure 5-11 (A)).

The relative frequency distribution of the circularity corresponding to this size-category is not dramatically changed either due to the presence of dextran, though, a slight shift towards lower circularity values was detected (see Figure 5-12 (A)).

More obvious, the average values of the width-to-length ratio of the small-sized category are unsystematically increased to about 0.7 for all dextran contents (see Figure 5-10 (B)). The distribution curves consistently show a clear shift towards higher width-to-length-ratios for all dextran contents (Figure 5-12 (B)). It is revealed that higher amounts of crystals with width-to-length-ratios of more than 0.7 were found within the small-sized category, which is again most pronounced for the lowest dextran content of 5000 mg/kg sucrose.

Here, too, according to the crystal shape dependent parameter change stated above (Figure 5-7 and Table 5-2), slightly increased circularities combined with an increase of the width-to-length-ratio point towards a higher amount of cube-shape crystals. Thus, the occurrence of cube-shaped crystals can be confirmed and additionally related to small-sized sucrose crystals, most prominent for the lower dextran content of 5000 mg/kg sucrose. For the samples produced in the presence of 10,000 or 15,000 mg dextran/kg sucrose, the distribution curves with respect to the width-to-length ratio become broader, containing more crystals with even higher width-to-length ratios. Thus, not only more cube-shaped crystals but also more agglomerates are indicated.

This trend for the shape-parameters also applies to dextran contents of 5,000 and 10,000 mg/kg sucrose in the mid-sized crystal category (1000-1250 µm), also pointing towards an increasing number of cube-shaped crystals.

The crystals produced in the presence of the highest dextran content show different characteristic, while showing a decreased averaged circularity (from 0.74 to 0.72) and a slightly decreased or rather unchanged averaged width-to-length-ratio (see Figure 5-11 (A) and (B), respectively).

Accordingly, the relative frequency distribution also indicates the occurrence of higher amounts of crystals with lower circularities ranging from 0.5 to 0.7 for the highest dextran content of 15,000 mg/kg sucrose (Figure 5-13 (A)), clearly indicating elongation or agglomeration. Besides, at this dextran content, the width-to-length-ratio distribution again shows higher amounts of both extremes, lower width-to-length-ratios (less than 0.55) and higher width-to-length-ratios (greater than 0.7), see Figure 5-13 (B). These changes of the width-to-length ratio distribution suggests that agglomeration and elongation simultaneously occur within the mid-sized category due to the highest dextran content of 15,000 mg/kg sucrose.

The analysis of sucrose crystals in the large-sized category corresponding to maximum feret diameters greater than 1250 µm reveals much more clearly a dose-response-related decrease of the averaged circularity, see Figure 5-11 (A). Thereby, the averaged circularity decreased from 0.73 (reference) to the lowest averaged circularity of 0.65 for the highest dextran load of 15,000 mg/kg sucrose.

In contrast, the average values of the width-to-length ratio corresponding to large-sized crystals show an increase for samples with a dextran load of 5,000 and 10,000 mg/kg sucrose in comparison with the reference. The highest dextran content of 15,000 mg/kg sucrose caused a decrease of the averaged width-to-length-ratio from roughly 0.63 to 0.55.

In general, the distribution curves of the width-to-length ratio for these large-sized crystals are broader than for the other crystal-size categories. Nevertheless, it can be concluded that samples with lower dextran contents correspond to smoother and less broad distribution curves.

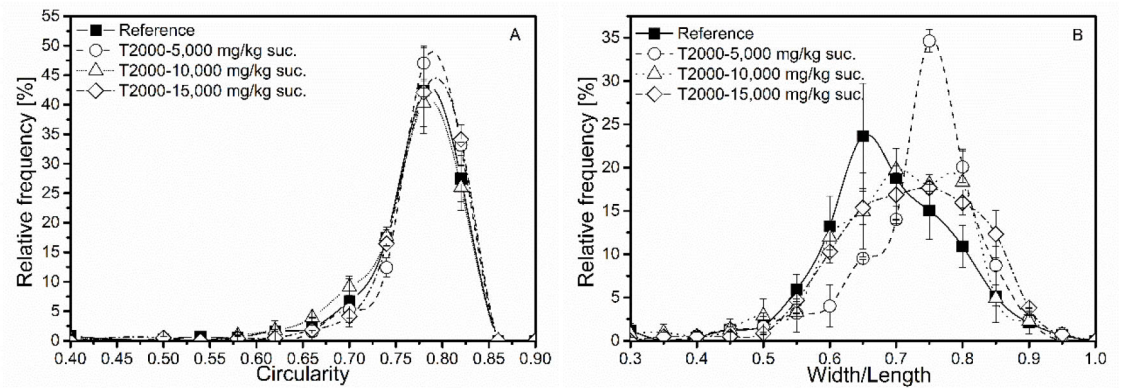

Figure 5-12 Sucrose crystal shape analysis by static image analysis. Relative frequency distribution curves of A) the circularity and B) the width-to-length ratio of sucrose crystals with maximum feret diameters below 1000 µm.

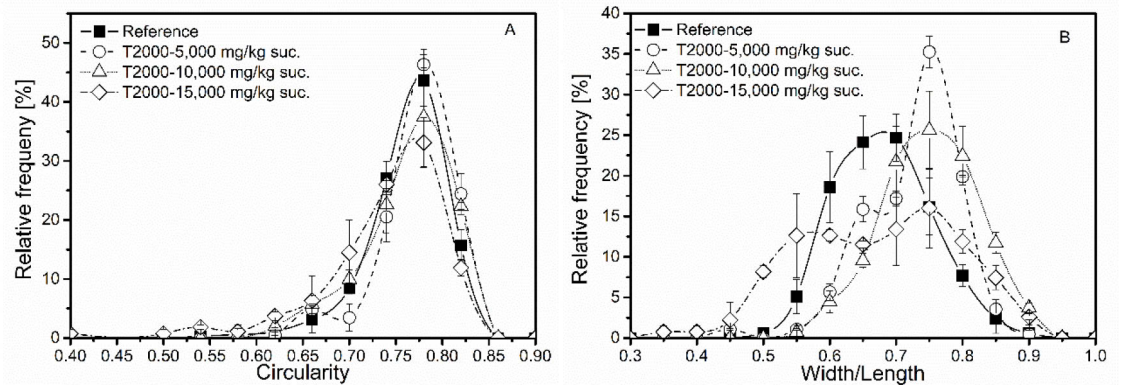

Figure 5-13 Sucrose crystal shape analysis by static image analysis. Relative frequency distribution curves of A) the circularity and B) the width-to-length ratio of sucrose crystals with maximum feret diameters ranging between 1000 and 1250 µm.

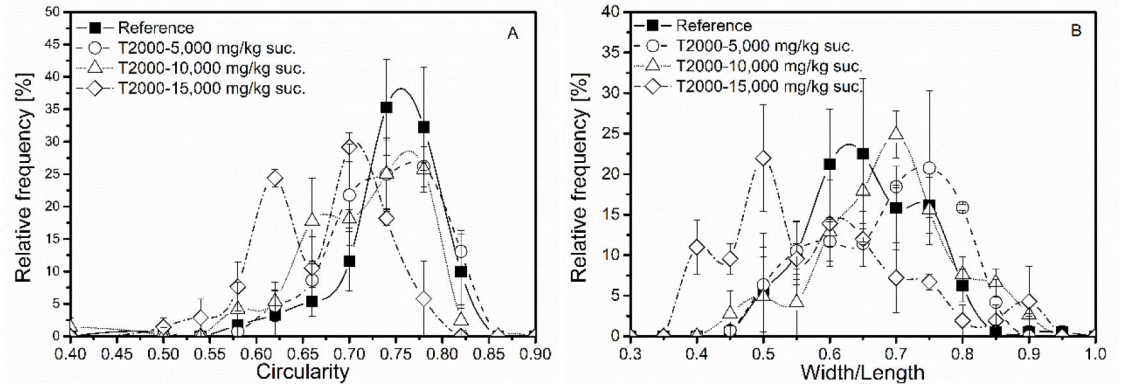

Figure 5-14 Sucrose crystal shape analysis by static image analysis. Relative frequency distribution curves of A) the circularity and B) the width-to-length ratio of sucrose crystals with maximum feret diameters above 1250 µm.

A systematic shift of the relative frequency distribution to low circularities of less than 0.7 is obvious, see Figure 5-14 (A). For the samples produced with 5,000 and 10,000 mg dextran/kg sucrose, the curve shifts to higher width-to-length ratios (above 0.7) than the reference. The decrease of the circularity combined with the increase of the width-to-length-ratio again indicates an increasing presence of agglomerates (see Table 5-1 and Table 5-2).

The distribution curve corresponding to the samples loaded with 15,000 mg/kg sucrose clearly shifts to lower values. Dramatically higher amounts of crystals with lower width-to-length-ratios of less than 0.55 are indicated by the relative frequency distribution (diamonds in Figure 5-14 (B)). This parameter change suggests that at such a high dextran content, mainly elongated crystal shapes occur within the large-sized crystal category. Due to the number-based evaluation and the fact that the small-sized crystals outnumber the larger ones in the sample, the presence of these elongated large-sized crystals category does not propagate into the average values concerning the whole sample.

To sum up, at the lowest dextran content of 5,000 mg/kg sucrose, the overall evaluation suggests that a higher number of cube-shaped crystals were formed. The categorised evaluation revealed that this especially relates to small- and mid-sized crystals, whereas the large-sized category seems to additionally contain higher amounts of agglomerates.

At a content of 10,000 mg/kg sucrose, the overall evaluation indicates that cube-shaped crystals and agglomerated crystals increasingly occur. The occurrence of cube-shaped crystals can again be related to the category of small and mid-sized crystals. Again large-sized crystals indicate agglomeration at this intermediate dextran content. Different to the lower dextran content, the occurrence of these large-sized crystals was more prominent and was found to impact the overall evaluation.

At a content of 15,000 mg/kg sucrose, the overall evaluation suggests that both, elongation and agglomeration predominantly occur. Again, evaluation by crystal-size categories reveals that for small-sized crystals more cube-shaped crystals occur, while mid-sized crystals are clearly characterised by parameter changes relating to elongation and agglomeration. In the large-sized category, the data clearly indicate a pronounced occurrence of elongated crystal shapes.

Conclusively, the size dependent evaluation of the samples using the two shape parameters, circularity and width-to-length ratio, confirmed the previous assumptions made by Faria et al. and Abraham et al. suggesting that three dextran-related shape-modifications of sucrose crystals occur, namely cube-shaped, elongated and agglomerated crystals. It has been shown that the occurrence of these crystal shapes relates to the dextran content and to certain sucrose crystal sizes. Cube-shaped crystals are clearly related to small-sized crystals. These were generally found for all dextran contents investigated, but predominantly for lower dextran contents of 5,000 mg/kg sucrose. Agglomeration and distinct elongation were clearly found to be related to mid-and large-sized crystals, while both effects increased with increasing dextran dosage. Distinctly elongated crystals were predominantly found for the highest dextran content and could clearly be related to large-sized crystals with high maximum feret diameters. Thus, the crystal-size related evaluation of the shape parameters made it possible to detect and to distinguish the different dextran-induced shape

modifications depending on the dextran addition and the maximum feret diameter of the sucrose crystals.

5.4 Conclusion

Evaporative crystallisation experiments using synthetic thick sucrose juices containing various contents of high molecular mass dextran (T2000) were performed. HPLC analysis of the dissolved sucrose crystals revealed that T2000 dextran present in the mother liquor gets incorporated into the sucrose crystal. Partition coefficients between mother liquor and growing crystal of roughly 2 % with respect to feed composition or 1.15 % with respect to the actual T2000 concentration were derived. By applying an additional affination step, which removes mother liquor and adsorbed non-sugars from the crystal surfaces, it could be shown that dextran is incorporated into the crystal lattice and not just adsorbed onto the surface of the crystal. Although the exact incorporation mechanism of dextran into the sucrose crystal is not known, it was expected, also based on literature, that due to the incorporation of dextran the crystal shape and size of the sucrose crystals is modified.

Subsequently, the study presented focuses on adequately and comparatively analysing dextran-induced modifications of sucrose crystal characteristics with regard to crystal size and shape. Therefore, static image analysis was implemented and compared to common sieve analysis as well as dynamic image analysis (Camsizer). All methods applied reveal consistent results for the crystal size distribution. All methods indicate an increase of crystals with lower minimum and especially lower maximum feret diameters due to the presence of T2000 dextran. Besides, three different dextran-related shape-modifications were found, namely cube-shaped crystals, elongated needle-shaped crystals and agglomerates. Evaluation of average values and relative frequency distributions suggest that the occurrence of these shapes relates to the dextran content present. A more detailed crystal size-related evaluation of the shape parameters confirms this and additionally suggests that the dextran-related crystal shapes can be allocated to certain crystal sizes. Thus, cube-shaped crystals could clearly be related to small-sized crystals, predominantly occurring at lower dextran contents. Agglomeration and distinct elongation were clearly found to be related to mid- and especially large-sized crystals. The latter two, especially distinct elongation, seem to increasingly occur for higher dextran contents.

Acknowledgement

The authors would like to thank the department of geo-technical engineering at the Technical University Berlin for providing the Camsizer measuring instrument.

References

Abdel-Rahman, E. A., Smejkal, Q., Schick, R., El-Syiad, S., & Kurz, T. (2008). Influence of dextran concentrations and molecular fractions on the rate of sucrose crystallization in pure sucrose solutions. *Journal of Food Engineering*, *84*, 501–508.

Abdel-Rahman, E.-S. (2007). Investigations on the influence of dextran during beet sugar production with special focus on crystal growth and morphology (PhD). Technische Universität Berlin, Berlin.

Abdel-Rahman, E.-S., Schick, R., & Kurz, T. (2007). Influence of dextran on sucrose crystallization. *Sugar Industry*, *132*(6), 453–460.

Abraham, K., Hagen, S., Schlumbach, K., Rohde, A., & Flöter, E. (2016). Dextranase application in sucrose solutions - towards a better understanding. *International Sugar Journal*, 604–610.

Asadi, M. (Ed.). (2007). *Beet-Sugar Handbook*. New Jersey: John Wiley & Sons.

Bubnik, Z., & Kadlec, P. (1992). Sucrose crystal shape factors. *Sugar Industry*, *117*(5), 345–350.

Chen, J. C., & Chou, C. C. (1993). Cane Sugar Handbook: A Manual for Cane Sugar Manufacturers and Their Chemists (12th ed.). New York: John Wiley & Sons.

Faria, N., Pons, M. N., Feyo de Azevedo, S., Rocha, F. A., Vibier, & H. (2002). Quantification of the morphology of sucrose crystals by image analysis. *Powder Technology*, *133*(1-3), 54–67. https://doi.org/10.1016/S0032-5910(03)00078-0

Fernlund, J. M. (1998). The effect of particle form on sieve analysis: a test by image analysis. *Engineering Geology*, *50*(1), 111–124. https://doi.org/10.1016/S0013-7952(98)00004-0

ICUMSA (Ed.). (2011). *ICUMSA Method Book*. Berlin: Dr. Albert Bartens KG.

Kaur, S., & Kaler, R. (2008). Dextran and its effect on the flow behaviour of molasses and crystallization rate. *Journal of Food Engineering*, *86*(1), 55–60. https://doi.org/10.1016/j.jfoodeng.2007.09.010

Khalikova, E., Susi, P., & Korpela, T. (2005). Microbial dextran-hydrolyzing enzymes: fundamentals and applications. *Microbiology and Molecular Biology Reviews*, *69*(2), 306–325. https://doi.org/10.1128/MMBR.69.2.306-325.2005

Mantovani, G., Vaccari, G., & Marignetti, N. (1960). Relationship between crystal elongation and the presence of some impurities in cane sugar processing. *Publication of Technical Papers and Proceedings of the Annual Meeting of Sugar Industry Technologists*.

Mathlouthi, M., & Reiser, P. (1995). *Sucrose Properties and Application: Properties and Application* (1st ed.). Frimley: Blackie Academic & Professional.

Schlumbach, K., Pautov, A., & Flöter, E. (2017). Crystallization and analysis of beet and cane sugar blends. *Journal of Food Engineering*, *196*, 159–169. https://doi.org/10.1016/j.jfoodeng.2016.10.026

Ferreira, Tiago, & Rasband, Wayne. (2012). ImageJ User Guide: IJ 1.46r.

Van der Poel, P. W., Schiweck, H., & Schwartz, T. (1998). *Sugar Technology: Beet and Cane Sugar Manufacture*. Berlin: Dr. Albert Bartens KG.

Witte, G. (1987). Untersuchungen zur Kristallfußarbeit bei Weißzucker. *Zuckerind.*, *112*, 581–587.

6 Effect of Dextran and Enzymatically Decomposed Dextran on the Sucrose Crystal Shape

Abraham, K. [ab], Brykczynski, H. [a], Rudolph-Flöter, E.S.J. [a], Schlumbach, K. [a], Schäfer, A. [a], Flöter, E. [a]

[a] TU Berlin, Department of Food Process Engineering, Seestraße 13, 13353 Berlin, Germany

[b] SternEnzym, Kurt-Fischer-Str. 55, 22926 Ahrensburg, Germany

Submitted to the Sugar Industry (2018)

Abstract

The effect of dextran's molecular mass distribution on the sucrose crystal shape was key to this study. Therefore, sucrose crystals were produced by evaporative crystallisation experiments using synthetic thick juices containing high (T2000) and low (T40) molecular mass dextran fractions as well as enzymatically decomposed dextran. The combined analysis of molecular mass distributions by size exclusion chromatography and sucrose crystal shapes by static image analysis were used to identify the least harmful reaction products resulting from the enzymatic decomposition of dextran. The combined evaluation of two shape parameters, circularity and width-to-length ratio, has shown that three different shape modifications can be related to the presence of dextran, namely cube-shaped crystals, elongated needle-shaped crystals and agglomerates. In the main, the data indicated that high T2000 contents and generally all T40 dextran contents led to an increased occurrence of agglomerated and occasionally elongated crystals. The latter was especially found for high T2000 dextran contents. In contrast, low T2000 dextran contents predominantly increased the amount of cube-like crystals.

The enzymatic decomposition of dextran resulted in a gradual reduction of the molecular mass. It was shown that an insufficient decomposition to broadly distributed low molecular mass dextran fragments, which are realistic to assume for sugar cane and beet raw juices, still dramatically affected the sucrose crystal shape. Once dextran was decomposed to molecules with molecular masses of less than 5 kDa, no dextran-related effects on the sucrose crystal shape were found.

6.1 Introduction

It is a well-known fact that the presence of impurities can affect the crystallisation process during sugar manufacture (Asadi, 2007). This inter alia concerns polysaccharides produced by microbial activity. Lactic acid bacteria, more specifically *Leuconostoc Mesenteroides* species, are known to produce the glucose polymer dextran, occurring in varying and broad molecular mass distributions (Abdel-Rahman, 2007b). The glucose monomers in dextran's main chain are linked via α-(1→6) glycosidic linkages. Besides, it was reported that sugar industry-relevant species produce dextran containing up to 5 % branching points via α-(1→2), α-(1→3) and α-(1→4) glycosidic bonds (Khalikova et al., 2005).

Considering the fact that dextran's molecular mass in beet and cane juices range from 15 to 2000 kDa, the extent and kind of effects during sucrose crystallisation can vary accordingly (Chen & Chou, 1993). Thus, depending on the molecular mass distribution present, dextran is known to affect the hydrodynamics of the solution as well as the characteristics of the final sucrose crystals (Abdel-Rahman et al., 2007). So far, there is general agreement that high molecular mass dextran is mainly responsible for a viscosity increase, impeding diffusion processes and thus the crystallisation rate (Kaur & Kaler, 2008). Besides, high and also low molecular mass dextran fractions are known to be involved in modifications of the final sucrose crystal characteristics with regard to size and shape distributions (Abdel-Rahman et al., 2007).

These dextran-related effects are usually mitigated by enzymatic decomposition. However, a targeted application of dextranase is still not established practice. More precisely, guidelines for enzyme dosages according to known enzyme-to-substrate ratios and a detailed understanding of the effects of dextran and the resulting reaction products are not available. Previously reported work of ours marks a major step towards this goal by developing a new analytical tool for dextran analysis in sugar industrial practice, see (Abraham et al., 2019a) and (Abraham & Flöter, 2018). Furthermore, the enzymatic decomposition of dextran with varying initial molecular mass distributions has been investigated in detail and the corresponding reaction products were identified (Abraham et al., 2019b). To complete this effort, the effects of dextran and enzymatically decomposed dextran during sugar manufacture need to be considered. The latter has already been studied with regard to sugar beet raw juice purification (Abraham K. et al., submitted for publication in 2019a). Besides, the effects on the final sucrose crystal quality are of particular interest.

The final sucrose crystal quality is inter alia determined by its shape. A theoretical three-dimensional sucrose crystal shape is shown in Figure 6-1 below. Its allocation to the monoclinic crystal system inter alia implies that the length of the three axes (A, B, C) differ from one another. In pure sucrose solutions, the B-axis is generally known to be most elongated (Mathlouthi & Reiser, 1995).

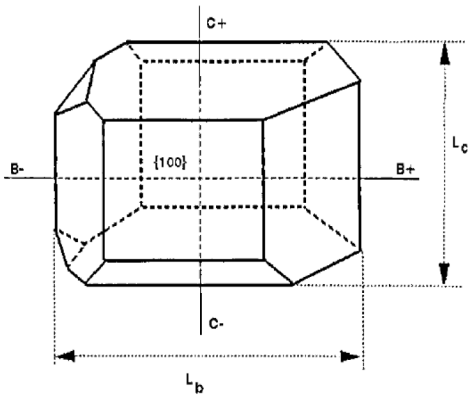

Figure 6-1 Theoretical sucrose crystal shape (Bubnik & Kadlec, 1992).

In view of dextran-related shape modifications, it was mainly reported that the presence of dextran causes a specific elongation along the initially shorter C-axis of the sucrose crystals (Mantovani et al., 1960). However, Faria et al. found that elongated crystals occur only occasionally. Instead, cube-shaped crystals and pronounced agglomeration were predominantly related to the presence of dextran (Faria et al., 2002). The simultaneous occurrence of different crystal shapes complicates a clear evaluation of crystal shape data. Previous work confirmed that different crystal shapes (cube-shaped, elongated and agglomerated crystals) can be related to the presence of dextran. Thereby, different particle analysis methods were compared in order to adequately detect effects of varying contents of high molecular mass dextran on the sucrose crystal characteristics (Abraham et al., submitted for publication in 2019b). During this effort, static image analysis has shown to be most meaningful for sucrose crystal shape analysis, also enabling a size-related evaluation. This way, the previously assumed different crystal shapes (cube-shaped, elongated and agglomerated crystals) could be distinguished and allocated to different crystal size categories. Nevertheless, cube-shaped crystals were found to predominantly occur in the presence of high molecular mass dextran, especially at dextran contents of 5000 mg/kg sucrose. A further increase in the dextran content additionally promoted agglomeration and elongation.

To complement on these previous results and to finally establish a controlled dextranase application with regard to sucrose crystallisation, effects of varying molecular mass distributions should be considered. Investigating the effects of enzymatically decomposed dextran is particularly of relevance because low molecular mass dextran is also known to affect the crystal morphology, which should hence be avoided (Sgualdino et al., 1997). Thus, in view of sucrose crystal characteristics, the effect of dextran's decomposition products and thus the optimum degree of dextran decomposition need specifically to be identified in order to exploit the maximum potential of dextranase applications.

The study presented focuses on the specific effects of varying molecular mass distributions on the sucrose crystal characteristics. To do so, sucrose crystals were produced by evaporative

crystallisation experiments using synthetic thick juices containing dextran fractions with varying molecular masses. The latter was managed by decomposing high molecular mass dextran with varying enzyme levels.

Static image analysis was used to determine two shape parameters, the width-to-length ratio as well as the circularity, which were evaluated in combination to distinguish the different dextran-related shapes. Therefore, relative frequencies according to different categories for the two shape parameters were calculated and used to identify the crystal shapes present. In addition, size exclusion chromatography was used to analyse the molecular mass distribution of dextran and the resulting reaction products. The combined analysis of sucrose crystal characteristics and molecular mass distributions aims at targeted dextranase application in industrial sugar manufacturing.

6.2 Material and Methods

6.2.1 Materials

Synthetic thick juices (66 % (m/m) sucrose solutions) with high (T2000) and low (T40) molecular mass dextran fractions were prepared for the crystallisation experiments. Therefore, dextran fractions with mass-average molecular masses of 2,000 kDa (T2000: Sigma-Aldrich, dextran with a molecular mass distribution ranging from 1,500 to 2,800 kDa) and 40 kDa (T40: Carl Roth, dextran with a molecular mass distribution ranging from 35 kDa to 45 kDa) were used. All dextran fractions originate from the lactic acid bacteria *Leuconostoc Mesenteroides* strain B512.

Due to the fact that the sucrose content is known to affect the dextranase reaction, enzyme treatments were performed in synthetic thin (15 % (m/m) sucrose solutions), which were then evaporated to thick juices. For both, synthetic thin and thick juices, refined sucrose (Nordzucker, extra-white sugar) was used.

For the enzymatic decomposition of T2000 dextran, a non-genetically modified dextranase originating from a *Chaetomium gracile* strain (Sugazym DX L, SternEnzym) was used. Its temperature and pH optimum ranges from 328 K to 338 K and from 4 to 7, respectively. The enzyme is known to specifically and randomly hydrolyse α-(1→6) glycosidic linkages in dextran molecules (Khalikova et al., 2005).

6.2.2 Crystallisation Experiments

6.2.2.1 Crystallisation Plant

Evaporative crystallisation experiments were performed at 5 liter lab scale using a crystallisation pilot-plant followed by centrifugation and drying. The plant design as well as the experimental procedure is described in detail elsewhere (Schlumbach et al., 2017). Schlumbach et al. also verified the experimental set-up on reproducibility and suitability for the production of sugar of industrially relevant quality. The crystallisation unit is composed of a double wall stainless-steel vessel with a

cylindrical glass vessel mounted on top. Both vessels are individually temperature controlled via two thermostats (F32-HD and F12-MC, Julabo). A Pt-100 thermocouple as well as a process refractometer (iPR 2-3, Schmidt & Haensch GmbH & Co) are attached on top and on the bottom of the vessel, respectively. This way, the temperature and the dry substance are continuously monitored throughout the crystallisation run. The vacuum is build up and held constant using a low-pressure pump (PC 3001, Vacuubrand GmbH & Co KG). An agitator (RZR 2102 control, Heidolph Instruments GmbH & Co. KG) is used to move a stirrer inside the vessel. A gastight permanent magnetic coupling on top of the vessel guarantees the vessel to be tightly closed in order to maintain the low pressure level. The agitator is further useful to measure the torque serving as an indication for the crystallisation end. The experimental set-up is computer-controlled and the data (temperature, pressure, dry substance) taken during the run are recorded online via a Lab-VIEW code, specifically developed for this purpose. Furthermore, all input and output flows are manually monitored in order to allow mass balances. An inlet and an outlet valve at the bottom of the vessel are useful for sample intake and collection, respectively. The steam resulting from evaporation leaves the system on top of the vessel, where it enters a vent condenser. The condensate produced is then collected and quantified in an Anschuetz-Thiele-receiver. The final sucrose crystals are subsequently separated from the mother liquor in a temperature controlled centrifuge. A washing unit with a flat-jet nozzle was furthermore used for removing residual syrup from the sucrose crystal surface. Finally, the sugar was dried in a fluidized bed dryer (Fluid bed dryer TG 1, Retsch).

6.2.2.2 Experimental Procedure

The feedstocks (66 % (m/m) sucrose solutions with varying dextran fractions) were filled into the vessel via the inlet valve supported by the vacuum created. The supersaturation was set to 1.05 based on the process data recorded. At this point, seed crystals of defined sizes were added (180 - 250 µm) representing the departure points for crystal growth. The amount of crystals required was calculated according to the following equation based on the d^3-rule, in which $n_{Cr,i}$ and $m_{Cr,i}$ refer to the number and mass of crystals, respectively (Witte, 1987). The indices 0 and 1 are related to the starting and end point of the crystallisation strike.

$$m_{Cr,0} = m_{Cr,1} \times \left(\frac{d_{Cr,0}}{d_{Cr,1}}\right)^3 \times \frac{n_{Cr,0}}{n_{Cr,1}} \tag{6-1}$$

The process was subsequently controlled in a way that at practically constant supersaturation approximately 50 % (m/m) crystalline material was generated. This state and therefore the crystallisation end is indicated by the increase of the agitator's torque of 0.06 Nm compared to the value at the time of seeding. The resulting crystals are then separated from the mother liquor via centrifugation. A fluidized bed was further used to dry the sugar at 333 K for 5 minutes. The crystallisation of the dextran-free reference was performed fourfold to ensure proper repeatability.

Subsequently, the other synthetic thick juices containing varying dextran contents were respectively crystallised in duplicate.

6.2.3 Enzyme Reaction

The enzyme treatments were performed in synthetic thin juices (15 % (m/m) sucrose solutions). Thus, a subsequent evaporated step was necessary to obtain thick juices with about 60 to 65 % (m/m) sucrose. Thin juices containing 5000 mg T2000 dextran/kg sucrose were incubated at 328 K for 10 min. Varying enzyme levels were used (4, 10, 50 mg/ kg solution) to observe the effects of reaction products with different molecular masses on the sucrose crystal shape. The resulting thick juices were then crystallised as described in 6.2.2.2 above.

6.2.4 Analysis of Sucrose Crystals - Static Image Analysis

Light microscopy images were recorded using a Zeiss-Axio Scope A1 microscope. Microscope slides were loaded with the dry sucrose crystals in a way that the whole area is exploited. A complete record of the microscope slide was taken by using the tile function included in the Zeiss software. The resulting images of three microscopic slides of each sample were subsequently analysed using ImageJ. In order to properly analyse the crystal size and shape, calibration as well as image editing are necessary. Thus, two-dimensional crystal shapes were analysed, assuming that the crystals lay on the largest 100-surface. In order to reduce potential errors due to dust or foreign matter, the crystal measurements were previously restricted to the highest possible circularity for sucrose crystals of 0.8.

Two shape parameters were chosen to analyse the dextran-related shape modifications, the width-to-length ratio as well as the circularity. The former refers to the ratio of the minimum and the maximum feret diameter, see equation (6-2).

$$Width/Length = \frac{Minimum\ diameter}{Maximum\ diameter} \tag{6-2}$$

According to the ImageJ user guide, the maximum and minimum feret diameter refer to the longest and shortest distance between any two points along the selection boundary, respectively (Fernlund, 1998). In squares and rectangles, this means that the maximum feret is represented by the maximum diagonal, see Figure 6-2.

The circularity is defined by the following equation (6-3) (Ferreira & Rasband, 2012).

$$Circularity = 4\pi \times \frac{Area}{Perimeter^2} \tag{6-3}$$

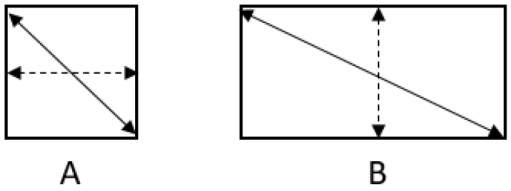

Figure 6-2 Determination of the maximum (solid arrow) and the minimum (dashed arrow) feret diameter by ImageJ.

In view of sucrose crystals, the maxima of the width-to-length ratio as well as the circularity is obtained when crystals are cube-like. The two shape parameters are depicted as relative frequencies according to three respective categories.

6.3 Results and Discussion

6.3.1 Chromatographic Analysis

Figure 6-3 shows the chromatograms of the non-decomposed T2000 and T40 dextran as well as of enzymatically decomposed T2000 dextran using varying enzyme levels. A secondary x-axis relates the molecular masses to the respective retention times as deduced from the calibration using pullulan standards and size-exclusion columns with defined separation ranges. As usual, the retention time increases with decreasing molecular mass. Thus, large molecules, such as T2000 dextran, elute first (black solid line). The broad and overlapping peaks of the T2000 chromatogram suggest a relatively high polydispersity, covering a molecular mass range from 60 kDa to 3000 kDa, according to the calibration system used. The chromatogram of the T40 dextran fraction indicates a monomodal, but still relatively broad main peak (black dashed line), covering a range from 3 kDa to 100 kDa.

Even though T2000 and T40 dextran fractions are obviously composed of molecules with different molecular masses, the proximity of the peaks indicates that T40 and T2000 dextran fractions partially comprise dextran molecules of similar molecular masses.

The chromatograms of the reaction products resulting from the enzymatic decomposition of T2000 dextran at 328 K and pH 6 for 10 min using varying enzyme dosages are additionally shown in Figure 6-3. Under these conditions - optimal for the dextranase activity according to the supplier – variation of the enzyme level was used to obtain reaction products with varying molecular mass distributions. Thereby, it is obvious that an increase of the enzyme level leads to a gradual decrease of the molecular mass indicated by a successive shift of the peaks towards higher retention times. Thus, high molecular mass dextran molecules were gradually converted into smaller molecules. The application of a comparatively low dextranase level of 4 mg/kg juice on a rather high T2000 content of 5000 mg/kg sucrose resulted in broadly distributed low molecular mass dextran fragments, see red solid line in Figure 6-3. According to the secondary x-axis, these reaction products covered a molecular mass range of 2 kDa to 300 kDa, which is very similar to the

chromatogram of the non-decomposed T40 dextran fraction. Therefrom, two main peaks can be identified, which have molecular masses of approximately 85 kDa and 10 kDa at their peak maxima, respectively.

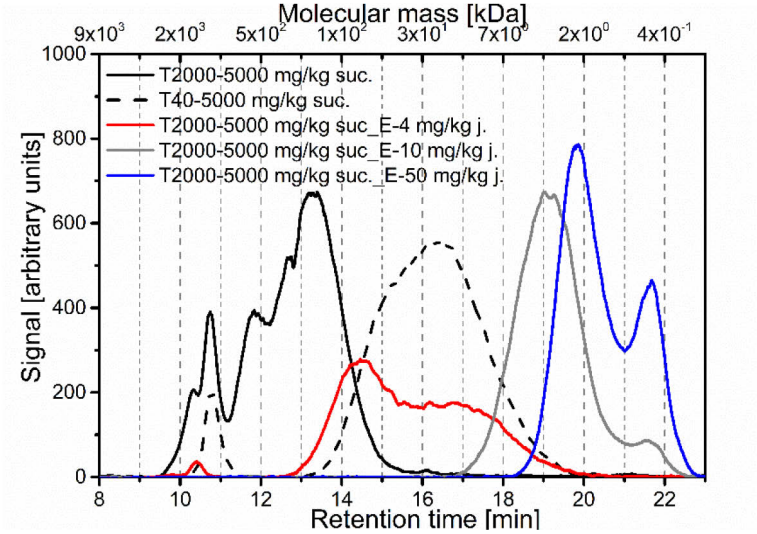

Figure 6-3 Size exclusion chromatograms of dextran fractions with varying molecular mass distributions (black solid line – non-decomposed T2000 dextran; dashed line - non-decomposed T40 dextran fraction; red line – 4 mg enzyme/kg juice on T2000 dextran; grey line - 10 mg enzyme/kg juice on T2000 dextran; 50 mg enzyme/kg juice on T2000 dextran).

The application of higher enzyme levels of 10 mg/kg juice resulted in a distinctly progressed decomposition, see grey solid line Figure 6-3. The data suggest more clearly a bimodal distribution, whereby the maximum of the main peak relates to a molecular mass of about 3 kDa. The distinctly smaller side peak indicates the additional presence of molecules with a molecular mass of about 0.6 kDa. Overall, the curve deviates from the base line at retention times corresponding to molecular masses ranging from 0.4 kDa to 10 kDa.

Similarly, the application of an even higher enzyme level of 50 mg/kg juice leads to a further shift of the main peak towards higher retention times relating to a molecular mass of 2.3 kDa in its peak maximum (blue solid line). Furthermore, the height of the side peak, indicating a molecular mass of 0.6 kDa, is distinctly increased. For this chromatogram, signals were obtained at retention times corresponding to molecular masses of 0.4 kDa to 5 kDa.

Thus, the increase of the enzyme level leads to a gradual reduction of the average molecular mass, resulting in reaction products of low molecular mass and reduced polydispersity. In the next step, the effects of these decomposition products identified on the sucrose crystal shape were investigated.

6.3.2 Impact of Dextran and Enzymatically Decomposed Dextran on the Sucrose Crystal Shape

6.3.2.1 Single Crystal Analysis

In order to analyse sucrose crystal shape modifications induced by the presence of dextran with various molecular mass distributions, two crystal shape parameters have been applied, the circularity and the width-to-length-ratio (see equation (6-2) and (6-3) above). Previous work has explained in detail how these two shape parameters are determined, illustrated by means of different theoretical geometrical shapes (Abraham et al., submitted for publication in 2019). Figure 6-4 shows realistic single sucrose crystal types identified in the dextran-free and dextran-loaded samples produced in this study. Thereby, a reference crystal (A) and crystal shapes found in the dextran-loaded samples (B) to (D) are depicted.

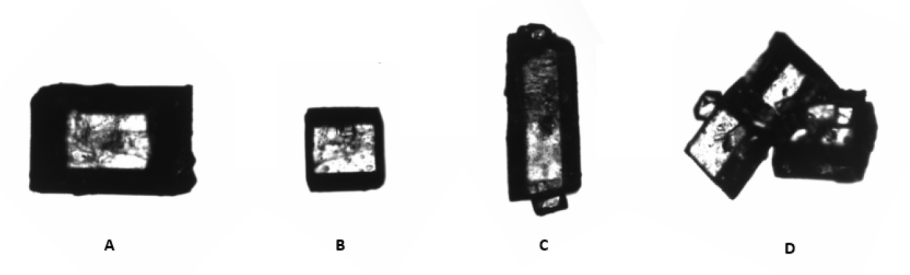

Figure 6-4 Sucrose crystal types identified from single crystal analysis using ImageJ, including a reference crystal (A), cube-shaped crystal (B), distinctly elongated crystal (C) and an agglomerated crystals (D).

The crystal shape-related changes of the width-to-length ratio and the circularity in comparison with the reference are summarised in Table 6-1. In view of this, the two-dimensional analysis of a reference crystal (type (A)) is as expected closest to a rectangular shape with a width-to-length ratio of 0.6 and a circularity of 0.75.

Table 6-1 Circularity and width-to-length ratio (=minimum feret/maximum feret) determined by Image J for the single sucrose crystals shown in Figure 6-4.

Shape	Reference	Cube-shape	Elongated	Agglomerates
Circularity	0,75	0,78 ↑	0,58 ↓	0,51 ↓
Width/Length	0,6	0,75 ↑	0,39 ↓	0,83 ↑

This crystal selection illustrates that cube-like crystals (type (B)) cause an increase in both, width-to-length ratio (0.75) and circularity (0.78) in comparison with the reference crystal (type (A)). Quite the opposite parameter change was found for distinctly elongated crystals (type (C)), for which the width-to-length ratio (less than 0.4) as well as the circularity (less than 0.6) were found to be distinctly decreased.

In case of agglomerates (type (D)), the width-to-length ratio (here 0.83) is similar to the value of the cube-like crystal. The latter is due to the fact that the minimum and the maximum feret length for irregular forms is determined based on the shortest and longest straight lines which fits in the contour of the crystal. The circularity of the agglomerate (D) is, however, distinctly decreased (0.51). Thus, in comparison with the reference, a significant decrease of the circularity combined with higher width-to-length-ratios is an indicator for higher amounts of agglomerates such as crystal type (D).

Previous work has shown that the latter three shapes ((B) to (D)) simultaneously occur when T2000 dextran was present during sucrose crystallisation, while the predominance of the different shapes seems to correlate with the concentration (Abraham et al., submitted for publication in 2019)

This work complements the previous work, while focusing on the specific role of the different molecular mass distributions explained above. This way, most harmless reaction products and therefore the optimum degree of enzymatic decomposition with regard to sucrose crystal shape modifications are supposed to be identified.

6.3.2.2 Effects of Non-Decomposed High and Low Molecular Mass Dextran Fractions

The relative frequencies for the two shape parameters were calculated according to three categories, respectively. Thereby, the categories were chosen in a way that the different shapes identified by the single crystal analysis can be distinguished. For the width-to-length ratio, relative frequencies for crystals with values of less than 0.5, ranging between 0.5 and 0.7 and greater than 0.7 were calculated. Also derived from the shape data of the single crystals, the relative frequencies of crystals with circularities of less than 0.7, ranging between 0.7 and 0.77 and greater than 0.77 were distinguished, see again Table 6-1. The relative frequency data corresponding to these categories for the samples loaded with varying molecular mass dextran fractions are shown in Figure 6-5 to Figure 6-7.

According to Figure 6-4, typical reference crystals belong to the intermediate category for both shape parameters, as marked in the central part of Figure 6-5 to Figure 6-7. The low width-to-length category includes elongated crystal shapes (<0.5) (left part in Figure 6-5 to Figure 6-7), while the high width-to-length ratio category (>0.7) is mainly populated by agglomerates and cubes (right part in Figure 6-5 to Figure 6-7). Crystals in the low circularity category (<0.7) are either agglomerated or elongated, while the high circularity category (>0.77) is obviously composed of cube-like crystals. As expected, the dextran-free reference sample is mainly composed of typical rectangular reference crystals, belonging to the intermediate category for both parameters, see filled bars in Figure 6-5 to Figure 6-7. The remaining smaller part is represented by cube-like and agglomerated crystals. Thus, the dominant crystal shape of the reference crystals produced in pure sucrose solutions in this study is confirmed to be rectangular. The presence of T2000 dextran causes

an increase of the relative frequency corresponding to crystals with high width-to-length ratios above 0.7 at the expense of crystals in the intermediate category, pointing towards an increased occurrence of cube-like and/or agglomerated crystals (Figure 6-5 (A)). A further increase in the dextran content caused a systematic reduction of the relative frequency corresponding to this high width-to-length ratio category. Instead, the amount of crystals with low width-to-length ratio is increased in comparison with the reference, mainly concerning the highest dextran load of 15,000 mg/kg sucrose.

The amount of crystals with high circularities is also increased due to the presence of T2000 dextran, again most pronounced for the low dextran content of 5,000 mg/kg sucrose (Figure 6-5 (B)). Here, too, on further dextran addition, the amount of crystals with low circularities is systematically increased. Thus, the shape data suggest that the occurrence of the dextran-related shape modifications depend on the T2000 content present. For the low dextran content of 5,000 mg/kg sucrose, the simultaneous increase in both, circularity and width-to-length ratio, clearly suggests a higher number of cube-like crystals. The additional increase in crystals with low circularities at high dextran contents indicates that agglomerates increasingly occur. For the high T2000 content, crystals with low width-to-length ratios are also increased, suggesting that additionally elongated crystals occur.

Similar to T2000 dextran, the presence of T40 dextran causes a distinct increase in crystals with high width-to-length ratios, also indicating cubes and/or agglomerates. Besides, a just slightly higher amount of crystals with low width-to-length ratios of less than 0.5 were found, again suggesting elongation. In this case, the amount of crystals with high circularities is just slightly increased for the T40 dextran-loaded samples. Similar to the samples loaded with higher T2000 dextran contents, a distinctly higher number of crystals with low circularities in comparison with the dextran-free reference were found instead. In this case, the amount of crystals with high circularities is just slightly increased for the T40 dextran loaded samples. Similar to the samples loaded with higher T2000 dextran contents, a distinctly higher number of crystals with low circularities in comparison with the dextran-free reference were found instead. The latter is even more pronounced for T40 dextran-loaded samples compared to T2000 dextran-loaded samples.

Combining the data of the two shape parameters, mainly agglomerates seem to increasingly occur when T40 dextran was present. Cube-like crystals as well as elongated crystals seem to additionally occur but apparently to a rather low extent. Different to T2000, the dextran-related crystal shape modifications seem to be similar all over the T40 dextran concentration range studied.

Consequently, it was generally found that the presence of both, T2000 and T40 dextran, affects the sucrose crystal shape. Thereby, the combined evaluation of the two shape parameters indicates that high T2000 contents and either T40 dextran content predominantly promote agglomeration accompanied by the occasional occurrence of cubes and elongated crystals.

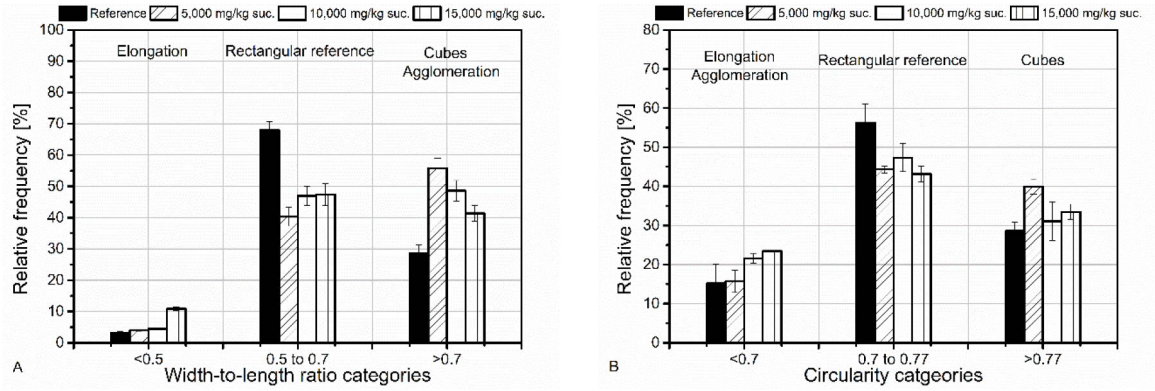

Figure 6-5 Sucrose crystal shape analysis. Relative frequencies of the circularity (A) and the width-to-length ratio (B) for T2000 dextran-loaded samples according to three categories.

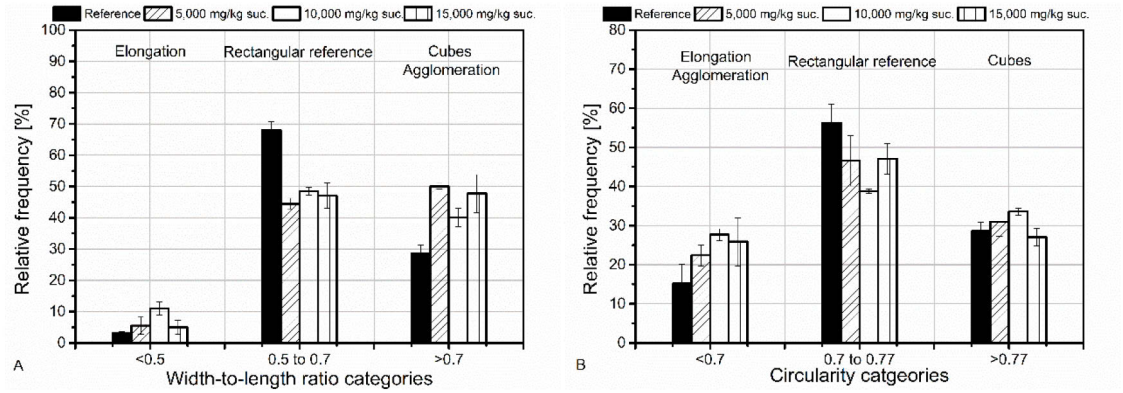

Figure 6-6 Sucrose crystal shape analysis. Relative frequencies of the circularity (A) and the width-to-length ratio (B) for T40 dextran-loaded samples according to three categories.

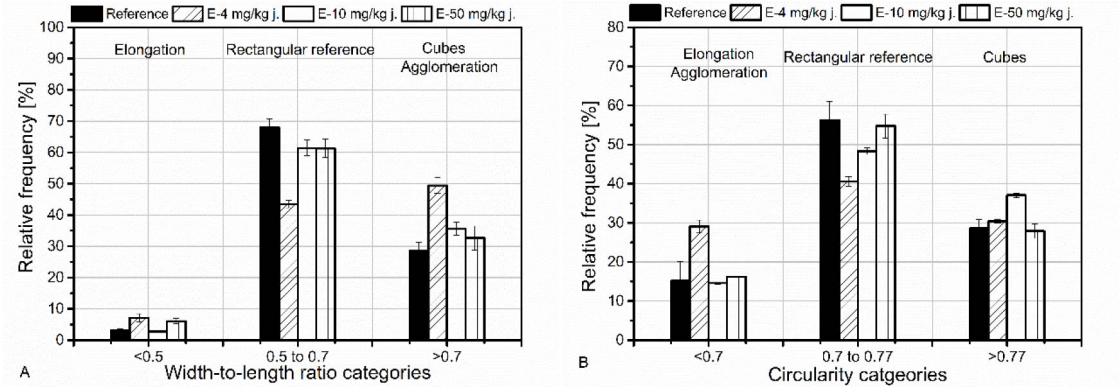

Figure 6-7 Sucrose crystal shape analysis. Relative frequencies of the circularity (A) and the width-to-length ratio (B) for samples containing enzymatically decomposed T2000 dextran according to three categories.

At low T2000 contents, cube-like crystals seem to dominate, while particularly high T2000 dextran contents caused especially distinct crystal elongation.

This clearly suggests that dextran's molecular mass distribution is relevant for sucrose crystal shape modifications during crystallisation. This also means that a sufficient enzymatic decomposition of

dextran needs to be ensured in order to mitigate and also to avoid a potential exacerbation of the dextran-related shape modifications.

6.3.2.3 Effects of Enzymatically Decomposed Dextran

Figure 6-7 (A) shows the relative frequencies corresponding to the width-to-length ratio of crystals produced in the presence of enzymatically decomposed T2000 dextran using varying enzyme levels.

The reaction products resulting from the application of the low enzyme level of 4 mg/kg juice (covering molecular masses from 2 kDa to 300 kDa) cause expectedly similar effects as the non-decomposed T40 dextran fraction, which are, however, even more pronounced. For this sample containing mildly decomposed T2000 dextran, the amount of crystals in the category with high width-to-length ratios is again distinctly increased, by 20 % in comparison with the dextran-free reference. A slight increase of crystals with low width-to-length ratios was also found. In addition, Figure 6-7 (B) illustrates that the mildly decomposed dextran fraction mainly causes an increase in crystals with low circularities, roughly doubled in comparison with the reference, similar to the effects caused by high T40 dextran contents.

Here, again, the increase of the width-to-length ratio combined with a decrease in circularity suggest that these broadly distributed low molecular mass dextran fragments mainly promote agglomeration. Besides, the additional occurrence of crystals with low width-to-length ratios also suggests that elongation also occasionally occur.

With progressing decomposition of dextran, the relative frequencies of the crystal shape data approaches the reference distribution. The reaction products resulting from the application of the intermediate dextranase level of 10 mg/kg juice on 5000 mg T2000/kg sucrose (covering molecular masses from 0.4 kDa to 10 kDa) still indicates slight deviations from the reference data. Thereby, the amounts of crystals with high width-to-length ratios and circularities were still slightly higher in comparison with the reference. No changes in the low circularity and low width-to-length category were found. Thus, only a slightly higher portion of cube-like crystals was indicated.

Further decomposition to products with molecular masses below 5 kDa using an enzyme level of 50 mg/kg juice leads to crystal shape characteristics very similar to the reference samples. The relative frequencies of the circularity and the width-to-length ratio approached the reference data. Thus, none of the dextran-related effects on the crystal shape could be detected anymore once dextran was sufficiently decomposed.

6.4 Conclusion

Static image analysis was used to analyse dextran-related sucrose crystal shape modifications, particularly focusing on effects due to varying dextran molecular mass distributions. Therefore, sucrose crystals were produced by evaporative crystallisation experiments using synthetic thick

juices containing dextran fractions with varying molecular mass distributions. Thereby, various contents of high (T2000) and low (T40) molecular mass dextran as well as enzymatically decomposed T2000 dextran were considered. The combined analysis of molecular mass distributions by size exclusion chromatography and sucrose crystal shape modifications were used to identify the least harmful reaction products resulting from the enzymatic decomposition of dextran.

Size exclusion chromatography data have revealed that even the two non-decomposed dextran fractions (T2000 and T40) are relatively polydisperse, covering molecular mass ranges of 60 kDa to 3000 kDa and 3 to 100 kDa, respectively.

For the crystal shape analysis, two shape parameters were considered, the width-to-length ratio as well as the circularity. These were used to detect dextran-related shape modifications. Thereby, three different dextran-related shape-modifications were confirmed as found in previous work. These are cube-shaped crystals, elongated needle-shaped crystals and agglomerates.

Evaluation of relative frequencies according to the different shapes identified suggests that high T2000 contents and generally all T40 dextran contents mainly led to an increased occurrence of agglomerated and also partly elongated crystals. The latter was especially found for the highest T2000 dextran content. In contrast, low T2000 dextran contents predominantly increased the amount of cube-like crystals.

In case of T40 dextran, the effects seem to be independent of the concentration, thus, even low T40 contents caused agglomeration and partially elongation. Differently, in case of T2000 dextran, the occurrence of the different dextran-related shape modifications seems to correlate with the dextran content present.

The enzymatic decomposition of dextran resulted in a gradual reduction of the molecular mass. Thus, the reaction products resulting from the application of the rather low enzyme level of 4 mg/kg juice on 5000 mg T2000/kg sucrose were still of relatively high molecular mass and broadly distributed (2 kDa to 300 kDa). This was quiet similar to the non-decomposed T40 dextran. Thus, effects on the crystal shape were also similar to the effects caused by T40 dextran, but were even more pronounced. Hence, broadly distributed low molecular mass dextran fragments, which are realistic to assume for sugar cane and beet raw juices, seem to cause most dramatic effects.

This clearly supports the necessity to ensure that dextran is sufficiently decomposed by knowing the dextran content as well as the initial molecular mass distribution. The application of higher enzyme levels of 10 mg/kg juice (0.4 kDa to 10 kDa) and 50 mg/kg juice (0.4 kDa to 5 kDa) has led to an approach of the shape data to the reference. No dextran-related effects on the sucrose crystal shape were found when dextran was decomposed to molecular masses of less than 5 kDa. The latter hence represents the target of dextranase application in order to avoid sucrose crystal shapes modifications.

References

Abdel-Rahman, E.-S. (2007). Investigations on the influence of dextran during beet sugar production with special focus on crystal growth and morphology (PhD). Technische Universität Berlin, Berlin.

Abdel-Rahman, E.-S., Shick, R., & Kurz, T. (2007). Influence of dextran on sucrose crystallization. *Sugar Industry*, *132*(6), 453–460.

Abraham, K., & Flöter, E. (2018). New approaches for the determination of dextran in the sugar production process. *Sugar Industry*, *143*(68), 138–146.

Abraham, K., Kunst, S., & Flöter, E. (2019). Membrane Characterisation for Fractionated Dextran Analysis in Sugar Industry. *Food Analytical Methods.* Advance online publication. https://doi.org/10.1007/s12161-019-01441-7

Abraham, K., Rudolph-Flöter, E., Schlumbach, K., Schäfer, A., & Flöter, E. Comparative Analysis of Dextran-Induced Sucrose Crystal Modifications. *Submitted for Publication in 2019*.

Abraham, K., Weigelt, J., Rudolph, S., & Flöter, E. (2019). Systematic study on the enzymatic decomposition of various dextran fractions. *Process Biochemistry.* Advance online publication. https://doi.org/10.1016/j.procbio.2019.01.024

Abraham K., Splett, L., Köster, E., & Flöter, E. Effect of Dextran and Enzymatically Decomposed Dextran on Calcium Carbonate Precipitation. *Submitted for Publication in 2019*.

Asadi, M. (Ed.). (2007). *Beet-Sugar Handbook.* New Jersey: John Wiley & Sons.

Bubnik, Z., & Kadlec, P. (1992). Sucrose crystal shape factors. *Sugar Industry*, *117*(5), 345–350.

Chen, J. C., & Chou, C. C. (1993). Cane Sugar Handbook: A Manual for Cane Sugar Manufacturers and Their Chemists (12th ed.). New York: John Wiley & Sons.

Faria, N., Pons, M. N., Feyo de Azevedo, S., Rocha, F. A., Vibier, & H. (2002). Quantification of the morphology of sucrose crystals by image analysis. *Powder Technology*, *133*(1-3), 54–67. https://doi.org/10.1016/S0032-5910(03)00078-0

Fernlund, J. M. (1998). The effect of particle form on sieve analysis: a test by image analysis. *Engineering Geology*. (50 (1)), 111–124. https://doi.org/10.1016/S0013-7952(98)00004-0

Kaur, S., & Kaler, R. (2008). Dextran and its effect on the flow behaviour of molasses and crystallization rate. *Journal of Food Engineering*, *86*(1), 55–60. https://doi.org/10.1016/j.jfoodeng.2007.09.010

Khalikova, E., Susi, P., & Korpela, T. (2005). Microbial dextran-hydrolyzing enzymes: fundamentals and applications. *Microbiology and Molecular Biology Reviews*, *69*(2), 306–325. https://doi.org/10.1128/MMBR.69.2.306-325.2005

Mantovani, G., Vaccari, G., & Marignetti, N. (1960). Relationship between crystal elongation and the presence of some impurities in cane sugar processing. *Publication of Technical Papers and Proceedings of the Annual Meeting of Sugar Industry Technologists*.

Mathlouthi, M., & Reiser, P. (1995). *Sucrose Properties and Application: Properties and Application* (1st ed.). Frimley: Blackie Academic & Professional.

Schlumbach, K., Pautov, A., & Flöter, E. (2017). Crystallization and analysis of beet and cane sugar blends. *Journal of Food Engineering*, *196*, 159–169. https://doi.org/10.1016/j.jfoodeng.2016.10.026

Sgualdino, G., Vaccari, G., Mantovani, G., & Aquilano, D. (1997). Glucose and Fructose Adsorption on Sucrose Crystals. Their Role as Habit-Modifiers. *Crystal Research and Technology*, *32*(8), 1057–1065. https://doi.org/10.1002/crat.2170320807

Ferreira, Tiago, & Rasband, Wayne. (2012). ImageJ User Guide: IJ 1.46r.

Witte, G. (1987). Untersuchungen zur Kristallfußarbeit bei Weißzucker. *Zuckerind.*, *112*, 581–587.

7 Systematic Study on the Enzymatic Decomposition of Various Dextran Fractions

Abraham, K. [ab], Weigelt, J. [a], Rudolph, S. [a], Flöter, E. [a]

[a] TU Berlin, Department of Food Process Engineering, Seestraße 13, 13353 Berlin, Germany

[b]SternEnzym, Kurt-Fischer-Str. 55, 22926 Ahrensburg, Germany

Originally published in the Journal of Process Biochemistry (2019).

https://doi.org/10.1016/j.procbio.2019.01.024

Abstract

Investigations on the enzymatic decomposition of dextran with varying initial average molecular masses, aiming at controlled dextran-related process effect mitigation during sugar manufacture, were key to this study. HPLC with size exclusion columns revealed that the enzymatic decomposition follows a gradual pattern leading to a successive reduction of the average molecular mass with the increase of the enzyme level and the incubation time. Affinity chromatography additionally revealed that oligo-, tri- and disaccharides constituted the smallest possible units. The amount of these small-sized saccharides increased with higher enzyme level and extended incubation time. Both effects were found to be further progressed when decomposing T40 as well as an equal-mass mixture of T2000 and T40 compared to exclusively T2000. The decomposition using unusually high enzyme levels leads to very similar reaction products for all substrates investigated. Besides, it was found that the presence of 15 % (m/m) sucrose seems to hardly affect the enzyme reaction so that the enzyme application in raw sugar juices seems to be appropriate. The work presented suggests that not only the dextran content, but also the average molecular mass and the polydispersity of dextran are decisive for targeted dextranase applications in sugar industry practice.

7.1 Introduction

The occurrence of polysaccharides in sugar cane and beet juices can cause several adverse effects during sugar manufacture. One of the main representatives of microbial polysaccharides in sugar cane and beet juices is dextran occurring in broad molecular mass distributions. In sugar industry, dextran is formed by enzymatic activity of lactic acid bacteria, more specifically by *Leuconostoc mesenteroides* species. This water soluble homogenous polysaccharide is composed of glucose units, which are mainly linked via α-(1→6) glycosidic linkages (Chen & Chou, 1993). However, up to 5 % of branching points via α-(1→2), α-(1→3) and α-(1→4) glycosidic linkages can occur when produced by sugar-industry-relevant species (Robyt & Eklund, 1982). Bashari et al. analysed dextran extracted from deteriorated cane, which revealed that the α-(1→3) glycosidic bond is the dominating branching point (Bashari et al., 2013). Dextran is co-extracted along with the sucrose and can adversely affect sugar processing in many ways. The kind and extent of these process effects not only depend on the total dextran content, but also on the molecular mass distribution. The latter refers to the potential occurrence of molecular masses in the range of 15 to 2,000 kDa (Chen & Chou, 1993).

Dextran is a prevailing topic in the sugar cane industry due to the abundant occurrence of mesophilic bacteria in the area, where sugar cane is cultivated. Dextran formation can nevertheless occur in sugar beet juices, mainly when beet cells are exposed to freeze-thaw cycles. Several authors determined dextran contents during sugar manufacture. In doing so, dextran contents ranging from roughly 2500 to 5000 mg/kg dry substance were determined in cane mixed juices (Rauh et al., 1999). Also, Morel du Boil et al. determined dextran contents ranging from 100 to 5000 mg/kg dry substance in cane raw juices. Furthermore, the authors found even higher dextran contents of up to 10,000 mg/kg dry substance in seriously deteriorated cane juices (Ravno & Purchase, 2005). In general, limited information is given for dextran contents in sugar beet raw juices. Nevertheless, dextran contents ranging from 800 to 1400 mg/kg dry substance in raw beet juices from different Egyptian factories were reported (Abdel-Rahman et al., 2007).

The total content and also the molecular mass distribution of dextran in raw juices can be influenced by several parameters such as climatic conditions, the extent of microbial infestation as well as the sucrose content in cane or beet. It is hence very likely that the total amount as well as the characteristics of dextran in sugar cane and beet juices vary, which causes deviation from a uniform dextran distribution with respect to branching as well as molecular mass (Falconer et al., 2011).

Aquino et al. generally identified two major groups, a higher and a lower fraction possessing molecular masses in the range of 10^3 kDa and 10^1 kDa, respectively (Aquino & Franco, 2009). Both molecular mass dextran fractions are known to be involved in the occurrence of dextran-induced process problems, whereas specific effects of the different molecular mass fractions are assumed (Chen & Chou, 1993). There is general agreement that the presence of high molecular

mass dextran leads to a viscosity increase impacting the filtration, evaporation as well as the crystallisation rate (Chen & Chou, 1993). Besides, an important effect concerns the modification of final sucrose crystal characteristics, which is known to be caused by both high and low molecular mass dextran (Abraham et al., 2016).

These dextran-induced process effects are usually mitigated by enzymatic decomposition representing a useful tool for years. However, a controlled and targeted enzyme application is still not established practice. Dextranases from various microbial origins can be used to depolymerise high-molecular mass dextran into smaller rather harmless low-molecular mass dextran fragments. In this respect, a sufficient decomposition of dextran while simultaneously avoiding over-dosages of cost-intensive dextranases is most challenging. The dextranase action, and hence the reduction in molecular mass, can be affected by the actual process conditions (e.g. pH, temperature) and also by the sugar beet and cane juice characteristics (e.g. sucrose content, dextran content and characteristics) (Eggleston & Monge, 2005).

The process parameters are relatively fixed, whereas the total dextran content as well as its molecular mass distribution are the most varying factors relevant for the adaption of the incubation conditions (mainly concerning enzyme dosage and reaction time).

Several authors already did some research on dextranase application in sugar industry. These studies mainly focused on the analysis of dextranase activity as well as residual dextran contents, while considering relevant process conditions during sugar manufacture. Thereby, residual dextran contents were mostly determined by common industry methods, such as the Enzyme-HPLC and the current standard Haze Method (Eggleston & Monge, 2005). However, these methods are affected by different molecular mass dependent detection limits and are generally rather inaccurate. In an earlier publication, it was shown that these methods are in particular not capable to actually identify the decomposition products resulting from dextranase action (Abraham & Flöter, 2018). In this respect, it should further be noted that a precise molecular mass dependent definition of dextran and, therefore, the actual targeted molecular mass for dextranase applications, is not existent. A sharp limit in terms of molecular mass, distinguishing harmless dextran fragments from initial harmful dextran, has not been clearly identified yet. Ideally, enzymes should only be applied to harmful dextran molecules in order to avoid unnecessary enzyme over-dosage, which is what this study aims at. The vague definition of harmful and harmless dextran combined with certain molecular mass dependent detection limits of the above-mentioned methods make the evaluation of the benefit of dextranase application based on residual dextran contents rather inaccurate. Nevertheless, these previous studies certainly helped to identify suitable process steps to add dextranases during sugar processing (Eggleston & Monge, 2005).

However, the border between harmless and harmful molecule sizes needs still to be identified. Therefore, the pattern of enzymatic decomposition has to be understood and the resulting products

need to be identified. This understanding about the enzymatic decomposition needs to be related to the effects of the various decomposition products on the different process steps of sugar manufacture. Only then enzyme application can be accomplished in a targeted manner. The latter is supposed to be part of future publications, whereas this work addresses the first initiative of analysing the influence of the initial molecular mass distribution of the substrates on the molecular mass distribution of the products resulting from dextranase action. Such a fundamental analysis requires reliable analytical methods, which do not necessarily need to be suitable for industrial practice.

It is a well-known fact that the enzyme-to-substrate ratio (dextranase-to-dextran) determines the yield of an enzyme reaction and therefore the resulting molecular mass distribution of decomposition products. According to the Michaelis-Menten-theory, at lower substrate levels, the reaction velocity directly correlates with the substrate level making it a reaction of first order (Berg et al., 2018). In contrast to this well-known impact, the effect of varying dextran molecule characteristics (e.g. molecular mass distribution) on the enzyme reaction has received only scant attention in the past.

While decomposing dextran with different initial average molecular masses, several factors can affect the molecular mass distribution of the resulting products. Thus, at the same incubation conditions, the progress of decomposition can differ when starting from different initial molecular mass distributions. Assuming that the decomposition pursues a gradual decrease of the molecular mass, as Eggleston et al. stated, means that high molecular mass dextran needs to pass through intermediate decomposition products of comparatively high and broadly distributed molecular masses.

The outline of the general mechanism of enzymatic reactions suggests that not only the gradual manner of the dextranase action causes differences when decomposing dextran with different initial molecular mass distributions. In general, an enzyme reaction is composed of three main steps concerning the substrate binding, the actual catalytic reaction and the product-enzyme-dissociation. The first step requires the encounter of the two participating reactants, here dextranase and dextran, which is then followed by a loose adhesion until the active site of the enzyme is reached. These steps are diffusion-controlled processes, whereas the subsequent catalytic step is reaction controlled. The diffusion limited steps are mainly determined by the diffusion coefficient, which relates to the type of the medium and its temperature as well as to the content and the size of the molecules (Einstein-equation) (Bisswanger, 2000). The solution properties as well as the specific characteristics of dextran and enzyme can hence decisively affect the progress of the enzymatic decomposition and are therefore reaction rate-determining. Besides, earlier work suggests that interactions between dextran molecules in a dextran mixture containing broadly distributed molecular masses (simultaneous presence of high and low molecular mass dextran fractions) occur,

which potentially also affects enzyme access (Abraham et al., 2019). Also, data published by Bertrand et al. give a first indication that the degree of polymerisation of dextran is relevant for the dextranase action (Bertrand et al., 2014). All these facts suggest that the incubation conditions should not only be adapted to the total dextran content, but also to the molecular mass distribution. The elucidation of these differences can help to adequately apply enzymes while achieving targeted molecular masses after enzyme treatment (e.g. adaption of enzyme dosage and incubation time).
This study aims at analysing the decomposition products resulting from the enzymatic decomposition of dextran using dextranase originating from a *Chaetomium gracile* strain (Sugazym DX L, SternEnzym). This work in particular focuses on potential effects due to different initial molecular mass compositions serving as a substrate for the enzyme reaction. Effects due to varying incubation times as well as the presence of sucrose were additionally considered. To adequately identify the decomposed dextran fragments, HPLC was used with columns either based on size exclusion or on affinity. The average molecular masses as well as percentage shares of the resulting dextran decomposition products were calculated based on the chromatographic data.

7.2 Material and Methods

7.2.1 Materials

Dextranase (Sugazym DX L, SternEnzym) was used to enzymatically decompose dextran fractions with different molecular mass distributions. This non-genetically modified dextranase originates from a *Chaetomium gracile* strain. Its temperature and pH optimum range from 328 to 338 K and from pH 4 to 7, respectively. It is known to specifically and randomly hydrolyse α-(1→6) glycosidic linkages in dextran. According to the manufacturer, the activity of this enzyme is 7000 U/g. Here, one dextranase unit refers to the activity of the amount of enzyme which liberates one micromole isomaltose per minute under specific conditions (pH 6.0, 310 K, reaction time of 30 min, 2 % (m/m) dextran 500).
Dextran with a high average molecular mass (T2000: Sigma-Aldrich, dextran 2000 with a molecular mass distribution ranging from 1,500 to 2,800 kDa) and one with a low average molecular mass (T40: Carl Roth, dextran 40 with a molecular mass distribution ranging from 35 to 45 kDa) were used as substrates for the enzymatic reactions in quasi-binary aqueous and aqueous sucrose solutions. Quasi-binary aqueous solutions are composed of distilled water and the respective dextran fractions. Aqueous sucrose solutions additionally contain 15 % (m/m) sucrose, which corresponds to realistic sucrose contents in sugar beet and cane raw juices (van der Poel et al., 1998). Both dextran fractions originate from lactic acid bacteria, more specifically from the *Leuconostoc mesenteroides s*train B512. Refined sucrose (Nordzucker, extra-white sugar) was used to investigate the influence of sucrose on the enzyme reaction.

7.2.2 Enzymatic Reaction

Quasi-binary aqueous and aqueous sucrose solutions containing dextran with varying molecular mass distributions were incubated. Variation of the enzyme level and the incubation time were investigated. Incubation of these samples took place in a shaking water bath in order to ensure good mixing. Temperature was monitored and the respective enzyme level was dosed once the desired temperature of 328 ± 1 K was reached. This is defined as the starting point of the enzyme reaction time. The enzymatic reaction was terminated by thermal inactivation, for which the samples were kept at a temperature of 353 ± 1 K using a second water bath for 20 min. Prior to chromatographic analysis, the samples were then cooled to room temperature. Previous experiments verified that dextran is still well-dissolved during this procedure. In general, every enzyme reaction was performed in duplicate.

7.2.3 Chromatographic Analysis

7.2.3.1 Size Exclusion Chromatography (SEC)

Chromatographic measurements in aqueous solutions were performed using high pressure liquid chromatography (HPLC, Chromaster system, Hitachi) equipped with an evaporative light scattering detector (ELSD 90 LT-Low Temperature, VWR). Two polymeric size exclusion columns with a separation range of 0.1 to 70 kDa (ABOA SuperOH-P-250, AppliChrom) and 2.5 kDa to 1,000 kDa (ABOA SuperOH-P-350, AppliChrom) were connected in series to enhance separation of enzymatically decomposed dextran based on size exclusion. An isocratic method with distilled water as the mobile phase was used with a flow rate of 1 ml/min. The sample volume was 20 µl. The temperature of the oven and the detector were set to 293 K and 323 K, respectively. The samples were pre-filtered using 0.45 µm syringe filters (Chromafil GF/PET-45/25, Macherey-Nagel) and were transferred into 1.5 ml vials without any dilution. Calibration to establish a relation of the molecular mass to the retention time was performed using pullulan standards of various molecular masses of very low polydispersity (Pulkit 08, Polymer Standard Service). According to the calibration data, the retention time correlates exponentially with the molecular mass of the pullulan standards, see Figure 7-1 below.

The extrapolation to retention times shorter than 12 minutes, describing really high molecular masses, might lead to increased inaccuracies due to the limited number of calibration samples in this range of high derivatives dM/dt. It has to be mentioned that the chromatographic separation is challenged by the spectrum of molecular masses dealt with in this work. A hampered separation, and therefore determination, of molecular masses above that limit was tolerated in order to allow a more precise separation of molecular masses relevant for enzymatically decomposed dextran, which was central to this study. Consequently, determination of dextran with molecular masses

above 1,000 kDa might be underestimated due to insufficient separation of dextran of particularly high molecular mass. However, these molecular masses are only contained in the high average molecular mass substrate, T2000, and not core of this research subject dealing with decomposition products.

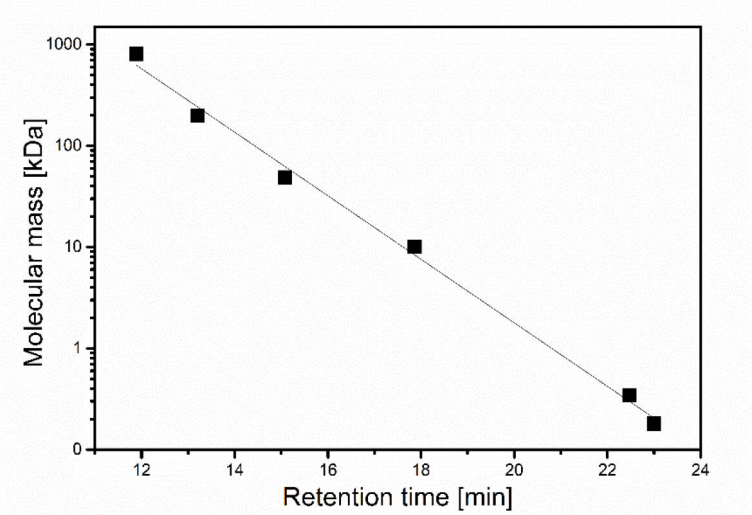

Figure 7-1 SEC-calibration data. Molecular mass as a function of the retention time deduced from calibrations using two polymeric size exclusion columns (ABOA SuperOH-P-250 and ABOA SuperOH-P-350, AppliChrom).

7.2.3.2 Affinity Chromatography

Analysis in aqueous solutions were performed using high pressure liquid chromatography (Chromaster system, Hitachi) equipped with an evaporative light scattering detector (ELSD 90 LT-Low Temperature, VWR). For the analysis of small-sized saccharides, a single column configuration was used to separate the saccharides based on affinity (ABOA SugarSep-Ca, AppliChrom).

Here, too, an isocratic method using distilled water as a mobile phase was applied. The flow rate was set to a constant value of 0.5 ml/min. A sample volume of 20 µl was injected. The temperature of the oven and the detector were set to 353 K and 323 K, respectively. The samples were pre-filtered using 0.45 µm syringe filters (Chromafil GF/PET-45/25, Macherey-Nagel) and were transferred into 1.5 ml-vials. Calibration was established using saccharide standards of high purity (Analytical standards, Supelco).

7.2.3.3 Data Processing

The chromatograms obtained when working with SEC were quantitatively and qualitatively analysed using the Peakfit software 4.12. In doing so, broad and multiple peaks could be separated by using a manually modified deconvolution method. The peaks were described by Gaussian peaks at their local maxima. If necessary, when two peaks were not completely separated, two different Gaussian peaks were separated at the so-called valley in between these two peaks. The peak width

of the single peaks was adapted in a way that the total area under the chromatogram is completely covered. To exclude noise of the baseline in the data processing, a fixed minimum amplitude was set.

The area A_i and molecular masses M_i of the individual peaks were determined. Subsequently, these were used to calculate the average molecular masses of the sample according to equation (7-1). M_i was obtained from relating the maximum respective peak retention time to the pullulan calibration curves (see Figure 7-1).

$$Average\ molecular\ mass = \Sigma \frac{A_i}{A_{total}} * M_i \tag{7-1}$$

Similarly, the chromatograms obtained using the affinity chromatography were quantitatively and qualitatively analysed using the Peakfit software 4.12 in combination with the calibration curve. Gaussian peaks were identified and, in this case, clearly allocated to small-sized saccharides included in the calibration. The individual areas of these peaks were again determined and summed up to the total area. Percentage shares of the area of the individual peaks corresponding to the small-sized saccharides in relation to the total area of the chromatogram were calculated.

7.2.4 Viscosity Analysis

The viscosity of aqueous solutions containing dextran with the different molecular mass distributions, serving as a substrate for the enzymatic reaction, was determined using a rheometer (MCR 302, Anton Paar) equipped with a cone-plate-system. Previous analysis confirmed a Newtonian behaviour of the dilute aqueous dextran solutions. Based on this, the shear rate was set to a constant value of 100 s^{-1}. The temperature was set to a constant value of 328 K, just as for the enzymatic reaction. Here, too, sample preparation and subsequent viscosity analysis was performed in duplicate.

7.3 Results and Discussion

7.3.1 Analysis of Enzymatic Decomposition Products by Size Exclusion Chromatography (SEC)

In order to analyse the effect of dextran's initial average molecular mass on the enzymatic decomposition, experiments in quasi-binary aqueous solutions at optimum conditions of the dextranase used were performed. To do so, the temperature and pH were set to 328 K and pH 6, respectively.

In the first set of experiments, the incubation time was kept constant at 5 min. Dextran fractions with average molecular masses relevant for sugar cane and beet industries were used, either alone or in combination, as initial substrates for the enzymatic reaction. In this study, these were represented by dextran fractions with an average molecular mass of 2000 kDa (T2000) and 40 kDa

(T40), according to manufacturer's specification. The products resulting from the enzymatic decomposition were analysed using size-exclusion chromatography (SEC) in order to determine the molecular mass distribution of the products.

For fundamental HPLC analysis of the enzymatic decomposition process, a rather high but still realistic dextran content of 0.075 % (m/m), corresponding to 5000 mg/kg dry substance in a 15 % (m/m) sucrose solution, was used. Figure 7-2 (A) shows the SEC-chromatograms of high (T2000) and low (T40) molecular mass dextran fractions and their equal-mass mixture at a mass percentage of 0.075 % (m/m) in quasi-binary aqueous solutions, which were used as substrates for the enzymatic reactions. The secondary x-axis relates the molecular masses to the respective retention times as deduced from the calibration with pullulan standards using size exclusion columns with defined separation ranges (see also Figure 7-1).

In general, size exclusion chromatography elutes large molecules first. Thus, the retention time increases with decreasing molecular masses, as illustrated in Figure 7-2 (A). The broad and overlapping peaks suggest a relatively high polydispersity for both dextran fractions, T2000 and T40 (continuous and dashed line in Figure 7-2 (A), respectively), which is also in alignment with the manufacturer's information.

Using the Peak fit evaluation explained above, the molecular masses of the separated individual peaks were additionally determined, and based on these data, the average molecular masses of the initial dextran fractions and their enzymatic decomposition products were calculated, shown in Figure 7-3.

The analysis of T40 dextran indicates a monomodal but broad main peak, which covers molecular masses from 3 kDa to 100 kDa, deduced from the separation-calibration-system used (see secondary x-axis in Figure 7-2).

The average molecular mass calculation of T40 dextran (approx. 36 kDa) is in good agreement with the average molecular mass given by the manufacturer. T2000 dextran is characterised by an even higher polydispersity, covering molecular masses of 60 kDa to 3000 kDa. The calculation of the average molecular mass of T2000 dextran underestimates (approx. 450 kDa) the manufacturer's specification, for reasons given above. However, as the focus of this work is on the analysis of the decomposition of high molecular mass dextran into low molecular mass dextran, this only affects the calculation of the average molecular mass of the T2000 substrate and not of the reaction products. Even though the T2000 and T40 dextran fractions are obviously composed of molecules with different molecular masses, the proximity of the peak's limits indicates that the two substrates, T40 and T2000, partially comprise dextran fractions of similar molecular masses.

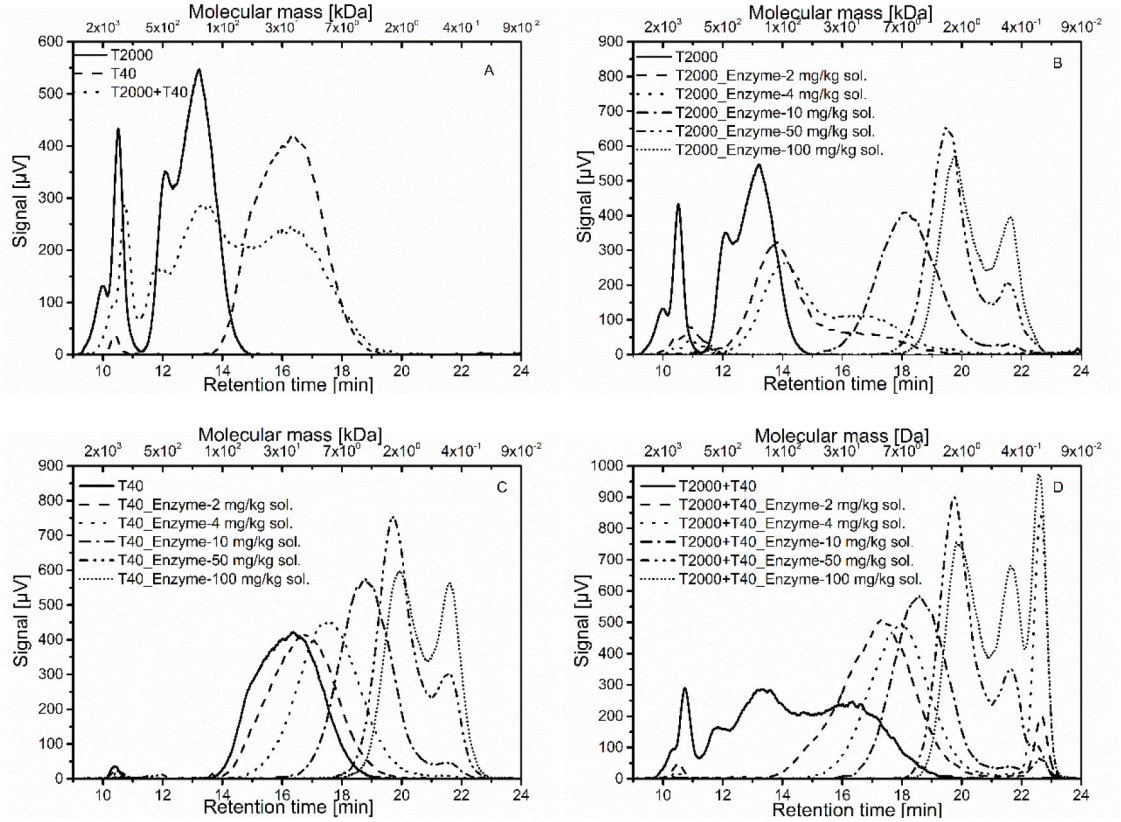

Figure 7-2 SEC-chromatograms of the initial and enzymatically decomposed dextran fractions. Incubation of 0.075 % (m/m) of T2000, T40 and the equal-mass mixture of T2000 and T40 at 328 K, pH 6 for 5 minutes. Figure (A) shows the initial dextran fractions (substrate). Figure (B), (C) and (D) show enzymatically decomposed T2000 and T40 as well as the equal-mass mixture of T2000 and T40, respectively.

The chromatogram of the equal-mass mixture of T2000 and T40 dextran is also shown in Figure 7-2 (A). It covers both fractions resulting in an even higher polydispersity, as expected ranging from 3 kDa to 3000 kDa.

Figure 7-2 (B), (C) and (D) show the SEC-chromatograms of enzymatically decomposed T2000 and T40 dextran as well as of the decomposed equal-mass mixture of T2000 and T40 dextran, respectively. Thereby, varying enzyme levels were considered, which are, as usual in sugar industry, given as mg per kg solution. The chromatograms of the substrates prior to enzyme application are again depicted as black continuous lines to facilitate comparison. For all three substrates, an increase of the enzyme level leads to a gradual decrease of the molecular mass due to enzymatic decomposition indicated by a successive shift of the peaks of the chromatograms towards higher retention times (Figure 7-2).

Consistently, a decrease of the average molecular mass with higher enzyme levels can be observed, see Figure 7-3. It is important to pay attention to the two y-axes in Figure 7-3, in which the primary y-axis relates to the average molecular masses of T40 dextran and the equal-mass mixture of T2000 and T40, while the secondary y-axis relates to the average molecular masses of T2000 dextran. For all dextran fractions, the decrease in average molecular mass as a function of the enzyme level

appears to follow a power model fairly well. Even though this general trend applies for all substrate compositions, the progress of the enzymatic decomposition differs when using the different substrates. This is in particular evident for the application of lower enzyme levels of 2 and 4 mg/kg solution (dashed and dotted line in Figure 7-2). The decomposition of high molecular mass T2000 dextran using these low enzyme levels of 2 and 4 mg/kg solution results in dextran fragments of comparatively high average molecular masses, roughly 180 kDa and 120 kDa, respectively (see squares in Figure 7-3). These average molecular masses are clearly higher than the average molecular masses determined for the products resulting from the decomposition of T40 dextran. For the latter, average molecular masses of 30 kDa and 10 kDa were respectively calculated (see dots in Figure 7-3).

Interestingly, the enzymatic decomposition of the equal-mass mixture of T2000 and T40 dextran results in very similar molecular masses as the decomposition of T40 dextran. It even seems that the decomposition was slightly further progressed in comparison with the decomposition of exclusively T40 dextran. On decomposition of the equal-mass mixture, an additional peak at about 23 min unsystematically occurs. This conspicuous peak occurs at retention times which would indicate the presence of an additional small-sized saccharide. Affinity chromatography was used to elucidate this in more detail, see further down.

Consequently, the calculated average molecular mass of the decomposition products starting from the equal-mass mixed substrate is slightly lower in comparison with the average molecular mass when exclusively decomposing T40 dextran. Average molecular masses of about 20 kDa and 6 kDa due to the application of 2 and 4 mg enzyme per kg solution were respectively achieved by decomposing the equal-mass mixture (see triangles in Figure 7-3).

On a further increase of the enzyme level to 10 mg/kg solution (dash-dot line in Figure 7-2), the average molecular masses of the decomposition products further decreased and seemed to level off at 16 kDa for T2000 dextran and 5 kDa for both, T40 dextran as well as the equal-mass mixture of T2000 and T40 dextran (Figure 7-3).

The application of unusually high enzyme levels of 50 mg/kg solution leads to significantly progressed enzymatic decompositions (dash-dot-dot line in Figure 7-2). The incubation of the three substrates with different molecular mass distributions results in products with very similar molecular masses. Apart from the unsystematic occurrence of the peak at 23 min for the equal-mass mixture, an increase of the enzyme level to 100 mg/kg solution (short dot line in Figure 7-2) seems not to affect the decomposition product characteristics greatly for the currently discussed incubation time of 5 min. For both high enzyme levels, the chromatograms show a further shift towards higher retention times and the average molecular masses decrease to single digit values independent of the average molecular mass of the initial substrate (Figure 7-3).

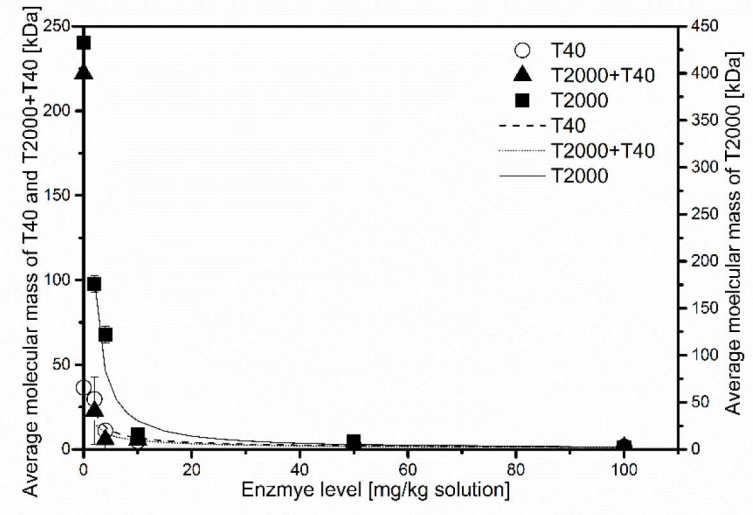

Figure 7-3 Average molecular masses [kDa] of the decomposition products calculated from SEC-data. Incubation of 0.075 % (m/m) of T2000, T40 and the equal-mass mixture of T2000 and T40 at 328 K, pH 6 for 5 minutes using various enzyme levels. Data are depicted as a function of the dextranase level applied. T2000: squares, T40: dots, equal-mass mixture of T2000 and T40: triangles.

These low average molecular masses determined can be explained by the formation of oligosaccharides and smaller molecules, whose precise composition will be discussed later in this work.

The data reconfirm that the enzymatic decomposition, and therefore the decrease of the molecular mass, follows a gradual pattern. A gradual decrease of the molecular mass means that the respective next smaller molecular mass is formed. Thus, high molecular mass dextran molecules are converted into smaller molecules while gradually delivering molecules of intermediate sizes. Under the same conditions (incubation time, enzyme and substrate level), intermediate products have higher molecular masses when starting from T2000 dextran in comparison with starting from T40 dextran. Thus, decomposition of T2000 dextran is less progressed than the decomposition of T40 dextran. However, the chromatograms of the decomposition products resulting from substrates with equal-mass mixed molecular masses suggest that the decomposition is not only affected by the sequential mode of action, which could be explained as follows:

For the decomposition reaction, dextran and dextranase need to get in contact, followed by loose adhesion before the actual catalytic step at the active sites of enzyme and substrate takes place. These first two steps are diffusion controlled and seem therefore to be prone to molecular mass variation of the substrate. It is a well-known fact that the viscosity of sugar cane and beet juices is affected by dextran's molecular mass (Kaur & Kaler, 2008). Generally, it can be assumed that the higher the viscosity, the lower the diffusion coefficient. Thus, the mobility of high and low molecular mass dextran molecules differs. The higher the substrate mobility is, the lower the solution viscosity, and thus the better the enzyme diffusion (Bisswanger, 2000). Hence, higher

viscosities can obviously affect the diffusion controlled parts of an enzyme reaction (Elmgren, 1980).

To prove the relevance of viscosity-related effects for the relatively low dextran contents used, the viscosity was experimentally determined. Figure 7-4 shows the viscosities of quasi-binary aqueous solutions containing dextran with the different average molecular masses at the currently discussed mass percentage of 0.075 % (m/m), which are realistic for raw juices at the beginning of sugar manufacture. The data indicate that there is no effect on the viscosity due to these rather low dextran contents. In contrast, higher dextran contents (mass percentage of 5 % (m/m)) show a clear increase of the viscosity. The higher the average molecular mass of dextran, the more distinct the effect on the viscosity. Figure 7-4 also shows the effect of the equal-mass mixture of T2000 and T40 dextran on the viscosity in quasi-binary aqueous solutions. The data indicate an intermediate viscosity, which is significantly lower than in the exclusive presence of T2000 dextran, but still higher than in the presence of solely T40 dextran. The fact that a clear molecular mass dependent trend is seen at the higher mass percentage of 5 % (m/m), gives reason to assume that dextran molecules of different molecular masses have different molecular mobilities. This can also play a role in the different decomposition progresses, even though it is not recognisable from the viscosity data at the low mass percentage of 0.075 % (m/m).

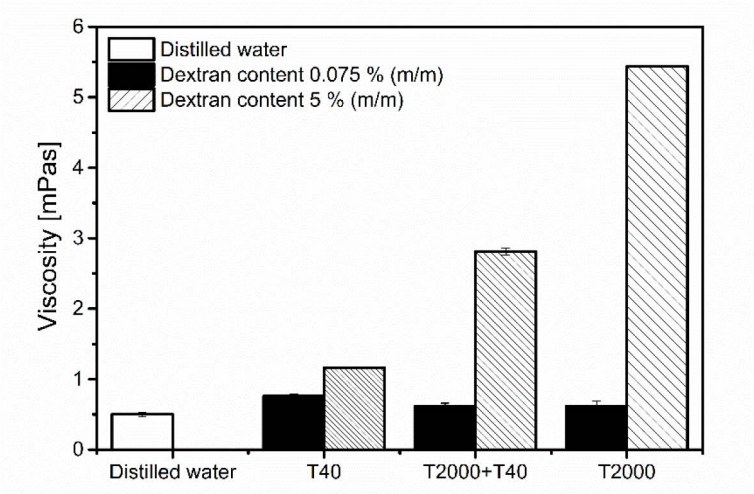

Figure 7-4 Viscosity of quasi-binary aqueous dextran solutions. Mass percentages of 0.075 % (m/m) and 5 % (m/m) and of pure distilled water at 328 K (temperature for enzyme reaction) were measured.

For one thing, the improved decomposition of the equal-mass mixture of T2000 and T40 dextran could be attributed to the gradual decomposition process and also to a higher molecular mobility deduced from the lower viscosity of the solution. However, the very similar or rather even slightly improved decomposition, of the equal-mass mixture in comparison with exclusively T40 dextran gives reason to assume that the presence of very broadly distributed dextran chain lengths additionally help enzyme access (e.g. dextran segment densities, spatial distributions, steric

hindrance can potentially be involved). However, at the current state of the research, all reasons involved still remain unclear needing further investigations. Nevertheless, the simultaneous presence of high and low molecular mass dextran has also shown conspicuous differences in previous work with regard to membrane separation (Abraham et al., 2019).

7.3.2 Analysis of Small-Sized Decomposition Products by Affinity Chromatography

In order to improve the characterisation of small-sized saccharides (mono-, di- and oligosaccharides) resulting from the dextranase action, the initial substrates and the decomposition products were additionally analysed by affinity chromatography. Besides, the conspicuous peak from SEC-data when decomposing the equal-mass mixture can be re-examined.

The affinity-chromatograms of the initial substrates with the different molecular mass distributions are shown in Figure 7-5 (A). As affinity chromatography was used to separate and to identify decomposition products with low molecular masses, differences in the chromatograms of the substrates with rather high but different initial average molecular masses are not as explicit as for the chromatograms from SEC-analysis. The chromatograms of the enzymatic decomposition products resulting from T2000, T40 and the equal-mass mixture of T40 and T2000 are shown in Figure 7-5 (B), (C) and (D), respectively. Since the focus is on the smaller molecules, the scale of the figure is chosen in a way that the peaks of the smaller molecules with a lower average molecular mass are clearly displayed, while the peaks for larger molecules with higher average molecular masses are not shown completely.

At low enzyme levels of 2 and 4 mg/kg solution, the chromatograms of the decomposition products do not show peaks relating to small-sized saccharides, such as oligo-, tri- and disaccharides (dashed and dotted lines in Figure 7-5). An increase of the enzyme level to 10 mg/kg solution applied to aqueous solutions containing T40 dextran or the equal-mass mixture (dash-dot line in Figure 7-5 (C) and (D)) resulted in the formation of di-, tri- and oligosaccharides (peak maxima at about 10 min, 11 min and 12 min, respectively).

However, analysis of the decomposition products of T2000 dextran (dash-dot line in Figure 7-5 (B)) at these enzyme levels revealed that hardly any small-sized saccharides were formed, again indicating a less progressed decomposition as it was already concluded from SEC. Nevertheless, for all substrates studied the application of even higher enzyme levels of 50 and 100 mg/kg solution (dash-dot-dot and short dot line in Figure 7-5 (B), (C) and (D)) results in increased and similar amounts of small-sized decomposition products.

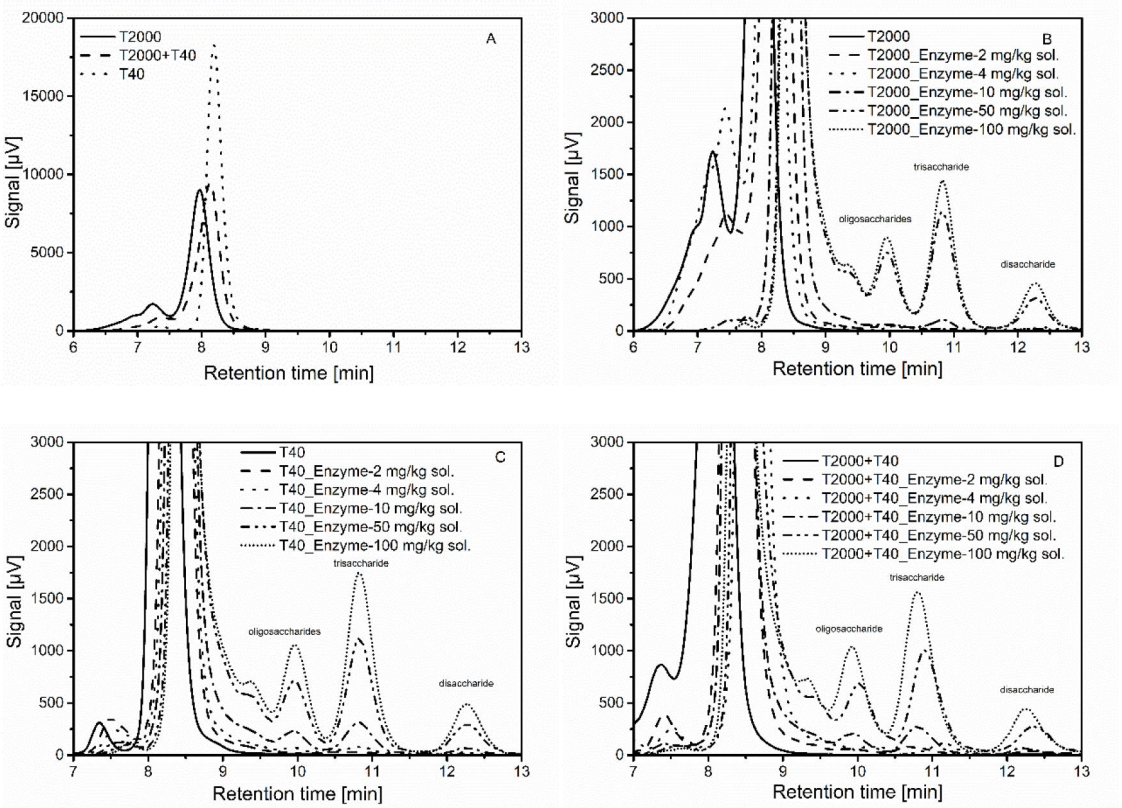

Figure 7-5 Affinity-chromatograms of the initial and enzymatically decomposed dextran fractions. Incubation of 0.075 % (m/m) of T2000, T40 and mixture of equal masses of T2000 and T40 at 328 K, pH 6 for 5 minutes. Figure (A) initial dextran fractions (substrates). Figure (B), (C) and (D) show enzymatically decomposed T2000 and T40 as well as the equal-mass mixture of T2000 and T40, respectively.

Evaluating the peak areas and relating them to the total area allows to determine the percentage shares of these small-sized decomposition products (Figure 7-6). The higher the enzyme level, the higher the amount of oligo-, tri- and disaccharides. Besides, it is found that trisaccharides generally constitute the largest shares among the small-sized saccharides, followed by oligosaccharides and then disaccharides. Decomposition products smaller than disaccharides were not found. Here, too, when using the high enzyme levels, the decomposition products are the same for the substrates with different initial average molecular masses. The data indicate that an even further increase of the enzyme level to 50 and 100 mg/kg solution lead to quantitatively and qualitatively similar compositions of the decomposition products for all substrates studied in this work.

For the equal-mass mixture substrate, SEC data of the decomposition products showed a conspicuous peak at retention times, indicating the additional presence of molecules with a really low molecular mass, e.g. representative for mono- or disaccharides. However, the additional analysis applying affinity chromatography shows that also for the equal-mass mixture substrate only oligo-, tri- and discaccharides are formed, but no mono-saccharides. This indicates that this peak rather relates to effects caused by interaction of dextran chains of different lengths during

separation in the SEC-columns as it was already observed for membrane separation in previous work (Abraham et al., 2019).

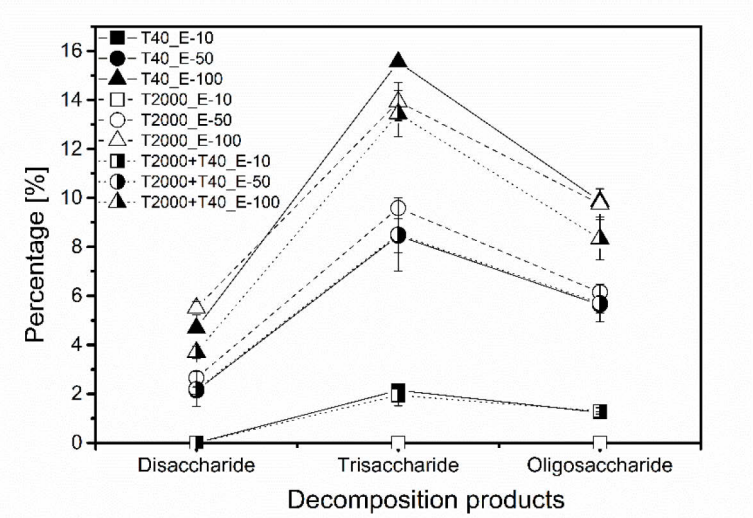

Figure 7-6 Percentages of the peak area corresponding to small-sized saccharides in the decomposition products in relation to the total area calculated from affinity-data. Incubation of 0.075 % (m/m) of T2000 (open symbols), T40 (filled symbols) and the equal-mass mixture of T2000 and T40 (half-filled symbols) at 328 K, pH 6 for 5 minutes using various enzyme levels. Enzyme levels of 10 (squares), 50 (dots) and 100 (triangles) mg/kg solution are depicted.

In general, dextranase attacks the α-(1→6) glyosidic linkages in dextran with both high and low molecular masses (Khalikova et al., 2005). The fact that mainly oligo- and trisaccharides are formed by the dextranase reaction is not surprising since branching in dextran's main chain occurs, representing uncleavable bonds. The theory of steric hindrance, as described by Rollings, states that due to branching the attack of the α-(1→6) glycosidic linkages by the enzyme is hindered. Not only the actual branching points are unhydrolyzable, but also the α-(1→6) linkages in the vicinity of such branching points (Rollings, 1985). Thus, similar final decomposition product compositions indicate that the amount as well as the overall distribution of branching points seem to be quite similar for the different molecular mass dextran fractions used in this study.

7.3.3 Variation of Incubation Time

The decomposition products are also affected by the incubation time, which is of great relevance for industrial practice as well. Therefore, experiments with T2000 dextran as a substrate at incubation times, varying between 5 and 360 min, were conducted. The temperature and pH were, as previously, set to 328 K and pH 6, respectively.

A constant mass percentage of substrate of 0.075 % (m/m) and also a constant enzyme level of 10 mg/kg solution were used. As previously, size exclusion chromatography and affinity chromatography were used to identify and quantify the decomposition products. The chromatograms were processed as described above.

In Figure 7-7, the average molecular mass of the decomposition products for each incubation time is given. The black squares in Figure 7-7 (A) represent the average molecular masses of the enzymatic decomposition in quasi-binary aqueous solutions, which means in absence of sucrose.

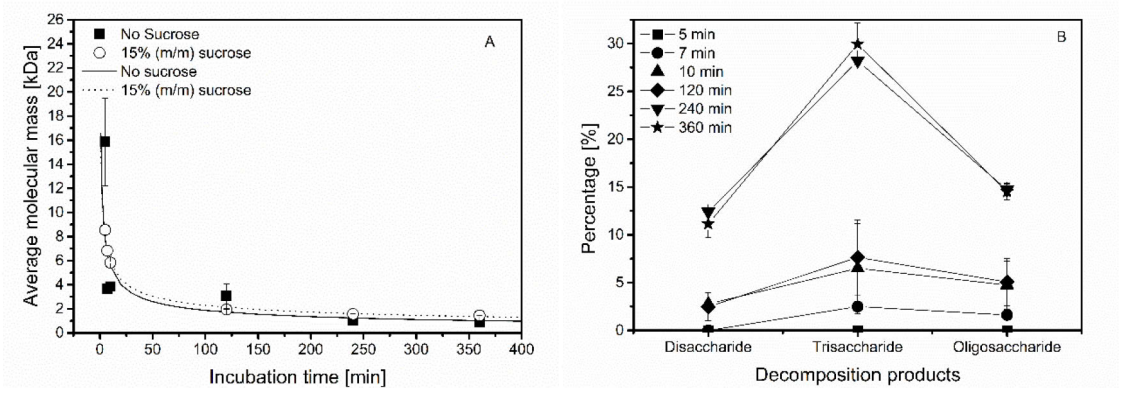

Figure 7-7 Influence of incubation time on enzymatic decomposition using a fixed enzyme level of 10 mg/kg solution. A) Average molecular mass [kDa] calculated from SEC-data. B) Percentages of small-sized saccharides contained in decomposition products calculated from affinity-data.

The average molecular mass resulting from an incubation time of 5 min stands out due to its comparatively large error bar. This appears to be related to the intermediate progress of the decomposition process of initially broad molecular mass distributions of the rather inhomogeneous T2000 dextran fractions. This results in broadly distributed reaction products, which exacerbate the determination of average molecular masses. Nevertheless, the average molecular masses of the duplicate determinations with approximately 12 kDa and 20 kDa are similar to each other and distinct from other compositions, but result in a large standard deviation, though. A general trend is apparent, namely a decrease of the average molecular mass with an increase in incubation time. The relation between the average molecular mass and the incubation time appears to fit a power model reasonably well. When using an enzyme level of 10 mg/kg solution, a decrease of the average molecular mass from 16 kDa to 4 kDa can be achieved by an increase of the incubation time to 7 min and 10 min. A further and significant increase of the incubation time to 120, 240 and 360 min does not dramatically affect the average molecular mass of the decomposition products. Long-time incubation for 240 min as well as 360 min result in average molecular masses of the decomposition products of 1 kDa. The rather marginal difference in the average molecular masses calculated after long-time incubation indicates that the major enzymatic action is largely exploited within 7 min of incubation.

The affinity chromatograms of the decomposition products using various incubation times reveal the formation of small-sized saccharides with increasing incubation time. The percentage shares of the individual area of the peaks corresponding to the above-discussed oligo-, tri- and disaccharides in relation to the total area are shown in Figure 7-7 (B).

The amount of oligo-, tri- and disaccharides obviously increases with higher incubation times. Here, too, the application of 10 mg/kg solution to T2000 dextran does not reveal any small-sized saccharides within 5 min incubation time. In the following, the formation of decomposition products as a function of the incubation time are discussed by giving the percentage of the respective kind of saccharide in relation to the total area. A small amount is formed within an incubation time of 7 min (2 % for tri and oligosaccharides, respectively). Incubation of T2000 dextran for 10 min and 120 min lead to very similar amounts of about 8 % of trisaccharides, 5 % of oligosaccharides and about 2 % of disaccharides. For an incubation time of 240 min or longer, almost 30 % of trisaccharides, about 10 % disaccharides and almost 15 % of oligosaccharides were produced. SEC-data indicate that the greatest advance in decomposition is achieved within the first 7 min. Affinity-data indicate that a distinctly elongated incubation time leads to an increase of small-sized saccharides. This also confirms the gradual mode of action of the dextranase used as stated above, in which dextran is gradually splitted into molecules of lower molecular masses until finally resulting in the just mentioned smallest possible units, namely oligo-, tri- and disaccharides. These smallest possible units are not necessarily wanted for an optimal sugar production. They might even be detrimental for a high-quality sugar production as it is known that a high amount of reducing sugars, such as isomaltose, can increase colour formation during sugar processing. Thus, there is no additional sugar industry-relevant benefit of long-time incubation.

This data set has indicated that the enzymatic decomposition is not only gradually accomplished with the increase of the enzyme level, but also with the incubation time. Nevertheless, it has been shown that for the enzyme level applied, incubation times between 5 min and 10 min are sufficient to widely exploit the enzyme potential needed, while simultaneously avoiding the formation of a high number of reducing sugars. Combined adaption of enzyme dosage and incubation time hence complements targeted enzyme applications.

7.3.4 Potential Effects due to the Presence of Sucrose

In general, it is recommended to apply dextranases as early as possible in the process (Jimenez, 2009). There are two reasons to do so: firstly, potential negative process effects due to the presence of dextran of higher molecular masses (e.g. filtration, evaporation, crystallisation) need to be avoided as early as possible in the process, and secondly, it is assumed that the presence of high sucrose contents as typical in the later process steps, negatively affects the dextranase activity (Eggleston & Monge, 2005). This issue has already attracted attention in earlier work, in which inhibiting effects due to a relatively high sucrose content of about 60 % (m/m), typical sucrose level in the last evaporation step during sugar manufacture, on the enzyme reaction could be observed (Abraham et al., 2016).

In order to analyse whether the relatively low sucrose contents found in raw juices also affect the enzyme reaction, enzymatic decomposition experiments in aqueous sucrose solutions were performed. Sucrose concentrations typically range between 14 % and 20 % (m/m) in sugar beet and 10 % and 18 % (m/m) in sugar cane raw juices (van der Poel et al., 1998). Therefore, an averaged and standardised level of 15 % (m/m) sucrose was used for this study. The resulting corresponding average molecular masses of the dextran fractions are shown as dots in Figure 7-7 (A).

Apart from the value at an incubation time of 5 min for the sucrose-free system that was discussed above, the average molecular masses of the systems containing sucrose are just slightly higher than those of the sucrose-free one. These rather small differences are further diminished at higher incubation times (longer than 120 min) indicated by very similar values for the average molecular mass determined for the decomposed dextran of about 2 kDa.

Conclusively, only a minor effect of the presence of sucrose (15 %) on the decomposition of high-molecular mass dextran was found. This is relevant for the application of dextranase to sugar cane and beet raw juices.

7.4 Conclusion

The enzymatic decomposition of dextran fractions with different average molecular masses (T2000, T40, equal-mass mixture of T2000 and T40) was investigated using high performance liquid chromatography equipped with two column configurations, either based on size exclusion (SEC) or affinity.

The SEC-data indicate that the enzymatic decomposition by dextranase follows a gradual pattern, meaning a successive reduction of the average molecular mass. The average molecular mass of the decomposition products decreases with the increase of the enzyme level as well as with the increase of the incubation time. This is indicated by a shift of the peaks within the chromatograms towards higher retention times and, thus, to lower average molecular masses. This gradual decreasing trend applies to all substrates, T2000 and T40 dextran as well as to the equal-mass mixture of T2000 and T40 dextran. However, the progress of decomposition differs when starting from the different initial molecular masses, especially when using lower enzyme levels. In this case, the enzymatic decomposition starting from T2000 dextran is less progressed in comparison with the decomposition starting from T40 dextran. Surprisingly, the enzymatic decomposition of the equal-mass mixture of T2000 and T40 dextran shows a very similar progress of decomposition as T40 dextran. It appears to be even slightly further progressed in comparison with the decomposition of solely T40 dextran. These differences in the average molecular masses of the decomposition products mainly diminish with the application of high enzyme levels, which would be cost-intensive and hence not advisable. Thus, the final composition of decomposition products is similar for the dextran substrates with different average molecular masses taking either long process times or high enzyme levels.

Affinity chromatography was additionally used to analyse the small-sized saccharides, such as oligo-, tri- and disaccharides, contained in the products resulting from the enzymatic decomposition. The affinity analysis is generally in good alignment with SEC analysis. Oligo-, tri- and disaccharides could be identified. Generally, the amount of small-sized saccharides increases with the increase of the enzyme level and the incubation time. Under the same conditions, the amount of small-sized saccharides is higher when starting from the equal-mass mixture as well as from exclusively T40 dextran than when starting from T2000 dextran. When using really high enzyme levels, the amount and kind of decomposition products are very similar for all substrates, again suggesting that the final product composition is similar.

The influence of the incubation time on the decomposition in quasi-binary aqueous and in 15 % (m/m) aqueous sucrose solutions was additionally investigated with an enzyme dosage of 10 mg/kg solution. A power model appears to describe the relation of average molecular mass and incubation time reasonably well. For both solutions, the average molecular mass just slightly decreases with the increase of the incubation time. At incubation times longer than 7 minutes, an increasing amount of small-sized saccharides were found, although the average molecular mass, obtained from SEC-data, was not dramatically affected. This rather marginal difference indicates that the major enzyme benefit sought for the application in sugar industry is largely realised within the first 7 min of incubation time at the specific dosage studied. Besides, the presence of 15 % (m/m) sucrose seems to hardly affect the enzyme reaction so that the enzyme application in raw juices seems to be appropriate.

The data gathered made clear that the progress in decomposition differs when decomposing dextran with varying molecular mass distributions. This suggests that the enzyme dosage should not only relate to the total dextran content, but also to the molecular mass distribution of the substrate. This way, targeted molecular masses can be achieved, while simultaneously avoiding enzyme over-dosage.

The work presented emphasises again that dextran analysis in sugar industry practice should cover these two aspects, total dextran contents (substrate content) and identification of molecular mass dextran fractions (type of substrate). The analysis with respect to these targets has already been focus of previous work (Abraham & Flöter, 2018).

References

Abdel-Rahman, E.-S., Shick, R., & Kurz, T. (2007). Influence of dextran on sucrose crystallization. *Sugar Industry*, *132*(6), 453–460.

Abraham, K., & Flöter, E. (2018). New approaches for the determination of dextran in the sugar production process. *Sugar Industry*, *143*(68), 138–146.

Abraham, K., Hagen, S., Schlumbach, K., Rohde, A., & Flöter, E. (2016). Dextranase application in sucrose solutions - towards a better understanding. *International Sugar Journal*, 604–610.

Abraham, K., Kunst, S., & Flöter, E. (2019). Membrane Characterisation for Fractionated Dextran Analysis in Sugar Industry. *Food Analytical Methods.* Advance online publication. https://doi.org/10.1007/s12161-019-01441-7

Aquino, F. W., & Franco, D. W. (2009). Molecular mass distribution of dextran in Brazilian sugar and insoluble deposits of cachaça. *Food Chemistry*, *114*, 1391–1395. https://doi.org/10.1016/j.foodchem.2008.11.019

Bashari, M., Lagnika, C., Ocen, D., Chen, H., Wang, J., Xu, X., & Jin, Z. (2013). Separation and characterization of dextran extracted from deteriorated sugarcane. *International Journal of Biological Macromolecules*, *59*, 246–254. https://doi.org/10.1016/j.ijbiomac.2013.04.046

Berg, J. M., Tymoczko, J. L., Gatto, G. J. jr., & Stryer, L. (2018). *Stryer Biochemie* (8. Auflage). Heidelberg: Springer Spektrum.

Bertrand, E., Pierre, G., Delattre, C., Gardarin, C., Bridiau, N., Maugard, T., Michaud, P. (2014). Dextranase immobilization on epoxy CIM disk for the production of isomaltooligosaccharides from dextran. *Carbohydrate Polymers*, *111*, 707–713. https://doi.org/10.1016/j.carbpol.2014.04.100

Bisswanger, H. (2000). *Enzymkinetik: Theorie und Methoden* (3. Auflage). Weinheim: Wiley-VCH.

Chen, J. C., & Chou, C. C. (1993). Cane Sugar Handbook: A Manual for Cane Sugar Manufacturers and Their Chemists (12th ed.). New York: John Wiley & Sons.

Eggleston, G., & Monge, A. (2005). Optimization of sugarcane factory application of commercial dextranases. *Process Biochemistry*, *40*(5), 1881–1894. https://doi.org/10.1016/j.procbio.2004.06.025

Elmgren, H. (1980). The mobility profile around polymer segments as calculated from microviscosity data on polymer solutions and gels. *Journal of Polymer Science: Polymer Letters Edition*, *18*(5), 339–350. https://doi.org/10.1002/pol.1980.130180504

Falconer, D. J., Mukerjea, R., & Robyt, J. F. (2011). Biosynthesis of dextrans with different molecular weights by selecting the concentration of Leuconostoc mesenteroides B-512FMC

dextransucrase, the sucrose concentration, and the temperature. *Carbohydrate Research*, *346*(2), 280–284. https://doi.org/10.1016/j.carres.2010.10.024

Jimenez, E. R. (2009). Dextranase in sugar industry: A review. *Sugar Tech*, *11*(2), 124–134. https://doi.org/10.1111/j.1468-0254.2009.00285.x

Kaur, S., & Kaler, R. (2008). Dextran and its effect on the flow behaviour of molasses and crystallization rate. *Journal of Food Engineering*, *86*(1), 55–60. https://doi.org/10.1016/j.jfoodeng.2007.09.010

Khalikova, E., Susi, P., & Korpela, T. (2005). Microbial dextran-hydrolyzing enzymes: fundamentals and applications. *Microbiology and Molecular Biology Reviews*, *69*(2), 306–325. https://doi.org/10.1128/MMBR.69.2.306-325.2005

Rauh, J. S., Cuddihy, J. A., & Opelka, M. J. (1999). Analyzing Dextran in the Sugar Industry: A Review of Dextran in the Factory and a New Analytical Technique. *Proc. American Society of Sugar Beet Technologist 30th Biennial Meeting*, 29–40.

Ravno, A. B., & Purchase, B. S. (2005). Dealing with Dextran in the South African Sugar Industry. *Proc S Afr Sug Technol Ass*, *79*, 28–47.

Robyt, J. F., & Eklund, S. H. (1982). Stereochemistry Dextransucrase Involved in the Mechanism of Action of Dextransucrase in the Synthesis of Dextran and the Formation of Acceptor Product. *Bioorganic Chemistry*, *11*, 115–132.

Rollings, J. (1985). Enzymatic Depolymerization of Polysaccharides. *Carbohydrate Polymers*, *5*, 37–82.

Van der Poel, P. W., Schiweck, H., & Schwartz, T. (1998). *Sugar Technology: Beet and Cane Sugar Manufacture*. Berlin: Dr. Albert Bartens KG.

8 New Approaches for the Determination of Dextran in the Sugar Production Process

Abraham, K. [ab]; Flöter, E. [a]

[a] TU Berlin, Department of Food Process Engineering, Seestraße 13, 13353 Berlin, Germany

[b] SternEnzym, Kurt-Fischer-Str. 55, 22926 Ahrensburg, Germany

Originally published in Sugar Industry (2018), 143 (7), 138-156.

Abstract

The presence of polysaccharides in sugar cane and beet raw juices causes several negative effects during the sugar manufacture. These are usually mitigated by enzymatic decomposition of dextran. Such effects not only depend on the content, but also on the molecular mass distribution. This means that the different dextran fractions specifically affect the process. An accurate process control hence requires the most precise knowledge about the existing content and the molecular mass distribution present. A detailed understanding of the specific processing problems and also a targeted enzyme application hence requires the determination of a total dextran content and also its characterisation including the differentiation between the different dextran fractions. An accurate analytical tool which equally satisfies industrial applicability is still lacking. To improve on this situation, two new approaches for the determination of dextran were developed and benchmarked against the commonly used and established Haze Method, which is rather inaccurate and also sensitive to molecular mass variation. The two new approaches are both based on polarimetry. These two methods indicate to be superior over the Haze Method with respect two molecular mass variation and hence enable the determination of a broader molecular size range including also low molecular mass dextran.

8.1 Introduction

The presence of polysaccharides in sugar beet and cane juices causes diverse negative effects during sugar manufacture. These polysaccharides can either originate from cell plant material or from microbial activity. The latter especially comprises the glucose polymer dextran formed by enzymatic activity of lactic acid bacteria, more specifically by *Leuconostoc mesenteroides* species. The main chain of dextran is composed of α-(1→6) linked glucose units. Branching points via α-(1→3) glycosidic linkages can occur up to 5 % and cause deviation from a strictly linear structure. Dextran is especially relevant for the sugar cane industry mainly due to the abundant occurrence of mesophilic bacteria in the area, where sugar cane is cultivated. Nevertheless, the presence of dextran is not negligible in the sugar beet industry either. The bacterial growth in this case is mainly initiated by freeze-thaw-cycles. In both cases, dextran is co-extracted along with the sucrose and can affect sugar manufacture in many ways. Among them, the presence of dextran causes a higher viscosity negatively affecting the filtration, evaporation and crystallisation rate (Promraksa, 2008).

During juice purification the modified shape and size of precipitated calcium carbonate crystals with adhering non-sugars is known to contribute to worsened filtration processes (Hein et al., 2012). Furthermore, dextran causes modifications of the sucrose crystal shape and size (Promraksa, 2008). This is more specifically about crystal elongation and agglomeration. Such modification effects not only depend on the existing content, but also on the molecular mass distribution of dextran. This implies that studying the effects of dextran additionally necessitates a view on the specific effects of the different molecular mass fractions. Different molecular masses can hence cause different processing problems to different extents.

It is a well-known fact that an increase in viscosity is mainly caused by high molecular mass dextran. The specificity of the aforementioned modification effects is, however, not yet clarified in detail. It is, however, well known that both, high and low molecular weight dextran, contribute to such effects (Abdel-Rahman, 2007).

Dextran analysis is hence a necessary prerequisite to understand the dextran induced processing problems in detail and also to reduce these effects in a controlled manner. Such effects are usually mitigated by enzymatic decomposition, which results in a gradual decrease of molecular mass. However, details of the decomposition process and intermediate reaction products including their specific effects on the sugar process are currently not understood in detail.

An adequate dextran analysis consequently demands to fulfil the following two main requirements. The first of these is represented by the determination of the total dextran content including also lower molecular mass dextran. This requires a response signal independent of molecular mass. Known methods mostly feature a response signal with an adverse sensitivity to molecular mass variation, which makes the determination of equally high and low molecular mass dextran nearly impossible.

In order to realise the most precise understanding of the dextran issue prevail, it is further necessary to characterise the molecular size distribution. The differentiation between high and low molecular mass dextran is hence additionally necessary to accomplish an adequate dextran analysis. The establishment of appropriate analytical tools is especially hampered by relatively low contents and broad molecular mass ranges in realistic raw juices (Day & Sarkar, 1986).

Besides, industrial suitability needs to be satisfied simultaneously, regarding time necessary to perform an analytical procedure, equipment and ease of operation. Established methods for the determination of dextran fail to comply with at least one of these requirements.

The usage of alcoholic precipitation of dextran is a popular tool in polysaccharide analysis. The commonly used Haze Method according to the ICUMSA description is based on alcoholic precipitation using 50 % (v/v) ethanol. Despite its ease of operation, the response signal of this method, the degree of alcoholic precipitation, is, however, sensitive to molecular mass variation. This results in a rather inaccurate dextran content determination, which is additionally limited to high molecular mass dextran.

Another established method is the Roberts' Copper Method. In this case all of the polysaccharides are precipitated with ethanol. In the following, dextran is selectively precipitated with alkaline copper sulfate. The formation of a phenol-sulfuric acid colour complex is subsequently determined in a spectrophotometer (485nm) (Chen & Chou, 1993). The high demand of time and chemicals renders this method unsuitable for industrial practice. Furthermore, the exact molecular size limit and amount of precipitated dextran using even 80 % (v/v) ethanol is not clearly delimited. The completeness of dextran precipitation by means of 80 % (v/v) ethanol is controversially discussed in literature. Earlier results based on polarimetry indicated that low molecular mass dextran with an average molecular weight of 40 kDa is not fully recovered using 80 % (v/v) ethanol.

This issue also applies to other methods using alcoholic precipitation as a preparatory step, such as the Enzyme-HPLC Method. The latter also uses alcoholic precipitation with 80 % (v/v) ethanol in order to isolate all polysaccharides. Dextran is subsequently enzymatically decomposed to its final decomposition products, which is assumed to be solely isomaltose. The isomaltose content is then used to calculate the initial dextran content. Anyhow, a decomposition to solely isomaltose is questionable. The occurrence of branching points in the chain is the most obvious contributing factor for a decomposition to a mixture of oligosaccharides and isomaltose. Hence, the preparation step of alcoholic precipitation and the assumption of complete conversion are potential sources of uncertainty. The main disadvantage of this method is, however, its non-conformity with industrial practice as it is time consuming and requires chromatographic equipment. Du Boil further reported that this method is similarly time-consuming as the Roberts' Copper Method (Du Boil, 2000).

Consequently, an industrially useful method for the analysis of total dextran contents comprising the whole molecular size range is still needed. In order to make a step towards this, new methods were investigated and benchmarked against the Haze Method.

Both new approaches are based on polarimetry requiring standard industrial equipment. These methods are not cumbersome or excessive in chemical consumption. The aforementioned basic requirements for industrial suitability are hence satisfied. The response signal of optical rotation is further assumed to be independent of the molecular mass of dextran. The evaluation of analytical methods for the determination of dextran contents requires a detailed understanding of the response signal and potential variations due to process parameters or other components. The signal strength and sensitivity is crucial for the definition of meaningful determination ranges with regard to content and molecular mass distribution of dextran.

The work presented consequently documents the progress in developing methods that satisfy the conditions of applicability, accuracy and differentiation for the determination of dextran. To this end, the determination of dextran was studied at varying contents and molecular sizes in order to evaluate the general applicability of the new methods proposed.

8.2 Materials and Methods

8.2.1 Materials

Different dextran molecular mass fractions were used in the work presented. Middle molecular mass dextran (Carl Roth, dextran 500) was used to prepare the calibration curve for all methods applied. High (Sigma-Aldrich, dextran 2000 with a molecular mass distribution of 1,500 to 2,800 kDa) and low molecular mass dextran (Carl Roth, dextran 40 with molecular mass distribution of 35-45 kDa) were further used for the preparation of synthetic thin juices containing 15 % (m/m) sucrose. All of these dextran fractions originate from lactic acid bacteria, more specifically from *Leuconostoc Mesenteroides* strain B512. Manufacturer specifications report very similar specific optical rotations for these different dextran fractions. The high molecular mass dextran fraction possesses a specific optical rotation of +199°. Middle and low molecular mass dextran show quite similar values for the optical rotation with +195° to +203° and +195° to+ 201°, respectively.

8.2.2 Determination of Dextran

8.2.2.1 Haze Method

The Haze Method according to the ICMUSA GS1/2/9-15 (2011) was adapted to analyse 15 % (m/m) sucrose solutions. Those 15 % (m/m) sucrose solutions were intended to represent synthetic thin juices. The sample preparation procedure included the removal of starch (enzymatic decomposition with amylase) and proteins (precipitation with 10 % (m/m) trichloracetic acid

solution) followed by filtration using filter aid (acid washed kieselguhr) and Whatman filter paper No. 5. Dextran was subsequently precipitated with ethanol and the resulting turbidity was measured in a spectrophotometer at 720 nm after 20 min ± 10 s (Nanocolor UV/VIS, Macherey-Nagel) (ICUMSA, 2011). The calibration procedure was modified in a way that the filtration step necessary in the actual measurement procedure of samples was also part of the sample preparation procedure for calibration purposes. This was done for complete adjustment of the calibration and measurement procedures. The following steps of the procedure were performed as described above in accordance with the ICUMSA description. Middle molecular mass dextran (Carl Roth, dextran 500) was used to prepare the calibration curve. The latter aims at a reduction of the sensitivity of the alcoholic precipitation and hence of the final results to molecular mass variations.

8.2.2.2 Enzymatic Method

The optical rotation of 15 % (m/m) sucrose solutions with defined dextran contents of different molecular masses were measured before and after a complete enzymatic decomposition. The difference in optical rotation between the initial dextran loaded solution and the solution containing specifically decomposed dextran was consequently used to calculate the initial dextran content. Samples were hence divided into two parts, of which one was incubated with dextranase in surplus (1000 mg/kg juice of Sugazym DX L, SternEnzym) for 60 minutes at 328 K in a shaking water bath (SW23, Julabo). The sucrose content in the synthetic juices was set to a constant value of 15 % (m/m) for both, the calibration and measurement procedure. This way, potential effects of the presence of sucrose on the enzymatic hydrolysis would also be reflected in the calibration curve. The calibration and the actual measurement procedure were hence fully adjusted. And again, middle molecular mass dextran (Carl Roth, Dextran 500) was used to prepare the calibration curve in order to reduce potential effects of the substrate's molecular mass on the mode of enzyme action. The procedure of measuring the optical rotation was performed as described in chapter 8.2.2.4. The measurement of the initial dextran loaded solution and the solution containing specifically decomposed dextran were performed in direct succession in order to avoid any deviations due to mutarotation.

8.2.2.3 Membrane Method

The optical rotation of 15 % (m/m) sucrose solutions with defined dextran contents of different molecular masses were measured before and after the separation of dextran via membrane filtration. Standard industrial equipment was used to perform the membrane filtration and to measure the optical rotation (Autofilt and high-performance circle polarimetry, Schmidt & Haensch). The Autofilt filter apparatus was equipped with a polyethersulfone membrane with a molecular weight cut-off of 4 kDa (Microdyn-Nadir, UH 004). A transmembrane pressure of 3 bar was set and the membrane filtration was performed at room temperature.

The separation of dextran via membrane filtration was also implemented in the calibration procedure intended to include potential effects of the sucrose on the membrane separation performance (separation efficiency and sucrose retention). Here, too, the calibration and the actual measurement procedure were hence fully adjusted. And again, middle molecular mass dextran (Carl Roth, dextran 500) was used to prepare the calibration curve. The measurement of the feed and permeate samples were performed in direct succession in order to avoid any changes in total optical rotation due to mutarotation. The difference in optical rotation between the feed and the permeate was used to calculate the amount of dextran retained by the membrane. Determination of optical rotation was done according to descriptions in chapter 8.2.2.4. Assuming that all dextran fractions are hold back by the membrane, this value is considered as the dextran load of the feed material. A first aliquot of the permeate of 10 ml was discarded before the actual sample of 20 ml was collected. A sample volume of 20 ml is necessary to allow a first rinse of the polarimeter tube using 5 to 7 ml.

8.2.2.4 Polarimetric Measurement

Optical rotations were measured at 589 nm using a high-performance circle polarimeter provided by Schmidt & Haensch with a resolution of 0.001° (Polartronic MH8). The measuring temperature was set to 293 ± 1 K. A glass tube with center cup filling of 200 mm length and a filling volume of 12 ml was used for all measurements in the polarimeter. The glass tube needs to be assembled carefully such that the optical rotation of the empty tube is not higher than 0.002°. Prior to the measurement, the tube was rinsed with a small amount of the sample. During filling, the obligatory care for avoiding any air bubbles was taken. The filled tube was placed in the polarimeter and the rotation was read out once the value remained constant.

8.2.2.5 Chromatographic Measurements

Chromatographic measurements in aqueous solutions were performed using high pressure liquid chromatography (Chromaster system, Hitachi) equipped with an evaporative light scattering detector (ELSD 90 LT-Low Temperature, VWR). Two polymeric SEC-columns (ABOA SuperOH, AppliChrom) were applied in series to enhance separation based on size exclusion. The composition of the mobile phase was kept constant throughout the 30-minute measurement time (isocratic application). The temperature of the oven and the detector were set to 293 K and 323 K, respectively. The flow rate was set to a constant value of 1 ml/min and the injection volume was 20 µl.

8.3 Results and Discussion

8.3.1 Discussion of Method and Calibration

8.3.1.1 Haze Method

The Haze Method is currently the most commonly used method for dextran analysis in the sugar industry. It is based on alcoholic precipitation and measures the resulting turbidity photometrically. Water-soluble polysaccharides such as dextran interact with water molecules via hydrogen bonds. The presence of ethanol consequently disrupts those interactions between dextran and water resulting in the desired turbidity to be measured. The solubility of polysaccharides is mainly influenced by their molecular structure and mass. This is expressed by a decrease of the solubility with an increase of molecular mass. The degree of alcoholic precipitation hence differs with molecular mass variation (Cui, 2005).

This sensitivity of the response signal to different dextran fractions leads to an unreliable dextran determination. Consequently, this method can be useful for specific sets of samples with limited variation of molecular size. In this case, the use of adequate material for the calibration curve is required. This is, however, impossible if the molecular size distribution of the samples to be measured is not given a priori. The choice of the calibration material is hence decisive for the final dextran determination. Either way, the actual problem of the preparation of the calibration curve cannot be overcome by that.

The amount of ethanol used to generate turbidity also influences the solubility and hence the precipitation process. According to the ICUMSA description, an equal aliquot of ethanol is used for the haze formation (50 % (v/v) ethanol). This setting aims at avoiding the precipitation of other non-sugars of lower molecular mass, such as pectin. However, this is the root cause for its limitation to mainly high molecular mass dextran. Besides, the Haze Method is not able to provide any information about the molecular composition of dextran present in a sample. Nevertheless, earlier results have shown that method combinations, such as the Haze and Roberts' Copper Method, can be useful to roughly identify characteristics of the molecular mass distribution (Abraham et al., 2016). This combination is, however, not suitable for industrial practice because the Roberts' Copper Method is both, cumbersome and chemically intensive.

As mentioned above, the Haze Method involves the removal of starch and proteins followed by filtration prior to the actual alcoholic precipitation. According to the ICUMSA method, this filtration step is omitted in establishing calibration curves. To evaluate the effect of this filtration step on the results of the Haze Method, the data depicted in Figure 8-1 (A) were generated. Solutions containing the corresponding amounts of dextran, trichloracetic acid and filter aid were analysed before and after filtration.

The differences in absorption illustrate a significant dextran loss during the filtration process. This is caused by adhesion to either or both, the inner filter pore surface and the surface of the filter aid particles. Figure 8-1 (B) illustrates the differences between establishing a calibration curve with or without the filtration step suitable to analyse 15 % (m/m) sucrose solutions. The data suggest that the omission of the filtration step during calibration can cause dramatic underestimation of dextran contents. It appears thus advisable to implement the respective change in the calibration procedure. The associated adhesive forces are inter alia related to size and geometry of contact areas. It is, however, beyond the scope of this work to evaluate the effect of the filtration step with respect to different filter materials or specificity to dextran molecular sizes. However, the Haze Method is nevertheless an established and commonly used method for the determination of dextran in sugar industry. Consequently, it served as a reference method for the two new approaches for dextran analysis discussed in this manuscript.

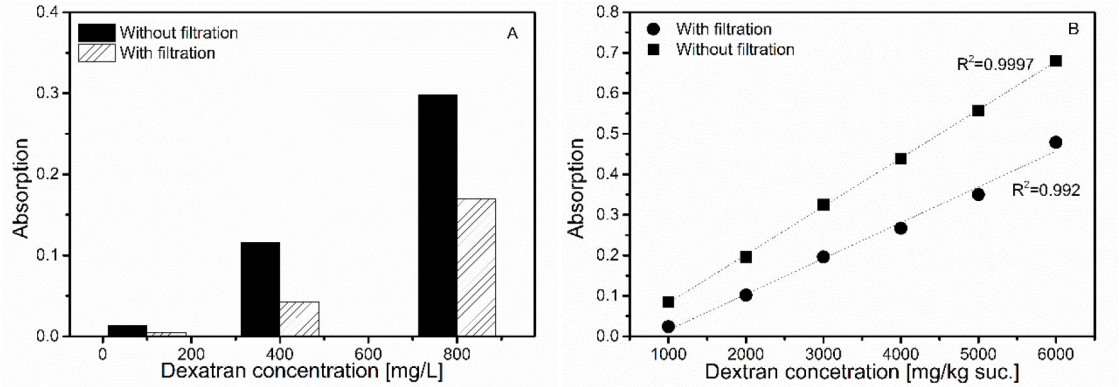

Figure 8-1 Fundamental analysis of the commonly used Haze Method. A) Filtration loss of middle molecular mass dextran solutions containing the corresponding amounts of trichloracetic acid and filter aid. B) Calibration curve with or without the filtration step for 15 % (m/m) sucrose solutions.

8.3.1.2 Enzymatic Method

The main principle of the Enzyme Method was first mentioned by Singleton et al. (Singleton et al., 2002). It is based on the change in optical rotation due to the complete enzymatic decomposition of dextran. It is generally assumed that high and low molecular mass dextran cause the same specific rotation rendering the signal independent of the molecular mass distribution. The decomposition products are assumed to be composed of oligosaccharides and isomaltose depending on the mode of enzyme action and the degree of branching of the substrate. These decomposition products have a lower specific rotation than dextran. The differences in optical rotation between the initial dextran containing solution and the solution containing decomposition products relates to the original dextran content. Prior to method related experiments at optimum conditions (explained in chapter 8.2.2.2), the enzyme reaction was continuously monitored in a different setting. To this end,

hydrolysis experiments in pure dextran solutions in the polarimeter tube were performed in order to monitor the change in optical rotation during an enzymatic decomposition over time.

The temperature of this hydrolysis experiment in the tube was set to 293 K due to the temperature limitation of the polarimeter. The change in optical rotation during an enzymatic hydrolysis seems to be almost identical for aqueous solutions of either high or low molecular mass dextran, shown in Figure 8-2 (A). This confirms the basic assumption made with respect to the independence of the response signal from molecular mass. This consequently means that the response signal is practically independent of molecular mass variation of the starting material in pure dextran solutions. This is a major advantage over the Haze Method potentially enabling the determination of total dextran contents. Furthermore, Figure 8-2 (A) reveals that after 20 minutes no change in optical rotation occurs when an adequate enzyme surplus is used at an incubation temperature of 293 K. Earlier work has shown that the presence of sucrose has an influence on the enzyme reaction indicating a possible non-competitive inhibition.

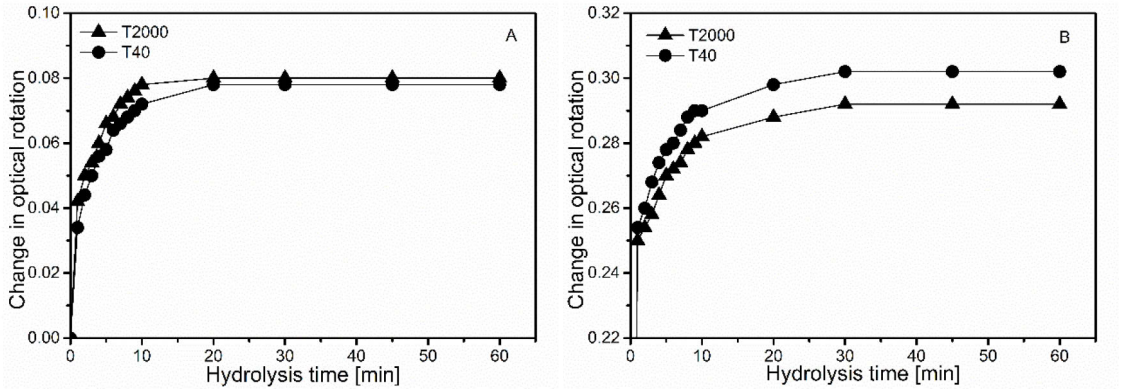

Figure 8-2 Fundamental analysis of the Enzymatic Method – Incubation of dextran in the polarimeter tube at 293 K. A) T2000 (triangles) and T40 (dots) dextran in binary solutions (no sucrose). B) T2000 (triangles) and T40 dextran (dots) in 15 % (m/m) sucrose solutions.

An enzyme-catalysed reaction is generally divided into three main steps comprising the formation of an enzyme-substrate-complex, the actual catalysed reaction and finally the product dissociation. The specific binding of the substrate to the active site of the enzyme is hence a prerequisite for an enzyme-catalysed reaction, which is either based on the key-lock-principle or on the induced fit model. In both cases, the final appearance of the active site of the enzyme is complementary to its docking site of the substrate (Bannwarth et al., 2007).

Conformational changes of the substrate due to the presence of other solution components may lead to changes of the enzyme-substrate-contacts. This potentially results in a modification of either the enzyme reaction time or of the kind and amount of decomposition products, which obviously affects the total change in optical rotation due to the enzymatic hydrolysis. In order to evaluate in how far the presence of sucrose affects the enzymatic decomposition of dextran, hydrolysis experiments containing 15 % (m/m) sucrose were additionally conducted. As Figure 8-2 (B) shows, these

experiments reveal similar results as those with pure dextran solutions (Figure 8-2 (A)). The data in Figure 8-2 (B) reveal that the complete decomposition of high and low molecular mass dextran in 15 % (m/m) sucrose solutions requires a slightly higher reaction time (30 minutes). In this case, relatively large changes in optical rotation occur. This is caused by not uncommon side effects during the decomposition process when using such extraordinary high enzyme contents. To reduce the effects of this side activity on the actual measurement, the calibration procedure was once again adjusted to the measuring procedure. This concerns the operation procedure as well as the sample composition. A constant sucrose level of 15 % (m/m) for the calibration as well as for the measurement procedure was hence fixed, which is supposed to always equally contribute to the difference in optical rotation.

In contrast to pure dextran solutions, the change in optical rotation for high and low molecular mass dextran due to an enzymatic decomposition seems to be slightly different in the presence of sucrose. The molecular mass of the substrate seems to influence the enzyme reaction pattern. Potential conformational changes of dextran molecules in solution need to be clarified in detail. To minimise possible effects of dextran's molecular size, the calibration curve was again prepared with middle molecular mass dextran just as for the other methods.

However, basic method analysis was performed using optimum conditions for the enzyme reaction in order to assure complete enzymatic decomposition. Therefore, an optimum temperature for the dextranase action of 328 K and an incubation time of 60 minutes were set. The enzyme reaction is hence assumed to occur even faster at this temperature. At this point, it is worth to mention that there is still some space to modify the enzyme reaction parameters in order to reduce the sample preparation time. It has to be further emphasised here that the change in optical rotation due to the enzymatic decomposition is relatively small. This necessitates very accurate handling and the usage of highly accurate circle polarimeters.

8.3.1.3 Membrane Method

The Membrane Method uses the well-established method of retention of macromolecules by mechanical means. The effect of the filtration on the permeate in relation to the feed solution is again evaluated using polarimetry. The main principle is quite similar to the Enzymatic Method, whereat the main difference is that there is a dextran separation step instead of an enzymatic decomposition. The separation of dextran via membrane filtration results in a difference in optical rotation between feed and permeate. This difference is subsequently used to calculate the dextran content of the feed solution. As discussed above, the response signal of the polarimeter is independent of dextran's molecular mass distribution.

The separation process via membrane filtration depends on the membrane and solution characteristics. The relationship between the membrane pore size and shape distribution and the

polymer conformation, more precisely the molecular appearance and hydrodynamic radius in solution, of the component to be separated is the key factor of the separation process.

Figure 8-3 (A) shows the effect of molecular size variation on the separation process in pure dextran solutions. The results indicate a separation efficiency of almost 100 % for high and middle molecular mass fractions in pure dextran solutions. In contrast, low molecular mass dextran shows a separation efficiency of approximately 60 to 70 % in pure dextran solutions.

It is well known that the monosaccharide sequence of specific polysaccharides is rather fixed. The glycosidic bonds are, however, flexible and enable the formation of different conformational structures implying flexible spatial arrangement of a polymer chain. In particular, the glyosidic bonds at the primary hydroxyl group are generally more flexible, indicating a higher flexibility of α-1,6-linkages in dextran molecules (Hänsel & Sticher, 2007). It is hence assumed that higher molecular mass dextran exhibits characteristics of an expandable random coil.

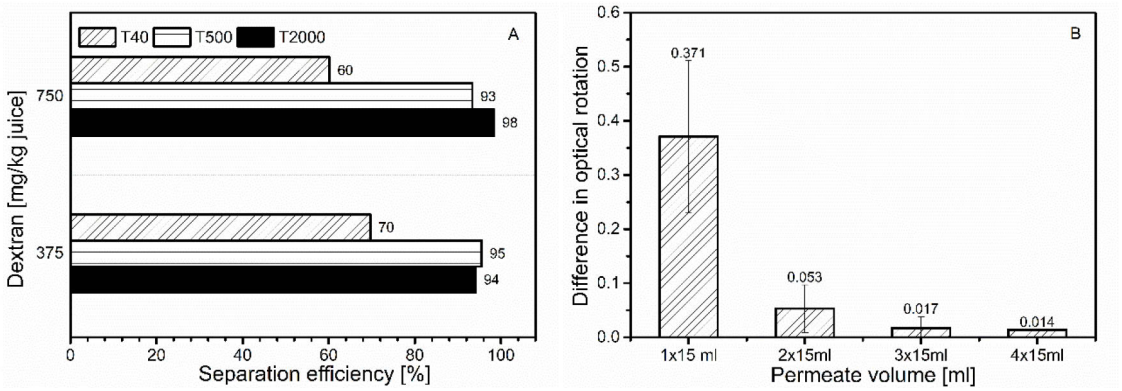

Figure 8-3 Fundamental analysis of the membrane process. A) Separation efficiency of dextran at varying molecular masses. B) Membrane filtration of 15 % (m/m) sucrose solutions investigated over a total permeate volume of 60 mL.

Other authors could also identify that there is a conformational transition of the polymer state depending on the molecular mass. This leads to a random coil conformation of high molecular mass dextran and an elongated rod-like conformation of low molecular mass molecules (Gasciolli et al., 1991).

This rod-like conformation of low molecular mass dextran and particularly the lower limit of this polydisperse fraction probably enables a partial ‘snake through’ effect. This term is supposed to describe the ability of linear molecules to pass the membrane pores despite the fact that membrane specification and molecular mass indicate otherwise.

It is well-known that both, the membrane as well as the polymer conformation, can be modified by the presence of other solution components. In this respect again, adhesion of major solution components to the inner surface of the membrane pores presumably occur, similar to the adhesion effects during the filtration step of the Haze Method. A higher inner surface of membranes yields

even higher susceptibility for adhesion. Even a minor retention of optical active sucrose in the membrane contributes to the difference in optical rotation between feed and permeate.

These sucrose retention effects were evaluated by analysing the differences in optical rotation between feed and permeate of pure sucrose solutions over a total permeate volume of 60 ml. Consecutive aliquots of 15 ml of the permeate were sampled. Each permeate sample was used to analyse the difference in optical rotation compared to the 15 % (m/m) sucrose feed solution. The results are shown in Figure 8-3 (B). There is a substantial difference in optical rotation between feed and the first aliquot of the permeate clearly indicating adhesion of sucrose to the membrane. The difference in optical rotation between feed and permeate aliquots subsequently decreases with the ongoing filtration process. To reduce this sucrose retention effect, the first aliquot of the permeate was discarded. Consequently, the second aliquot is used for the actual measurement throughout this work. An averaged difference in optical rotation of 0.05° was obtained for the second aliquot of the permeate of pure 15 % (m/m) sucrose solutions (see Figure 8-3 (B)). This value corresponds to the signal of about 700 mg dextran per kg sucrose. Using this aliquot hence admittedly still shows a slight difference in optical rotation caused by sucrose retention. An additional measure to eliminate these residual effects of sucrose retention is the inclusion of this membrane filtration step in the calibration procedure. This also incorporates a potential dependence of the sucrose retention on the existing dextran content. Samples were again standardised to a constant sucrose content of 15 % (m/m). Furthermore, middle molecular mass dextran was used to prepare the calibration curve, here, too.

8.3.1.4 Determination of Dextran at Varying Contents and Molecular Masses

After discussing the fundamentals of each analytical method, the following dextran determination data are supposed to proof their applicability to the analysis of different molecular mass dextran fractions in sucrose solutions. Figure 8-4 (A) shows the results for samples containing high molecular mass dextran in synthetic thin juices using the three different methods discussed above. All methods use calibration curves based on middle molecular mass dextran.

The Haze Method significantly overestimates high molecular mass dextran. This confirms the aforementioned sensitivity of this method to molecular mass variation due to differences in their solubility. The determination of low molecular mass dextran contents is shown in Figure 8-4 (B). The Haze Method apparently underestimates low molecular mass dextran, which is in complete agreement with previous reasoning. This commonly used analytical method hence appears of limited quality for the determination of total dextran contents when molecular mass variations are considered. The determination of high molecular mass dextran using the Enzymatic and the Membrane Method shows dextran contents very close to the actual values of the prepared solutions (Figure 8-4 (A)).

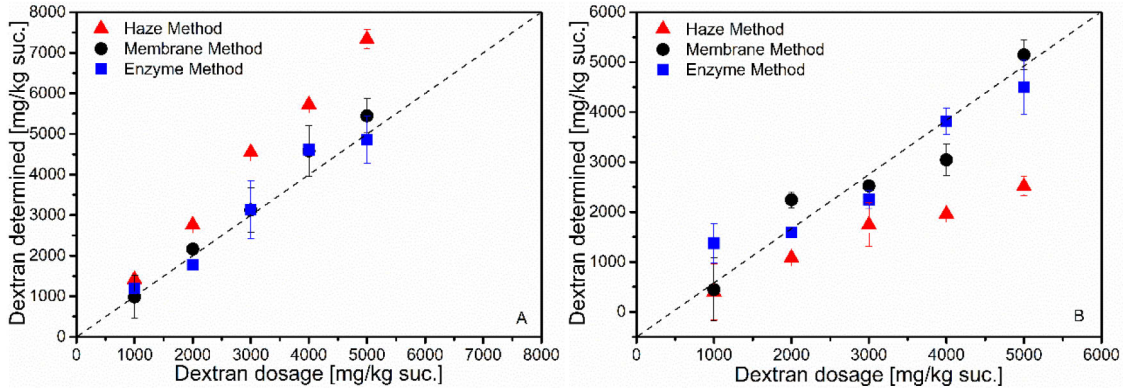

Figure 8-4 Determination of high and low molecular mass dextran fractions in 15 % (m/m) sucrose solutions. A) High molecular mass dextran. B) Low molecular mass dextran.

The determination of low molecular mass dextran contents (Figure 8-4 (B)) shows also an improved detection for both methods compared to the Haze Method. Both methods yield values close to the actual contents, but the data indicate less accuracy as found for high molecular mass dextran. The good results obtained by the Enzymatic Method are somewhat surprising because it appears to be influenced not only by the effects of conformation of enzyme and dextran but also operates at the lower end of polarimetric measurement range. To further improve on these promising results, a more accurate measurement of the optical rotation could reduce the residual deviations.

The black dots in Figure 8-4 (B) represent the determination of low molecular mass dextran contents in synthetic thin juices using the Membrane Method. The data obtained reveal higher dextran contents than could be expected from the analysis of the separation efficiency in binary dextran solutions (see Figure 8-3 (A)). In ternary solutions, this can be caused by either a higher sucrose or a higher dextran retention. To better understand such effects, chromatographic measurements of the feed and permeate of membrane-filtered dextran-loaded solutions with and without sucrose were performed. Figure 8-5 (A) shows the chromatograms for feed and permeate of binary solutions at two different dextran contents. The data confirm the above mentioned incomplete separation of low molecular mass dextran in binary solutions. This is indicated by the presence of a dextran peak in the chromatograms of the permeate depicted as a dashed line.

Other solution components can alter the membrane pore structure as well as the polymer conformation due to specific interactions. The chromatographic analysis of synthetic thin juices containing additionally 15 % (m/m) sucrose is illustrated in Figure 8-5 (B). In particular, the zoom to the dextran peak is shown in Figure 8-5 (C). This reveals a complete retention of low molecular mass dextran present in the feed, dashed curve coincides with the baseline. This confirms an improved separation efficiency of the low molecular mass dextran fraction due to the presence of sucrose. This is most likely caused by a conformational difference between the rod-like dextran structure in aqueous solution and a more bulky spherical structure in sucrose solution due to specific interactions between sucrose and dextran.

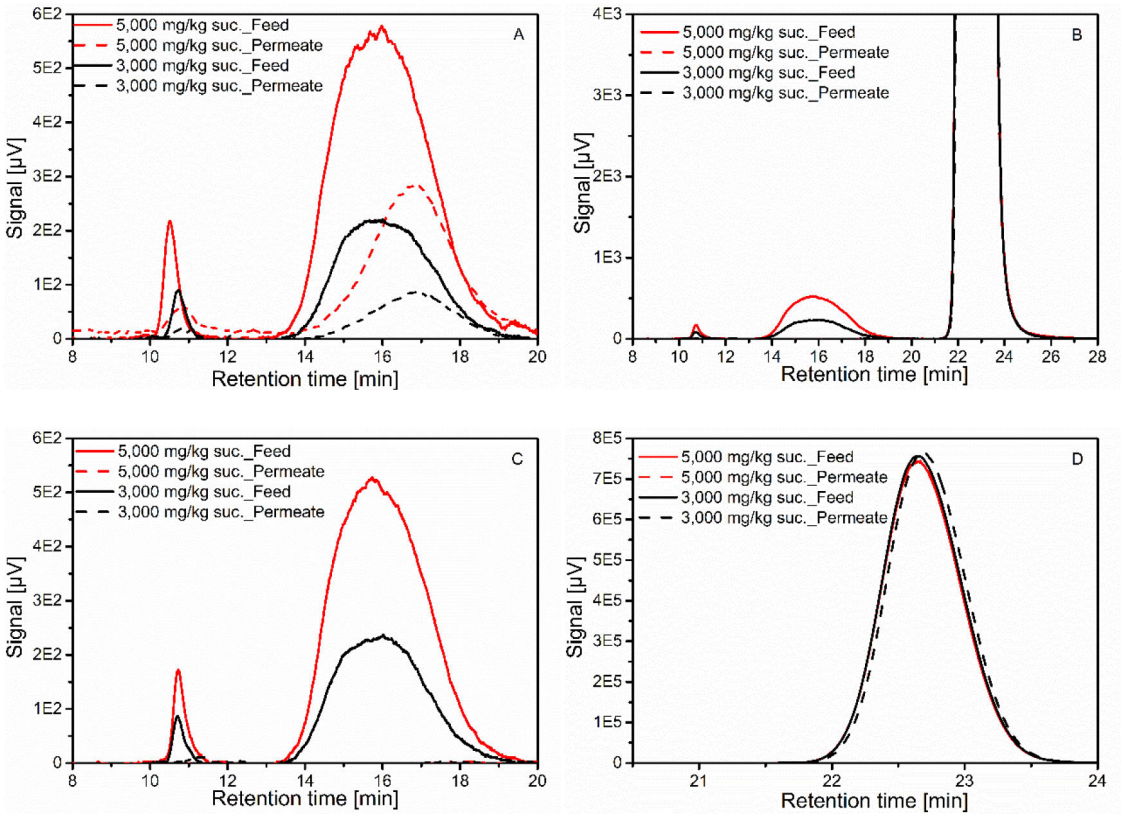

Figure 8-5 Chromatographic measurements of feed and permeate obtained from membrane filtration. A) Separation of low molecular mass dextran in binary solutions. B) Separation of low molecular mass dextran in the presence of 15 % (m/m) sucrose. C) Zoom to low molecular mass dextran peak of B. D) Zoom to sucrose peak of B. Red continuous line (feed solution) and red dotted line (permeate solution) containing 5000 mg dextran/kg sucrose; black continuous line (feed solution) and black dotted line (permeate solution) containing 3000 mg dextran/kg sucrose.

These possible coil formation effects induced by the presence of other carbohydrates may hamper or completely suppress the snake through of low molecular mass dextran. As pointed out earlier, attention should further be given to possible changes of the membrane characteristics. This concerns the deposition of sucrose molecules on the membrane surface and/or the adhesion of sucrose to the inner surface of the membrane pores. Possible occurrence of narrowed or even blocked pores, certainly impacts the membrane permeability. Even if the initial heterogeneous membrane pore structure is not affected, accumulation of dextran and possibly sucrose on the membrane surface could occur. Such deposition layer commonly affects the filtration process itself.

Considering the zoom to the sucrose peaks shown in Figure 8-5 (D), no significant change of the sucrose content between the feed and the permeate could be identified. This confirms that effects of sucrose retention can be counteracted by discarding the first aliquot of the permeate. In this manuscript, changes of the polymer conformations induced by sucrose were suspected to play a role in both, the modification of the kinetics of enzyme reactions for high and low molecular mass dextran and membrane retention of low molecular mass dextran. On the one hand, it appears important to verify or rather understand the assumption of this induced conformational change to

develop robust analytical methods. On the other hand, more detailed knowledge on this phenomenon may enable deliberate coil development to better understand membrane separation processes in general. Nevertheless, both, the Enzymatic and Membrane Method have proven to be superior over the Haze Method for the determination of dextran contents considering different molecular mass fractions. The reliable determination of a broader molecular size range is a prerequisite to any advanced dextran analysis.

8.4 Conclusion

Two new approaches for the determination of dextran contents, the Enzymatic and the Membrane Method, were developed and compared to the commonly used Haze Method. Both methods are based on determining differences in optical rotation and hence require highly sensitive circle polarimeters. The assumption that polarimetry is basically independent of the molecular size distribution of dextran was verified. It follows that these methods are suitable to quantify the full molecular size spectrum of dextran. The prototypes of the new methods indicate to be suited for industrial practice since type of equipment, conduction time and chemical consumption are within reasonable ranges. Detailed evaluation of these methods revealed that the incorporation of all sample preparation steps in the procedure to establish calibration curves is generally beneficial to avoid artefacts. Specifically, the methods presented suffered from adhesion of solution components to filter or membrane materials.

Besides, operating at fixed sucrose contents throughout calibration and analysis increased accuracy since methods based on polarimetry are sensitive to variations in sucrose contents. The presence of sucrose is furthermore suspected to induce conformational changes of dissolved dextran. The products resulting from complete enzyme catalysed hydrolysis of dextran appear to vary between high and low molecular mass dextran in the presence of sucrose. This difference could not be observed in aqueous dextran solutions. The retention of smaller initially linear dextran molecules by membranes appeared also to be affected by the presence of sucrose. The resulting entanglement of the smaller chain molecules significantly improved the separation efficiency. This improved retention, from 60 % to practically 100 %, was verified by chromatographic measurements.

The data gathered reveal that the two new methods to determine dextran contents are superior over the Haze Method. This is particularly true when considering that dextran occurs with significant molecular mass variations. The results mark a promising step towards a reliable and practical method that enables a more targeted mitigation of dextran contaminations. The ongoing work is further aiming at the characterisation of the molecular mass distribution of the dextran present in a sample. For this endeavour, the application of multiple membrane separations and analysis of the kinetic of enzymatic decomposition appear to be useful departure points.

References

Abdel-Rahman, E. (2007). Investigation on the influence of dextran during beet sugar production with special focus on crystal growth and morphology (PhD), Berlin.

Abraham, K., Hagen, S., Schlumbach, K., Rohde, A., & Flöter, E. (2016). Dextranase application in sucrose solutions - towards a better understanding. *International Sugar Journal*, 604–610.

Bannwarth, H., Kremer, B. P., & Schulz, A. (2007). *Basiswissen Physik, Chemie und Biochemie*. Heidelberg: Springer-Verlag.

Chen, J. C., & Chou, C. C. (1993). Cane Sugar Handbook: A Manual for Cane Sugar Manufacturers and Their Chemists (12th ed.). New York: John Wiley & Sons.

Cui, S. W. (2005). Food Carbohydrates: Chemistry, Physical Properties and Applications. Boca Raton: Taylor & Francis.

Day, D. F., & Sarkar, D. (1986). Methods of Analysis for Dextran in Sugar Molasses and Juice. *Proc. Int. Soc. Sugar Cane Technol*, 748–754.

Du Boil, P. M. (2000). An Enzymic-HPAEC Protocol for the Analysis of Polysaccharides in Sugarcane Products - Dextran and Sarkaran. *Proc S Afr Sug Technol Ass*, *74*, 317–327.

Gasciolli, V., Choplin, L., Paul, F., & Monsan, P. (1991). Viscous properties and molecular characterization of enzymatically size-controlled oligodextrans in aqueous solutions. *Journal of Biotechnology*, *19*, 192–202. https://doi.org/10.1016/0168-1656(91)90058-4

Hänsel, R., & Sticher, O. (2007). *Pharmakognosie - Phytopharmazie* (8. Auflage). Heidelberg: Springer.

Hein, W., Bauer, H., & Emertorfer, F. (2012). Processing of long-stored sugar beet. *Sugar Industry*, *137*(1), 25–32.

ICUMSA (Ed.). (2011). *ICUMSA Method Book*. Berlin: Dr. Albert Bartens KG.

Promraksa, A. (2008). Reduction of Dextran Contamination in Raw Sugar Production (PhD). Suranaree University of Technology, Nakhon Ratchasima.

Singleton, V., Horn, J., Bucke, C., & Adlard, M. (2002). A New Polarimetric Method for the Analysis of Dextran and Sucrose. *American Society of Sugar Cane Technologists*. (Vol. 22), 112–119.

9 Membrane Characterisation for Fractionated Dextran Analysis in Sugar Industry

Abraham, K. [ab]; Kunst, S. [a]; Flöter, E. [a]

[a] TU Berlin, Department of Food Process Engineering, Seestraße 13, 13353 Berlin, Germany

[b] SternEnzym, Kurt-Fischer-Str. 55, 22926 Ahrensburg, Germany

Originally published in the Journal of Food Analytical Methods (2019).

https://doi.org/10.1007/s12161-019-01441-7

Abstract

The separation characteristics of two polyethersulfone membranes (molecular weight cut-off (MWCO) specification of 4 kDa and 10 kDa) for the retention of different dextran fractions (T2000, T40, T10) from aqueous solutions were systematically investigated, aiming at implementing them as a preparatory step for dextran analysis in sugar industry practice. Ultrafiltration is used to cause differences in optical rotation due to mechanical separation of dextran from aqueous solutions. The membrane separation performance was evaluated using polarimetry and size exclusion chromatography. It was found that the presence of sucrose leads to dramatically improved separation efficiencies for both membrane settings. Specific cut-off values for the separation of dextran from aqueous sucrose solutions have been determined, 10 kDa and 50 kDa for the membranes with a MWCO specification of 4 kDa and 10 kDa, respectively. The data indicate that the basic membrane setting (MWCO of 4 kDa) enables the complete separation and therefore the analytical quantification of the whole molecular mass spectrum relevant for sugar industry. The combination of both membranes, furthermore, indicates that it is suited for the differentiation between a high and a low molecular mass dextran fraction. The application of this new approach for the determination of dextran with varying molecular masses at various contents in synthetic thin juices as well as in real sugar beet raw juices indicates promising prospects.

9.1 Introduction

The occurrence of polysaccharides in sugar cane and beet juices can cause diverse negative effects during sugar manufacture. These polysaccharides can either originate from cell plant material or from microbial activity. Microbial polysaccharides are in this case mainly related to dextran formed by enzymatic activity of lactic acid bacteria, more specifically by *Leuconostoc mesenteroides* species. The water soluble homogenous polysaccharides are composed of glucose units, which are mainly linked via α-(1→6) glycosidic linkages (van der Poel et al., 1998). Branching points can additionally occur. It is known that sugar industry-relevant species produce dextran containing up to 5 % branching points via α-(1→3) glycosidic linkages, which cause deviations from a strictly uniform structure (Promraksa, 2008).

Dextran is a prevailing topic in the sugar cane industry due to the abundant occurrence of mesophilic bacteria in the area, where sugar cane is cultivated. Dextran formation can nevertheless occur in sugar beet juices, mainly when beet cells are exposed to freeze-thaw cycles. Naturally-produced dextran is generally of relatively high average molecular mass and high polydispersity. This refers to the potential occurrence of molecular masses in the range of 15 kDa to 2,000 kDa (Chen & Chou, 1993). Aquino et al. further identified two major groups, a lower and a higher fraction possessing molecular masses in the 10^3 kDa and 10 kDa range, respectively (Aquino & Franco, 2009).

The co-extraction of dextran along with the sucrose can lead to various adverse effects during processing. There is general agreement that high molecular mass dextran is mainly responsible for a viscosity increase negatively affecting the filtration, evaporation as well as the crystallisation rate (Chen & Chou, 1993). On the basis of current knowledge, dextran can also modify the shape and size of precipitated particles during juice purification (Wojtczak et al., 2015). Besides, sucrose crystal size and shape distributions are known to be affected during crystallisation (Abdel-Rahman, 2007). The main mechanism is, however, not yet understood in detail. Anyhow, there is certainty about the involvement of both, high as well as low molecular mass dextran fractions in such effects. Nevertheless, there is reason to assume that the specific process effects relate to defined molecular masses. These dextran-induced process effects are usually mitigated by enzymatic decomposition of dextran.

In order to assess and also to reduce these process effects in a controlled manner, the quantification of preferably the whole molecular mass range and additionally the identification of the two main dextran fractions is a necessary prerequisite. This is especially relevant since targeted cost-intensive enzyme applications not only depend on the actual dextran content, but also on the initial molecular mass distribution. However, relatively low dextran contents and the just mentioned broad molecular mass distribution in the initial raw juices generally impede the analytical initiatives of quantification and identification (Day & Sarkar, 1986). So far, existing methods for dextran analysis in sugar industry practice do not satisfy these two demands.

Recently published work discusses existing methods in detail and in particular introduces the prototype of a new method based on optical rotation, called Membrane Method (Abraham & Flöter, 2018). It uses the separation of dextran via membrane filtration as a preparatory step for dextran analysis. The difference in optical rotation of the feed and the permeate is used to determine the dextran content. Optical rotation as a response signal is particularly promising due to its independence of molecular mass variation, equally detecting high and low molecular mass dextran. Effects of other optically active components present in juices are considered as background noise because these are assumed to not be removed during the filtration step. Furthermore, the sole application of mechanical separation ensures that no polarisation effects due to decomposition falsify the results.

A benchmark study made particularly clear that the current standard Haze Method is, as is well-known, mainly restricted to high molecular mass dextran. The new Membrane Method proved to be better suited for dextran analysis of the complete molecular mass spectrum in sucrose solutions with regard to concentration and relevant molecular masses (Abraham & Flöter, 2018).

Interestingly, the experimental observations indicated a 'snake through' effect of dextran molecules in binary aqueous solutions clearly above the manufacturer's specification of the membrane. However, an advantageously higher separation efficiency could be observed due to the presence of sucrose. The achieved complete separation of low molecular mass fractions in sucrose solutions laid the foundation of determining total dextran contents. Thereby, the whole molecular mass spectrum relevant for dextran-related effects during sugar manufacture is covered (Abraham & Flöter, 2018).

The separation of dextran by mechanical means is theoretically based on molecular sieving requiring an ultrafiltration system. Ultrafiltration membranes are generally characterised by the so-called molecular weight cut-off (MWCO). This term concerns the molecular mass at which 90 % of a monodisperse globular marker protein is rejected. It should be emphasized here that there are no general valid definitions for the determination of this parameter, resulting in rather vague and often inconsistent values. The separation performance of macromolecules, such as dextran, from aqueous solutions is more precisely determined by the relation of the membrane pore size to the radius of the molecule in solution. The rather heterogeneous membrane pore structure as well as the polymer's molecular conformation and its chain mobility in solution are hence the key factors for the retention of certain macromolecules (Baker, 2004).

The radius of a macromolecule, such as dextran, (often described as the radius of gyration) is generally determined by its molecular structure, which is in turn described by its chemical composition, its configuration and its conformation. The monosaccharide sequence and their type of linkages are relatively fixed and do not change unless chemical bonds are broken. The only feature relevant for the membrane filtration experiments in this study is hence the conformation of

dextran in solution. It arises from the conformation of the individual monosaccharides integrated in the chain (e.g. chair or boat conformation) and their type of linkages. The possibility of conformational transitions of single monosaccharides as well as the rotation of single bonds in-between these monosaccharides decisively contribute to the overall conformation of a polymer (Lee et al., 2004). This generally results in the formation of rod-like, compact sphere-like or random coil structures (Pasch & Trathnigg, 1998).

When dissolved in water, linear molecules have hence a higher likelihood to pass through the membrane pores than globular coil shaped molecules, such as proteins. The latter is, however, generally used for the determination of the MWCO for the characterisation of ultrafiltration membranes (Baker, 2004). Polysaccharides containing glycosidic linkages at the primary hydroxyl group play a very specific role due to the presence of an additional rotation angle. Two glucose units linked via an α-(1→6) bond can hence occur in various conformations characterised by three rotation angles, as illustrated in Figure 9-1.

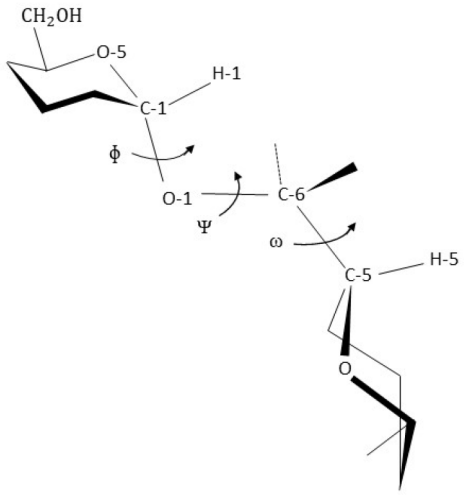

Figure 9-1 Two α-1,6-linked glucose units with three different rotation angles (Tvaroska et al., 1978).

This unusually flexible backbone of dextran enables a large number of conformations, which can easily be transformed into each other (Lee et al., 2004). It is assumed and confirmed by several authors that high molecular mass dextran exhibits characteristics of an expandable random coil, which generally allows the separation from aqueous solution by molecular sieving (Hirata et al., 2003).

Generally speaking, an impairment of the measurement due to the potential separation of other optically active polysaccharides present in real sugar raw juices by the membrane is assumed to be low. This presumption is based on the fact that the most common polysaccharides (e.g. pectin, starch and pullulan) in sugar beet and cane juices do not show coil characteristics in solution. Due to the generally acknowledged expanded linear structure of most of these macromolecules, low

efficiency of the separation via ultrafiltration is expected (Belitz et al., 2008). Dextran, however, has an exceptional molecular conformation making it prone to coiling, differentiating it from other major polysaccharides contained in raw juices. Nevertheless, a detailed understanding of the separation process of the different molecular mass dextran fractions is a prerequisite to identify membranes suitable for the application in quantitative dextran analysis including fractionation.
This study is hence aiming at investigating the separation of dextran from aqueous solutions using two different polyethersulfone membranes. The feasibility of fractionating different dextran molecular mass fractions by membrane application was the focus of this research.
Size exclusion chromatography and highly accurate circle polarimetry were used to evaluate the respective separation processes in binary aqueous and in aqueous sucrose solutions. Small angle x-ray scattering (SAXS) measurements were further used to respectively analyse the conformation of the different dextran fractions in both solvents supporting a detailed understanding of the underlying separation phenomena. Finally, the general applicability of the very method was evaluated by determining dextran contents of various molecular masses in different juices.

9.2 Material and Methods

9.2.1 Materials

Dextran fractions with different molecular masses were dissolved in binary aqueous and aqueous sucrose solutions. These were used as feed solutions for the membrane filtration experiments. Dextran fractions with a high and a low mass-average molecular mass of 2,000 kDa (Sigma-Aldrich, dextran T2000 with a molecular mass distribution of 1,500,00 to 2,800,000 Da) and 40 kDa (Carl Roth, dextran 40) were used. According to the manufacturer's specifications, the high and the low molecular mass dextran fraction possesses a very similar specific optical rotation of +199° and +195° to + 201°, respectively. Further manufacturer's information are given for the low molecular mass dextran fraction. Dextran T40 is characterised by a mass-average molecular mass of 40.5 kDa and a number-average molecular mass of 21.4 kDa. The polydispersity index, the ratio of these two terms, is 1.894. Furthermore, the molecular mass distribution, according to the manufacturer, appears to vary in a way that up to 10 % of molecules with molecular masses above 100 kDa as well as less than 10 kDa are respectively present. This is why a dextran fraction with an even lower mass-average molecular mass (T10) of 9.4 kDa and a number-average molecular mass of 5.5 kDa (polydispersity of 1.705) was additionally included in this study. All dextran fractions originate from the lactic acid bacteria *L. Mesenteroides* strain B512. Refined sucrose (Nordzucker, extra-white sugar) was used to investigate the influence of sucrose on the separation process via membrane filtration in order to stepwise approach more realistic conditions. Furthermore, a realistic sugar beet raw juice was further subject to this study, which was obtained

from a German sugar beet factory and immediately frozen after sampling. The frozen state was continuously maintained until the actual experimental execution took place.

9.2.2 Methods

9.2.2.1 Membrane Filtration

Membrane filtration was performed in static manner (dead-end membrane filtration) using a modified Autofilt filter apparatus (Schmidt & Haensch) equipped with the respective polyethersulfone membranes. This most widely used material for ultrafiltration systems are composed of polysulfone or polyethersulfone giving membranes a hydrophilic character and high pH and temperature stability. Hence, polyethersulfone membranes with two different MWCOs were used, 4 kDa (Microdyn-Nadir, UH 004) and 10 kDa (Microdyn-Nadir, UP010). Application of a single membrane to determine total dextran contents was already reported elsewhere (Abraham & Flöter, 2018). A transmembrane pressure of 0.3 MPa was set and the membrane filtration was performed at ambient temperature. The feed and the permeate obtained from the membrane separation were sampled and analysed using highly accurate circle polarimetry and size exclusion chromatography. A first aliquot of the permeate of 10 ml was discarded before the actual sample of 20 ml was collected. A sample volume of 20 ml is necessary to allow both, adequate performance of polarimetric and chromatographic analysis. Comparisons of these two analyses were used to evaluate the membrane separation process. The analysis of the feed and the permeate samples were performed in direct succession in order to ensure same conditions. The subsequent calculation of the separation efficiencies and the determination of molecular masses were used to actually characterise the respective membrane separation. The separation efficiency was calculated according to the following equation, whereas c_P [g/100g] and c_F [g/100g] refer to the dextran concentration of the permeate and the feed, respectively (Hamid et al., 2011).

$$Separation\ efficiency\ [\%] = \left(1 - \frac{c_P}{c_F}\right) \times 100 \tag{9-1}$$

The actual principle of the Membrane Method for the determination of dextran in aqueous sucrose solutions and raw juices builds on the difference in optical rotation caused by the separation of dextran from aqueous solutions by membrane filtration. The difference in optical rotation between the feed and the permeate enables the determination of dextran retained by the membrane. The calibration procedure was completely adjusted to the actual measuring procedure. In particular, the sucrose levels for the calibration as well as the measurement procedure were kept identical in order to eliminate any contributions of sucrose on the membrane performance. Dextran with a mass-average molecular mass of 500 kDa (Carl Roth, dextran 500) was used for calibration purposes. This dextran fraction has the broadest molecular mass spectrum, covering the most common occurring mass fractions of high and low molecular mass dextran. The dextran contents were

deducted from the calibration curve, covering the differences in optical rotation for varying dextran contents in 15 % (m/m) sucrose solutions, by linear interpolation. Further details on calibration and basic method procedure are described elsewhere (Abraham & Flöter, 2018). The analysis of realistic raw juices further requires a preparatory clarification step, which was performed according to the official standard method, ICUMSA GS8-2 (ICUMSA, 2011). In general, every analysis was performed in duplicate.

9.2.3 Analytics

9.2.3.1 Chromatographic Measurement

Chromatographic measurements in aqueous solutions were performed using high pressure liquid chromatography (Chromaster system, Hitachi) equipped with an evaporative light scattering detector (ELSD 90 LT-Low Temperature, VWR). Two polymeric size exclusion columns with a separation range of 0.1 kDa to 70 kDa (ABOA SuperOH-P-250, AppliChrom) and 2.5 kDa to 1,000 kDa (ABOA SuperOH-P-350, AppliChrom) were applied in series to enhance separation based on size exclusion. An isocratic method with distilled water as the mobile phase was used. The flow rate was set to a constant value of 1 ml/min and a sample volume of 20 µl was injected. The temperature of the oven and the detector were set to 293 K and 323 K, respectively. Calibration for qualitative molecular mass analysis was performed using pullulan standards of very low polydispersity (Pulkit 08, Polymer Standard Service). For the calibration curve for purely quantitative determination of the dextran concentrations in the feed and in the permeate, the area for various concentrations of the respective dextran fractions was evaluated and plotted. The dextran concentration was deducted from this curve by linear interpolation. The chromatograms obtained were subsequently quantitatively and qualitatively analysed using the Peakfit software 4.12.

9.2.3.2 Polarimetric Measurement

A high-performance circle polarimeter (Polartronic MH8, Schmidt & Haensch) with a resolution of 0.001° was used for determining the optical rotation of a sample at a wavelength of 589 nm. The measuring temperature was set to 293 ± 1 K. A glass tube with a center cup filling of 200 mm length and a filling volume of 12 ml was used for all measurements. The glass tube needs to be assembled carefully in a way that the optical rotation of the empty tube is not higher than 0.002°. Prior to the analysis, the surplus volume of the collected permeate was used to rinse the tube. Values for the optical rotation were read out once the value remained constant.

9.2.3.3 Small Angle X-ray Scattering Measurement

Small angle x-ray scattering measurements (SAXS) were performed at the Federal Institute for Materials Research and Testing (A. Thuenemann, BAM-Bundesanstalt für Materialforschung und -prüfung, Unter den Eichen 87, 12205 Berlin, Germany). The different dextran fractions (T2000, T40 and T10) at a mass percentage of 2 % (m/m) were analysed in both, binary aqueous and aqueous sucrose solutions. Measurements were performed in a flow through capillary with a Kratky-type instrument (SAXSess from Anton Paar, Austria) at 294 $\pm$ 1 K. A sample-to-detector distance of 0.309 m was set, which allows to adequately investigate dispersions with low scattering intensities (Bergmann et al., 2000). The measured intensity was converted to absolute scale according to Orthaber et al. (Orthaber et al., 2000). The so-called scattering vector is defined as $q = 4\pi n/\lambda sin\theta$, whereas Θ and λ represent the scattering angle and the wavelength of radiation ($\lambda = 0.154\ nm$), respectively. Deconvolution (slit length desmearing) of the SAXS curves was performed with the SAXS-Quant software. SASfit software was further used for curve fitting (Breßler et al., 2015).

9.3 Results and Discussion

9.3.1 Membrane Separation of Different Single Dextran Fractions in Binary Aqueous Solutions

Dextran fractions with relevant molecular masses as found in sugar cane and beet industry are in this study represented by fractions with mass-average molecular masses of 2,000 kDa and 40 kDa. According to manufacturer's data, a relatively high proportion of dextran with an even lower molecular mass occurs within the T40-fraction. Therefore, experiments with a dextran fraction with a mass-average molecular mass of 10 kDa were also included in this study. Figure 9-2 (A) inter alia shows size exclusion chromatograms of the different dextran fractions at a mass percentage of 0.075 % (m/m) in aqueous solutions, shown as continuous lines. This concentration represents realistic dextran contents in contaminated sugar beet and cane raw juices. The above-mentioned fractions were used as a feed solution for the respective membrane separations. The secondary x-axis depicted in Figure 9-2 relates the molecular masses to the respective retention times. Size exclusion chromatography usually elutes large molecules first. The chromatograms of the feed solutions clearly indicate relatively high polydispersities for all fractions. The polydispersity increases with higher average molecular masses. The high molecular mass dextran fraction shows therefore relatively broad and distinct overlapping peaks, while the analysis of the dextran fractions of lower molecular masses indicates a monomodal but broad distribution. These dextran fractions successively elute. There are, however, some overlapping areas indicating the presence of identical molecular sizes within the respective fractions. The overlap found for the T40- and T10-fraction is in accordance with manufacturer's information.

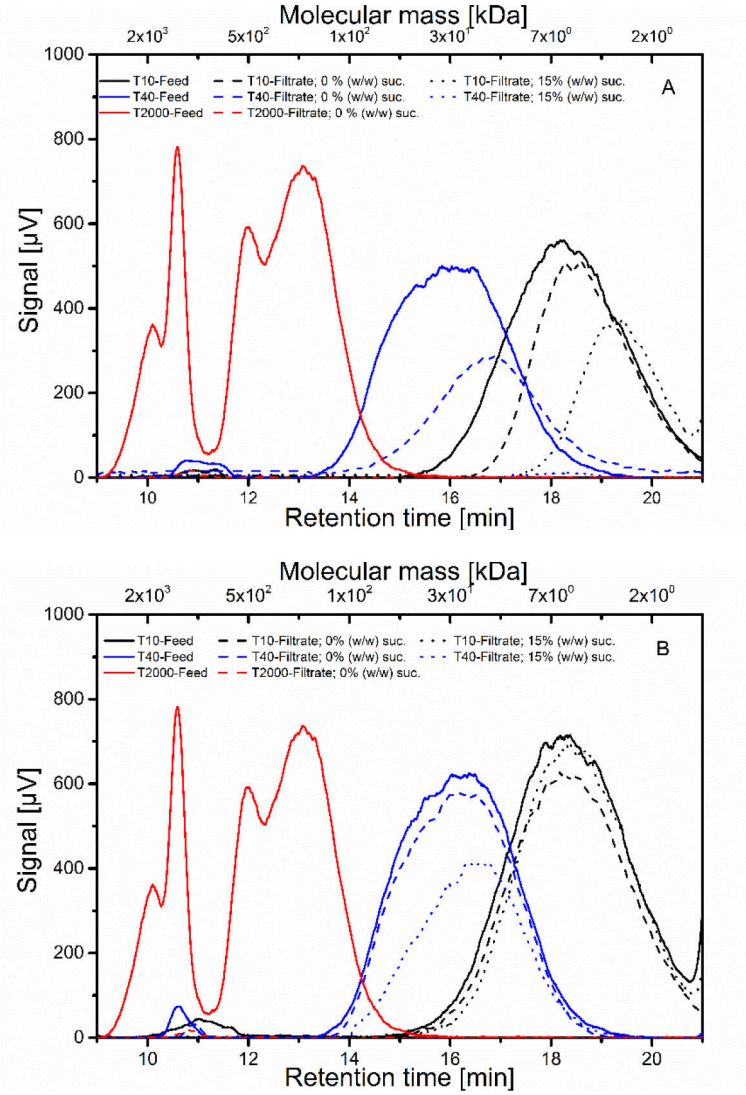

Figure 9-2 Chromatograms of the feed (continuous line) and the permeate solutions obtained from membrane separations of different dextran fractions (T2000, T40 and T10 - red, blue and black line, respectively) in binary aqueous (dashed lines) and in 15 % (m/m) aqueous sucrose solutions (dotted lines). A) Membrane separation via the MWCO of 4 kDa. B) Membrane separation via the MWCO of 10 kDa.

In order to obtain detailed knowledge about the membrane and polymer characteristics, the membrane process was firstly investigated in binary aqueous solutions solely consisting of dextran and distilled water using the above mentioned membranes with cut-offs of 4 kDa and 10 kDa. The chromatograms of the corresponding permeates of binary aqueous solutions obtained from the membrane separations are shown as dashed lines in Figure 9-2 (A) and (B).

It is obvious that there is a discrepancy between the cut-off specification and the actual separation limit for the respective dextran fractions. This is indicated by the slip-through of molecular masses clearly above the cut-off specification. The separation efficiencies of the two different membranes calculated from chromatographic as well as polarimetric analysis are additionally and comparatively given in Figure 9-3 (A) and (B), 4 kDa and 10 kDa, respectively. The higher the separation efficiency, the better was the actual separation from aqueous solutions of the respective

molecular mass fractions. Both analytical methods reveal quite similar separation efficiencies and indicate a separation of about 60 % for the low molecular mass dextran fraction (T40) using the membrane with a cut-off of 4 kDa. In contrast, practically no separation of T40-dextran was detectable for the membrane filtration using the higher cut-off of 10 kDa. An incomplete separation of the T40-fraction is obvious. This fact is, however, interesting considering the expectation of a material with a molecular weight specification of 40 kDa.

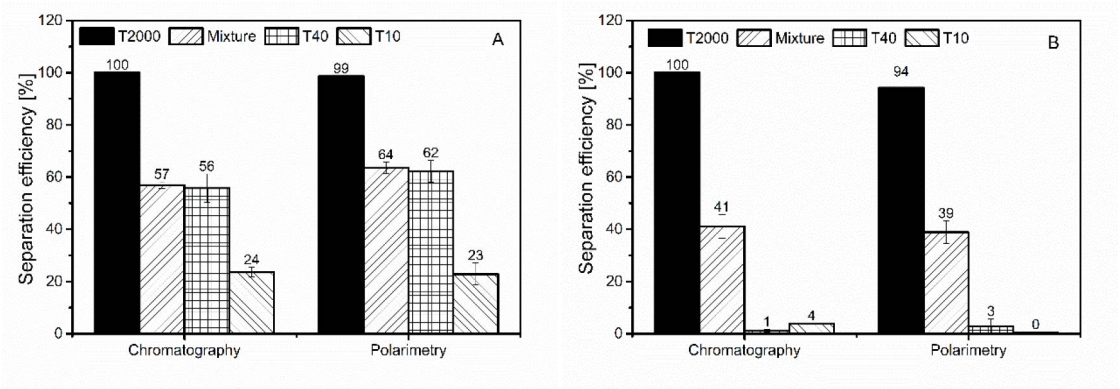

Figure 9-3 Comparative graphs of the separation efficiencies [%] of different dextran fractions in binary aqueous solutions calculated from chromatographic and polarimetric measurements. A) Membrane separation via the MWCO of 4 kDa. B) Membrane separation via the MWCO of 10 kDa.

To further elucidate the effect of the relatively high polydispersity of T40, another dextran fraction with lower molecular masses was included. The individual data of the T10-fraction (lower end fraction of the T40-dextran fraction) - very low separation efficiencies of roughly 25 % and 0 % using the membranes with the cut-offs of 4 kDa and 10 kDa, respectively - corroborate this view. This indicates that especially dextran of low molecular mass contribute to the incomplete separation of the T40-fraction. The partial or rather complete slip-through of these low molecular mass dextran fractions using these two types of membranes is especially surprising, since membrane cut-offs clearly suggest otherwise. The partial slip-through of dextran with average molecular masses clearly above the cut-off specification confirms the uncertainty of using the cut-off as a selection criterion for the separation of dextran molecules from aqueous solutions. This supports the necessity of separately assessing the suitability of membranes for the separation of certain macromolecules and in particular of dextran.

It is well-known that the membrane separation process is not only a function of the actual molecular mass distribution, but especially of conformational structure in solution. The retention of specific macromolecules is mainly determined by the relation of molecular radius to membrane pore size. The presence of α-(1→6) glycosidic linkages in dextran's main chain leads to an unusually flexible backbone most likely enabling the stretching of the original conformation of an expandable random coil into a rather expanded linear structure. Several authors already analysed the molecular structure of different dextran fractions with various molecular masses in diverse solvents. Hirata et al, for

instance, clearly concluded a random coil structure of T40- and T70-dextran in binary aqueous solutions and also postulated a more compact structure in solvents in which dextran is less soluble (Hirata et al., 2003). Gasciolli et al identified a random coil conformation of high molecular mass dextran and an elongated rod-like conformation of low molecular mass molecules. This, however, relates to molecules of less than an average-number molecular mass of 2 kDa obtained from viscosity measurements (Gasciolli et al., 1991). However, viscosity depends on several characteristics of the polymer as well as on the nature of the solvent, which makes the identification of this conformational transition rather inaccurate.

In order to clarify whether this conformational transition is relevant for the molecules studied here, small angle x-ray scattering (SAXS) measurements were performed (Thuenemann, BAM, Berlin, Germany). Therefore, dextran concentrations were elevated to a mass percentage of 2 % (m/m) to obtain strong and reliable signals. The scattering curve for T10-dextran and for T2000- and T40-dextran, consistently indicate typical characteristics of a polymer coil structure in binary aqueous solutions (see Figure 9-5). Thus, a 'snake-through' of molecules larger than the cut-off specification of the membrane can hence solely be caused by conformational modifications due to the application of pressure. As introduced, the monosaccharide conformation as well as the mobility of their linkages are relevant for the overall polymer conformation. The high flexibility of α-(1→6) linkages in dextran molecules is attributable to an extra bond (C_5 -C_6), resulting in a higher degree of freedom. Several authors, inter alia Lee et al., tried to analyse the forced induced transitions in α-(1→6) linked polysaccharides. Lee et al. concluded from single molecule atomic force microscopy and molecular dynamic simulations that dextran molecule extension due to forced induced conformational transitions occur. This was related to rotations around the additional C_5 -C_6 bond and to chair-boat transitions of the pyranose ring. Both effects can be involved in dextran molecule extension. Rotation around C_5 -C_6 to different conformational states can lead to an overall increase of the molecule extension. Furthermore, the contribution of the individual monomers in dextran chains can increase due to the transition from chair to boat conformation. These mechanisms are supposed to vary with the external force applied (Lee et al., 2004). Neelov et al. formulated that the relative contribution of both effects is pressure dependent. This suggests that the forces generated by the applied transmembrane pressure induced conformational changes during the separation process. Such an extended molecular structure is probably responsible for the 'snake-through' of dextran molecules clearly above the cut-off specification. In the case of binary aqueous solutions, effects of other solutes can be excluded.

9.3.2 Membrane Separation of Different Single Dextran Fractions in Aqueous Sucrose Solutions

The manufacturing target, and therefore the predominating, component in sugar beet and cane raw juices is sucrose. Concentrations typically range between 14 % and 20 % (m/m) in sugar beet and 10 % and 18 % (m/m) in sugar cane raw juices (van der Poel et al., 1998). Therefore, an averaged and standardised level of 15 % (m/m) sucrose was maintained for further investigations of the membrane separation process.

The chromatograms of the permeate solutions containing sucrose are additionally illustrated in Figure 9-2 (A) and (B) for both membrane settings, depicted as dotted lines. Furthermore, the separation efficiencies calculated from chromatographic measurements are compared in Figure 9-4 (C).

Different from the binary aqueous dextran solution discussed above, separation efficiencies cannot easily be determined by polarisation. This is due to the contribution of sucrose. Thus, polarimetry was not used for the determination of separation efficiencies for these systems. Only with mechanical separation of optically active dextran, a reliable dextran content could be derived. This approach independent of polarimetry is of fundamental importance to evaluate the separation process. The observations show a dramatic effect due to the presence of sucrose. The presence of sucrose leads to significantly increased separation efficiencies for both membrane settings. A complete separation of the low molecular mass T40-fraction in 15 % (m/m) sucrose solutions using the membrane with cut-off of 4 kDa was observed and is manifested by the coincidence of the permeate curve with the baseline (dotted line Figure 9-2 B). These findings laid the foundation for the method to completely quantify dextran contents including high as well as low molecular mass dextran fractions (Abraham & Flöter, 2018). Similar tendencies were found for the T10-fraction, whereas an increase of the separation efficiency from roughly 25 % in binary aqueous solution to 65 % in aqueous sucrose solutions could be determined (see Figure 9-4 (C)).

Furthermore, a shift of the first deviation from the baseline of the sucrose containing samples to higher retention times indicate the slip-through of smaller molecules. Comparing the data in Figure 9-2 (A) and (B), it is apparent that the effect of the presence of sucrose is more pronounced, when the membrane with a smaller cut-off is used. However, the general effect of an improved separation due to the presence of sucrose is found during the application of both membranes, shift of the T40-peak (see Figure 9-2 (B)), elimination of the T40-peak and shift of the T10-peak (Figure 9-2 (A)). Consequently, it was found that the presence of sucrose decisively improves the membrane separation process of relevant low molecular mass dextran fractions. Either or both, membrane as well as dextran's polymer characteristics can be responsible for this.

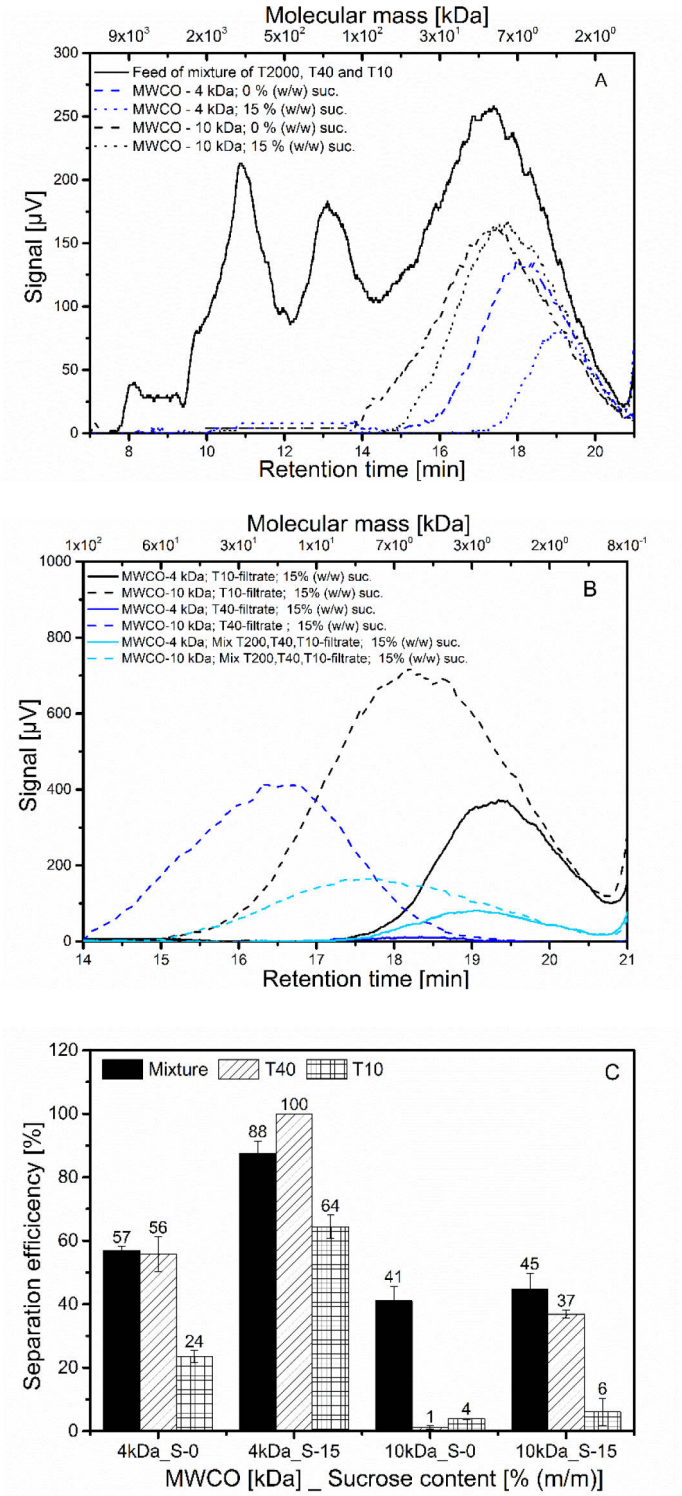

Figure 9-4 Evaluation of the effect of sucrose on the membrane separation performance. A) Chromatograms of permeate solutions of a mixture of equal amounts of T2000, T40 and T10 with (dotted lines) and without (dashed lines) 15 % (m/m) sucrose. B) Comparison of chromatograms of permeate solutions containing 15 % (m/m) sucrose using a MWCO of 4 kDa (solid lines) and 10 kDa (dashed lines). C) Comparison of all separation efficiencies [%] calculated from chromatographic measurements.

There is reason to assume that the molecular conformation of dextran changes depending on the solvent composition. In so-called good solvents polymer-solvent interactions prevail over polymer-

polymer interactions, resulting in a rather expanded structure. Decreasing the solubility of dextran in the solvent supposedly leads to a contraction of the dextran coils assumed to be caused by decreasing the level of dextran-solvent hydrogen bonds (Antoniou et al., 2010). A decrease of polymer-solvent interactions due to an increase in either or both polymer-sucrose or sucrose-solvent interaction hence may lead to generally modified molecular conformations, e.g. expanded structures. And again, SAXS measurements were used to identify potential basic conformational transitions of these different dextran fractions in 15 % (m/m) aqueous sucrose solutions in comparison with the initial binary aqueous dextran solutions. The scattering curves for the sucrose loaded samples are exemplary shown for the T10-fraction in Figure 9-5.

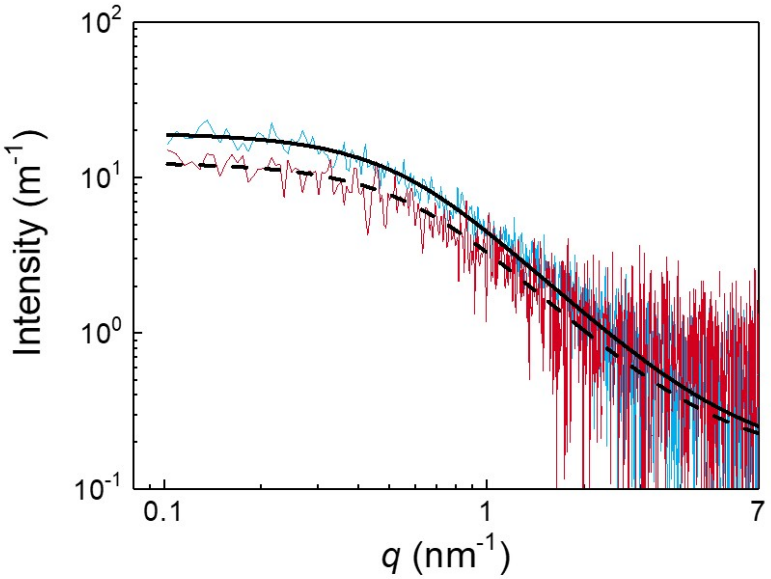

Figure 9-5 Scattering curves of T10-dextran fractions in binary aqueous and 15 % (m/m) aqueous sucrose solutions (blue and red line, respectively). Application of the Gaussian model results in the following $R_g$values for the different dextran fractions in binary aqueous and in aqueous 15 % (m/m) sucrose solutions (black solid and dashed line, respectively). T2000 in binary aqueous solutions = 9.3 ± 0. 1 nm and T2000 in 15 % (m/m) aqueous sucrose solution 10.9 ± 0.1 nm. T40 in binary aqueous solutions = 4.4 ± 0.1 nm and T40 in 15 % (m/m) aqueous sucrose solutions = 4.5 ± 0.1 nm. T10 in binary aqueous solutions = 2.8 ± 0. 1nm and T10 in 15 % (m/m) aqueous sucrose solution = 2.6 ± 0.1 nm.

First of all, it is important to mention that the scattering intensities of dextran in binary aqueous solutions are generally larger than in aqueous sucrose solutions (blue and red curves, respectively). This is caused by the higher density difference between the solvent solution and the polymer in binary aqueous solutions in comparison with aqueous sucrose solutions. However, very similar scattering patterns are identifiable for dextran dissolved in either binary aqueous or in aqueous sucrose solutions. A dramatic change of the molecular structure due to the presence of 15 % (m/m) sucrose in pressureless applications could hence not be detected.

Applying the so-called Gaussian model to the scattering data, ideally assuming free rotatability of any two bonds, allows the comparison of the radius of gyration R_g for dextran in both solutions. The application of this model results in R_g values of (2.8 ± 0. 1) nm and (2.6 ± 0.1) nm for T10 in binary aqueous (black solid line) and aqueous sucrose solutions (black, dashed line), respectively. Furthermore, $R_g$values of (4.4 ± 0.1) nm and (4.5 ± 0.1) nm for T40 in binary aqueous and in 15 % (m/m) aqueous sucrose solution were determined. Both sample compositions, binary aqueous and aqueous sucrose solutions, show hence very similar values for the radius of gyration of these random coil structures. However, the determined radius of gyration of T2000 in binary aqueous and in aqueous sucrose solutions is slightly different, (9.3 ± 0.1) nm and (10.9 ± 0.1) nm, respectively. The latter is anyhow completely separated by both membranes in binary aqueous as well as in aqueous sucrose solutions. These comparative SAXS measurements could not reveal any changes of the overall polymer conformation of dextran in solution without any pressure applied. Thus, the SAXS data do not underpin the possible explanation of the increased separation efficiency due to the presence of sucrose.

Alternatively, a slightly modified flow behaviour or attachment of sucrose molecules on dextran chains may hamper the forced induced conformational transitions. Furthermore, adhesion of sucrose to the inner surface of the membrane pores can lead to slightly modified membrane properties, e.g. reduced apparent pore sizes. However, within this study, it remains open which mechanism is responsible for the improved membrane separation due to the presence of sucrose. Nevertheless, this improved separation due to sucrose was repeatedly observed and is highly functional for this method to work at the extended applicability covering relevant ranges of molecular mass.

9.3.3 Membrane Separation of Mixed Dextran Fractions in Binary Aqueous and Aqueous Sucrose Solutions

In order to further approach realistic conditions of solutions containing molecules with broadly distributed molecular masses, mixtures containing equal amounts of the three dextran fractions (T2000, T40 and T10) with an overall mass percentage of 0.075 % (m/m) were analysed.

The separation characteristics of these mixtures for both membrane settings and solvent conditions are shown in Figure 9-4 (A). In binary aqueous solutions, separation efficiencies of about 60 % and 40 % when using membranes with the 4 kDa and 10 kDa cut-off were found. The separation efficiencies are slightly higher than expected from the separation efficiencies of the individual dextran fractions in binary aqueous solutions. Besides, the chromatograms of the permeates of mixed dextran fractions start to deviate from the baseline at slightly higher retention times than for the separation of single dextran fractions (see Figure 9-4 (B)). The presence of broadly mixed chain lengths seems hence to slightly affect the separation process. And again, the separation efficiencies

are dramatically increased due to the presence of sucrose. The mixture of T2000, T40 and T10 in aqueous sucrose solutions shows separation efficiencies of almost 90 % and 45 % by membranes with the 4 kDa and 10 kDa cut-off, respectively.

To finally derive an actual analytical method, concrete number-based parameters need to be identified, so that the separation of these mixed broadly distributed dextran fractions in aqueous sucrose solutions can be optimised. To get details on this, the determination of the 'snake-through'-molecular masses and the point of deviation from the baseline were determined (see Figure 9-4 (A)).

The peak maxima of the dextran molecules in the permeates of these mixtures correspond to molecular masses of about 4.3 kDa and 10.5 kDa for the respective membranes. These values appear to be nearly incidental with the molecular weight cut-off specification of the membranes. It has to be noted that they exclusively apply to the peak maxima in 15 % (m/m) aqueous sucrose solutions. These peaks are, however, not assigned to a uniform but rather to a relatively broad molecular mass distribution. The point of deviation of these curves from the baseline starts at earlier retention times indicating the passing through of molecules of also higher molecular masses than the peak maxima indicate. The permeate of the 10 kDa-membrane contains dextran molecules with a maximum molecular mass of 50 kDa. The maximum molecular mass found in the permeate after separation with the 4 kDa-membrane was 10 kDa. These molecular masses hence indicate the specific cut-off for dextran of these two membranes in 15 % (m/m) sucrose solutions. These different determination limits using the two different membrane settings suggest that this could be a way to roughly differentiate between a high and a low molecular mass dextran fraction. Consequently, the implementation of membrane separation as a preparatory step for macromolecule analysis seems to be a promising tool for industrial practice. The actual applicability of the basic single membrane application and also of the sophisticated membrane combination needs now to be regarded.

9.3.4 Application of the Membrane Method

9.3.4.1 Fractionated Dextran Analysis in Synthetic Thin Juices

The general applicability of the Membrane Method using the cut-off of 4 kDa for the determination of varying dextran contents and molecular masses in synthetic thin juices, meaning 15 % (m/m) aqueous sucrose solutions, was previously shown elsewhere (Abraham & Flöter, 2018).

To further evaluate the possibility of fractionated dextran analysis, the two different membrane settings were used to determine the two relevant dextran fractions and their combination in 15 % (m/m) sucrose solutions. In sugar industry, dextran contents are usually given in mg per kg sucrose, which was hence used for the application experiments. The fractionated dextran analysis was firstly considered for a constant dextran content of 5000 mg per kg sucrose, which corresponds

to the previously investigated mass percentages of 0.075 % (m/m). The related dextran values determined are shown in Figure 9-6 (A).

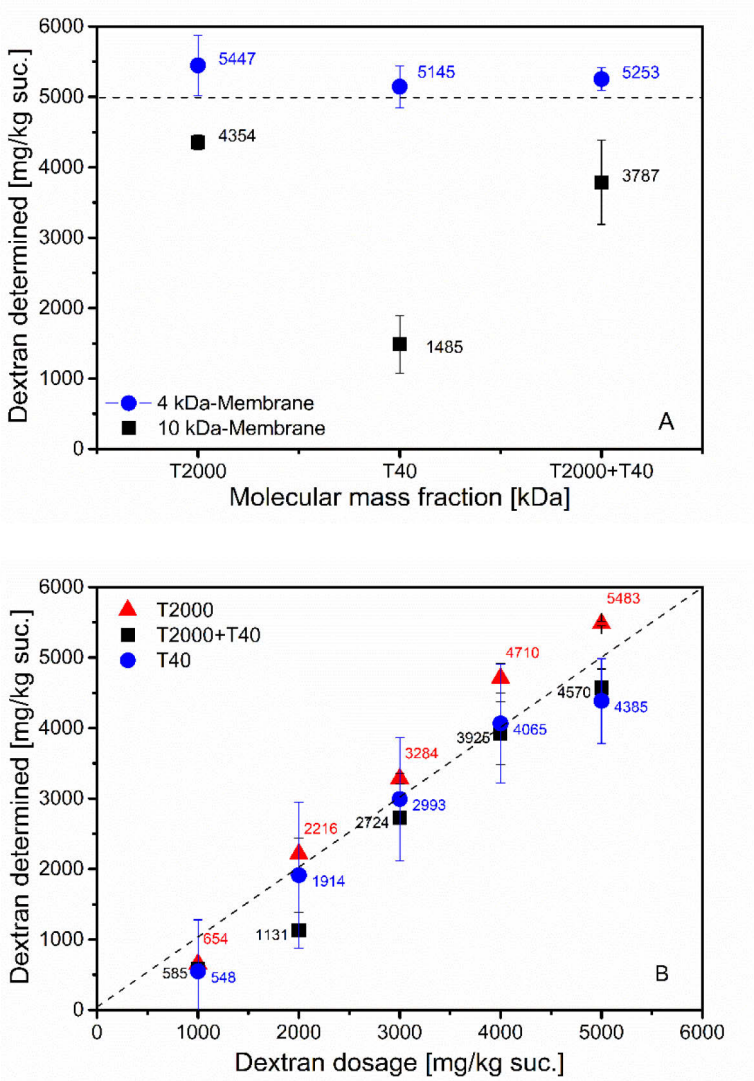

Figure 9-6 Application of the new Membrane Method for the determination of various dextran fractions and contents. A) Determination of various dextran fractions at a constant dextran content of 5000 mg/kg suc. (corresponds to 0.075 % (m/m)) using the MWCO of 4 kDa (blue dots) and 10 kDa (black cubes). B) Determination of different dextran fractions at various contents and molecular masses using the MWCO of 4 kDa.

First of all, the application of the membrane with the 4 kDa cut-off results in dextran values very close to the actual dextran dosage (5000 mg/kg sucrose; dashed line) independent of the molecular mass present. This once again confirms that the basic setting, using the membrane with the 4 kDa cut-off, seems to be capable of fully quantifying dextran covering the whole molecular mass spectrum relevant for dextran-related effects. The determination of total dextran contents using the membrane with the cut-off of 10 kDa is less successful. The value determined of high molecular mass dextran is relatively close to the actual dextran dosage of 5000 mg/kg sucrose. The separation of the T40-fraction happens as expected just to a small extent, which results in a low dextran value

determined of about 1500 mg/kg sucrose. This is in alignment with the previously established knowledge about the membrane separation characteristics.

According to that, this value obviously concerns the upper end of the molecular mass distribution of the T40-dextran fraction. This hence relates to dextran molecules larger than 50 kDa occurring in the molecular mass distribution of the T40-fraction. The determination of the mixture of equal amounts of T2000- and T40-dextran also reveals lower values when using the membrane with the 10 kDa cut-off (about 3800 mg /kg suc.). The combination of the separation performances identified for both membranes makes fractionated dextran analysis possible. The difference between the dextran values determined by the two different membranes should pertain to the dextran content with molecular masses ranging between the different separation limits of the respective membranes, here 10 kDa and 50 kDa.

9.3.4.2 Quantitative Analysis in Realistic Sugar Beet Raw Juices

To verify that the findings on synthetic thin juices are also valid for realistic settings, the basic single membrane configuration (cut-off of 4 kDa) was applied to real sugar beet juices. The raw juices were spiked with the respective molecular mass dextran fractions at various contents. In doing so, it was looked for potential effects due to other high molecular mass components present in sugar beet raw juices. Figure 9-6 (B) shows the determination of varying contents of the different dextran fractions in realistic sugar beet raw juices.

The data gathered clearly confirm that both, high and low molecular mass dextran fractions as well as their combination are very well separated. The absence of a systematic deviation actually indicates that the presence of other components in such real beet raw juice, e.g. the ever present pectin, do not significantly affect the determination of dextran. Pectin is known for rather low molecular masses and extended worm-like conformations in solution, probably enabling them to pass the membrane pores in a ‘snake-through’ manner as well (Morris & Ralet, 2012). These results mark an initial confirmation of the assumption made that other linear polysaccharides in real sugar beet raw juices do not interfere with the determination of dextran concentrations according to the method described above.

9.4 Conclusion

The prototype of a new method for the analysis of dextran with a broad molecular mass spectrum in sugar industry practice was systematically evaluated. The method proposed is based on determining differences in optical rotation caused by the mechanical separation of dextran by membrane filtration. Therefore, the separation characteristics of two polyethersulfone membranes for the retention of different dextran molecular mass fractions (T2000, T40, T10) from aqueous solutions was investigated. Polarimetry as well as highly accurate size exclusion chromatography

were used to evaluate the separation performance of the two membranes for dextran in binary aqueous solutions and aqueous sucrose solutions.

The study showed that the specific separation limits of these membranes for dextran are clearly above the manufacturer's MWCO specification. A 'snake-through' effect of larger dextran molecules through membrane pores above the cut-off specification of the respective membranes could be observed. This can possibly be related to the high flexibility of dextran chains.

The separation of relevant dextran fractions from binary aqueous solutions only works with limitations. However, the presence of sucrose leads to advantageously improved separation efficiencies for both membrane settings. The specific cut-off values for dextran in aqueous sucrose solutions have been determined. These dextran-related separation limits are 10 kDa and 50 kDa for the membranes with a MWCO of 4 kDa and 10 kDa, respectively.

This demonstrates that the basic membrane setting with a MWCO of 4 kDa is suited to completely separate and therefore to fully quantify the whole molecular mass spectrum relevant for dextran-related process effects in sucrose solutions, independent of the molecular mass present. The membrane with the MWCO of 10 kDa can be used for the determination of dextran with molecular masses above 50 kDa. The combination of these membranes seems hence to be useful to distinguish between the dextran-related cut-off values determined. The data obtained indicate that not only the complete quantification, but additionally the fractionation of dextran into high and low molecular mass fractions seems to be feasible. The application of this new approach for the determination of dextran with varying molecular masses at various contents in synthetic thin juices as well as in real sugar beet raw juices reveal very promising results.

It should be noted that the quality and therefore the composition of sugar cane and beet raw juices vary depending on several conditions (e.g. climate, harvest). Even though the data gathered indicate that pectin does not interfere significantly with the method suggested, other major polysaccharides have to be considered as potentially problematic in membrane filtration. In case that these problems materialise, it is recommended to fall back on established methods of sample preparation such as specific enzymatic decomposition prior to the membrane filtration. This subject is part of ongoing work studying more realistic raw juices of varying quality.

Anyhow, the work presented here, combined evaluation of the method and supporting HPLC analysis, shows the potential of the membrane method. This approach to develop a method with easy applicability suitable for industrial practice could be filling a gap of currently unknown information on dextran in sugar industry.

Acknowledgement

The authors would like to thank the Federal Institute for Materials Research and Testing (BAM-Bundesanstalt für Materialforschung und –prüfung) for performing and evaluating SAXS measurements.

References

Abdel-Rahman, E.-S. (2007). Investigations on the influence of dextran during beet sugar production with special focus on crystal growth and morphology (PhD). Technische Universität Berlin, Berlin.

Abraham, K., & Flöter, E. (2018). New approaches for the determination of dextran in the sugar production process. *Sugar Industry*, *143*(68), 138–146.

Antoniou, E., Themistou, E., Sarkar, B., Tsianou, M., & Alexandridis, P. (2010). Structure and dynamics of dextran in binary mixtures of a good and a bad solvent. *Colloid and Polymer Science*, *288*(12-13), 1301–1312. https://doi.org/10.1007/s00396-010-2259-x

Aquino, F. W., & Franco, D. W. (2009). Molecular mass distribution of dextran in Brazilian sugar and insoluble deposits of cachaça. *Food Chemistry*, *114*, 1391–1395. https://doi.org/10.1016/j.foodchem.2008.11.019

Baker, R. W. (2004). *Membrane technology and applications* (2nd ed.). Chichester, New York: J. Wiley.

Belitz, H.-D., Grosch, W., & Schiberle, P. (2008). *Lehrbuch der Lebensmittelchemie* (6. Auflage). Berlin Heidelberg: Springer Berlin Heidelberg.

Bergmann, A., Orthaber, D., Scherf, G., & Glatter, O. (2000). Improvement of SAXS measurements on Kratky slit systems by Göbel mirrors and imaging-plate detectors. *Journal of Applied Crystallography*, *33*(3), 869–875. https://doi.org/10.1107/S0021889800000881

Breßler, I., Kohlbrecher, J., & Thünemann, A. F. (2015). SASfit: a tool for small-angle scattering data analysis using a library of analytical expressions. *Journal of Applied Crystallography*, *48*(5), 1587–1598. https://doi.org/10.1107/S1600576715016544

Chen, J. C., & Chou, C. C. (1993). Cane Sugar Handbook: A Manual for Cane Sugar Manufacturers and Their Chemists (12th ed.). New York: John Wiley & Sons.

Day, D. F., & Sarkar, D. (1986). Methods of Analysis for Dextran in Sugar Molasses and Juice. *Proc. Int. Soc. Sugar Cane Technol*, 748–754.

Gasciolli, V., Choplin, L., Paul, F., & Monsan, P. (1991). Viscous properties and molecular characterization of enzymatically size-controlled oligodextrans in aqueous solutions. *Journal of Biotechnology*, *19*, 192–202. https://doi.org/10.1016/0168-1656(91)90058-4

Hamid, N., Ismail, A. F., Matsuura, T., Zularisam, A.W., Lau, W. J., Abdullah, M. S. (2011). Morphological and separation performance study of polysulfone/titanium dioxide (PSF/TiO 2) ultrafiltration membranes for humic acid removal. *Desalination*, *273*(1), 85–92. https://doi.org/10.1016/j.desal.2010.12.052

Hirata, Y., Sano, Y., Aoki, M., Shohji, H., Katoh, S., Abe, J., Yamamoto, H. (2003). Small-angle X-ray scattering studies of moderately concentrated dextran solution. *Carbohydrate Polymers*, *53*(3), 331–335. https://doi.org/10.1016/S0144-8617(03)00107-3

ICUMSA (Ed.). (2011). *ICUMSA Method Book*. Berlin: Dr. Albert Bartens KG.

Lee, G., Nowak, W., Jaroniec, J., Zhang, Q., & Marszalek, P. E. (2004). Molecular dynamics simulations of forced conformational transitions in 1,6-linked polysaccharides. *Biophysical Journal*, *87*(3), 1456–1465. https://doi.org/10.1529/biophysj.104.042879

Morris, G. A., & Ralet, M. C. (2012). The effect of neutral sugar distribution on the dilute solution conformation of sugar beet pectin. *Carbohydrate Polymers*, *88*(4), 1488–1491. https://doi.org/10.1016/j.carbpol.2012.02.020

Orthaber, D., Bergmann, A., & Glatter, O. (2000). SAXS experiments on absolute scale with Kratky systems using water as a secondary standard. *Journal of Applied Crystallography*, *33*(2), 218–225. https://doi.org/10.1107/S0021889899015216

Pasch, H., & Trathnigg, B. (1998). *HPLC of Polymers*. Berlin Heidelberg: Springer.

Promraksa, A. (2008). Reduction of Dextran Contamination in Raw Sugar Production (PhD). Suranaree University of Technology, Nakhon Ratchasima.

Tvaroska, I., Pérez, S., & Marchessault, R. (1978). Conformational Analysis of (1->6)-alpha-D-Glucan. *Carbohydrate Research*, *61*, 97–106. https://doi.org/10.1016/S0008-6215(00)84470-5

Van der Poel, P. W., Schiweck, H., & Schwartz, T. (1998). *Sugar Technology: Beet and Cane Sugar Manufacture*. Berlin: Dr. Albert Bartens KG.

Wojtczak, M., Gruska, R., MIkos, P., Antczak-Chrobot, & Aneta. (2015). Dextran molecular mass effect on particle size distribution of CaCO3 for 1st and 2nd carbonatation. *Sugar Industry*, *140*(11), 703–706.

10 Conclusion

The presence of microbial polysaccharides in sugar beet and cane juices is known to cause diverse negative effects during sugar manufacture. One of the most important polysaccharides produced by microbial activity is the glucose polymer dextran, which was therefore key to this study.

The dextran-induced effects during sugar manufacture from beet and cane are usually mitigated by enzymatic decomposition using dextranase, which specifically hydrolyses the α-(1→6) glycosidic bonds in dextran's main chain. However, a targeted and controlled application of dextranase in sugar industrial practice is still not established practice, whereas this work has made major steps towards this.

First of all, a targeted mitigation of dextran-induced process effects requires a detailed understanding of the effects of dextran with varying molecular mass distributions, also including enzymatically decomposed dextran. Thereby, the work presented focuses on the two most relevant sub-process steps of sugar manufacture with regard to dextran: juice purification including filtration as well as sucrose crystallisation. To specifically analyse the effects of dextran depending on its content and molecular mass distribution, experiments were generally performed in synthetic thin and thick juices.

Thus, the effects of dextran during sugar beet raw juice purification by means of lime and carbonation gas were investigated. Thereby, it was shown that dextran is involved in size and shape modifications of the calcium carbonate particles precipitated during carbonation. More precisely, the data indicate that the presence of dextran with molecular masses above 10 kDa promotes calcium carbonate agglomeration. This was most pronounced for broadly distributed intermediate but rather low molecular mass dextran. Thus, a mixture of high and low molecular mass dextran fractions as well as mildly, insufficiently decomposed high molecular mass dextran caused the most dramatic increase in the size of calcium carbonate particles.

Besides, a size-related evaluation of particle shape parameters has additionally revealed that particularly the shape of large-sized agglomerates was modified. The shape data indicated that the calcium carbonate agglomeration in dextran-free samples as well as in samples loaded with low molecular mass dextran is oriented. Once dextran of higher molecular mass was present (>85 kDa),

the shape data suggest that the agglomeration was non-oriented. Additionally, consulting viscosity measurements, it was shown that the effect of dextran contents relevant for raw juices in the beginning of sugar manufacture on the flow behaviour is minor. Thus, the major cause for impeded filtration performances as a part of beet raw juice purification is assumed to be caused by the just mentioned particle size and shape modifications, whereby it is assumed that the filter cake pore structure is modified due to the presence of more round agglomerates with smoother surfaces. Apart from effects on filtration performances, the actual purification performance, and thus the purity, can additionally be affected by these size and shape modifications of the calcium carbonate particles precipitated during juice purification.

These dextran-induced particle modifications were reduced by the enzymatic decomposition of dextran, while the progress in decomposition and thus the molecular mass of the reaction products are decisive. In this case, the latter was managed by applying varying enzyme levels. When decomposing dextran to reaction products with molecular masses of less than 10 kDa, no effects on the particle size and shape were found anymore, hence, representing the target of dextranase application with regard to particle modifications during carbonation.

Similarly, the effects of different dextran fractions on the size and shape distribution of sucrose crystals were investigated. Here, too, this includes the effects of the reaction products resulting from the application of varying enzyme levels, again aiming at identifying the most harmless reaction products. The data from evaporative crystallisation experiments using synthetic thick juices indicate that three different crystal-shapes can be related to the presence of dextran, namely, cube-like, elongated as well as agglomerated crystals.

For high molecular mass dextran, the occurrence of these shapes seems to depend on the dextran content present. Thus, low contents of high molecular mass dextran predominantly caused an increase in cube-like crystals, while at high contents agglomeration and elongation increasingly predominantly occur. Similar to higher contents of high molecular mass dextran, low molecular mass dextran, independent of the concentration present, mainly caused an increase in agglomerated crystals, accompanied by a low amount of elongated crystals.

Consequently, it has been shown that high as well as low molecular mass dextran affected the sucrose crystal characteristics in an undesirable way. This again gives reason to assume that not only the total dextran content, but also the molecular mass distribution seems to play an important role in the extent and kind of the effects on the sucrose crystal characteristics.

Here, again, it was found that mildly, insufficiently decomposed high molecular mass dextran still affects the sucrose crystal size and shape distribution, again negative effects were most pronounced. Thus, here again, broadly distributed intermediate molecular masses, which are realistic for naturally produced dextran in sugar cane and beet juices, caused most dramatic effects on the sucrose crystal characteristics. Here, too, the dextran-induced shape modifications could be reduced

by sufficient enzymatic decomposition. In this case, no dextran-related effects on the sucrose crystal characteristics were found once dextran was decomposed to reaction products with molecular masses below 5 kDa.

In order to decompose dextran to these most harmless reaction products identified, a detailed understanding of the dextranase reaction on various dextran contents and initial molecular mass distributions is necessary. A comprehensive study on that was done using size-exclusion and affinity chromatography. In doing so, it was confirmed that dextran is decomposed in a gradual manner.

In addition, it was found that not only the total dextran content, but also the initial molecular mass distribution is decisive for the progress in decomposition and thus for the molecular mass of the reaction products. Thereby, the decomposition of high and low molecular mass dextran fractions and an equal-mass mixture of these two were enzymatically decomposed while varying the enzyme level as well as the incubation time. For all molecular mass distributions, the molecular mass of dextran was gradually reduced with the increase in enzyme level and incubation time. As expected, the enzymatic decomposition of low molecular mass dextran was distinctly further progressed in comparison with the high molecular mass dextran fraction. Interestingly, the equal-mass mixture of the high and low molecular mass dextran fraction was similarly, even slightly further, progressed than the individual low molecular mass dextran fraction. Thus, interactions between high and low molecular mass dextran chains seem to be likely, assumed to facilitate enzyme-dextran-contacts.

The data clearly suggest that for the application of dextranase in a targeted manner, aiming at the most harmless reaction products mentioned above, the dextran content as well as its molecular mass distribution need to be known. This means, the total dextran content, including the whole molecular mass range relevant, must be determined and at best the two main molecular mass dextran fractions need be distinguished to adequately dose dextranase.

For this purpose, a practical tool for dextran analysis in sugar industrial practice was developed and benchmarked against the commonly used Haze Method, which is rather inaccurate and also sensitive to molecular mass variation. The method proposed is based on determining differences in optical rotation caused by the mechanical separation of dextran as a macromolecule from the juices by membrane filtration. To implement the latter as a preparatory step for dextran analysis in sugar industry practice, the separation characteristics of two polyethersulfone membranes for the retention of different dextran fractions from aqueous solutions were investigated, using polarimetry and size exclusion chromatography.

It was found that the presence of sucrose leads to dramatically improved separation efficiencies for both membrane settings. This advantage has led to specific cut-off values for the separation of dextran from aqueous sucrose solutions of 10 kDa and 50 kDa for the membranes with declared molecular weight cut-off specification of 4 kDa and 10 kDa, respectively. The data indicate that the

basic membrane setting (MWCO of 4 kDa) enables the complete separation and therefore the analytical quantification of the whole molecular mass spectrum relevant for sugar industry. The combination of both membranes, furthermore, indicates that this principle is suited for the differentiation between a high and a low molecular mass dextran fraction. Thus, investigations on the method proposed revealed promising prospects for complete and fractionated dextran analysis in sugar cane and beet juices, completing the demand for targeted enzyme applications.

To conclude, the first-time combination of these basic scientific findings on the whole dextran issue provides the basic framework for dextranase application in sugar industrial practice.